ANALYSIS OF CARBON DIOXIDE AND METHANE CYCLING IN FOREST SOILS USING STABLE CARBON ISOTOPES

By

Kern Y. Lee
B.Sc., University of Waterloo, 2005

A Thesis Submitted in Partial Fulfillment of the
Requirements for the Degree of

MASTERS OF SCIENCE

in the School of Earth and Ocean Sciences

Analysis of Carbon Dioxide and Methane Cycling in Forest

Soils using Stable Isotopes

By

Kern Y. Lee
B.Sc., University of Waterloo, 2005

Supervisory Committee

Dr. Michael J. Whiticar, Supervisor
(School of Earth and Ocean Sciences)

Dr. Jay T. Cullen, Departmental Member
(School of Earth and Ocean Sciences)

Dr. Kevin Telmer, Departmental Member
(School of Earth and Ocean Sciences)

Dr. Real Roy, Outside Member
(Department of Biology)

Dr. Steven Hallam, External Examiner
(Microbiology and Immunology, University of British Columbia)

Supervisory Committee

Dr. Michael J. Whiticar, Supervisor
(School of Earth and Ocean Sciences)

Dr. Jay T. Cullen, Departmental Member
(School of Earth and Ocean Sciences)

Dr. Kevin Telmer, Departmental Member
(School of Earth and Ocean Sciences)

Dr. Real Roy, Outside Member
(Department of Biology)

Dr. Steven Hallam, External Examiner
(Microbiology and Immunology, University of British Columbia)

ABSTRACT

Understanding the role of forests in the cycling of methane (CH_4) and carbon dioxide (CO_2) is of importance to the elucidation of global greenhouse gas budgets. Previous studies have shown aerated forests soils to be net sinks of atmospheric CH_4 and sources of carbon dioxide. While much research has focused on the role of forest soils as CO_2 sources and CH_4 sinks, few studies have utilized ^{13}C-isotope studies to clarify the nature of subsurface CO_2 production and CH_4 consumption. The present study, carried out in 3 temperate forest environments on Vancouver Island during 2006 and 2007, and a boreal forest in northern Quebec in 2005, is intended to address this paucity of information.

The isotope and concentration data corroborates previous studies in suggesting that both temperate and boreal forest environments act as net CH_4 sinks and CO_2 sources. No clear evidence of methanogenesis is apparent in either Vancouver Island or northern

Quebec, where the isotopic composition of subsurface CH_4 is influenced by diffusive and biological fractionation. Near-surface photosynthetic uptake may have a strong influence on the isotopic composition of soil CO_2 and the resultant fluxes, acting to reduce apparent fluxes due to CO_2 consumption.

Intra-site variability of CH_4 and CO_2 fluxes indicates that the use of two static chambers in a single site, while sufficient for the confirmation of gas uptake or emission, may be less adequate in the determination of actual rates of efflux/influx. Future studies should address this by either sampling a larger area, installing a greater number of chambers, or by utilizing entirely different methods, such as the use of eddy covariance techniques.

TABLE OF CONTENTS

List of Figures

List of Tables

ACKNOWLEDGEMENTS

I would like to thank my supervisor, Michael Whiticar, for his patience and willingness to put time aside from his busy schedule to address my many questions and concerns. His careful guidance also proved invaluable throughout the course of my studies. As well, I appreciate the efforts of my supervisory committee to assist me in the progression of my thesis. I am grateful to Drs. Cullen, Roy and Telmer for adjusting their busy schedules to look over and correct my thesis, and to participate in my thesis defense. My thanks are also extended to Dr. Hallam, who enthusiastically agreed to take on the responsibilities of external examiner.

Outside of the University of Victoria, the help of Marc-Andre Giasson in accommodating site transport and sample collection at the Quebec site made possible the boreal forest study. To my labmate, Joe Melton, thanks for answering any additional pesky questions that I had, and also by providing a welcome distraction as a formidable foozball opponent. As your record shows, you have indeed proved to be a worthy foe.

To all my friends here in Victoria who bore the brunt of my complaints and frustrations when things went badly, thanks for all your encouragement and your willingness to be guinea pigs for my many practice presentations. Finally, I am especially grateful for the constant support of my mother and father. Without them, I would not be were I am today.

1.0 Introduction and Background

1.1 Atmospheric Carbon Dioxide/Methane and Global Trends

Two of the most significant greenhouse gases in the Earth's atmosphere, in addition to water vapour, are methane (CH_4) and carbon dioxide (CO_2). Although present in lower mixing ratios than CO_2 (1.80 ppm vs. ~379 ppm for CO_2), CH_4 has a proportionately larger climate forcing effect: one additional mole of CH_4 provides roughly 24 times more radiative forcing as a greenhouse gas as compared to an additional mole of CO_2 (Wuebbles and Hayhoe, 2002).

The quantity of atmospheric CH_4 has increased rapidly since pre-industrial times. From a concentration of about 0.7 ppm, it has taken only 200 years for atmospheric CH_4 to reach its present day global mixing ratio of 1.8 ppm. Although the rate of increase has declined in recent years, the evidence is insufficient to extrapolate further trends and a continuing accumulation of atmospheric CH_4 remains the most likely scenario for the near future (Dlugokencky et al., 2003).

Natural wetlands constitute the largest single source of atmospheric CH_4 (~100 Tg/yr, or roughly 20 % of global CH_4 output) followed by animal and rice agriculture (~80 and 60 Tg/yr, or about 12 % and 16 % respectively), which represent the largest anthropogenic sources of CH_4 (Khalil, 2000). Smaller contributions include biomass burning, coal mining, natural gas leakage, landfill outgassing, termites, wastewater treatment, and open ocean emissions, with each source contributing 10 % or less of the global CH_4 output.

The largest sink of atmospheric CH_4 is within the troposphere, where CH_4 is removed via reactions with OH radicals. It is estimated that this sink alone removes about 440 Tg/yr of CH4 (90 % of the global CH_4 sink), which is more than 80 % of all methane released to the atmosphere. CH_4 removal also occurs in the stratosphere via reactions with OH and $O(^1D)$ (~15 Tg/yr or 3 % of the global CH_4 sink), and within aerated soils where oxidation occurs (~30 Tg/yr or 6 % of the global CH_4 sink) (Khalil et al., 2000).

Since the industrial revolution, atmospheric CO_2 mixing ratios have also been subject to large increases, having risen 100 ppm from a pre-industrial level of about 280 ppm (IPCC, 2007). Due to the higher atmospheric mixing ratio of CO_2, this gas species provides the bulk of the radiative forcing caused by all greenhouse gases present (water vapour excluded) in the atmosphere.

The burning of fossil fuels is the single largest contributor to this rapid growth rate, emitting about 7.2 ± 0.3 GtC/yr into the atmosphere during the period of 200-2005 (IPCC, 2007). This efflux is partially balanced by a net terrestrial and oceanic uptake of -0.9 ± 0.6 GtC/yr and -2.2 ± 0.5 GtC/yr, respectively (IPCC 2007). Current trends anticipate a continuing increase in atmospheric CO_2 well into the foreseeable future, which will augment the current imbalance between global CO_2 sources and sinks.

1.2 Bacteria and the Methane Cycle

Bacteria and Archaea play a major role in the methane cycle, and act as both sinks and sources of atmospheric CH_4. Methane-producing Archaea (or methanogens) constitute the largest source of atmospheric CH_4 and are ubiquitous in environments such as natural wetlands, rice paddies, animal digestive tracts, landfills, water treatment systems, and freshwater and marine sediments (Le Mer and Roger, 2001). Methanogenesis is mainly achieved via three pathways: carbonate reduction, fermentation of acetate and other organic acids, and fermentation of various methylated substrates, i.e., methylamines, methylated organic sulphur compounds, etc.

The carbonate reduction (or hydrogenotrophic) pathway is represented by the following equation:

$$CO_2 + 8H^+ + 8e^- \rightarrow CH_4 + 2H_2O \qquad (1.2.1)$$

This process is the dominant methanogenic pathway in marine sediments, but it can also occur in freshwater environments following the depletion of alternative substrates (e.g., Whiticar et al., 1986). In marine environments, the abundance of dissolved sulphate supports an extensive sulphate-reducing bacteria (SRB) population within marine sediments. These bacteria are able to out-compete methanogens for carbon substrates and methanogenic activity in these environments is minimal. However, methanogenesis can occur at greater depths where the dissolved sulphate pool has been exhausted. In these

zones, carbonate-reducing methanogenesis occurs due to the depletion of other substrates by SRB.

The other primary methanogenic pathway, acetate fermentation, proceeds via the reaction:

$$^{*}CH_3COOH \rightarrow {}^{*}CH_4 + CO_2 \qquad (1.2.2)$$

In the above Equation the "*" indicates the methyl group of acetate has been transferred fully intact to the methane molecule. In freshwater environments acetate fermentation represents the main mechanism of methanogenesis, comprising roughly 70% of total emissions (e.g., Whiticar, 1999). However, after depletion of acetate and other organic substrates, methane fermentation then proceeds via carbonate reduction. This often occurs at greater sediment depths, where the quantity of organic matter is much smaller.

The relative importance of the third methanogenic pathway, fermentation of methylated compounds, is not well known. A generic reaction for this mechanism is shown below:

$$CH_3\text{-}A + H_2O \rightarrow CH_4 + CO_2 + A\text{-}H \qquad (1.2.3)$$

In this Equation, "A" represents the chemical group to which the methyl molecule is attached. This mechanism is known to exist in freshwater environments concurrently with acetate fermentation, albeit in less significant quantities. Other modes of methanogenesis,

such as those utilizing alcohols, exist but their importance to the methane cycle is likely minor (Whiticar 2000).

Certain types of bacteria can also exploit CH_4 as an energy source. These organisms are known as methanotrophs, and all members of this group utilize CH_4 as their only carbon and energy source (Hanson and Hanson, 1996). The general reaction governing the process of methanotrophy is as follows:

$$CH_4 + O_2 \rightarrow CO_2 + 2H_2O \qquad (1.2.4)$$

There are three main groups of methanotrophs: type I, II and X. They are distinguished by differences in the arrangement of cytoplasmic membranes, as well as differences in carbon incorporation pathways (Higgins et al., 1981). Type I methanotrophs utilize the Ribulose Monophosphate (RuMP) pathway to assimilate carbon, while type II methanotrophs instead use the serine pathway for carbon incorporation. The third group, type X, utilizes RuMP as the primary pathway but contain small amounts of a serine-pathway chemical as well.

All known methanotrophs oxidize CH_4 via methane monoxygenase enzymes (MMOs). These are present in two forms: a soluble methane monoxygenase (sMMO) and a particulate membrane-bound MMO (pMMO). All described methanotrophs are capable of forming pMMO, while only a few type II and X methanotrophs can form sMMO. Methanotrophic bacteria play an important role in the CH_4 cycle by intercepting and consuming large amounts of CH_4 that would otherwise be emitted into the atmosphere.

1.4 Stable Carbon Isotopic Analyses

Studies of the stable carbon ($^{13}C/^{12}C$) isotope ratio of CH_4 can provide an indication of specific formation/consumption processes. Isotope ratios are presented in delta notation and are expressed in units of "per mil"(or ‰), which is obtained by the following Equation:

$$\delta Rx(‰) = \frac{R_{sample} - R_{std}}{R_{std}} \times 10^3 \qquad (1.4.1)$$

Where "R" represents the ratio of the heavier elemental isotope to the lighter one, and the subscripts "*sample*" and "*std*" refer to the ratios present, respectively, in the sample of study and a standard. In the case of stable carbon isotope ratios, the standard used for comparison is Vienna Pee-Dee Belemnite (V-PDB). It has an accepted $^{13}C/^{12}C$ value of 0.0112372 (Slater et al., 2001) and a $\delta^{13}C$ of 0 ‰.

Different types of CH_4, i.e., formed by different pathways, display distinctive ranges of isotopic values. For example, abiogenic, i.e., mantle or volcanic, CH_4 has a $\delta^{13}C$ range of –5 ‰ to –12 ‰ while biogenic (biologically produced) gases tend to have more ^{12}C-enriched values ranging from –21 ‰to –80 ‰ (Whiticar, 2000). The ^{12}C-enriched isotope ratios of biogenic CH_4 result from mass dependent isotope effects. Due to its lighter mass, ^{12}C within the precursor substrate has a higher enzymatic reaction rate than ^{13}C.

The result is the formation and emission of ^{12}C-enriched CH_4, relative to precursor materials. This isotope separation is commonly expressed in the form of a fractionation factor (α), obtained by the equation:

$$\alpha_{a-b} = \frac{\delta_a + 1000}{\delta_b + 1000} \quad (1.4.2)$$

Where subscript "*a*" represents precursor materials and "*b*" denotes the product. Using this notation, an α range of 1.04 to 1.09 has been observed for bacterial CH_4 production from substrates such as acetate and CO_2 (Whiticar et al., 1986). This corresponds to a ^{12}C-enrichment of 40 ‰ to 90 ‰ relative to the $\delta^{13}C$ of the substrate.

Within this range, $\delta^{13}C$ values can also distinguish between specific pathways of biogenic CH_4 production. For example, $\delta^{13}C$ values between -60 ‰ and –100 ‰ are characteristic of CH_4 derived from carbonate reduction, while values of –50 ‰ to -70 ‰ are normally associated with methyl-type fermentation processes. CH_4 oxidation is another process that can be ascertained from $\delta^{13}C$ data. Methanotrophic bacteria, like methanogens, will also favour the utilization of ^{12}C-enriched substrates due to the quicker reaction rates of ^{12}C. Thus, as a pool of CH_4 undergoes oxidation, the residual gas will become more ^{12}C-depleted.

The $\delta^{13}C$ of coexisting CO_2 can also help to elucidate methanogenic pathways. As with methane production and oxidation, consumption of CO_2 will tend to favour the reaction of ^{12}C enriched substrate, leaving behind a relatively ^{12}C-depleted pool of CO_2.

Past studies have found isotopic fractionations of 1.003-1.020 associated with this process (Templeton et al., 2006).

Thus, increasing $\delta^{13}CO_2$ values coupled with decreasing $\delta^{13}CH_4$ are indicative of an environment where CO_2-reduction is the dominant methanogenic mechanism. Furthermore, $\delta^{13}CO_2$ data used in conjunction with $\delta^{13}CH_4$ data can further clarify methanogenic pathways (Figure 1). For example, a plot of $\delta^{13}CO_2$ versus $\delta^{13}CH_4$ can reveal the processes affecting CH_4 and CO_2 by clarifying "regions" of acetoclastic/hydrogenotrophic methanogenesis, as well as methanotrophy (Whiticar *et al.*, 1986).

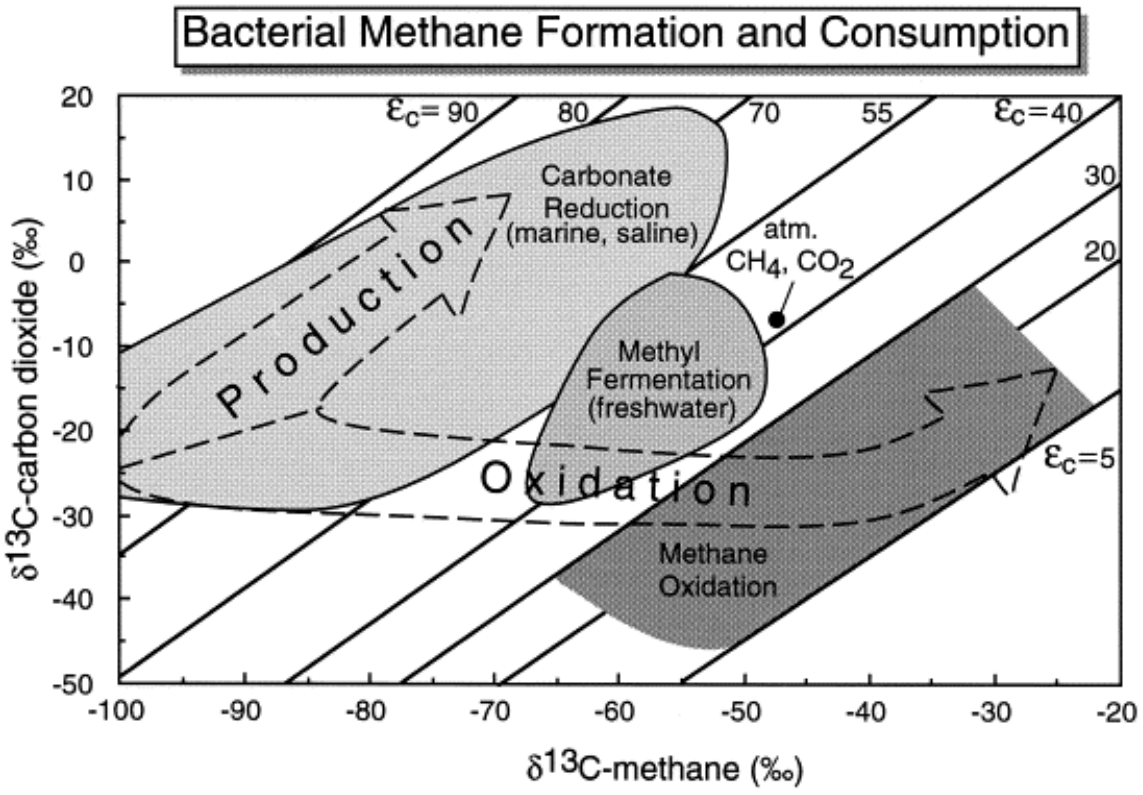

Figure 1: A plot of $\delta^{13}CO_2$ vs. $\delta^{13}CH_4$, showing regions of methane production and consumption (from Whiticar, 1999). Values of ε_c represent isotope fractionation values expressed in units of ‰ ($[\alpha - 1] \cdot 1000$).

The study of $\delta^{13}CO_2$ on its own can also provide important information on carbon cycling processes. As with bacterial uptake of carbon substrate, a discriminatory effect against ^{13}C is associated with plant uptake of CO_2. This is due to a combination of the higher diffusivity of ^{12}C as CO_2 is transported through the internal airspaces of plants, and the more favourable thermodynamics of ^{12}C incorporation into plant matter.

The result is an isotope fractionation that is around 18 ‰ for C_3 plants and 5 ‰ for C_4 plants, leading to average plant matter $\delta^{13}C$ values of –27 ‰ and –14 ‰ for C_3 and C_4 plants respectively (Amundson et al., 1998). Soil and plant respired CO_2 have $\delta^{13}C$ values largely indistinguishable from that of the parent plant, and thus bulk soil CO_2 can be assumed to have values similar to the $\delta^{13}C$ of the dominant flora in any given environment.

A distinction exists between soil CO_2 and soil-respired CO_2, the latter referring to the CO_2 residing at any given depth in the soil and the former referring to the flux of soil-derived CO_2 passing through a certain area. Cerling et al. (1991) made this observation through the use of Keeling Plot analyses of forest soil CO_2. The Keeling Plot method is a technique pioneered by Charles Keeling (1958), who found that plotting $\delta^{13}CO_2$ against $[CO_2]^{-1}$ resulted in a linear mixing line in situations where the $\delta^{13}C$ composition of CO_2 was only influenced by two endmembers.

A determination of the source $\delta^{13}CO_2$ introduced into such a system is then achieved by inspection of the y-intercept of the resultant plot, where soil-derived CO_2 is expected to be the only CO_2 source. The application of this technique by Cerling et al. (1991) reveals that soil $\delta^{13}CO_2$ is offset from known plant values by about –4.2 ‰, which is similar to the theoretical difference of -4.4‰ predicted by the difference in diffusion

coefficients of $^{13}CO_2$ and $^{12}CO_2$. Thus, Cerling et al. (1991) surmised that the more rapid diffusion of $^{12}CO_2$ versus $^{13}CO_2$ was responsible for the observed offset.

1.5 Carbon Dynamics in Forest Soils

Previous studies have shown that most forest soils consume more CH_4 than is produced, acting as net sinks for atmospheric methane (Reeburgh, 1997). CH_4 uptake estimates range from -0.04 to -8.96 $mg \cdot m^{-2} \cdot d^{-1}$, with a mean value of -1.9 $mg \cdot m^{-2} \cdot d^{-1}$ (Jang et al., 2006). The main factors influencing CH_4 uptake are soil water content and CH_4 soil diffusivities. Smaller influences include rates of microbial CH_4 uptake, soil pH, N content, and temperature (Le Mer and Roger, 2001).

Forest soils are known to be net CO_2 sources, with diffusion being the main mechanism of gas transport (Cerling et al., 1991). Within one of the sites featured in this study, a mature forest in Vancouver Island, previous work by Drewitt et al. (2002), and Jassal et al. (2004) measured efflux rates ranging from 2 to 10 $\mu mol \cdot m^{-2} \cdot s^{-1}$, with low values measured in winter and high values observed during summer months.

Soil CO_2 in these environments is derived from subsurface decay of organic matter, and moves through the soil to the surface via diffusive movement. The dominant influences on CO_2 fluxes from forest soils are soil temperature and moisture. Soil temperature has been known to affect rates of microbial activity, with CO_2 production normally increasing with higher temperatures.

The Drewitt et al. (2002) study found such correlations in DF49, where a positive correlation between CO_2 flux and soil temperature at 5 cm depth was observed over a

temperature range of 0 ^{o}C to 15 ^{o}C. Soil moisture can also affect CO_2 fluxes by decreasing the amount of air-filled pore-space through which gas can freely move, thus acting as a diffusive barrier. However, past studies have found soil temperature to be a dominant influence on soil CO_2 effluxes, with soil moisture having a smaller effect on efflux rates (Certini et al., 2003; Humphreys et al., 2006; Jassal et al., 2005).

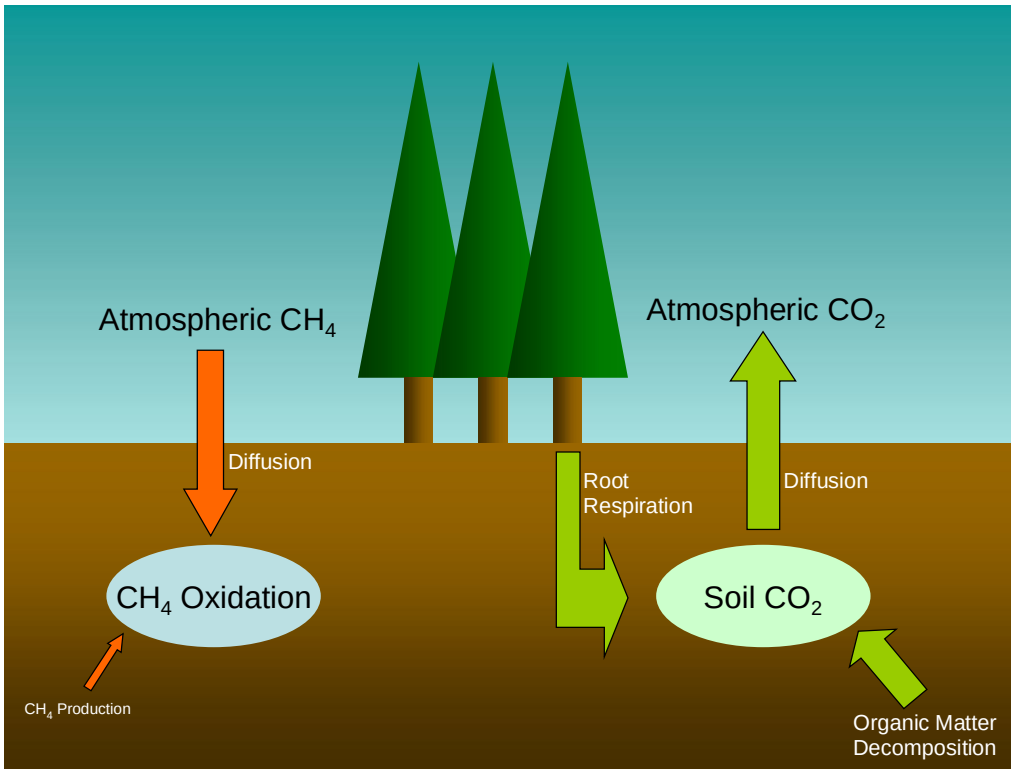

Figure 2: Simple diagrammatic summary of forest soil carbon cycling.

Isotope studies undertaken within forest soils have used the Keeling Plot method to ascertain the $\delta^{13}C$ of soil CO_2, which have been estimated at –24 ‰ to –28 ‰ for various forest environments (Cerling et al., 1991). Separate analyses of plant matter $\delta^{13}C$ show that these values are good approximations of $\delta^{13}C$ values for bulk organic matter at

a particular site, which are usually found to be representative of the dominant vegetation types within each setting.

1.6 Study Objectives

While much work has focused on CO_2 dynamics within forest environments, to the author's knowledge there are no studies that directly compare CH_4 cycling dynamics within coastal temperate forests of differing ages over a complete growing season. This project aims to assess the role of forest age on rates of soil CH_4 uptake in these environments, as well as changes in CH_4 sink characteristics brought about by major ecological disturbances.

Considering the prevalence of land-clearance for lumber harvesting and urban expansion, clarification of deforestation effects on the global CO_2 and CH_4 cycle is an additional objective of the current study. Such information would be valuable in future long-term climate change studies, given methane's importance as a strong climate forcer.

This study also has more specific aims. It provides a comparison between methods of CH_4/CO_2 flux determination that use either static chambers or soil profile data and ascertain whether, or why, these approaches provide significantly different flux estimates. As well, the isotope data will help elucidate sub-surface processes that affect both CH_4 and CO_2 cycling in these regions.

2.0 Methods

2.1 Site Description

Work was carried out as part of the Fluxnet Canada Research Network Program (*www.fluxnet-canada.ca*) at three sites on Vancouver Island (Figure 4), and one in Northern Quebec (Figure 5). Two of the Vancouver Island sites are located near the town of Campbell River, and consist of a mature forest and one that was harvested in the winter of 1999/2000 (Humphreys et al., 2006).

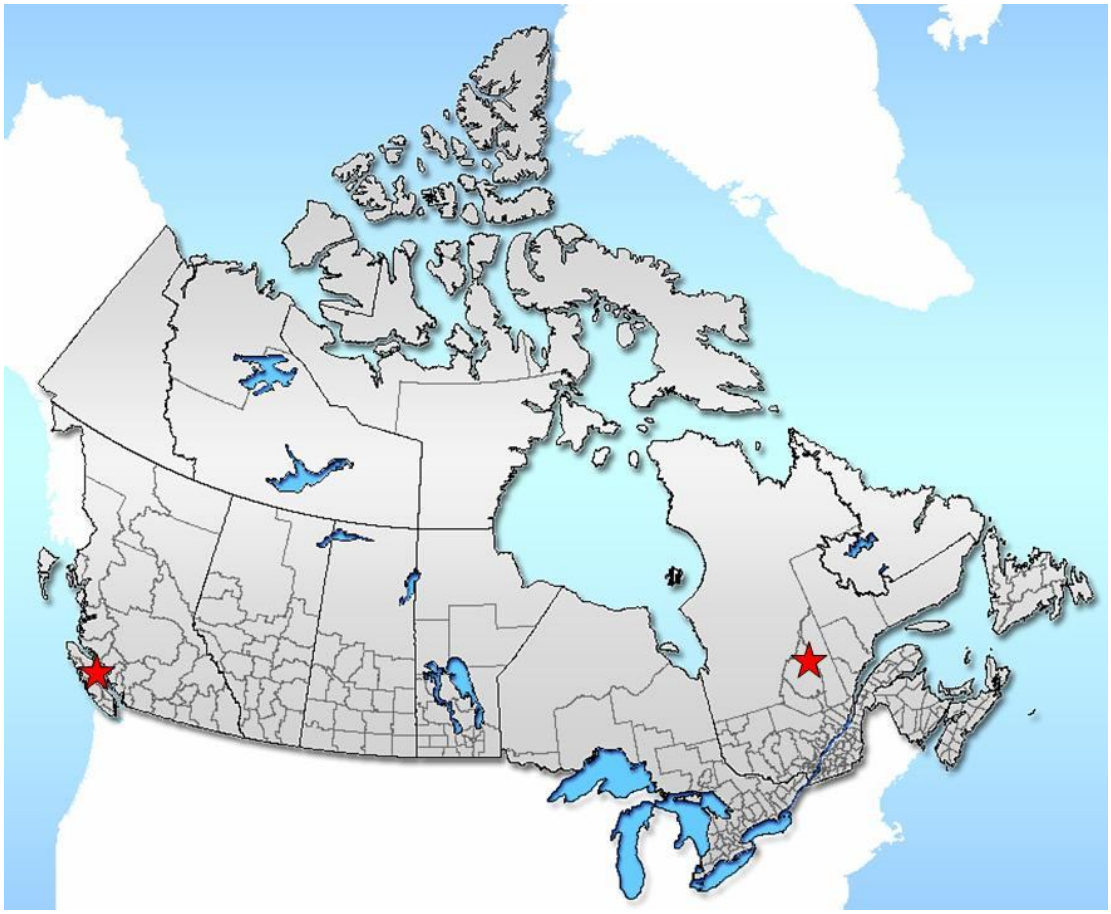

Figure 3: General overview of the BC and Quebec sites, indicated by the red stars (from http://commons.wikimedia.org).

The mature site (Douglas Fir 1949, or DF49) was subjected to a forest fire in 1949 (Jassal et al., 2005), but is now fully recovered. This site is located at an altitude of 320 m, and is dominated by Douglas fir (*Pseudotsuga menezeisii*) with some western red cedar (*Thuja plicata*) and red hemlock (*Tsuga heterophylla*) (Humphreys et al., 2006). The ground is covered by an organic layer between 1 and 10 cm thick, and the underlying soil is a humo-ferric podzol, with dense compacted till present at a depth of 1 m (Drewitt *et al*., 2002).

The clear-cut site (Harvested Douglas Fir 2000, or HDF00) located near Campbell has an elevation of 180 m. This site is devoid of significant tree cover, and smaller woody shrubs and grasses comprise most of the vegetative cover. Both DF49 and HDF00 experience an average annual temperature of 8.3 ^{o}C and mean annual precipitation of 1461 mm (see Table 5; all data from the Fluxnet-Canada database: *www.fluxnet-canada.ca*).

The third site (Harvested Douglas Fir 1988, or HDF88) is located near the town of Courtney at an elevation of 120 m, and is an area of forest that was clear-cut in 1988 (Humphreys, 2006; *www.fluxnet-canada.ca*). This makes the forest intermediate in age between the other two Vancouver Island sites, and young Douglas fir trees are the main vegetation type at this site. Present in lesser quantities are fireweed (*Epilobium angustifolium*), salal (*Gaultheria shallon*), Oregon grape (*Mahonia aquifolium*), bracken fern and huckleberry (REF). The mean annual temperature at HDF88 is 9.7 ^{o}C with an average precipitation of 1179 mm per year (Table 1) (data from the Environment Canada National Climate and Information Archive, retrieved from the online database: *http://www.climate.weatheroffice.ec.gc.ca/climateData/canada_e.html*).

Table 1: Site characteristics

Site	Province	Elevation (m)	Latitude/Longitude	Mean Annual Temperature (^{o}C)	Mean Annual Precipitation (mm)
DF49	BC	320	49°52' N, 125°20' W	8.3 °C	1461
HDF88	BC	120	49°31' N, 124°54' W	9.7 °C	1179
HDF00	BC	180	49°52' N, 125°17' W	8.3 °C	1461
OBS	QC	393	49°69' N, 74°34' W	0 °C	961.3

(Temperature and precipitation data from the Environment Canada National Climate and Information Archive; all other data from www.fluxnet-canada.ca)

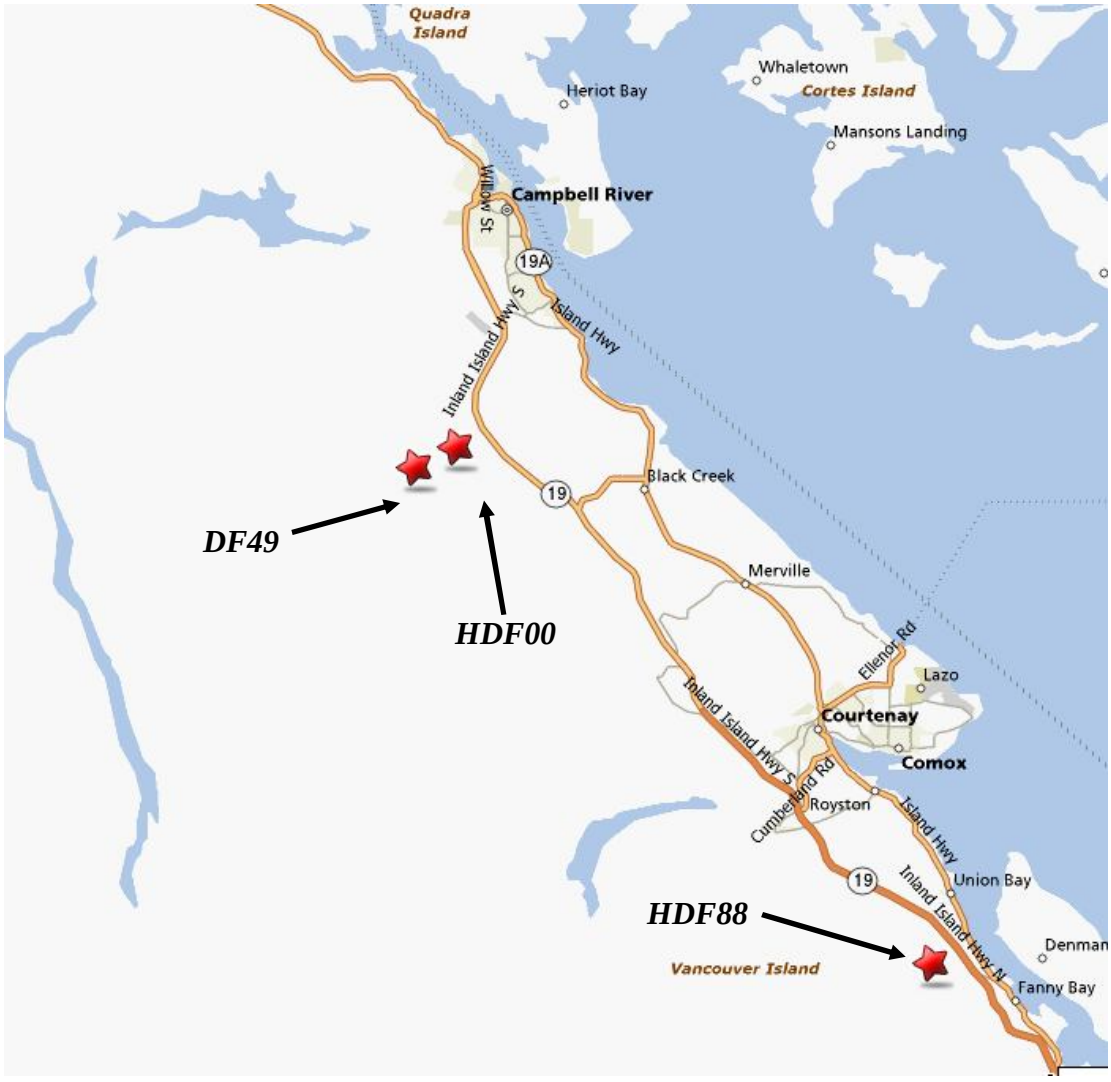

Figure 4: Map showing the three BC site locations (www.mapquest.ca).

The Chibougamau site (Old Black Spruce, or OBS) is a mature black spruce forest (*Picea mariana*), located 90 km from the town of Chibougamau. While black spruce is the dominant tree species, paper birch (*Betula papyrifera*) and balsam fir (*Abies balsamea*) are also present in lesser densities (Prévost, 1997). The undergrowth consists mainly of sheep laurel (*Kalmia angustifolia)* and moss (*Pleurozium schreberi*), and the soil type is moderately to well-drained silty sand (Prévost, 1997). At OBS, the mean annual temperature is 0^{o}C and average yearly precipitation is about 961.3 mm (Table 5) (data from the Environment Canada National Climate and Information Archive: *http://www.climate.weatheroffice.ec.gc.ca/climateData/canada_e.html*).

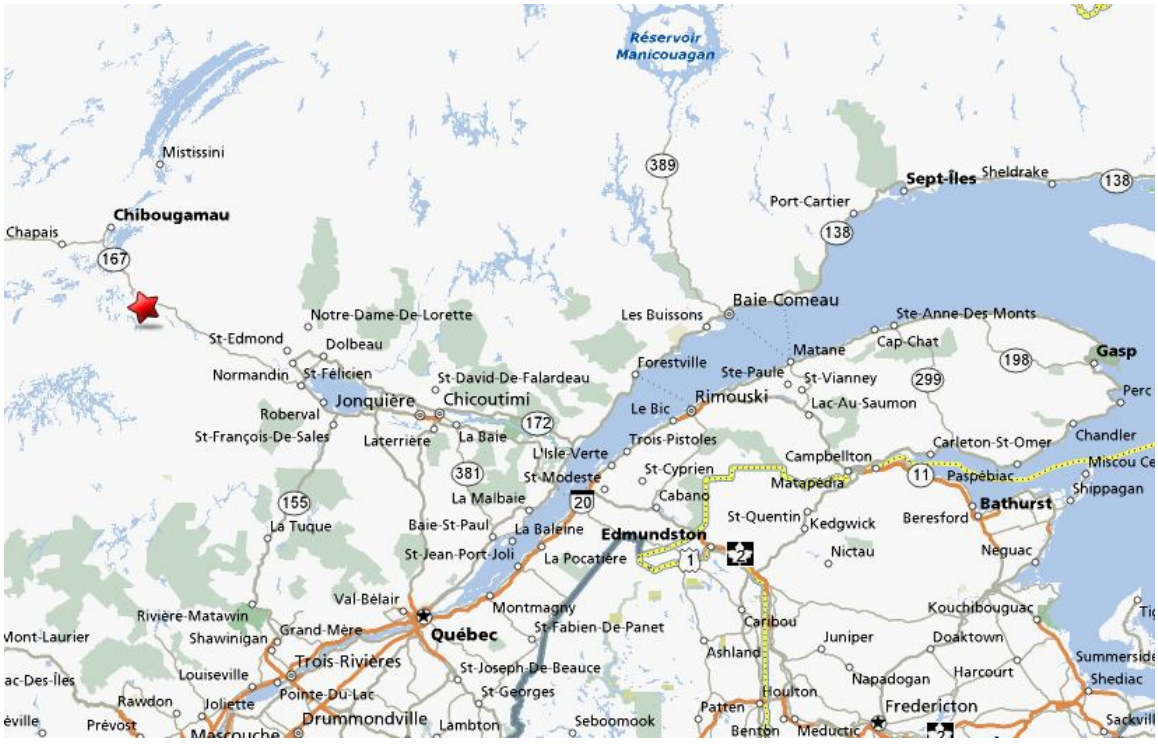

Figure 5: Map showing the OBS site in northern Quebec, marked by a red star (from www.mapquest.com).

2.2 Sampling and Collection

At all sites, soil air sampling (SAS) tubes were inserted into the soil from the surface, at depth intervals of 5, 10, 15, 20 and 30 cm. In OBS, DF49 and HDF00, SAS tubes of 80 cm length were also installed. These SAS probes (Figure 6) consist of plastic tubing capped by a plastic stopcock, surrounded by a 1/8" stainless steel tube.

At the mature forest site, six SAS tube sites were established, each containing two 5-30 cm depth profiles (Figure 8). In addition, two 80 cm probes were installed in a different location starting in August 2006. As well, two PVC static flux chambers were installed near two of the SAS tube sites (Figure7).

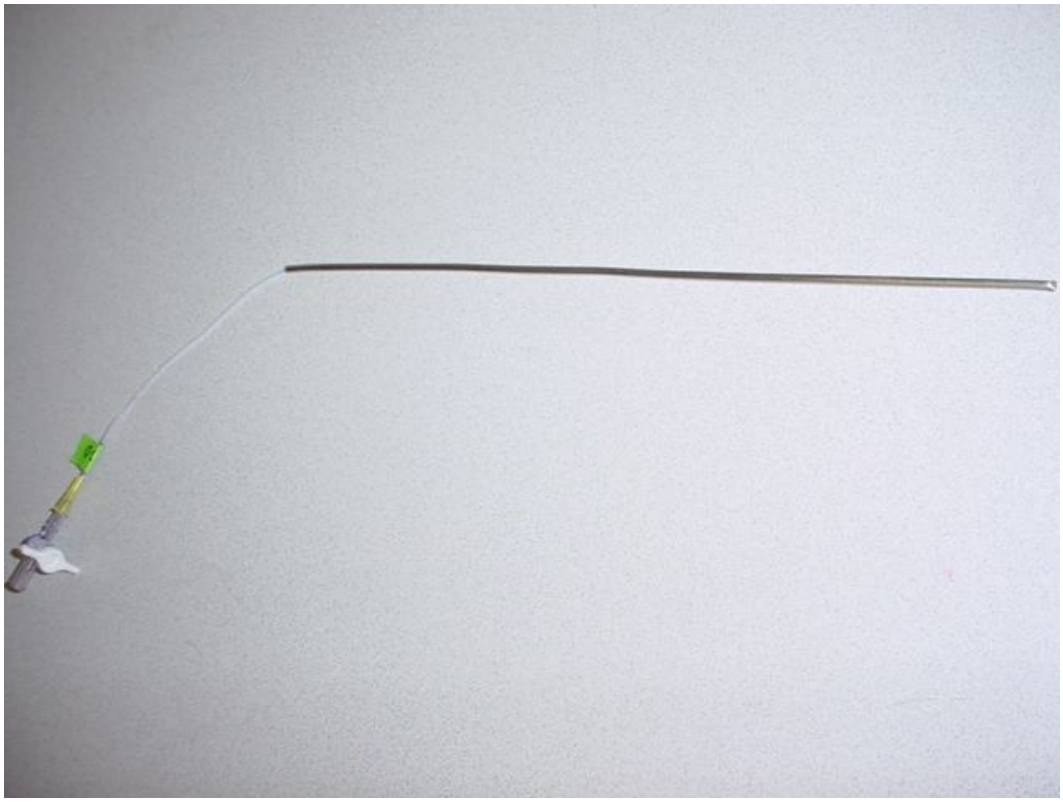

Figure 6: An example of a 30 cm SAS tube.

Three SAS tube sites were set up in HDF00, as well as two separate 80 cm SAS probes (also installed in August) and two PVC chambers. The values for one of the 80 cm SAS tubes at HDF00 was consistently similar to atmospheric values, and assumed to be the result of a compromised SAS probe. This left only one 80 cm $\delta^{13}CH_4$ measurement, which was retained in this study.

In HDF88, four SAS sites were present but no chambers or SAS tubes of 80 cm length were installed. The site layout at the Quebec forest site is similar to that in BC; three SAS tube sites are set up with two duplicate depth profiles of 5-30 cm depth, with an additional 80 cm SAS tube present at each site.

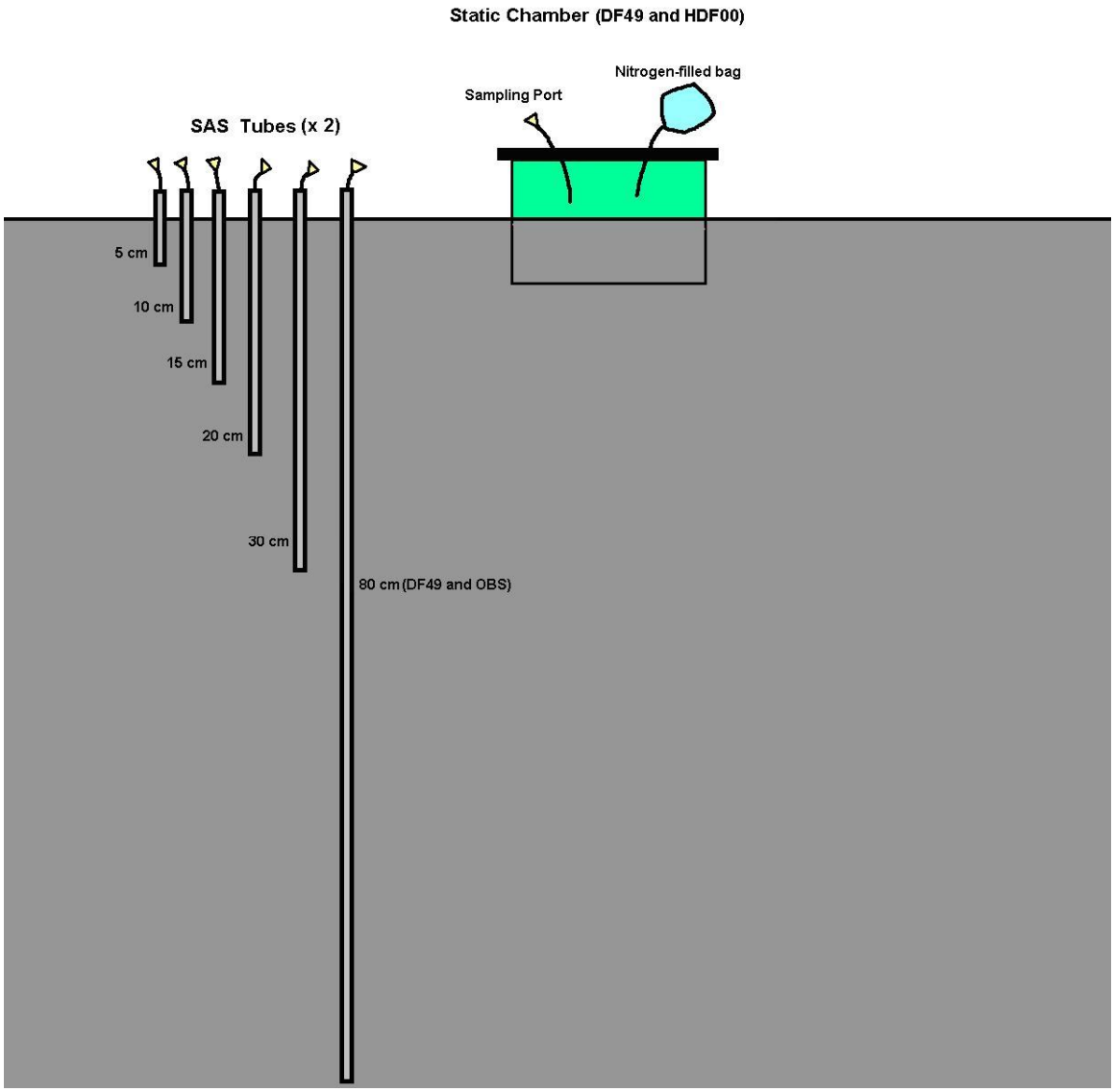

Figure 7: Generic diagram of the site set-up at all locations.

Soil gas was withdrawn from the SAS tube via a 30 ml airtight syringe and injected into 30 ml and 40 ml glass Wheaton bottles, which are capped with thin grey butyl rubber septa. For samples intended for CO_2 analyses, 15 ml of soil gas was injected directly into evacuated 20 ml Wheaton bottles capped with thick blue butyl rubber septa (Bellco Glass).

A different approach was used for CH_4 samples, whereby 20 ml of gas was injected into 30 ml Wheaton bottles filled with brine made from commercial table salt (NaCl). These bottles were capped with thinner butyl rubber septa (Chromatographic Specialties Inc.) for easier sampling, and stored inverted to prevent the contamination or escape of soil CH_4 from the bottles. The larger volume relative to the CO_2 samples was taken to compensate for the much smaller mixing ratios (<1.80 ppm) of CH_4, while the brine acted as a barrier between the stored CH_4 and the compromised rubber septa at the mouth of the Wheaton bottle.

In total (including both CO_2 and CH_4 samples), 2,544 samples were collected at the BC sites over the entire sampling period, including the months of April, May, June, July, August and November 2006, as well as January 2007. Thirty-three samples, taken during July, August and September 2005 were collected at the OBS site (see Table 2).

Before sampling of chamber gases, the static flux chambers were covered with plastic lids, with rubber O-rings placed in grooves milled into the lids. This provided an airtight seal to prevent escape of gas from the chambers. To further facilitate a secure seal, a layer of water was placed on the chamber rim prior to closure to seal any gaps between the rubber O-ring and the chamber rim.

A 1 L bag of N_2 gas was attached to the lid and opened to the chamber interior in order to offset the vacuum caused by the withdrawal of gas samples from a sealed chamber. Samples were taken from the chamber by syringe via a piece of plastic tubing capped with a stopcock. These samples were taken over the course of an hour, at intervals of 0, 5, 15, 30 and 60 minutes after chamber closure. After withdrawal, the gases were stored as mentioned above in Wheaton bottles for $\delta^{13}CO_2$ and $\delta^{13}CH_4$ measurements.

Table 2: Gas samples collected during 2005-2007

Site	Year	Date(s)	CO_2 Samples	CH_4 Samples
OBS	2005	Jun 29	33	33
		Aug 2	33	33
		Aug 30,31	33	33
DF49	2006	Apr 17,18	70	70
		May 17	70	70
		Jun 19	70	70
		Jul 19	70	70
		Aug 24	72	72
		Nov 4,5,18	72	72
	2007	Jan 17-21	72	72
HDF88	2006	Apr 17,18	60	60
		May 17	60	60
		Jun 19	60	60
		Jul 19	60	60
		Aug 24	60	60
		Nov 4,5,18	60	60
	2007	Jan 17-21	60	60
HDF00	2006	Apr 17,18	50	50
		May 17	50	50
		Jun 19	50	50
		Jul 19	50	50
		Aug 24	52	52
		Nov 4,5,18	52	52
	2007	Jan 17-21	52	52

2.3 $\delta^{13}CH_4$ and $[CH_4]$ Analyses

Methane measurements are made on a Finnigan-MAT 252 continuous flow GC-IRMS (Figure 8). After first passing through a –50 ^{o}C ethane water trap, the soil gas is flushed through a HaySep trap with a temperature of –125 ^{o}C. This traps and concentrates methane, while allowing most N_2 and O_2 to pass through. The trap is then warmed and the sample gas is released onto a second trapping stage which consists of a section of blank capillary tubing immersed in liquid N_2 that traps CO_2 present in the soil gas, while a portion of GSQ column is used in a similar manner to trap CH_4.

Only the CH_4 is then released after a few minutes, which passes through a GSQ column in order to separate the methane from other constituents. After this stage, the CH_4 is combusted into CO_2 with O_2, via a Ni-Pt catalyst at temperatures of 1080^{o}C. The gas is then re-trapped onto a section of blank capillary before being released onto a second GSQ column used to separate the combusted CH_4 (in CO_2 form) from any remaining compounds. Lastly, the CO_2 is injected into the mass spectrometer, where it is analyzed for m/z (mass-to-charge ratio) 44, 45 and 46. Concentration measurements are obtained by analyzing the area of the m/z 44 peak.

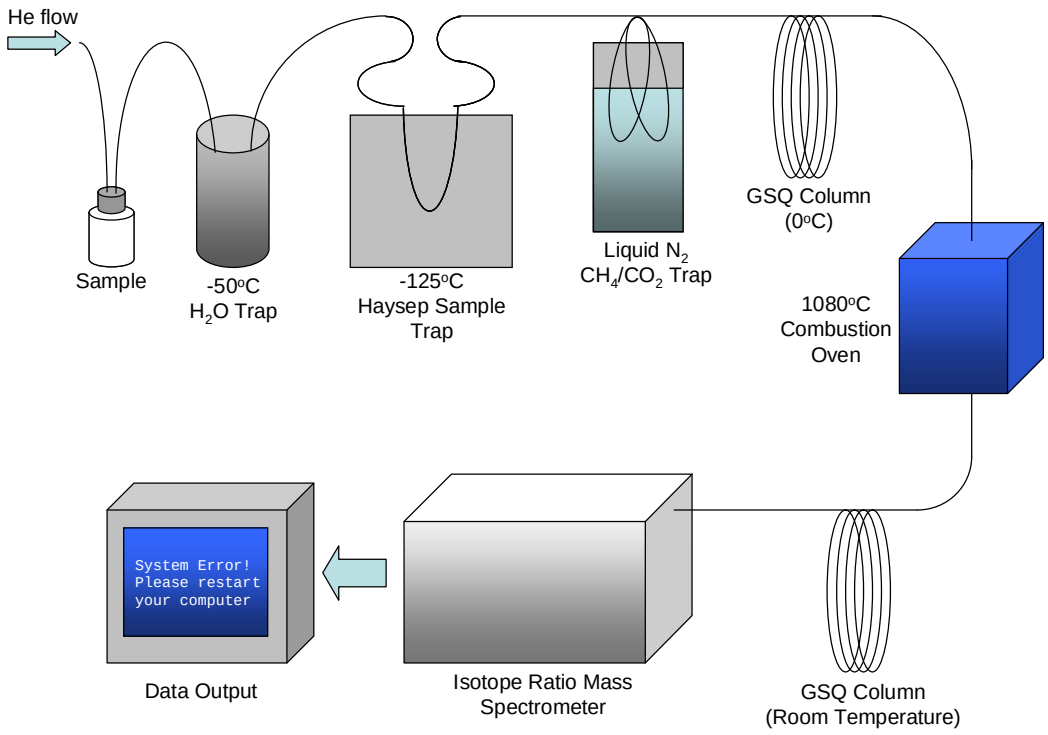

Figure 8: GC-IRMS scheme for CH_4 analysis.

Outdoor air is used as the laboratory standard against which carbon isotope ratios and concentration measurements are calibrated. The laboratory standard is taken to have a $\delta^{13}CH_4$ value of -47.7 ‰ and a mixing ratio of 1.8 ppm based on northern hemisphere literature values (Gupta et al., 1996; Quay, 1999; Stevens, 1988; Sugawara et al., 1996). Subsequent data plots in this study will also use these numbers as reference ambient values, for comparison purposes. In addition, an artificial air standard holding values of –48.3‰ and 1.8 ppm was used for calibration of the OBS samples.

Standard deviations in both $\delta^{13}CH_4$ and $[CH_4]$ are calculated for samples within the same depth, site and sampling month via the Equation:

$$s = \sqrt{\frac{\sum_{i=1}^{i=N} (x_i - \bar{x})^2}{N}} \qquad (2.3.1)$$

Where x_i represents a single measurement, $\bar{x}$ is the mean for a set of measurements, and N is the number of measurements. Analysis of outdoor air over the period of analysis (see Table 3 for details) yielded standard deviations (1σ) of ± 0.23 ‰ for $\delta^{13}C$ and ± 0.23 ppm (N = 213), while the artificial air showed values of ± 0.23 ‰ and ± 0.27 ppm (N = 40).

Table 3: CH_4 analysis dates

Site	Sampling Year	Sampling Month	Analysis Start Date	Analysis End Date
OBS	2005	Late June	8-Mar-06	12-Mar-06
		Early August	12-Mar-06	15-Mar-06
		Late August	15-Mar-06	18-Mar-06
DF49	2006	April	30-Apr-07	4-May-07
		May	10-May-07	15-May-07
		June	22-May-07	25-May-07
		July	3-Jul-07	26-Nov-07*
		August	11-Jun-07	13-Jun-07
		November	21-Jun-07	25-Jun-07
	2007	January	28-Oct-07	29-Oct-07
HDF88	2006	April	4-May-07	9-May-07
		May	18-May-07	21-May-07
		June	2-Jul-07	19-Aug-07**
		July	18-Aug-07	20-Aug-07
		August	20-Aug-07	22-Aug-07
		November	23-Aug-07	24-Aug-07
	2007	January		
HDF00	2006	April	9-May-07	10-May-07
		May	16-May-07	18-May-07
		June	27-May-07	5-Jun-07
		July	7-Jun-07	9-Jun-07
		August	14-Jun-07	19-Jun-07
		November	25-Jun-07	27-Jun-07
	2007	January		

*Samples run on two separate periods: June 3-6, and November 25-26
**Samples run on July 2, and August 17-19

Running known dilutions of outdoor air in Helium gas, ranging from atmospheric to 0.6 ppm CH_4 tested the assumption of a linear relationship between peak area and concentration. Data retrieved over the course of several months was shown to give a good linear fit ($R^2 = 0.91$), and calibration curves made from samples ran during the same day gave an even stronger relationship. Thus, a single point representing ambient CH_4 was deemed sufficient for calibration purposes (Figure 9).

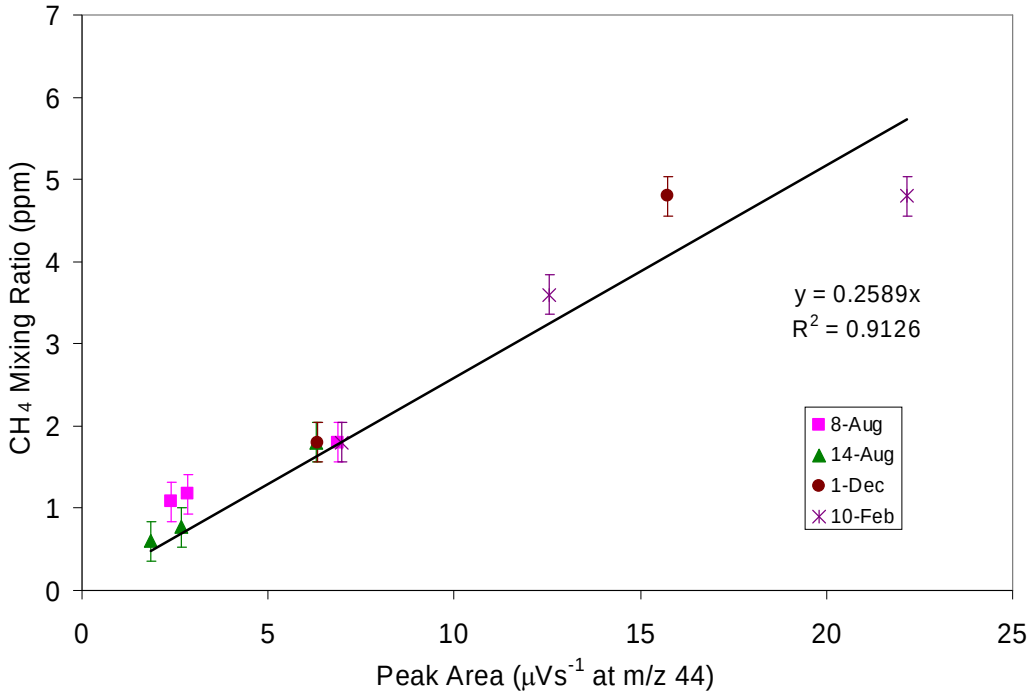

Figure 9: Calibration curve for [CH_4], made from outdoor air dilutions in helium. Data retrieved from calibration curves constructed at various months, with error bars representing 1σ.

2.4 $\delta^{13}CO_2$ and $[CO_2]$ Analyses

The $\delta^{13}CO_2$ samples are analyzed both on a Finnigan-MAT 252, as well as a Delta XL Plus GC-IRMS. With both machines, the gas is injected directly into a section of capillary leading to the GSQ column. After passing through the column, the gas is sent to the mass spectrometer, where it is analyzed for m/z 44, 45, and 46. The samples are measured against an in-house gas standard with a $\delta^{13}CO_2$ of -49.44 ‰ against V-PDB. Over the entire analysis period (see Table 4), a $\delta^{13}CO_2$ standard deviation (SD) of ± 0.11 ‰ was achieved on the Delta XL Plus (N = 64), while a SD of ± 0.16 ‰ was obtained from analyses performed with the MAT 252 (N = 36). With $[CO_2]$, standard deviations of ± 124 and ± 115 ppm were obtained on the Delta XL Plus and the MAT 252, respectively (1σ).

Table 4: CO_2 analysis dates

Site	Sampling Year	Sampling Month	Analysis Start Date	Analysis End Date
OBS	2005	Late June	22-Sep-06	27-Sep-06
		Early August	27-Sep-06	28-Sep-06
		Late August	29-Sep-06	30-Sep-06
DF49	2006	April	11-May-06	19-May-06
		May	12-Jul-06	14-Jul-06
		June	21-Jul-06	24-Jul-06
		July	26-Jul-06	28-Jul-06
		August	24-Oct-07	25-Oct-07
		November	26-Oct-07	27-Oct-07
	2007	January	28-Oct-07	29-Oct-07
HDF88	2006	April	7-Jul-06	12-Jul-06
		May	17-Jul-06	20-Jul-06
		June	24-Jul-06	25-Jul-06
		July	28-Jul-06	31-Jul-06
		August	26-Oct-07	26-Oct-07
		November	28-Oct-07	28-Oct-07
	2007	January	22-Nov-07	23-Nov-07
HDF00	2006	April	4-May-06	11-May-06
		May	20-Jul-06	21-Jul-06
		June	25-Jul-06	24-Oct-07*
		July	31-Jul-06	1-Aug-06
		August	25-Oct-07	26-Oct-07
		November	27-Oct-07	28-Oct-07
	2007	January	29-Oct-07	22-Nov-07

*Bulk of samples analyzed on July 25-26, with the remainder completed on October 24

Various concentrations of CO_2/He mixtures were made to confirm a linear relationship between [CO_2] and peak area, as well as to test the sensitivity of the machine to differing amounts of CO_2. Data retrieved over the course of the sampling period gave good linear fits, and a single data point was deemed sufficient for calibration purposes (Figure 10). All values are reported against the V-PDB standard.

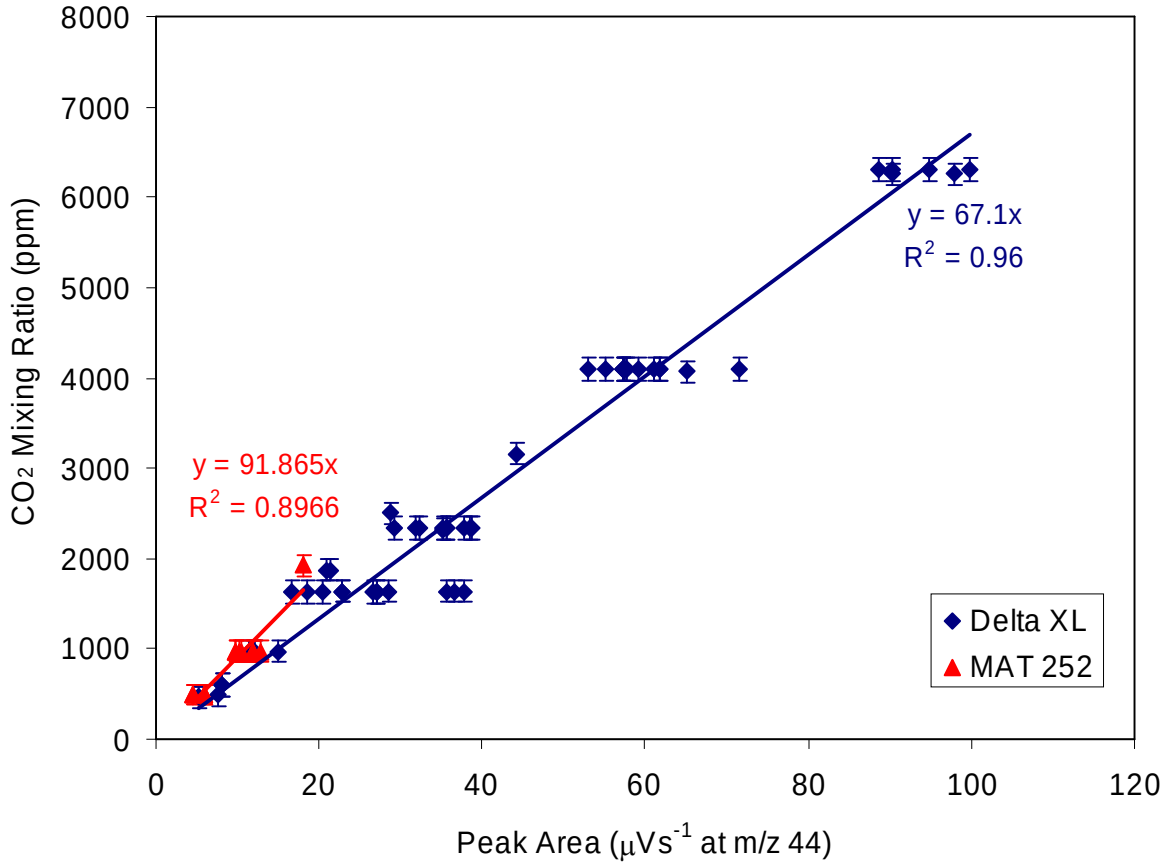

Figure 10: CO_2 calibration curves constructed with MAT 252 and Delta XL data retrieved over the entire sampling period, using various CO_2/He dilutions. Error bars represent analytical 1σ.

For comparison purposes, all $\delta^{13}CO_2$ and [CO_2] results are compared to averaged annual ambient values, based on observations of near ground (2 m and 0.5 m height) CO_2 during 2005 at DF49 (used for all BC sites; see Table A25 in appendix) and OBS (both OBS and DF49 data is available from the Fluxnet Canada database, courtesy L. Flanagan; see Table A24 in appendix). From this data, a yearly average ambient $\delta^{13}CO_2$ of –10 ‰ and [CO_2] of 417 ppm was obtained from DF49, and average values of –10 ‰ and 433

ppm from the OBS data. This data is included in all plots that include "ambient CO_2" values for reference purposes, in the subsequent sections of this study.

During the months of November and January, many CO_2 measurements matched ambient values, even when retrieved from 80 cm depth within the soil column. These were assumed to be the result of compromised samples, likely due to defective rubber septa. Given the consistency of these anomalous values (424 ± 40 ppm and –10.9 ± 0.6 ‰), they were excluded from the depth plots and subsequent calculations, and only measurements that showed values outside of the standard deviation range of the suspect measurements were used.

2.5 Flux Estimates

Both the static chamber measurements and the soil concentration profiles are used to estimate CH_4 and CO_2 fluxes within the BC and Quebec sites. The depth profiles were used to compute fluxes based on Fick's First Law of Diffusion, following the formula:

$$J = -D_s \frac{\delta C}{\delta z} \qquad (2.5.1)$$

Where J = gas flux ($\mu mol \cdot m^{-2} \cdot s^{-1}$ and $mg \cdot m^{-2} \cdot d^{-1}$ for CO_2 and CH_4, respectively), D_s = apparent soil gas diffusion coefficient ($m^2 \cdot s^{-1}$), and $\delta C/\delta z$ = change in concentration with depth ($\mu mol \cdot m^{-1}$ and $mg \cdot m^{-1}$for CO_2 and CH_4, respectively).

As the concentration data is initially in units of ppm, a conversion factor is required. Raw concentration data is multiplied by $P/(10^6 \cdot RT)$ to convert into units of $mol \cdot m^{-3}$, where P is ambient air pressure in Pa (data obtained from the Fluxnet-Canada

database), T is air temperature in Kelvin, and R is the universal gas constant in units of $m^3 \cdot Pa \cdot K^{-1} \cdot mol^{-1}$. For CH_4, the mixing ratio data must also be multiplied by the molecular weight of the gas (16.04 $g \cdot mol^{-1}$) and scaled by 10^3 to obtain units of $mg \cdot m^{-3}$.

Equation 2.5.1 assumes a steady state system, whereby either the amount of CO_2 produced and emitted by soil, or the quantity of CH_4 supplied and consumed by soil remains constant with time. This is a reasonable assumption for the sites of study, as the supply of CO_2 (soil respired) or CH_4 (atmospheric) into the soil system and the rates of CO_2/CH_4 production/uptake can be taken as constant over the time period of sampling (2-4 hours). D_s is calculated from the formula:

$$D_s = D_m \varepsilon \tau \qquad (2.5.2)$$

where D_m = free air gas diffusivity, ε = soil air-filled porosity, and τ = tortuosity, accounting for the non-linear movement of gas through the soil. The quantity $\varepsilon\tau$ can be defined as a "tortuosity factor" ξ, which is related to ε via the Equation $\xi = n\varepsilon^m$, where n and m are empirically determined constants (Currie, 1965).

Jassal *et al*. (2005) found that diffusivity measurements at DF49 were best described by:

$$\xi = 1.18\varepsilon^{2.27} \qquad (2.5.3)$$

Jassal et al. made a comparison between Equation 3 and previously proposed models by Penman (1940), Marshall (1959), Millington-Quirk (1961) and Moldrup et al. (1999). It was found that within the DF49 site, Equation 3 was the only formulation that gave

diffusivities in good agreement with observations, at all ranges of ε. While all other models gave good agreement at high ε values, the Penman and Marshal models were found to overestimate diffusivities at low ε, while the Millington-Quirk (1961) and Moldrup *et al.* (1999) models tended to underestimate diffusivities (Figure 11). Total soil air-filled porosity (ε) values used in Equation 2.5.3 were 0.49 and 0.56 for DF49 and OBS respectively, based on observations from past studies (Drewitt et al., 2002; Prévost, 2004). The DF49 value of 0.49 was also used for HDF88 and HDF00, given the similar soil properties and environmental characteristics present at all BC sites (Humphreys et al., 2006).

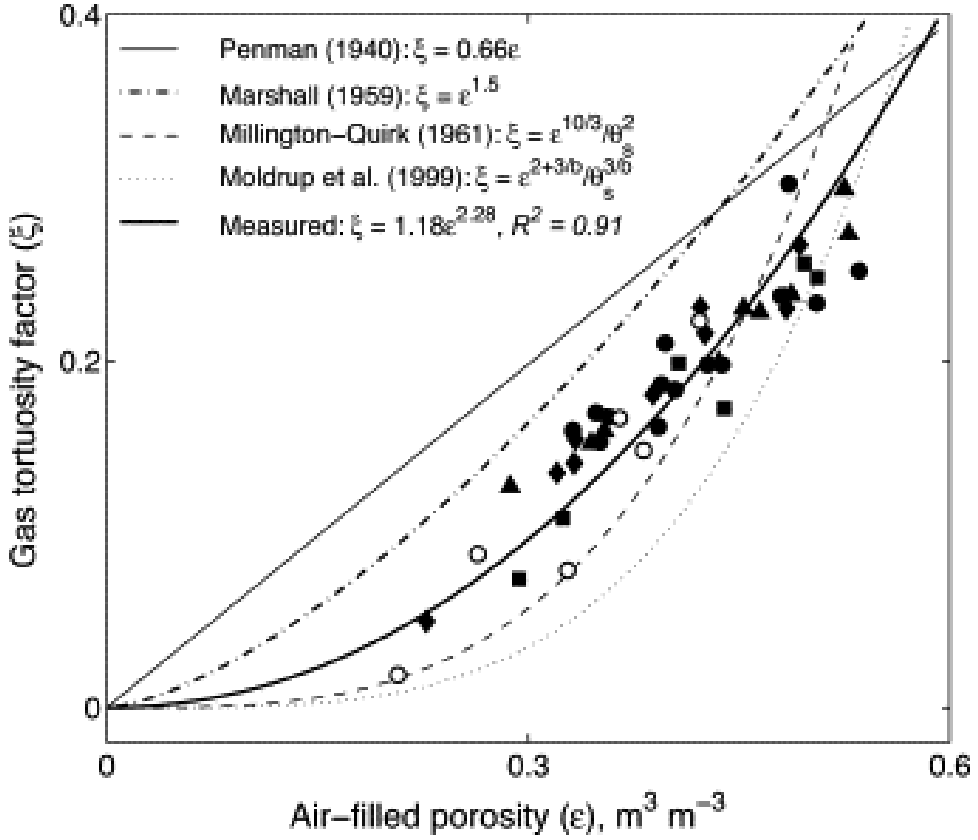

Figure 11: Comparison of Equation 3 against other diffusivity models, using DF49 data (Jassal et al., 2005).

Table 5: Soil Temperature and moisture data for all sites (see Tables A16-18 in appendix for more detailed soil moisture data)

Site	Year	Month	Time of Sampling	Averaged Soil Moisture to 30 cm depth (%/100 Vol)	Averaged Soil Temperature at 5 cm depth (°C)
DF49	2006	April	13:00-16:00	0.2599	3.35
		May	14:30-17:00	0.2072	9.94
		June	12:00-16:00	0.2259	10.46
		July	12:00-15:00	0.1250	12.72
		August	11:45-15:30	0.0710	13.55
		November	12:18-16:00	0.2302	6.50
	2007	January	9:30-13:00	0.2361	0.91
HDF88	2006	April	16:00-18:00	0.3233	5.35
		May	11:00-13:00	0.1453	10.64
		June	20:00-23:00	0.1253	11.11
		July	20:00-23:00	0.0921	12.90
		August	19:00-22:30	0.0661	13.19
		November	11:00-13:00	0.1906	6.46
	2007	January	11:00-14:00	0.2821	1.69
HDF00	2006	April	17:00-19:00	0.1993	5.22
		May	18:30-20:30	0.1436	16.05
		June	16:44-19:00	0.1701	14.51
		July	15:40-19:00	0.0702	16.35
		August	16:00-18:00	0.0491	18.34
		November	17:30-19:30	0.2105	6.18
	2007	January	16:00-19:00	0.1997	-1.88
OBS	2005	Late June	9:00-12:00	0.1560	14.00
		Early August	9:00-12:00	0.1783	12.70
		Late August	9:30-12:00	0.1527	13.30

Soils from all sites are podzols and have similar textures of loamy or silty sand at the BC sites and OBS respectively (Humphreys, 2006; Prévost, 2004). Therefore, Equation 3 was also used for HDF00, HDF88 and OBS, in addition to DF49. Soil moisture and temperature data available in the online Fluxnet-Canada data portal was used to calculate D_s for all sites (Table 5). Ambient [CO_2] data was retrieved from the Fluxnet-Canada database for the appropriate months, times and height above the soil

surface: 2 m above ground surface for DF49 and HDF88, and 0.5 m for HDF00 and OBS (Table 6).

Table 6: Near-Ground CO_2 Mixing Ratios (ppm)

Year	Month	DF49 (2m)	HDF88 (2m)	HDF00 (0.5 m)	OBS (0.5 m)
2005	Late June	N/A	N/A	N/A	391.47
	Early August	N/A	N/A	N/A	401.17
	Late August	N/A	N/A	N/A	518.94*
2006	April	400.64*	380.50	374.12*	N/A
	May	436.05	446.38	363.72	N/A
	June	413.67	348.07	364.38	N/A
	July	459.87	368.09	375.44	N/A
	August	389.16	351.36	377.08	N/A
	November	399.53*	395.90	396.83*	N/A
2007	January	404.67*	383.76	379.58*	N/A

*Samples taken over two days: values represent averaged [CO_2] over the period of sampling.

This value was then used as a near-surface [CO_2] value for the calculation of Fickian fluxes, which are calculated as the CO_2 flux between ambient air, and soil air at a depth of 5 cm. CH_4 fluxes were calculated in the same fashion, except that a northern hemispheric value of 1.80 ppm was used for all sites. Although global [CH_4] undergoes some seasonal variation, these changes (~0.05 ppm, from Quay, 1999) are smaller than those observed with ambient [CO_2] and are within the analytical standard deviation range observed in the laboratory. Thus, the general global [CH_4] value was deemed adequate for the purposes of flux calculations using Fick's law.

Changes in chamber concentration were fit best by an exponential curve of the form:

$$C(t) = Ae^{-kt} + C_d \qquad (2.5.4)$$

Where *A* is an integral constant, subscript *d* is a depth of constant [CH_4], and $k = D_s/hd$ (h = headspace height of chamber) (Nakano et al, 2004). The chamber flux is described by a modification of Fick's First Law:

$$F(t) = D\frac{C_d - C(0)}{d} \qquad (2.5.5)$$

From this Equation, the flux at t=0 (*F(0)*) can be calculated using *C(0)*, and values of *d* are obtained from the fitted curves.

Initial [CH_4] values occasionally appeared anomalous and out of line with subsequent values, possibly due to initial disturbances related to chamber closure. Some of the anomalous [CH_4] values were as much as 8 ppm lower than expected ambient values, which were often followed by an increase in the subsequent measurement then a decrease in all remaining samples. In this case, samples that were in excess of 0.3 ppm lower (i.e., greater than analytical error) than the following data point were discarded, and a sample from the next interval was used as an initial value.

The anomalous initial values are assumed to be a result of chamber pressurization effects, immediately following chamber closure. This has been observed in previous studies, in which a degree of "noise" was present in CO_2 concentrations measured immediately following chamber placement (Davidson et al., 2002). While all t=0 values for CO_2 appeared in line with subsequent measurements, it may be that the much large concentrations of CO_2 present at the soil surface are less sensitive to chamber pressurization effects than CH_4 or that a finer time resolution (>5 min) may be needed to record these initial disturbances.

While global atmospheric values (1.8 ppm) could also have been used in lieu of the t = 0 samples, the variability of the initial measurements indicated that the broad application of this value to all chambers would be less appropriate. Gas fluxes are in units of $\mu mol \cdot m^{-2} \cdot s^{-1}$ for CO_2, and $mg \cdot m^{-2} \cdot d^{-1}$ for CH_4.

3.0 Results

3.1 $\delta^{13}CH_4$ and $[CH_4]$ Trends

3.1.1 $\delta^{13}CH_4$ and $[CH_4]$ in OBS (Quebec Fluxnet Site)

The OBS soils show a general trend of increasing ^{12}C-depletion in $\delta^{13}CH_4$ and decreasing $[CH_4]$ with increasing soil depth. The $\delta^{13}CH_4$ values range from -48.5‰ to -40.8 ‰, and $[CH_4]$ has a range of 0.4 to 1.4 ppm (Figure 12). These trends are more apparent with the inclusion of the 80 cm SAS data, which show the most ^{12}C-depleted $\delta^{13}CH_4$ and lowest $[CH_4]$ in the entire soil profile.

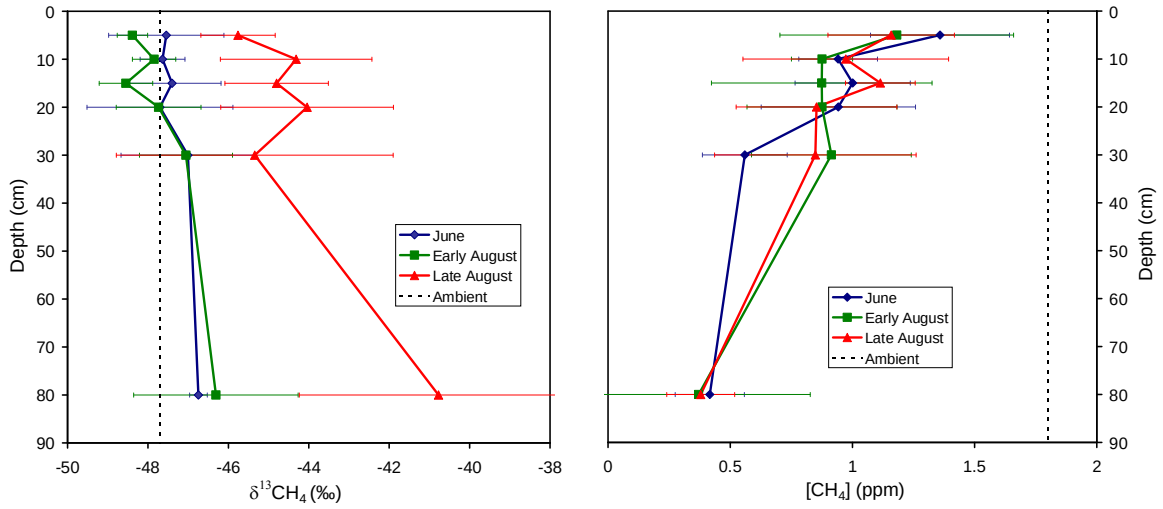

Figure 12: $[CH_4]$ and $\delta^{13}CH_4$ depth profiles at OBS. Error bars indicate standard deviation of sampling (1σ).

Within the upper 30 cm of soil, trends are less clear due to data scatter but $\delta^{13}CH_4$ values remain more ^{12}C-depleted, and $[CH_4]$ lower than ambient values. Some temporal trends are present in $\delta^{13}CH_4$, whereby a maximum value is displayed in late August, with all depths either decreasing or remaining constant during the preceding months. During late August, $\delta^{13}CH_4$ values in all depths are ^{12}C-depleted relative to global atmospheric values by 2 ‰ to 7 ‰. By comparison, the most ^{12}C-depleted value in all previous months and depths was 1.4 ‰ higher than ambient values. This was found during early August at a depth of 80 cm.

Concentration trends are less consistent, but a pattern of decreasing concentration from June to August is observed in many depths (Figure 13). Spatial variation is large for both $\delta^{13}CH_4$ and $[CH_4]$ data: standard deviation values range from ± 0.13 ppm to ± 0.5 ppm for $[CH_4]$, while $\delta^{13}CH_4$ shows a range of ± 0.4 ‰ to ± 3.5 ‰.

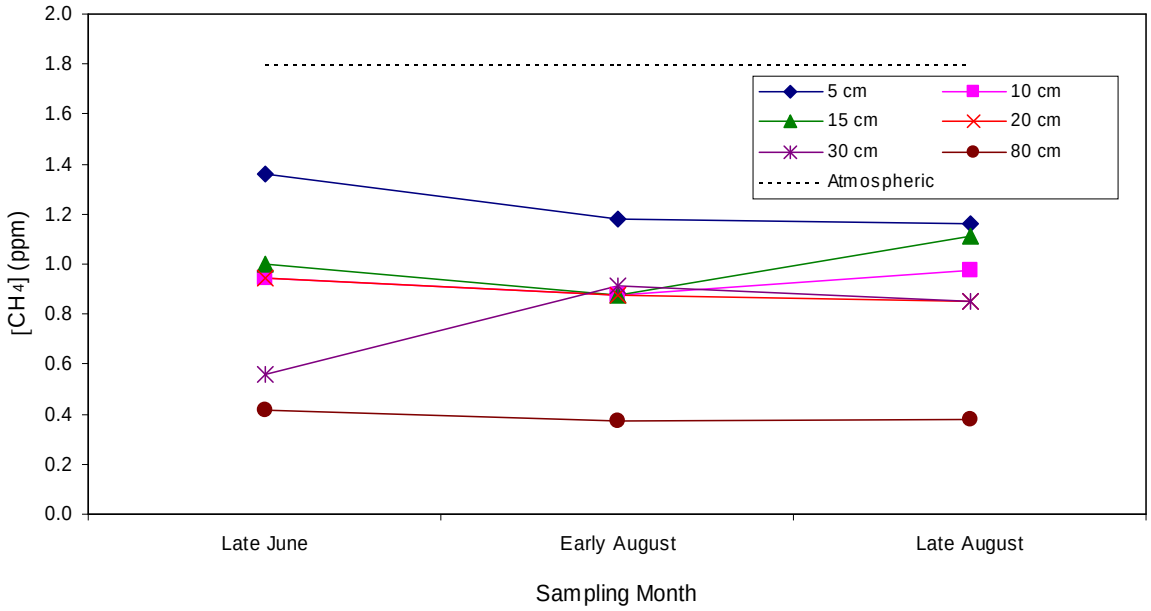

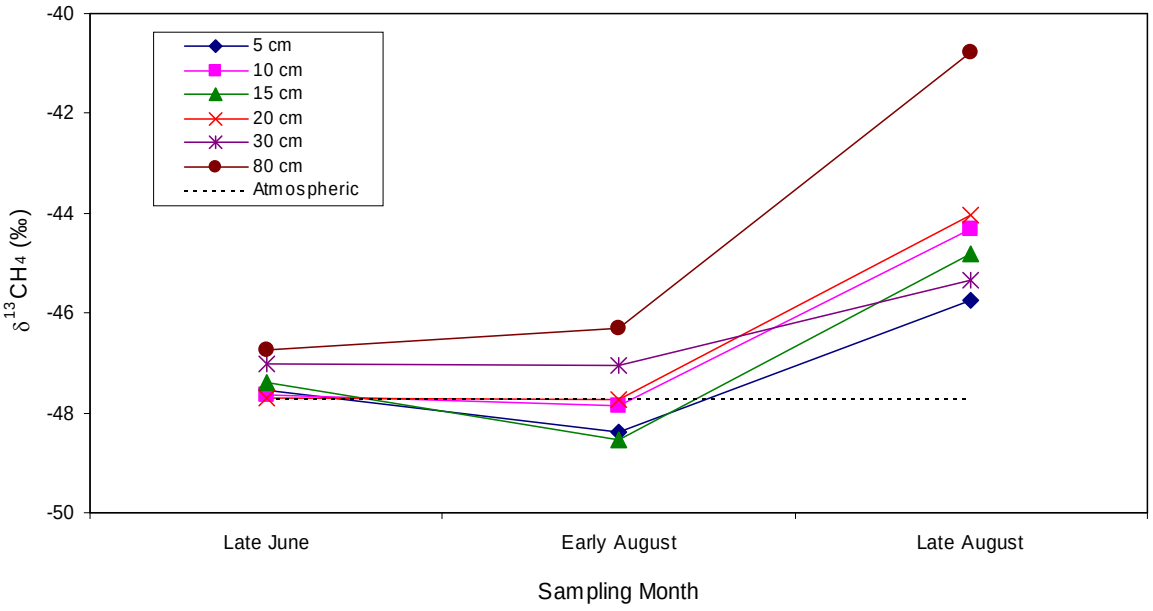

Figure 13: Monthly [CH_4] and $\delta^{13}CH_4$ plots for OBS.

3.1.2 $\delta^{13}CH_4$ and $[CH_4]$ in Vancouver Island, BC

The $[CH_4]$ depth profile trends within the BC sites are less well defined than those in OBS and there are no distinct depth-based trends during April to July 2006 (Figure 14). One feature at HDF88, however, seems consistent across all months of sampling except January 2007: a concentration minimum is present at 15 to 20 cm depth (0.8 to 1 ppm lower than $[CH_4]$ at 5 cm) from April 2006 until January 2007, during which the lowest $[CH_4]$ is instead found at 30 cm depth (Figure 15).

During all months and in most depths, $[CH_4]$ is low relative to the ambient value of 1.8 ppm. Soil $[CH_4]$ shows a range of 0.5 ppm to 1.7 ppm in DF49, 0.8 ppm to 1.9 ppm in HDF88, and 0.3 ppm to 1.8 ppm in HDF00, within the upper 30 cm of soil. The 80 cm probes show lower $[CH_4]$ values of 0.4 to 0.8 ppm from August 2006 to January 2007. As with OBS, spatial variation is significant even within the same depths at the same sites. Site DF49 shows standard deviations ranging from ± 0.04 ppm to ± 0.70 ppm, while HDF88 displays a range of ± 0.04 ppm to ± 0.95 ppm and HDF00 values range from ± 0.05 ppm to ± 0.76 ppm.

Seasonal $[CH_4]$ trends, if present, are only weakly expressed. A decrease in concentration from April to August is present in all sites, although the scatter of the data points makes it hard to determine whether this is a genuine feature (Figure 17). Within DF49 there is an abrupt increase in concentration during January, which is not seen in HDF00 or HDF88. In general, with the exception of the January maximum seen in DF49, CH_4 concentrations are consistent throughout the year.

The $\delta^{13}CH_4$ depth trends in the BC sites show more variability than [CH_4], with each depth within the same site showing large standard deviation (1σ) values (± 0.7 ‰ to ± 5 ‰ in DF49, ± 0.8 ‰ to ± 3.4 ‰ in HDF88, and ± 0.1 ‰ to ± 4.6 ‰ in HDF00). A $\delta^{13}CH_4$ range of –50 ‰ to –38 ‰ is present in DF49, -49 ‰ to –43 ‰ in HDF88 and –44 ‰ to –50 ‰ in HDF00 (Figure 15).

In general, values are ^{12}C-depleted as compared to global atmospheric CH_4 although deviations exist. Within HDF00, $\delta^{13}CH_4$ values that are ^{12}C-enriched relative to atmospheric CH_4 by 0.7 ‰ to 1.5 ‰ are apparent in the 15-20 cm depth range during the months of April and June (Figure 16). ^{12}C-enriched $\delta^{13}CH_4$ relative to atmospheric values are also seen in DF49 within the 15-20 cm depth range during April and June (0.3 ‰ to 2.5 ‰ more enriched), and from 5 to 30 cm depth in August (0.8 ‰ to 1.8 ‰ more enriched).

Within DF49, the 80 cm SAS tubes show more ^{12}C-depleted values below 30 cm as compared to shallower horizons, displaying a range of –46 ‰ to –38 ‰. Site HDF00 differs in showing 80 cm $\delta^{13}CH_4$ similar to, or more ^{13}C-depleted than atmospheric values, with values spanning –47.4 ‰ to –49.6 ‰.

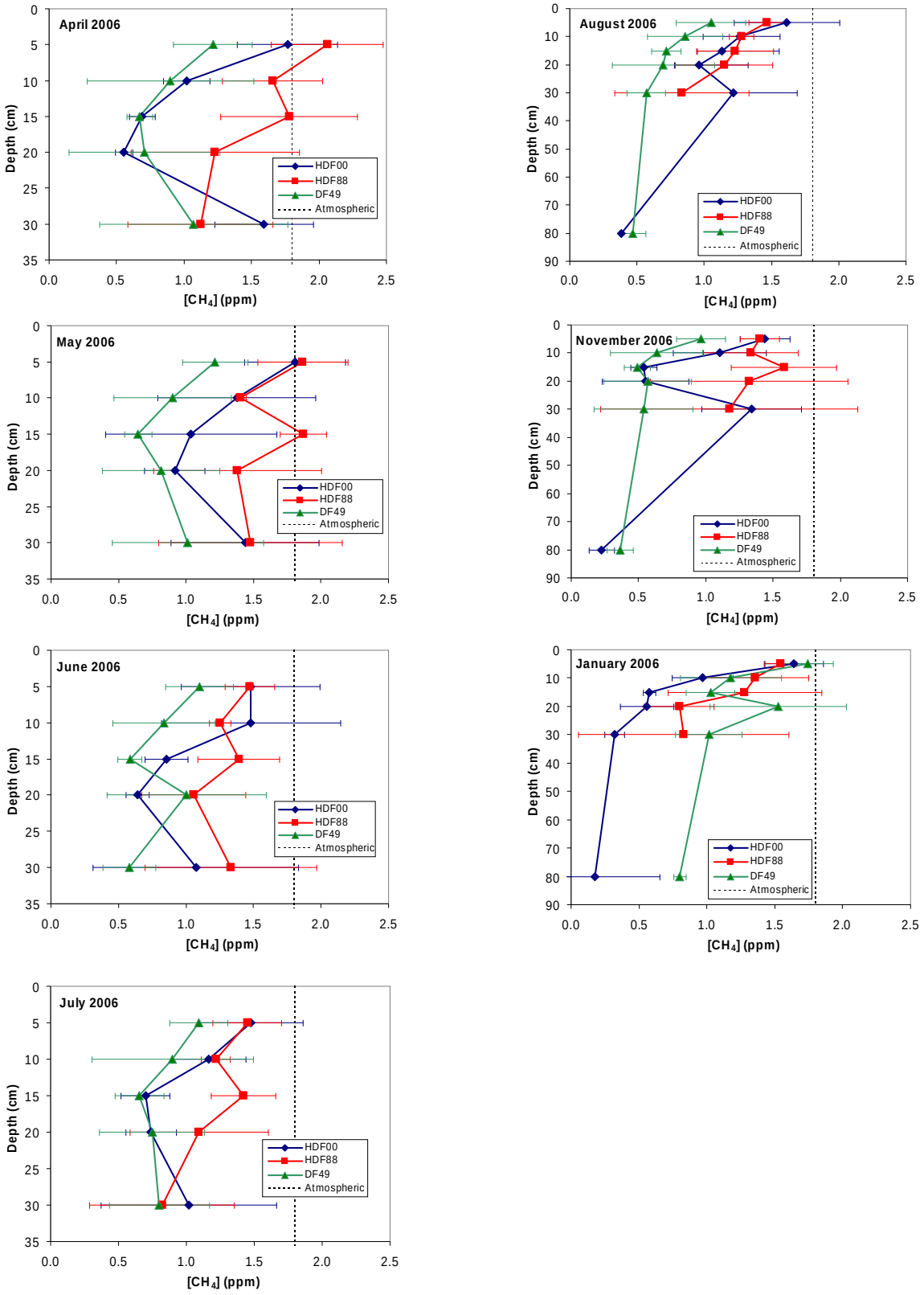

Figure 14: BC [CH_4] profile. Error bars indicate standard deviation of sampling (1σ).

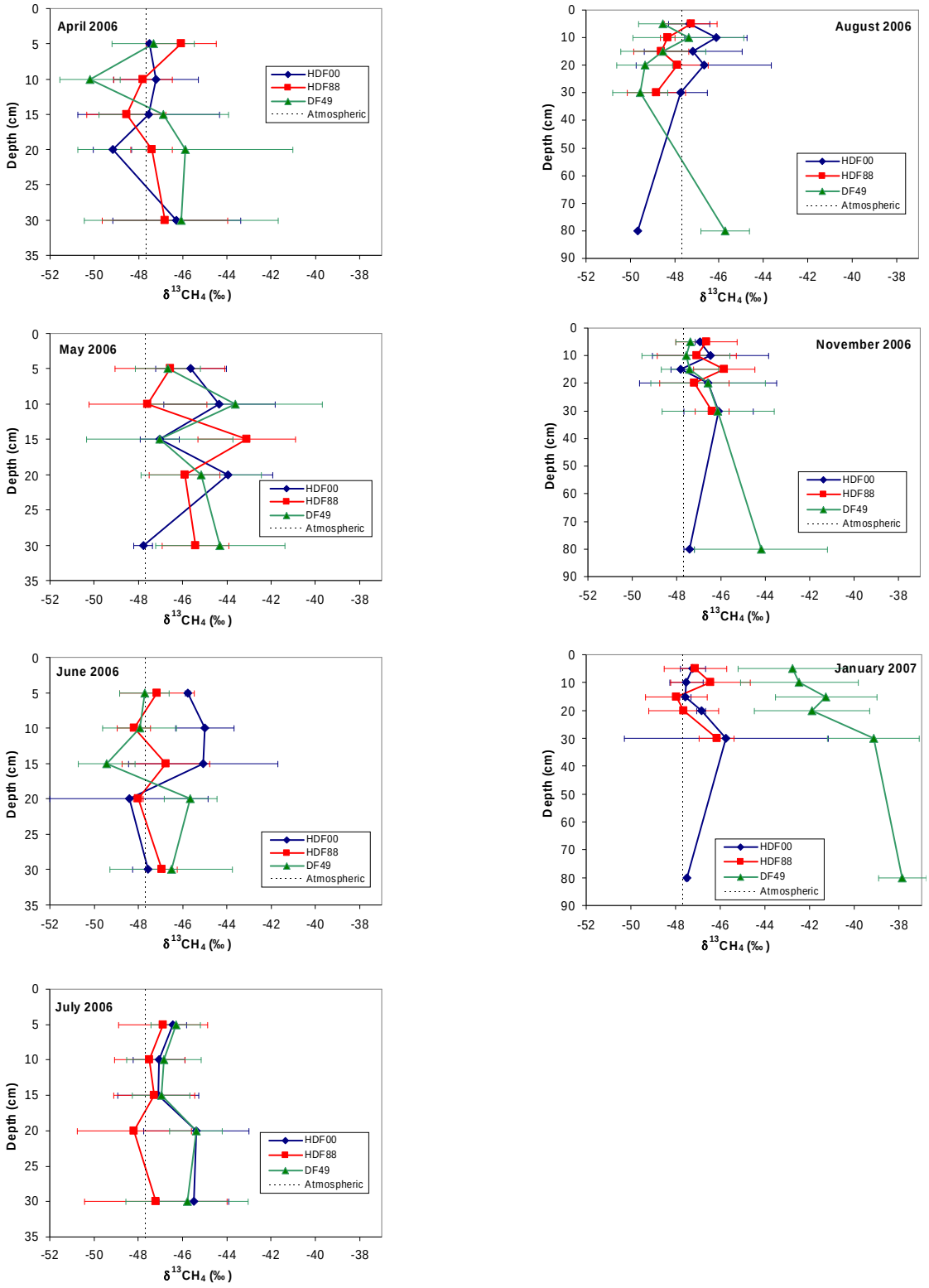

Figure 15: BC $\delta^{13}CH_4$ profiles. Error bars indicate standard deviation of sampling (1σ).

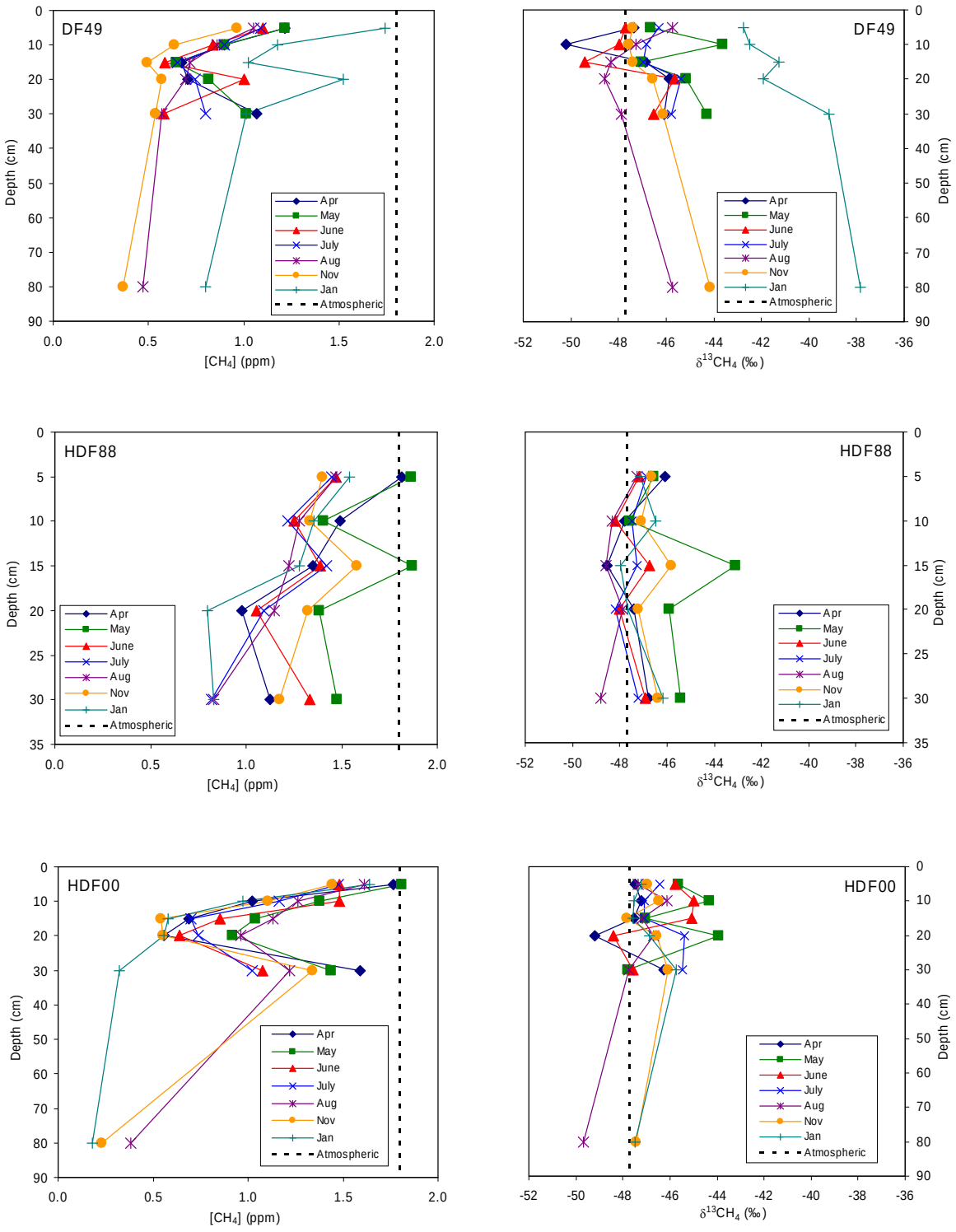

Figure 16: Monthly [CH_4] and $\delta^{13}CH_4$ profiles in the upper 30 cm of soil at DF49, DF88, and HDF00.

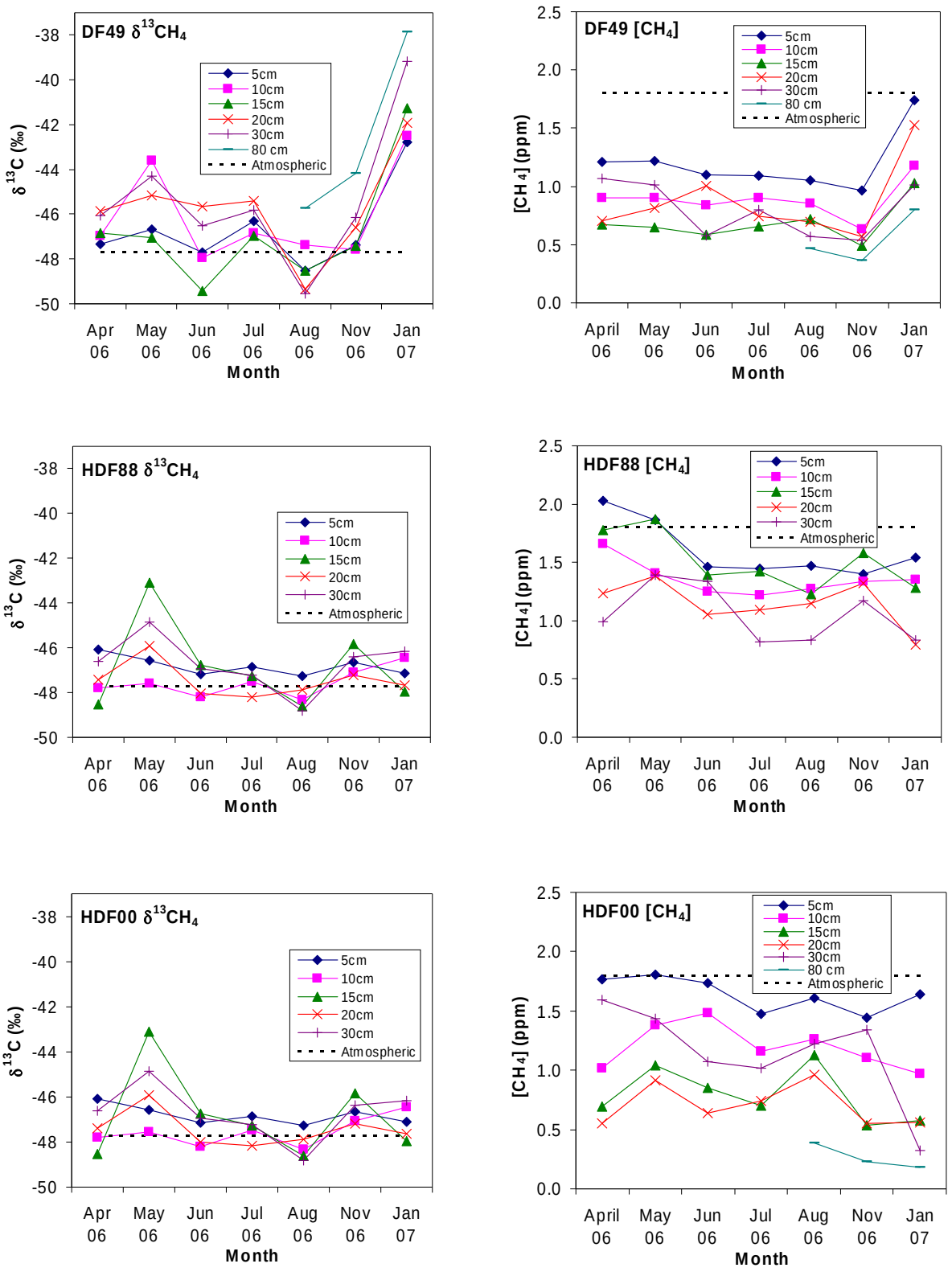

Figure 17: Seasonal CH_4 plots for the BC sites on Vancouver Island.

The month of June shows a ^{12}C-depleted shift with depth in DF49 and a ^{12}C-enriched one at HDF00, while the month of July instead shows a trend of more ^{12}C-enriched CH_4 relative to atmospheric values at lower depths in HDF88, while DF49 and HDF00 instead show more ^{12}C-depleted values. There are no trends in the May data, which does not show a concentration decrease with depth at DF49, HDF88, or HDF00.

All 3 BC sites exhibit similar $\delta^{13}CH_4$ and $[CH_4]$ ranges throughout the year, although some temporal variation is present. HDF88 and DF49 show the most ^{12}C-depleted soil CH_4 in May and the largest ^{12}C-enrichment in August, with a weaker ^{12}C-depletion in June. Site DF49 differs from HDF88 and HDF00 in having a strong ^{12}C-depletion of $\delta^{13}CH_4$ in January. HDF88 shows more ^{12}C-depleted $\delta^{13}CH_4$ in the same month, and no discernable trends are present in HDF00.

The BC chamber flux results show clear temporal trends, with generally increasing ^{12}C-enrichment and decrease in $[CH_4]$ over the course of an hour (Figures 17 and 18). Some exceptions are observed, such as with DF49 Chamber 1 and HDF00 Chamber 2 during April, when both $\delta^{13}CH_4$ and $[CH_4]$ show little change with time. When clear $\delta^{13}CH_4$ and $[CH_4]$ changes do occur relative to initial ($t = 0$) values, $\delta^{13}CH_4$ becomes ^{13}C-enriched by 2 ‰ to 9 ‰, while $[CH_4]$ decreases by 0.2 to 1.7 ppm.

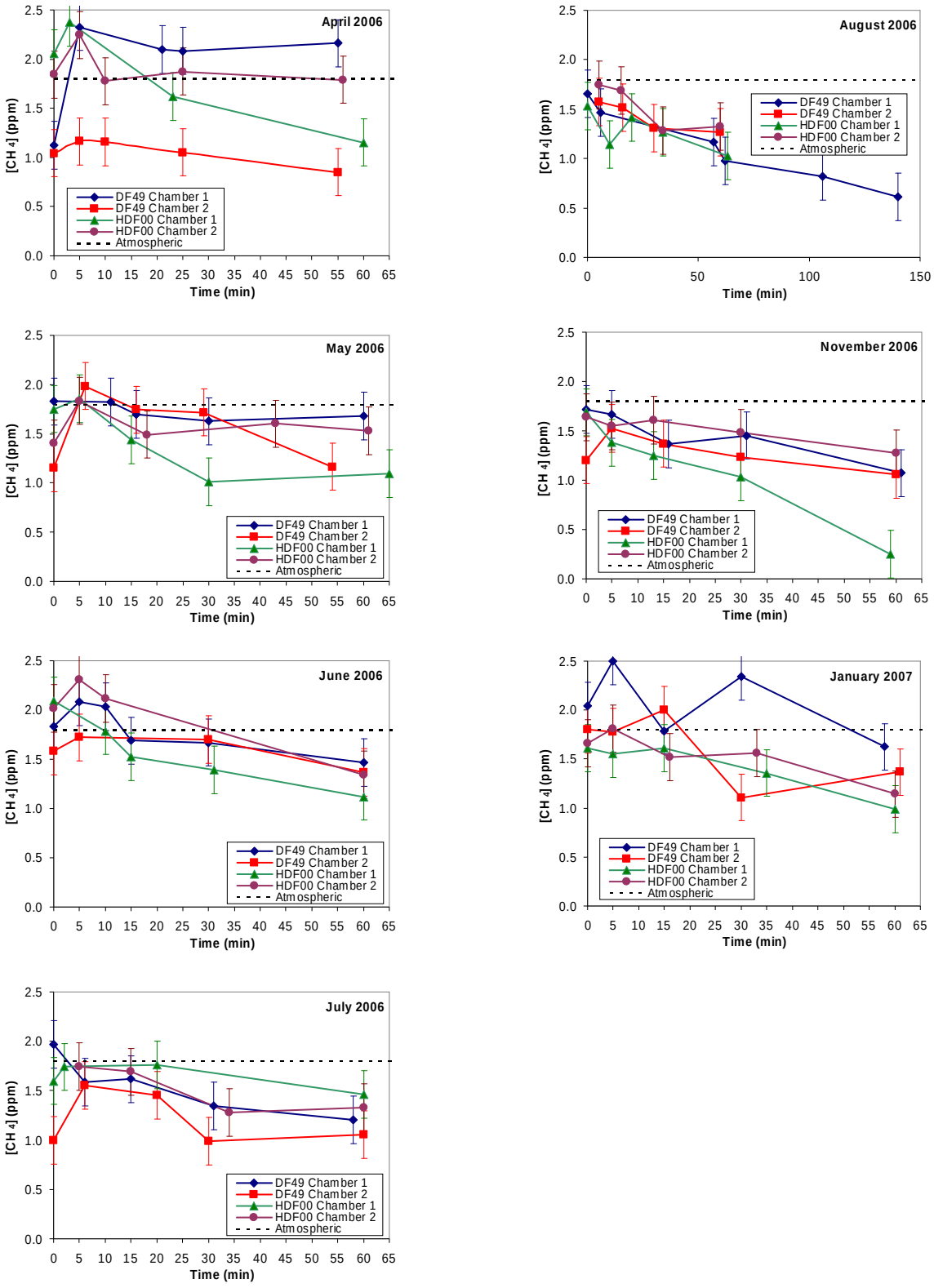

Figure 18: BC [CH_4] static chamber data. Error bars indicate standard deviation of analysis (1σ).

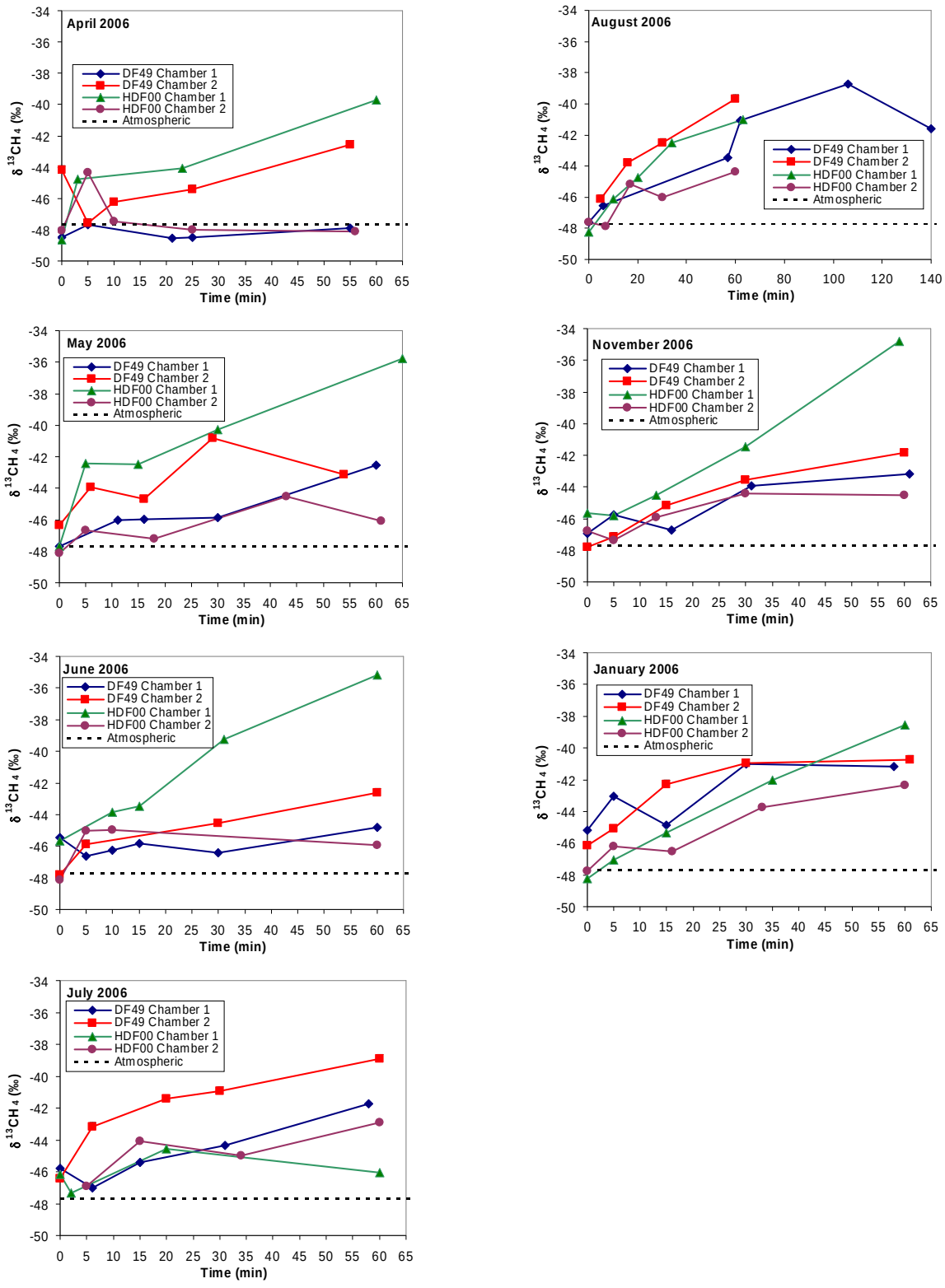

Figure 19: BC $\delta^{13}CH_4$ static chamber data. Error bars indicate standard deviation of analysis (1σ).

3.2 $\delta^{13}CO_2$ and $[CO_2]$ Trends

3.2.1 $\delta^{13}CO_2$ and $[CO_2]$ at Quebec OBS site

Site OBS shows decreasing $\delta^{13}CO_2$ and increasing $[CO_2]$ with depth (Figure 20). The $\delta^{13}C$ values span –12 ‰ to -23 ‰ from 5 to 80 cm depth, with concentrations of 790 ppm to 3,400 ppm over the same depth interval. Data scatter in the 5-30 cm range obscures depth trends, but $\delta^{13}CO_2$ values at 80 cm are more ^{13}C-depleted by at least 1.5 ‰ and $[CO_2]$ higher by at least 980 ppm as compared to all shallower depth intervals.

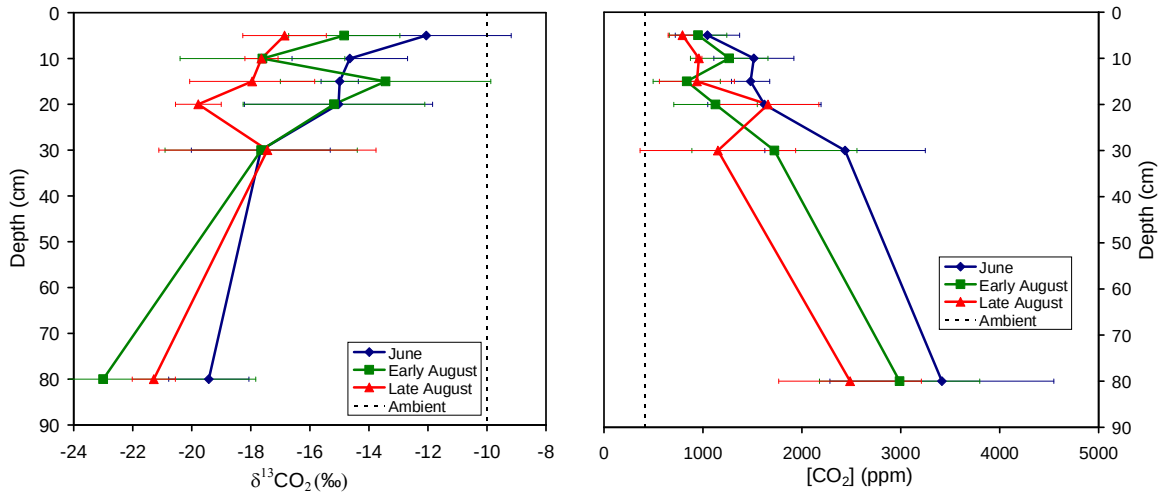

Figure 20: OBS $\delta^{13}CO_2$ and $[CO_2]$ depth profiles. Error bars indicate standard deviation of sampling (1σ).

Most depths show increasingly ^{12}C-enriched soil CO_2 from June to late August. Seasonal trends in concentration are more variable, with some depths showing a decrease in concentration across the 3 months of sampling (at 5, 10, 30, and 80 cm), and others displaying a minimum in late August (15, 20 cm).

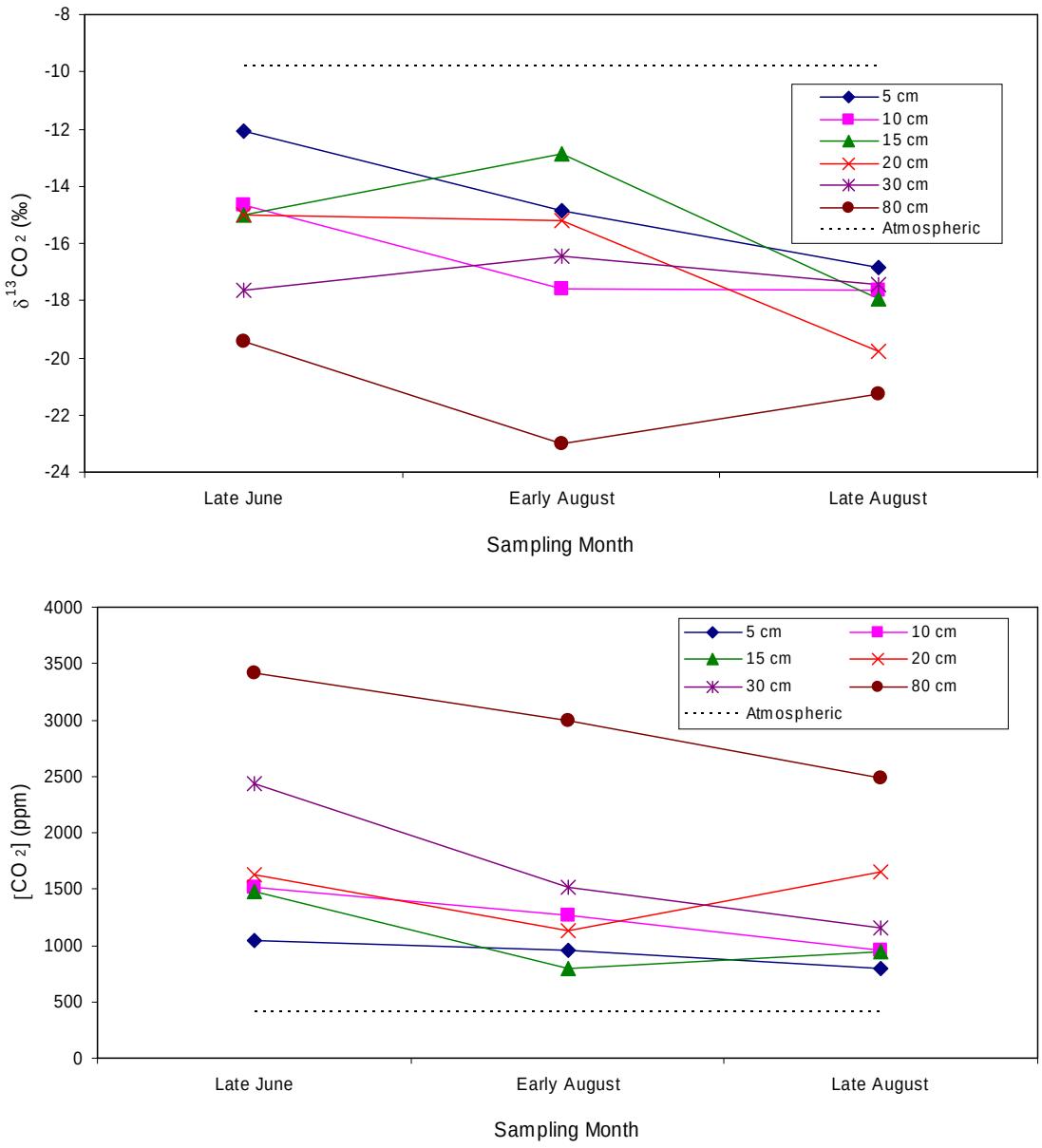

Figure 21: Monthly Changes in $[CO_2]$ and $\delta^{13}CO_2$ at OBS.

3.2.2 $\delta^{13}CO_2$ and $[CO_2]$ on Vancouver Island, BC

Within the BC sites, there are some differences in $\delta^{13}C$ ranges between the three sites, but these variations are inconsistent and change from month to month. At DF49, $\delta^{13}CO_2$ values range from –14 ‰ to –21 ‰ in all depths throughout the sampling period. Similar $\delta^{13}CO_2$ ranges of –12 ‰ to –24 ‰ and –11 ‰ to –22 ‰ are present in HDF88 and HDF00, respectively (Figure 23).

In contrast, the concentration estimates show more constant differences across the three profiles. In all months the HDF00 soils contain the lowest CO_2 concentrations, with a range of 890 ppm to 5,500 ppm. The DF49 soil shows a range of 1,200 ppm to 7,000 ppm, which overlaps the HDF88 range of 1,200 ppm to 8,100 ppm (Figure 22).

All BC locations show temporal variability, with all locations displaying similar trends of constant or increasingly ^{12}C-enriched values within the entire depth profile from May until June 2006, followed by increasingly ^{12}C-depleted values until August (Figure 25). Later in the season, trends appear more variable. DF49 $\delta^{13}CO_2$ values show a ^{12}C-enrichment from August to November at all depths, while HDF00 shows the same enrichment in all depths except for 20 and 30 cm. Within HDF88, on the other hand, all depths except for 20 and 30 cm show a slight ^{12}C-depletion in November. In January, both DF49 and HDF88 show more ^{12}C-enriched CO_2 than in August, while HDF88 shows the most ^{12}C-depleted $\delta^{13}CO_2$ at all depths except for 5 and 30 cm.

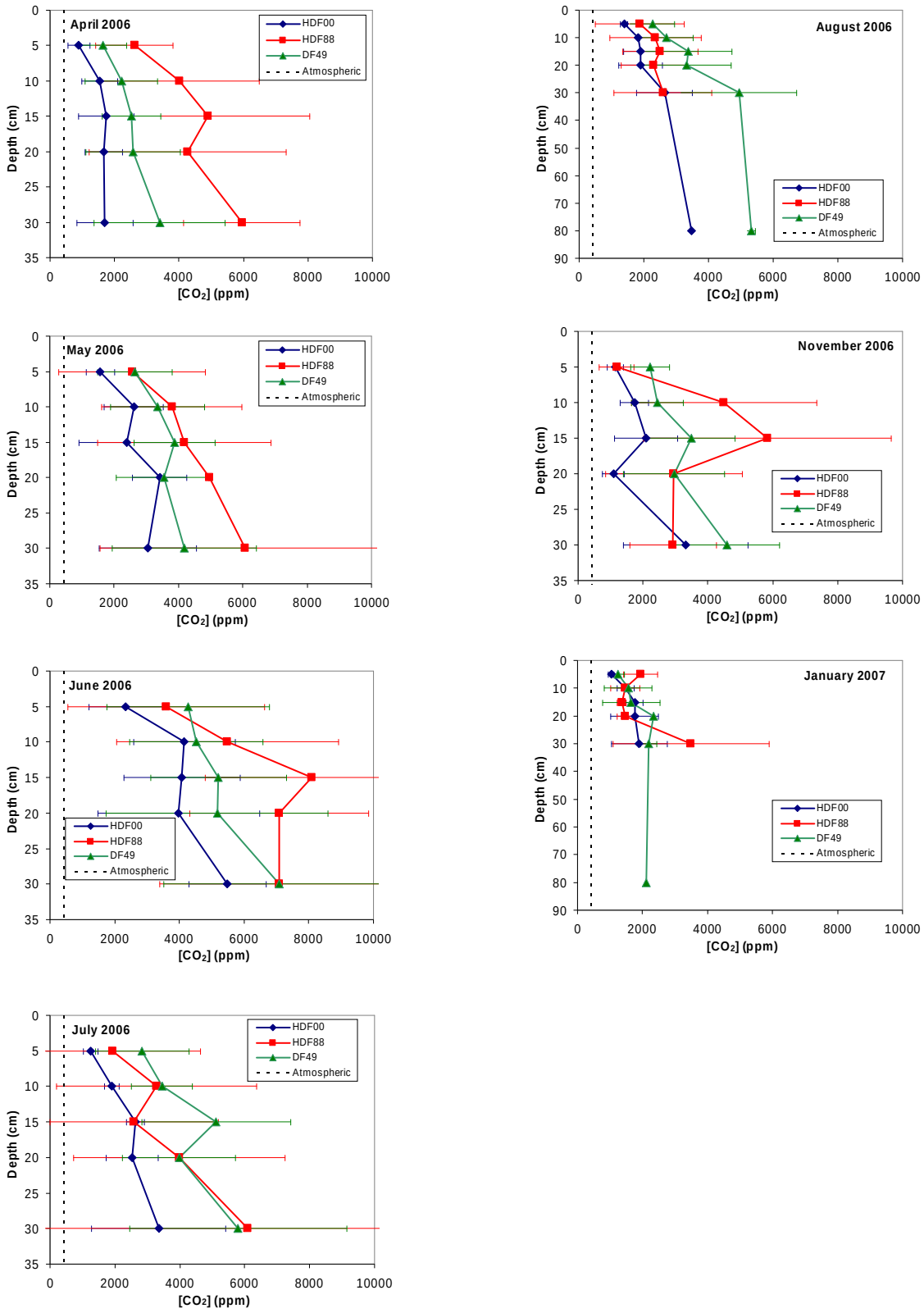

Figure 22: BC [CO_2] profiles. Error bars indicate the sample standard deviation (1σ).

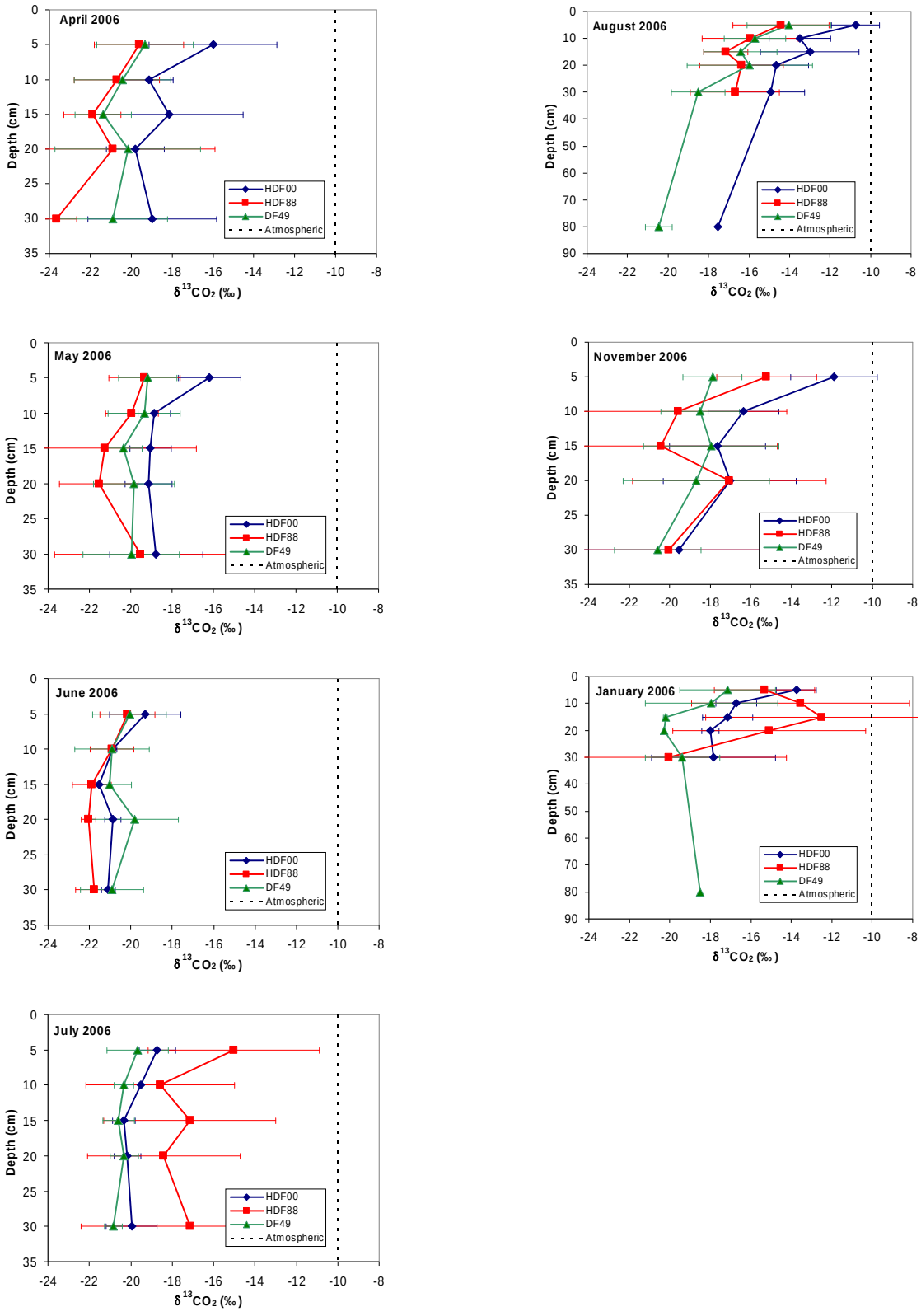

Figure 23: BC $\delta^{13}CO_2$ profiles. Error bars indicate the sample standard deviation (1σ).

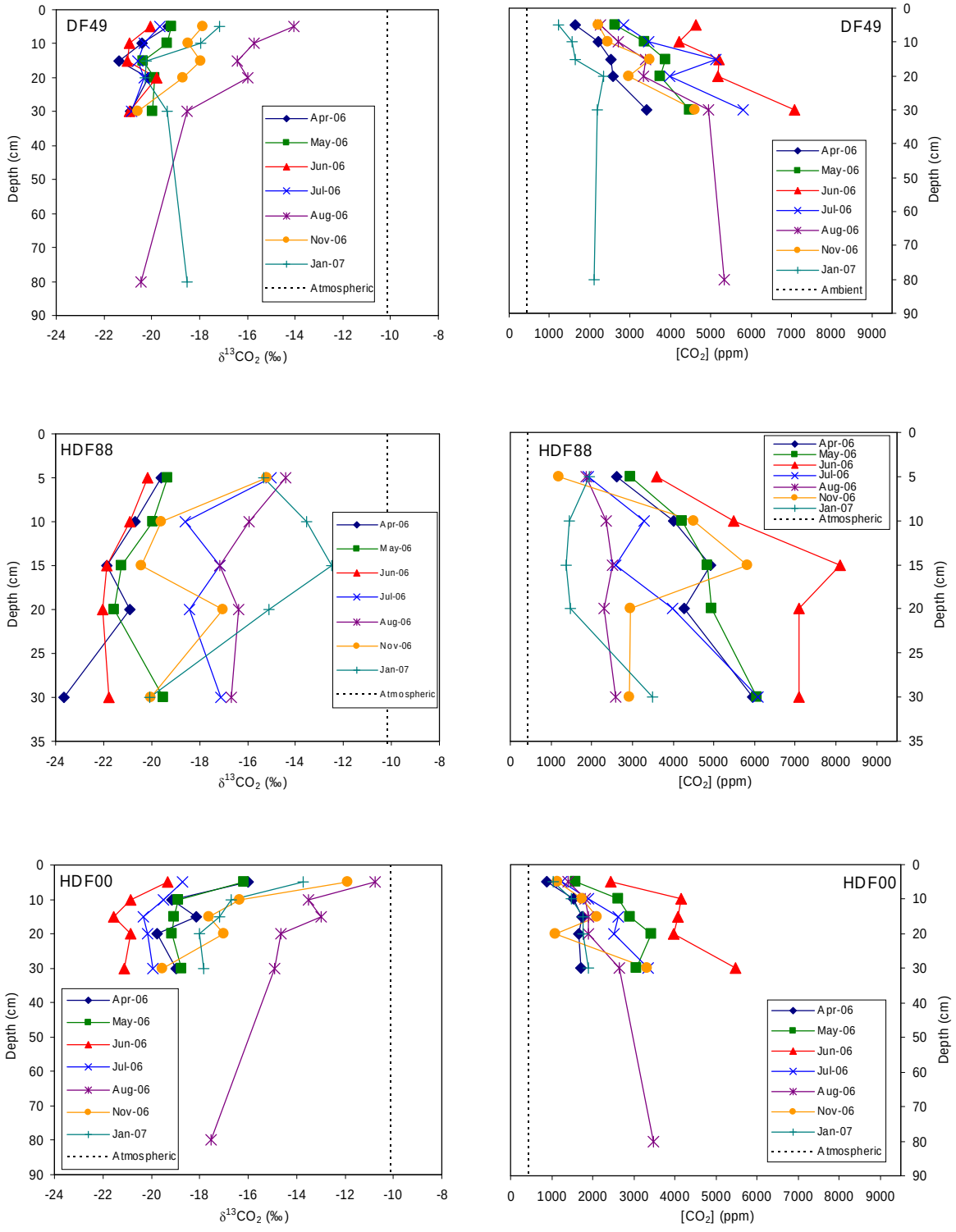

Figure 24: Monthly [CO_2] and $\delta^{13}CO_2$ profiles in the upper 30 cm of soil at DF49, DF88, and HDF00.

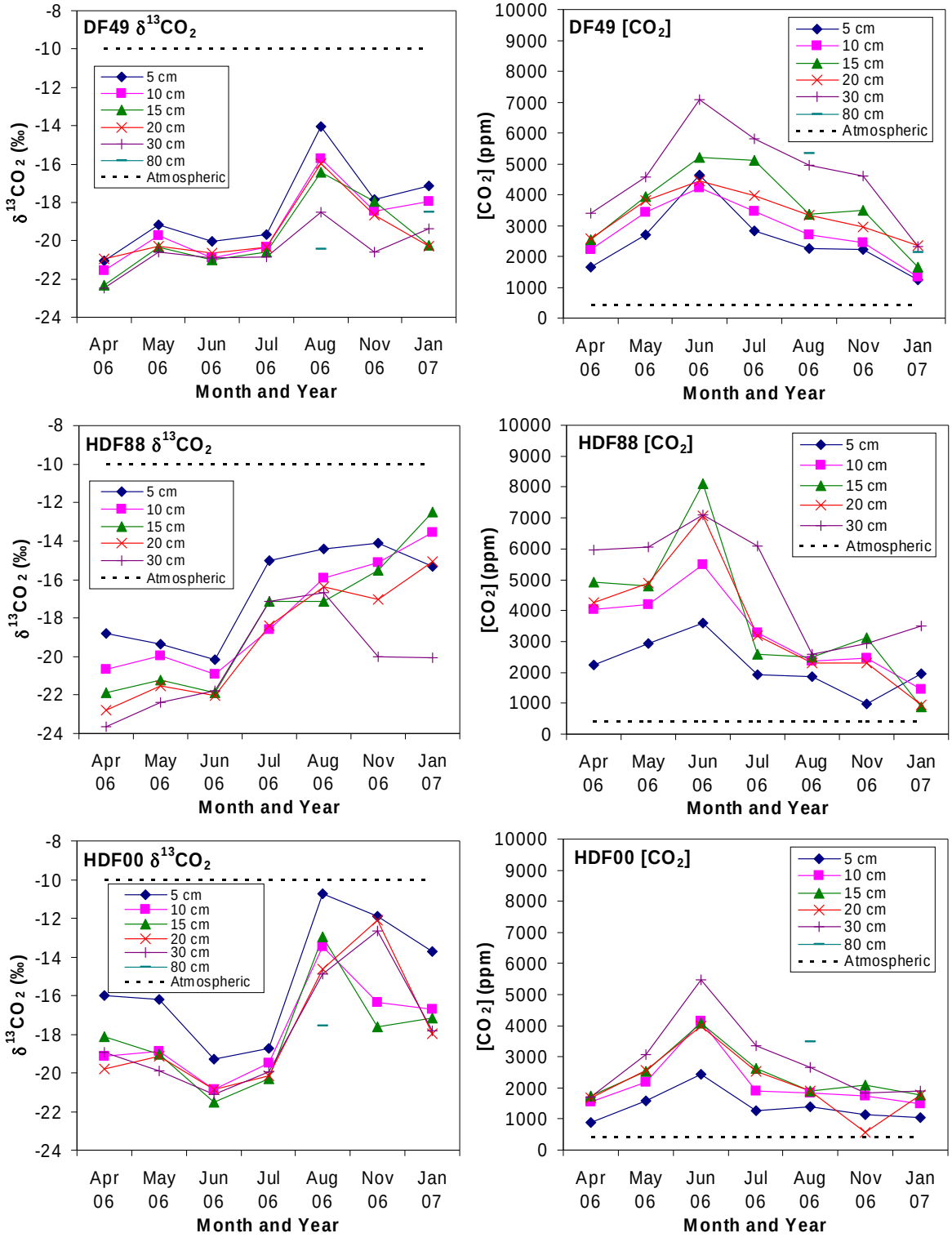

Figure 25: Seasonal CO_2 plots for the BC sites on Vancouver Island.

The [CO_2] data shows an increase in 2006 from April to a maximum value in June at all sites and depths. In the following months, most sites show a steady decrease in [CO_2] until November, although HDF88 differs slightly from the others by showing [CO_2] increases from August to November at 10, 15 and 30 cm depth. All sites show at most depths the lowest CO_2 concentrations being present in January of 2007.

The BC flux chamber studies in DF49 and HDF00 show increasing [CO_2] and decreasing $\delta^{13}CO_2$ with time, supporting the soil profile data in showing net CO_2 efflux (Figures 24 and 25). Site DF49 shows the highest accumulation rates, with an hourly [CO_2] increase ranging from 606 ppm to 2,021 ppm and corresponding ^{12}C-enrichment ranging from 1.8 ‰ to 11.2 ‰. Within HDF00, the changes in $\delta^{13}CO_2$ and [CO_2] were smaller. Over the course of the hour-long sampling period, [CO_2] increases of 328 ppm to 1,602 ppm and ^{13}C-depeltions of 1.7 ‰ to 8.4 ‰ were observed.

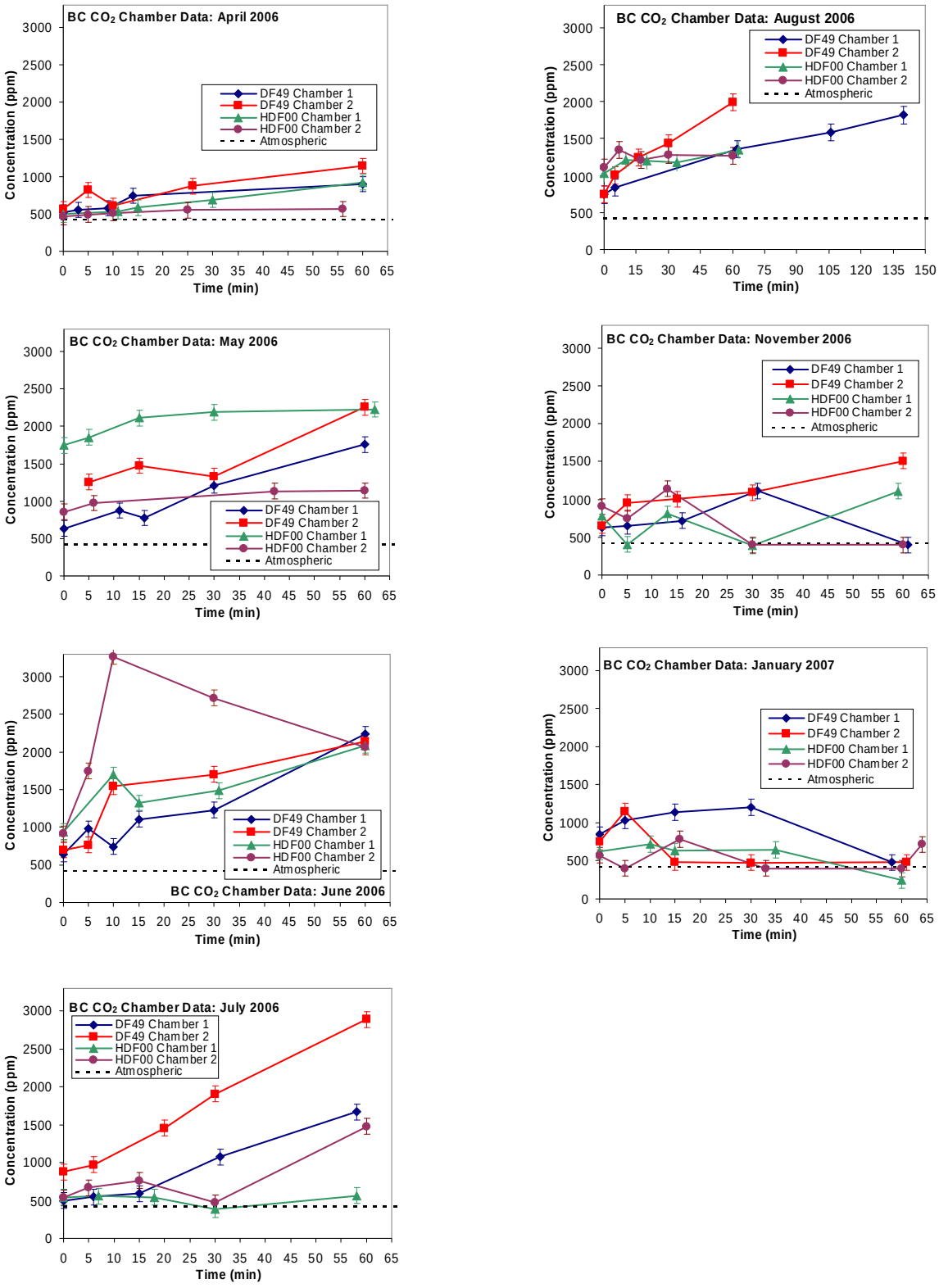

Figure 25: BC [CO_2] static chamber data. Error bars indicate sample standard deviation (1σ).

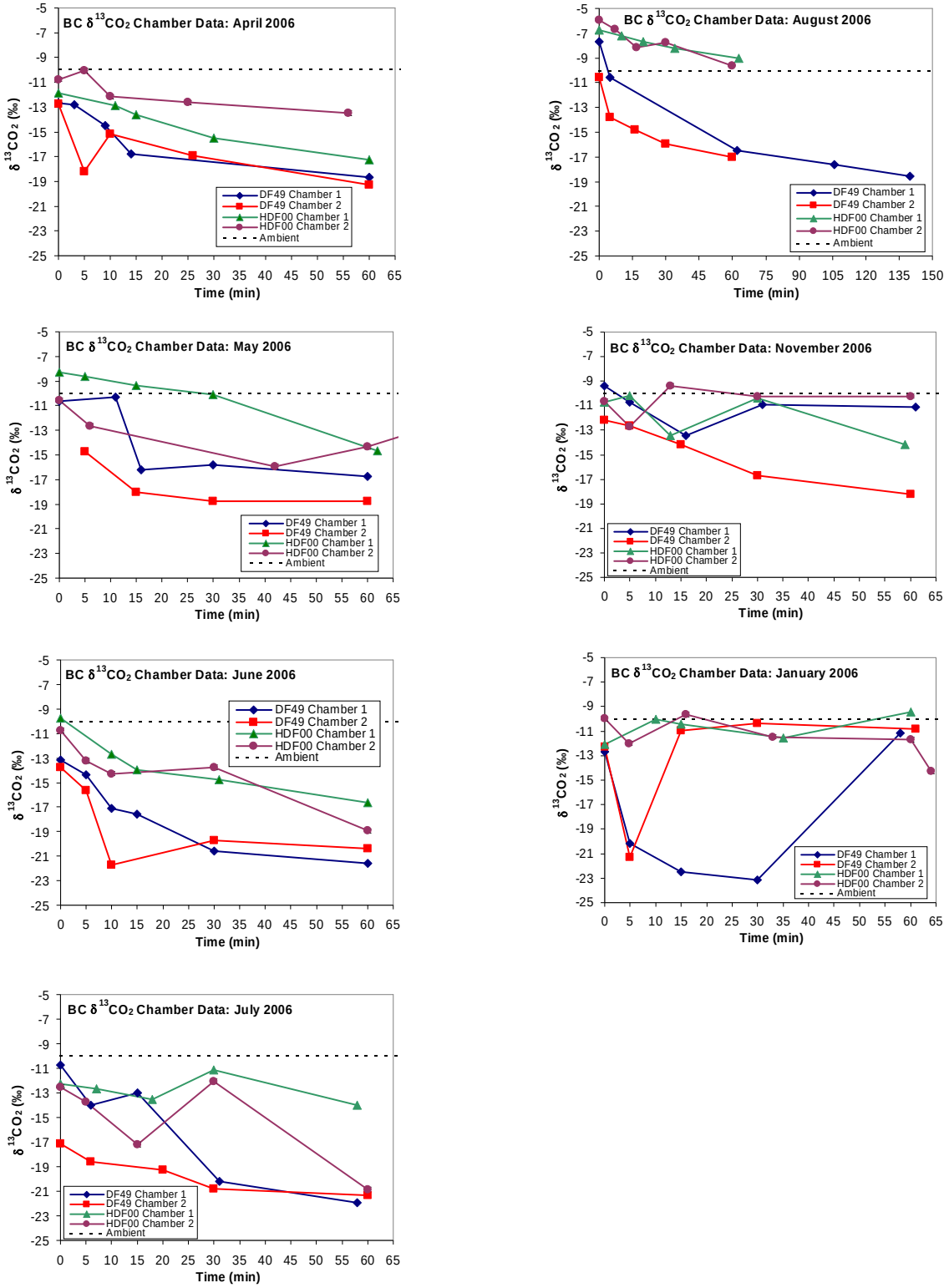

Figure 26: BC $\delta^{13}CO_2$ static chamber data. The analytical standard deviation has been omitted from this Figure, due to its small magnitude.

4.0 Discussion

4.1 CH_4 Cycling

4.1.1 CH_4 Uptake at OBS, Quebec

The soil [CH_4] and $\delta^{13}CH_4$ data from OBS suggests the presence of a methane-oxidizing environment. Predominantly ^{12}C-depleted soil $\delta^{13}CH_4$ and lower [CH_4] relative to atmospheric values indicate diffusion of CH_4 into the soil, where consumption by methanotrophic organisms takes place (Reeburgh et al, 1997). These findings imply that if any methanogenic activity is present in these soils, it occurs to a lesser degree than methanotrophy, making the OBS soils net sinks of atmospheric CH_4.

The concentration data is used to model simulated $\delta^{13}CH_4$ depth profiles and obtain estimates of the biological isotope fractionation factor (α_{bio}). The Equation used is based on Fick's second law in the following form (from Reeburgh et al., 1997):

$$\frac{d[CH_4]}{dt} = D_s \frac{d^2[CH_4]}{dz^2} - L[CH_4] \qquad (4.1.1.1)$$

Where D_s is the soil diffusion coefficient of CH_4 (with soil water content and tortuosity accounted for; see section 2.5), z is soil depth measured positively downwards, and L is a first order rate constant (s^{-1}) describing the consumption of CH_4.

Assuming steady state ($d[CH_4]/dt = 0$) and with the appropriate boundary conditions ($[CH_4]_z = [CH_4]_0$ at z = 0, and $d[CH_4]/dt = 0$ at z = ∞), Equation 4.1.1.1 can be solved:

$$[CH_4]_z = [CH_4]_\infty + ([CH_4]_0 - [CH_4]_\infty)e^{-z\sqrt{L/D_s}} \qquad (4.1.1.2)$$

Where $[CH_4]_\infty$ is the steady state concentration at depth. Equation 4.1.1.2 is identical for both ^{12}C and ^{13}C, with the necessary substitution of $^{13}D_s = {}^{12}D_s/1.0195$ (^{12}C diffuses faster than ^{13}C by a factor of 1.0195; Reeburgh, 1997). Values of $^{13}[CH_4]_0$ and $^{12}[CH_4]_0$ are set at northern hemisphere atmospheric abundances, based on a total concentration of 1.8 ppm and a $\delta^{13}CH_4$ value of -47.7 ‰.

For $[CH_4]_\infty$, concentration values at 80 cm are used, since $[CH_4]_\infty$ obtained by un-constrained exponential fits are similar (differing by an amount equal to, or less than, analytical standard deviation) to 80 cm values. Depth distributions of $[^{12}CH_4]$ and $[^{13}CH_4]$ are first obtained from the $\delta^{13}CH_4$ data using Equation 1.4.1. Equation 4.1.1.2 is then fitted to the concentration data to obtain L and $[CH_4]_\infty$ (see Table A21 in appendix). The biological fractionation factor can be calculated from L using the relationship $^{12}L/^{13}L = \alpha_{bio}$. Flux rates at z = 0 are calculated via differentiation of Equation 4.1.1.2 for ^{12}C (since $^{12}[CH_4] \approx [CH_4]$), and substituting the resulting Equation into 2.5.1:

$$J = -\frac{D_s}{z^*}(C_0 - C_\infty)e^{-z_0/z^*} \qquad (4.1.1.3)$$

Where z* = $\sqrt{D_s / L}$, a quantity often referred to as the "relaxation depth" (Reeburgh et al., 1997).

The application of Equation 4.1.1.2 results in good agreement with the $\delta^{13}CH_4$ profiles at OBS (Figure 27). The modeled curve based on the early August data agree with observations in showing ^{12}C-enriched $\delta^{13}CH_4$ values, relative to atmospheric CH_4, within the upper 30 cm of soil. The calculated α_{bio} values range from 1.016 to 1.028 (see Table 7), with a mean of 1.021 ± 0.006.

The observed α_{bio} values are similar to the range of 1.008 to 1.025 found in previous studies involving aerated soils, and the standard deviation is also within the range found in the literature, which has been measured at ± 0.0004 to ± 0.008 (Snover and Quay, 2000). This suggests that the ^{12}C-enriched CH_4 relative to atmospheric values observed during early and late August could arise solely as a result of diffusive fractionation and biological consumption, with minor to negligible methanogenic input.

Table 7: Calculated CH_4 flux and α_{bio} values from OBS

	Late June 2005	Early August 2005	Late August 2005
α	1.019	1.016	1.028
Eqn. 4.1.1.3 Fluxes ($mg \cdot m^{-2} \cdot d^{-1}$)	-0.80	-1.86	-1.89
Eqn. 2.5.1 Fluxes ($mg \cdot m^{-2} \cdot d^{-1}$)	-0.88	-1.33	-1.25

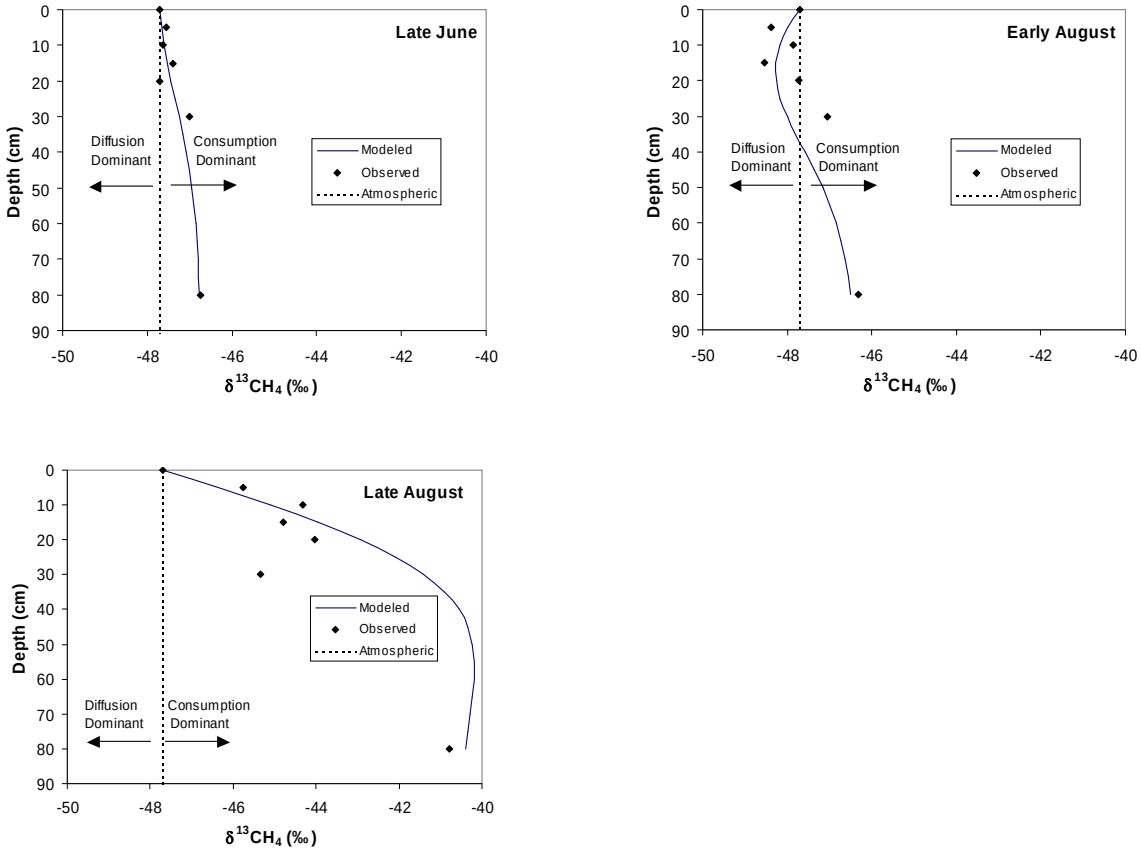

Figure 27: Comparisons between modeled and observed $\delta^{13}CH_4$ at OBS.

While the late August plot shows increasingly ^{12}C-depleted $\delta^{13}CH_4$ from 0 to 55 cm, a ^{12}C-enrichment is shown at depths greater than 60 cm. This may indicate that in regions of low methanotrophic activity, such as those expected deeper in the soil where soil moisture is higher and O_2 levels low, diffusive movement becomes the dominant influence on $\delta^{13}CH_4$ (see Figure 27). Thus, one would expect some degree of ^{12}C-enrichment at deeper soil horizons due to diffusive fractionation, which would overcome any ^{12}C-depletion brought about by methanotrophy. While a ^{12}C-enrichment of CH_4 deeper in the soil is not observed in late June and early August, it is possible that soil

moisture was higher and O_2 levels were lower during late August below a depth of 60 cm, resulting in lower methanotrophic activity at those depths.

Surface (z = 0) fluxes calculated using Equation 4.1.1.2 show the largest fluxes occurring in late June, with lower fluxes observed in August (Figure 28). Uptake rates range from –1.6 to –2.2 $mg \cdot m^{-2} \cdot d^{-1}$, with the lowest and highest fluxes observed in June and early August, respectively. These estimates are within the range of summertime fluxes observed in another mature Black Spruce forest by Savage et al. (1997), who measured CH_4 flux rates of 0.6 to –2.6 $mg \cdot m^{-2} \cdot d^{-1}$ using static chambers.

While the bulk atmospheric value of 1.80 ppm is assumed to be an appropriate near-ground value, the sensitivity of calculated fluxes using Equation 4.1.1.3 to assumed near-ground [CH_4] was tested by recalculating fluxes based on near-ground values of 1.50 ppm and 2.30 ppm. This represents a variation of ± 0.3 ppm, and is based on the standard deviation observed from the t = 0 chamber samples at DF49 and HDF00. As all t = 0 values (including those excluded from flux calculations) are included to determine this standard deviation, and since this variance is 6 times greater than the seasonal change observed by previous studies, the value of ± 0.3 ppm likely represents the upper range of possible near-ground [CH_4] variation.

Based on an assumed near-ground value of 2.3 ppm, recalculated fluxes are up to twice as high as those based on near-ground mixing ratios of 1.8 ppm, while the lower near-ground [CH_4] of 1.5 ppm result in fluxes that are up to two times lower (see Table 8). However, even accounting for this maximum possible variation in near-ground CH_4, the fluxes remain within the range of values found in the literature. As well, the variation in near-ground CH_4 is unlikely to be this strong, especially in the space of three

consecutive months within the same season. Thus, a near-surface value of 1.8 ppm will be assumed for all subsequent calculations.

Table 8: CH_4 calculated using 1.5 and 2.3 ppm near-ground CH_4 values, using Equation 4.1.1.3

Near-ground [CH_4] (ppm)	Fluxes ($mg \cdot m^{-2} \cdot s^{-1}$)		
	2005		
	Late June	Early August	Late August
1.5	-0.48	-0.70	-0.69
1.8	-0.88	-1.33	-1.25
2.3	-1.72	-2.66	-2.48

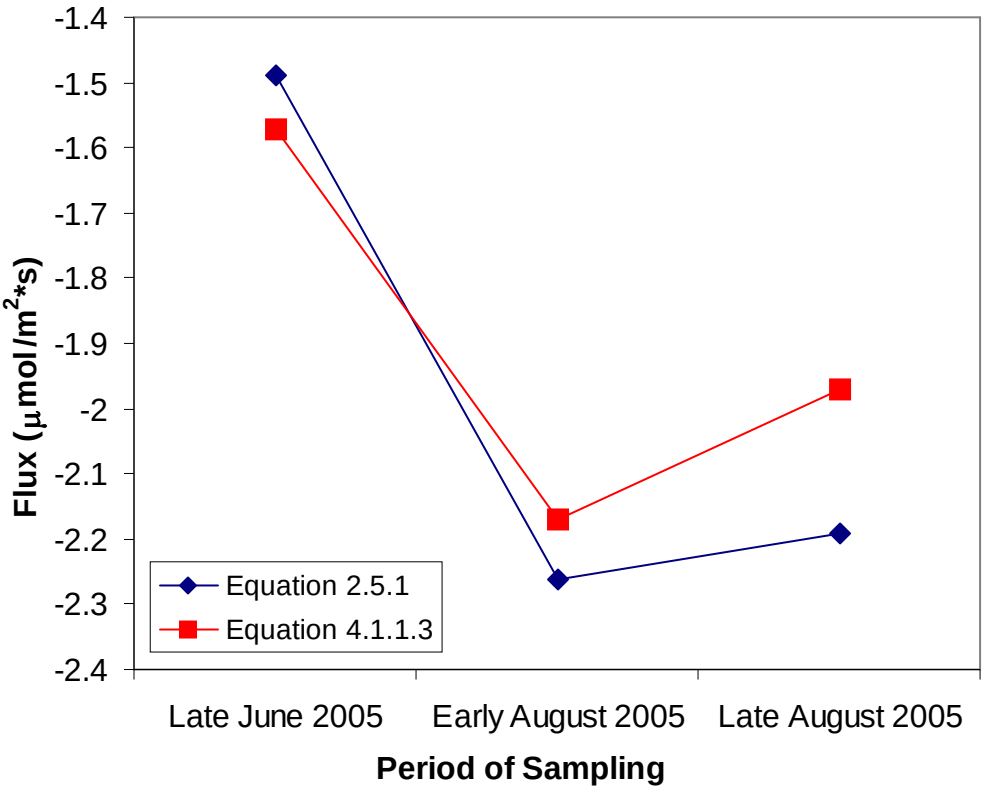

Figure 28: Comparison of CH_4 uptake rate calculations (fluxes) at OBS soil surface uptake using Eq 2.5.1 and 4.1.1.3.

Uptake rates derived from Equation 4.1.1.3 are compared to fluxes calculated from Equation 2.5.1, using the method outlined in Section 2.5 (see Table 7). Fluxes obtained using both equations show good agreement (Figure 28), suggesting that Equation 2.5.1 may provide a reasonably accurate assessment of CH_4 uptake rates. The two approaches show decreasing fluxes from late June to early August, followed by a slight increase in late August. The larger fluxes in early and late August as compared to June is due to the lower soil moisture observed during those periods of time, which result in a larger D_s value (see Figure 9).

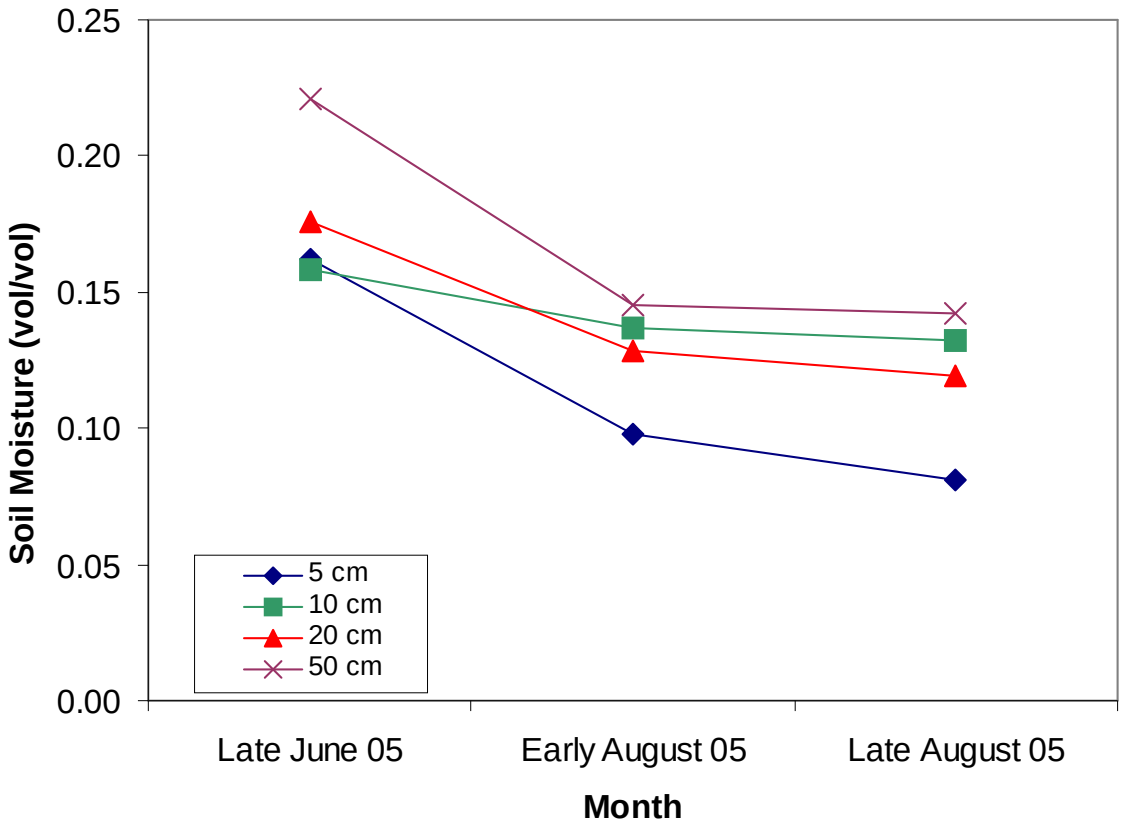

Figure 29: Observed soil moisture at OBS, from various depths (data from the Fluxnet-Canada Database, courtesy of H. Margolis; see Table A19 in appendix).

Using both observed and modelled [CH_4], the fraction of atmospheric CH_4 oxidized at each depth (F_{ox}) is calculated by subtracting [CH_4] at any given depth from values in the preceding depth interval, and then dividing the resulting number by atmospheric [CH_4]. The modelled data show the largest fraction of CH_4 being oxidized at 5 cm depth, with a general decrease in F_{ox} with depth (Figures 30). Negative F_{ox} values are occasionally present, although this is likely due to the large standard deviation present in the depth profile [CH_4] measurements.

Similar trends are apparent from observed [CH_4] values, which show a general correspondence with the calculated F_{ox} data. However, observed F_{ox} at 80 cm depth is as much as 30 % larger than in preceding depths. This may be due to the larger depth interval between 30 cm and 80 cm that is used to calculate F_{ox} at 80 cm, as compared to F_{ox} computed in shallower depths, which are based on 5-10 cm depth differences. This may result in less accurate F_{ox} estimates, which can be improved with sampling of additional depths between 30 cm and 80 cm.

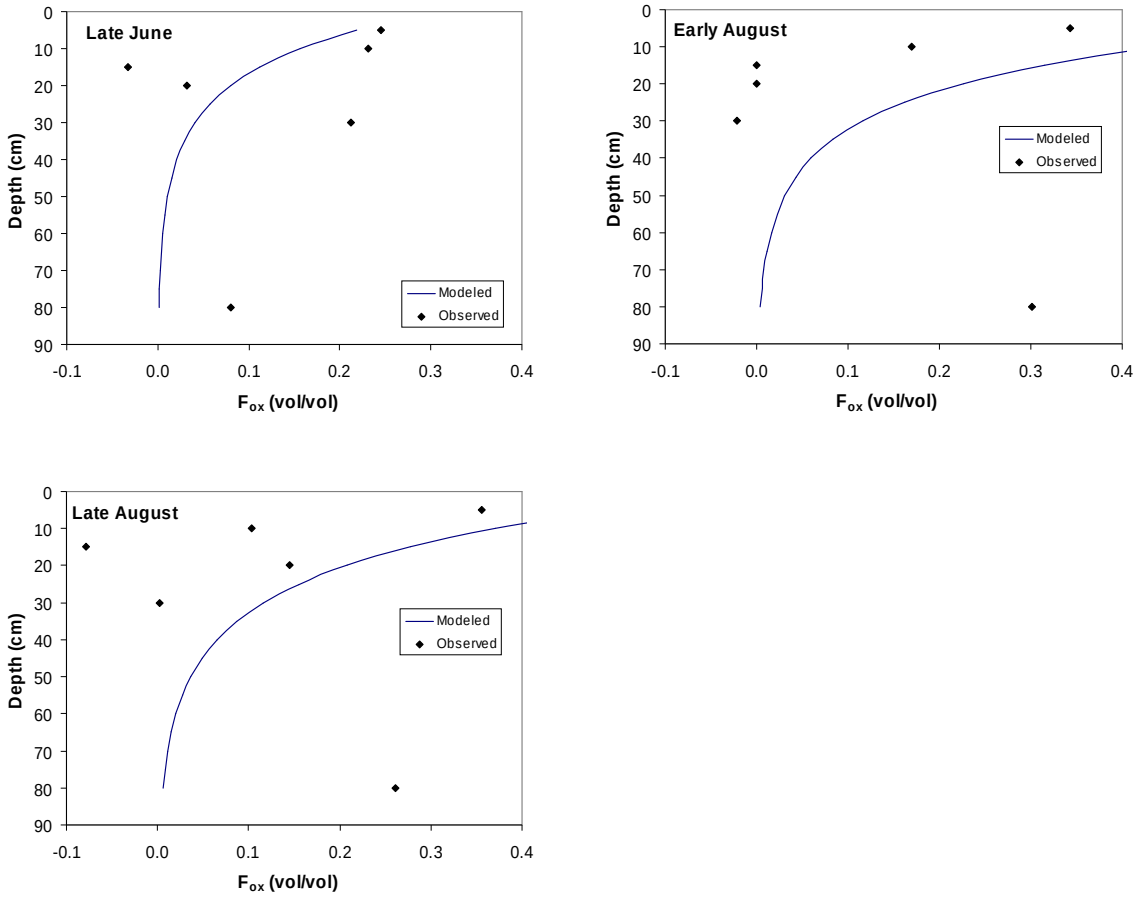

Figure 30: Comparisons of calculated and observed F_{ox} at OBS.

Figure 31 shows a cross plot of $\delta^{13}CO_2$ vs. $\delta^{13}CH_4$, constructed using the OBS data from all months. The lines α=1.03 and α=1.005 in Figure 29 represent the range of isotope fractionation factors between precursor CH_4 and product CO_2 that bound the region of methanotrophy within these plots (Figure 31; region of methanotrophy magnified for clarification, as compared to Figure 1). While the co-existing CO_2 is not likely to be strongly coupled with CH_4 at OBS due to the dominance of soil respired CO_2

over any CO_2 produced by methanotrophy, the general positioning of the data points supports the notion of methanotrophy in the OBS soils.

There are also many data points from shallower depth intervals (5 to 30 cm depth) that lie outside the region of methanotrophy, and trend towards atmospheric values (assumed $\delta^{13}CO_2$ of -10 ‰ and $\delta^{13}CH_4$ of -47.7 ‰). This may be partially due to the dominance of diffusive fractionation over methane oxidation within the 30 cm depth interval, resulting in more ^{12}C-enriched CH_4 as compared to data from 80 cm depth.

However, it is also likely that the influence of atmospheric CH_4 is stronger within shallower depth intervals given their proximity to the soil surface, resulting in enhanced mixing between soil gas and near-surface CH_4. This process could be facilitated by the lower soil moisture and greater air-filled pore space within the upper 30 cm of the OBS soil. Thus, a combination of both diffusive fractionation and mixing may be occurring within this region of the soil profile, resulting in the observed trend towards atmospheric values.

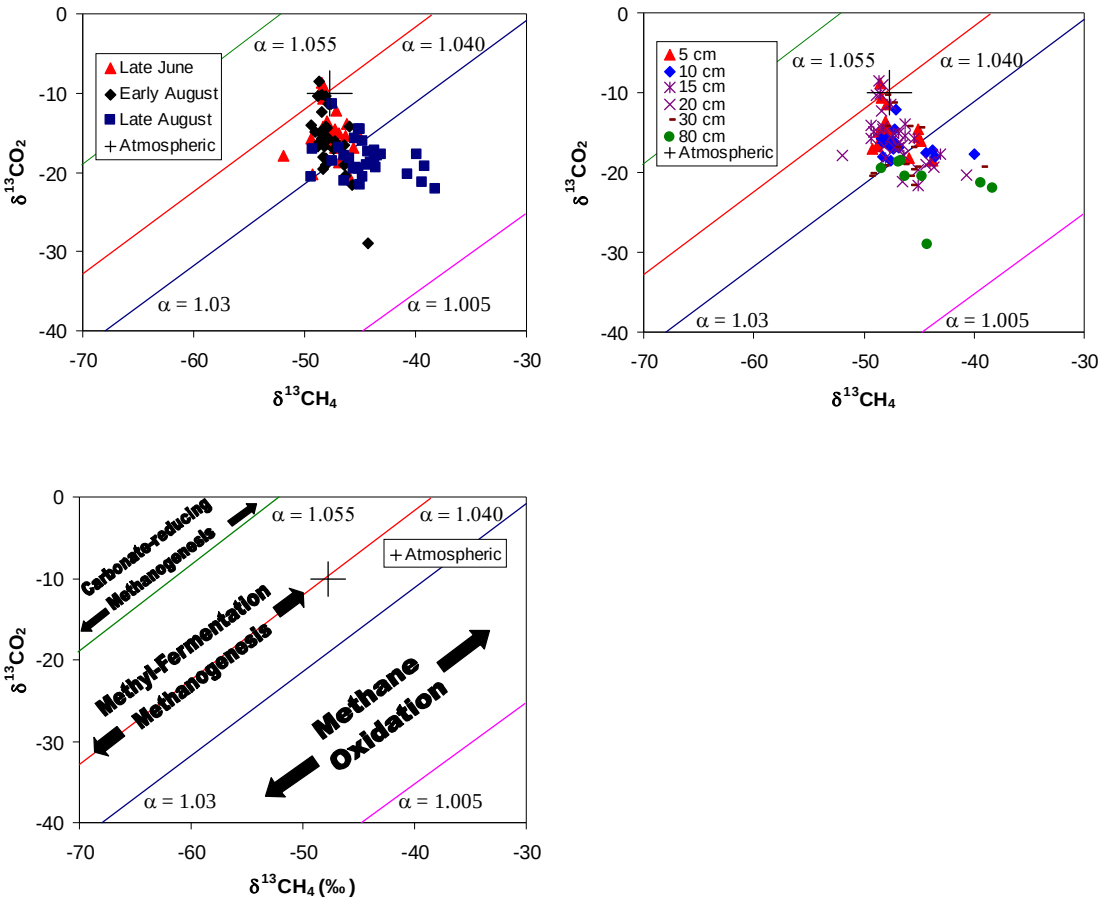

Figure 31: $\delta^{13}CO_2$-$\delta^{13}CH_4$ cross plot for all months of sampling at OBS, with a blank plot for reference.

4.1.2 CH_4 Dynamics in Vancouver Island

All BC sites during most months show lower soil [CH_4] and ^{12}C-depleted $\delta^{13}CH_4$ as compared to atmospheric values. This is similar to the findings at OBS, indicating that the BC soils at all locations act as net methane sinks. The decreasing headspace [CH_4] and increasing $\delta^{13}CH_4$ with time found in the DF49 and HDF00 chamber measurements further support this. These findings demonstrate that the process of methanotrophy

dominates over methanogenesis through the entire period of sampling, thus resulting in net CH_4 consumption in the soils.

Chamber fluxes are calculated using Equation 2.5.5 and compared to flux estimates derived from soil profile measurements, using both Equations 2.5.1 and 4.1.1.3, for comparison purposes. As 80 cm data was unavailable for the first 4 months of sampling at DF49 and HDF00, and for the entire sampling period in HDF88, concentration profiles are more roughly fit to Equation 4.1.1.2 by setting the lowest observed concentration as the C_∞ value while still assuming near-ground mixing ratios of 1.80 ppm.

From the chamber data, uptake rates ranging from –1.0 to –6.7 $mg \cdot m^{-2} \cdot d^{-1}$ are calculated from DF49 and fluxes calculated from HDF00 span 0 to –6.5 $mg \cdot m^{-2} \cdot d^{-1}$ (Figure 32; see Table 9). Both flux ranges are within the range of forest CH_4 uptake rates (0.00 to 8.96 $mg \cdot m^{-2} \cdot d^{-1}$) found in the literature (Jang et al., 2006). There are no consistent patterns emerging through the sampling season, therefore the uptake rates do not appear to have a seasonal dependence.

The Chamber fluxes show strong spatial variation in both sites, with fluxes differing by as much as 5.9 $mg \cdot m^{-2} \cdot d^{-1}$ in DF49 and 5.5 $mg \cdot m^{-2} \cdot d^{-1}$ in HDF00. Previous studies using similar chambers have also found strong variation in CH_4 flux within the same site and sampling period.

Prieme et al (1996) found CH_4 fluxes ranging from an uptake rate of –2.2 $mg \cdot m^{-2} \cdot d^{-1}$ to an efflux of 0.20 $mg \cdot m^{-2} \cdot d^{-1}$ using 122 static chambers encompassing 0.0078 m^2 of surface area (roughly half the size of those used in this study). All measurements were made during the same day in a Danish forest soil.

These authors concluded that in order to obtain more precise bulk flux estimates, a larger number of smaller chambers or a smaller number of larger chambers of 64 m^2 are needed. This suggests that the use of two smaller chambers at HDF00 and DF49 is insufficient for derivation of bulk area fluxes and that Equation 4.1.1.3 may provide a more accurate estimate of average CH_4 uptake rates, as it accounts for a larger sampled area.

Table 9: Calculated CH_4 Fluxes at all BC Sites

		Fluxes ($mg \cdot m^{-2} \cdot d^{-1}$)						
		2006						2007
Site	Method	Apr	May	Jun	Jul	Aug	Nov	Jan
DF49	Chamber 1	-2.54	-1.43	-6.70	-4.59	-1.35	-1.68	
	Chamber 2	-1.04	-2.10	-0.85	-4.84	-2.17	-2.53	
	Equation 2.5.1	-0.80	-1.86	-1.89	-2.55	-3.04	-1.97	-0.12
	Equation 4.1.1.3	-0.88	-1.33	-1.25	-1.92	-3.23	-0.26	-0.31
HDF88	Equation 2.5.1	0.25	0.20	-1.01	-1.26	-1.39	-0.75	-0.37
	Equation 4.1.1.3	-0.12	-0.27	-1.03	-1.21	-1.49	-0.52	-0.22
HDF00	Chamber 1	-3.83	-5.58	-5.38	-0.43	-0.75	-2.83	-1.38
	Chamber 2	-1.93	-0.07	-6.48	-1.96	-2.81	-0.75	-1.45
	Equation 2.5.1	-0.03	0.01	-0.36	-1.18	-0.90	-0.53	-0.12
	Equation 4.1.1.3	-0.68	-0.73	-0.87	-2.28	-1.09	-0.61	-0.66

This spatial variation in CH_4 Chamber fluxes may be related to intra-site heterogeneities in the subsurface distribution of soil moisture and organic matter, both of which can be strong influences on CH_4 diffusion and uptake rates. Within another temperate forest environment located in Massachusetts, soil moisture has been known to affect CH_4 both by acting as a barrier to diffusion at percentages greater than 50 %, or by reducing microbial activity via cell desiccation at quantities lower than 20 % (Castro et al., 1995; Czepiel et al., 1995).

As well, the distribution of organic matter can influence CH_4 uptake within forest soils by changing the ability of the soil to retain moisture (Castro et al., 1995) and studies

in other aerated soils show that organic matter can also provide substrates for certain types of methanotrophic organisms (West and Schmidt, 1999). While the precise methanotrophic pathway in the BC sites remains unknown, it is possible that organic matter may act as a source of methanotrophic substrate as well, influencing the magnitude of CH_4 uptake rates.

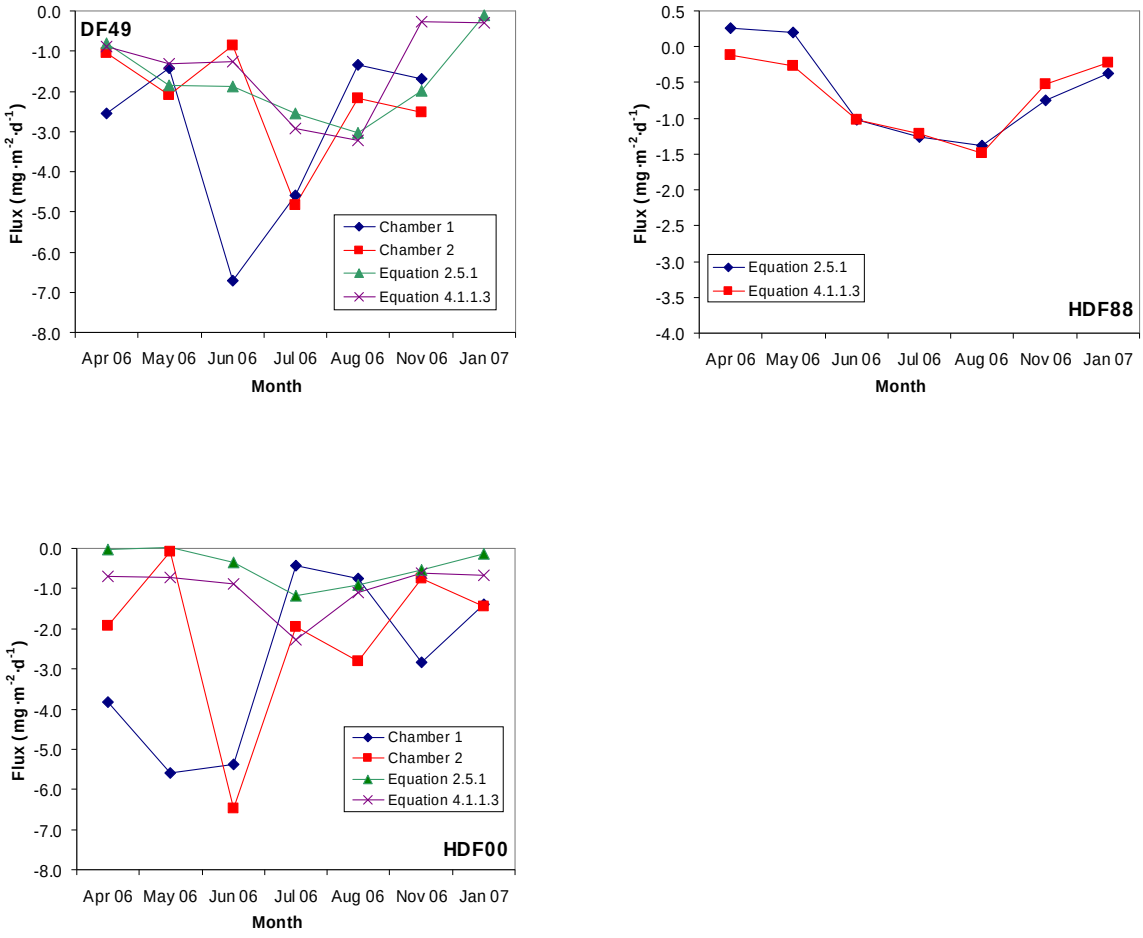

Figure 32: CH_4 flux estimates at the BC sites.

Lower flux values are obtained from Equation 4.1.1.3, with ranges of –0.3 to –3.2 $mg \cdot m^{-2} \cdot d^{-1}$ and –0.6 to –2.3 $mg \cdot m^{-2} \cdot d^{-1}$ present in DF49 and HDF00, respectively. Uptake rates calculated from Equation 2.5.1 are of a similar magnitude, showing ranges of –0.1 to –3.0 $mg \cdot m^{-2} \cdot d^{-1}$ and 0.01 to –1.2 $mg \cdot m^{-2} \cdot d^{-1}$ in DF49 and HDF00, respectively. The positive flux rate of 0.01 $mg \cdot m^{-2} \cdot d^{-1}$ observed during May is unlikely to represent true efflux rates. This assumption is based on the small flux value, the relatively ^{12}C-depleted $\delta^{13}CH_4$ value associated with the 5 cm [CH_4] measurement (-45.6 ‰), and the high standard deviation associated with this depth measurement (0.37). Thus, the calculated CH_4 efflux is likely due to spatial variation in near surface [CH_4] and minimal methanotrophy occurring within the soil.

Some temporal variation appears to be present, with both Equations showing the highest fluxes during the interval of June to August in DF49, with the lowest values observed in April and January. Within HDF00, Equations 2.5.1 and 4.1.1.3 show high fluxes during June to July, with lower values in early spring, fall, and winter.

Flux values from HDF88 are similar to those from HDF00 and DF49, ranging from 0.3 to -1.4 $mg \cdot m^{-2} \cdot d^{-1}$, and -0.1 to -1.5 $mg \cdot m^{-2} \cdot d^{-1}$, using Equations 2.5.1 and 4.1.1.3 respectively (Figure 32; see Table 9). Both equations show similar trends of low fluxes in spring, fall and winter, and a flux maximum present in August. As with HDF00, the positive fluxes calculated from 2.5.1 during April and May are probably artefacts of spatial variability in near surface [CH_4] values, coupled with minimal methanotrophic activity occurring at shallower soil depths.

CH_4 fluxes derived from Equation 4.1.1.3 are recalculated with near-ground CH_4 mixing ratios of 1.5 ppm and 1.8 ppm to determine their sensitivities to assumed near-

ground [CH_4] values. The recalculated fluxes occasionally showed some substantial differences, as compared with fluxes based on an assumed near-ground value of 1.8 ppm. With near-ground mixing ratios of 1.5 ppm, the recalculated fluxes are up to 5 times lower, while the substitution of a 2.3 ppm mixing ratio result in fluxes that are up to 4.3 times higher (see Table 10). However, as with OBS, actual variations in near-ground CH_4 are likely to be much lower than the 0.3 ppm variation used in these calculations, given that global seasonal variations in atmospheric CH_4 do not exceed 0.05 ppm (Quay, 1999).

Table10: Recalculated CH_4 fluxes derived from Eqn. 4.1.1.3, based on alternative near-ground [CH_4] values.

Site	Near-ground [CH_4] (ppm)	Fluxes ($mg \cdot m^{-2} \cdot s^{-1}$)						
		2006						2007
		Apr	May	Jun	Jul	Aug	Nov	Jan
DF49	1.5	-0.48	-0.70	-0.69	-1.65	-1.88	-0.20	-0.11
	1.8	-0.88	-1.33	-1.25	-2.93	-3.23	-0.26	-0.31
	2.3	-1.72	-2.66	-2.48	-2.79	-6.30	-0.34	-0.81
HDF88	1.5	-0.04	0.00	-0.27	-0.50	-0.61	-0.10	-0.05
	1.8	-0.12	-0.27	-1.03	-1.21	-1.49	-0.52	-0.22
	2.3	-0.31	-1.44	-3.06	-2.78	-3.38	-2.12	-0.94
HDF00	1.5	-0.30	-0.24	-0.44	-1.19	-0.65	-0.65	-0.70
	1.8	-0.68	-0.73	-0.87	-2.28	-1.09	-0.61	-0.66
	2.3	-1.56	-1.95	-1.87	-4.69	-4.34	-2.28	-2.48

Thus, the usage of the northern hemispheric CH_4 mixing ratio of 1.8 ppm is likely a suitable substitute for measured values in the Vancouver Island sites. While near-ground chamber measurements could have been used in substitution of this value, the observed variance in t = 0 [CH_4] within the same sampling period was as high as 0.24 ppm (within HDF00 during August 2006; see Figure 19 and Table A15 in appendix), making these measurements less suitable for the determination of CH_4 uptake rates averaged over larger areas.

To determine the influence of soil moisture and temperature on methanotrophic activity rather than diffusive gas movement through the soil column, flux estimates from all approaches are re-calculated with soil temperatures of 0 ^{o}C incorporated into the [CO_2] conversion factor calculations (from ppm to mg·m^{-3}) and the soil moisture fraction set at 0 % for the determination of D_s (see Table 11). Both variables are also accounted for due to an observed negative correlation between soil temperature and moisture (Figure 33). The adjusted fluxes are then plotted against observed soil temperature at 5 cm and averaged soil moisture content measured to 30 cm depth.

Table 11: CH_4 fluxes at all BC sites, adjusted for soil moisture and temperature variations

		Adjusted Fluxes (mg·m^{-2}·d^{-1})						
		2006						2007
Site	Method	Apr	May	Jun	Jul	Aug	Nov	Jan
DF49	Chamber 1	-2.66	-1.48	-6.96	-4.81	-1.42	-1.72	
	Chamber 2	-0.87	-2.18	-0.88	-5.06	-2.27	-2.59	
	Equation 2.5.1	-3.32	-3.31	-3.96	-4.02	-4.24	-4.74	-0.33
	Equation 4.1.1.3	-4.86	-4.52	-5.01	-6.83	-4.51	-1.07	-1.36
HDF88	Equation 2.5.1	0.00	0.00	-1.86	-1.99	-1.88	-2.26	-1.45
	Equation 4.1.1.3	-1.36	-0.56	-1.86	-1.78	-1.89	-1.48	-1.52
HDF00	Chamber 1	-3.91	-5.91	-5.66	-0.45	-0.81	-2.89	-1.38
	Chamber 2	-1.96	-0.07	-6.82	-2.08	-3.00	-0.76	-1.44
	Equation 2.5.1	-0.19	0.04	-1.81	-1.83	-1.08	-2.03	-0.90
	Equation 4.1.1.3	-2.21	-1.56	-2.24	-3.15	-1.34	-2.16	-2.18

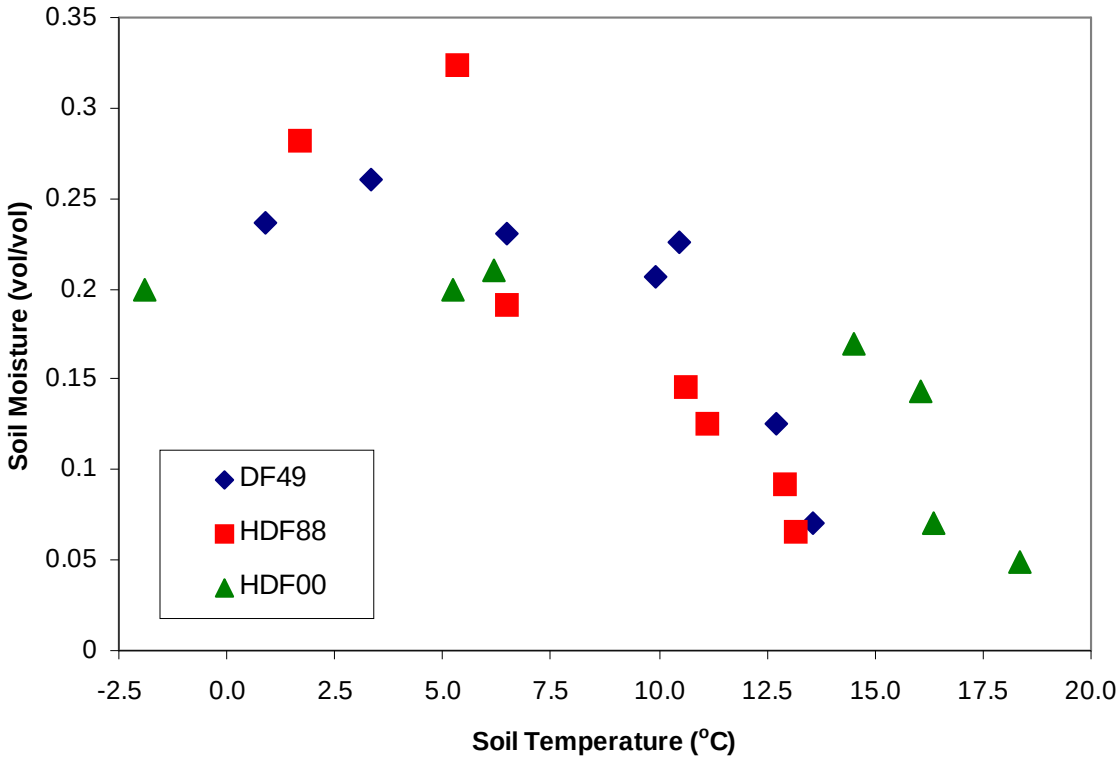

Figure 33: Relationships between soil moisture and temperature at all BC sites.

The chamber fluxes correlate poorly with soil moisture and temperature at both DF49 and HDF00, with $R^2 \leq 0.26$ for soil temperature and $R^2 \leq 0.43$ for soil moisture (Figure 34). Uptake rates calculated from Equation 4.1.1.3 also show poor correlation with both variables at all sites with $R^2 \leq 0.43$ for soil temperature and $R^2 \leq 0.26$ for soil moisture. As well, the CH_4 fluxes obtained from Equation 2.5.1 are poorly correlated to soil temperature ($R^2 \leq 0.20$) and soil moisture ($R^2 \leq 0.24$) (Figure 34), although trends of increasing uptake rates with increasing temperature, and decreasing uptake rates with increasing soil moisture are weakly apparent at DF49 and HDF88.

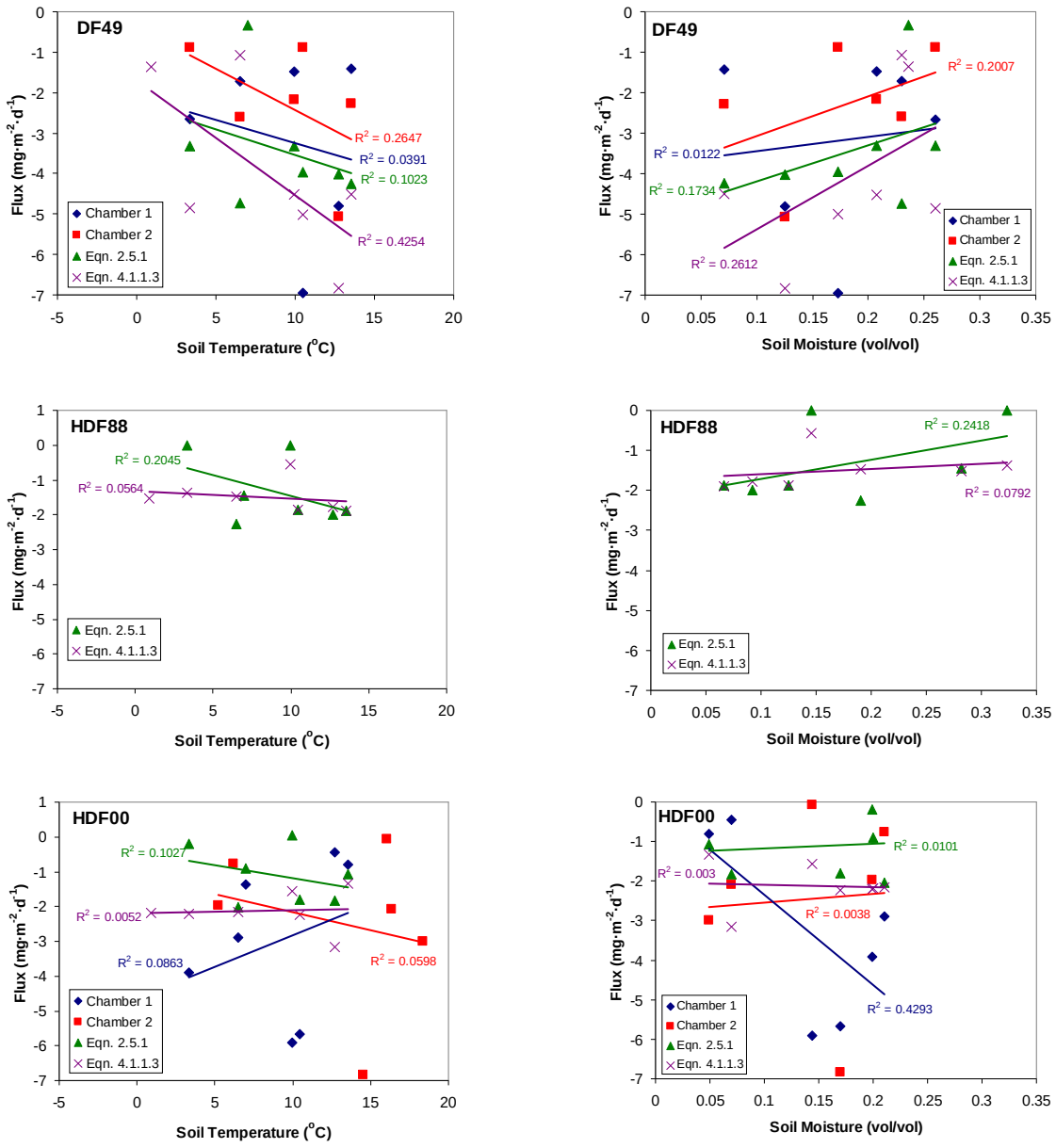

Figure 34: Correlations of BC fluxes with soil temperature and moisture.

These findings suggest that soil temperature and moisture yield only a minor influence on soil CH_4 uptake. However, the soil moisture values used are averaged measurements and especially in the case of the chamber measurements, these data may

not be representative of the areas being sampled. Soil temperature at 5 cm depth is likely to be more consistent as it is influenced mainly by ambient air temperature. It is possible that in this case, organic matter content holds a stronger influence on CH_4 uptake within the BC sites. A detailed assessment of soil organic matter spatial distribution in all BC sites may be required before any conclusion is certain.

Using Equation 4.1.1.2 and with the same assumptions applied to the OBS data (see Table A20 in appendix for curve-fitted concentration data), $\delta^{13}CH_4$ depth distributions are modeled for all months at HDF00, HDF88 and DF49 (Figures 35, 36, and 37). The modeled data compares well with observations during months when [CH_4] uniformly decreased with depth, and the range and standard deviation of calculated α_{ox} (average values of 1.021 ± 0.009, 1.027 ± 0.012 and 1.025 ± 0.004 at DF49, HDF88 and HDF00, respectively) is similar to the range of literature values (see Table 12). As well, the modelled data also show occasional ^{12}C-enrichment of subsurface CH_4, as seen in the observed $\delta^{13}CH_4$ depth profile.

This suggests that both diffusion and oxidation are the dominant processes at the BC sites during those periods. Thus, the occasionally ^{12}C-enriched CH_4 relative to atmospheric values may be due to the stronger influence of diffusive fractionation relative to methanotrophic activity within certain depths (see Figures 35, 36 and 37).

Table 12: Calculated α_{bio} values at all BC sites

	Biological Carbon Isotope Fractionation Factor (α_{bio})						
	2006						2007
Site	Apr	May	Jun	Jul	Aug	Nov	Jan
DF49	1.015	1.032	1.016	1.025	1.012	1.015	1.032
HDF88	1.021	1.054	1.026	1.020	1.020	1.026	1.023
HDF00	1.026	1.023	1.032	1.026	1.022	1.025	1.021

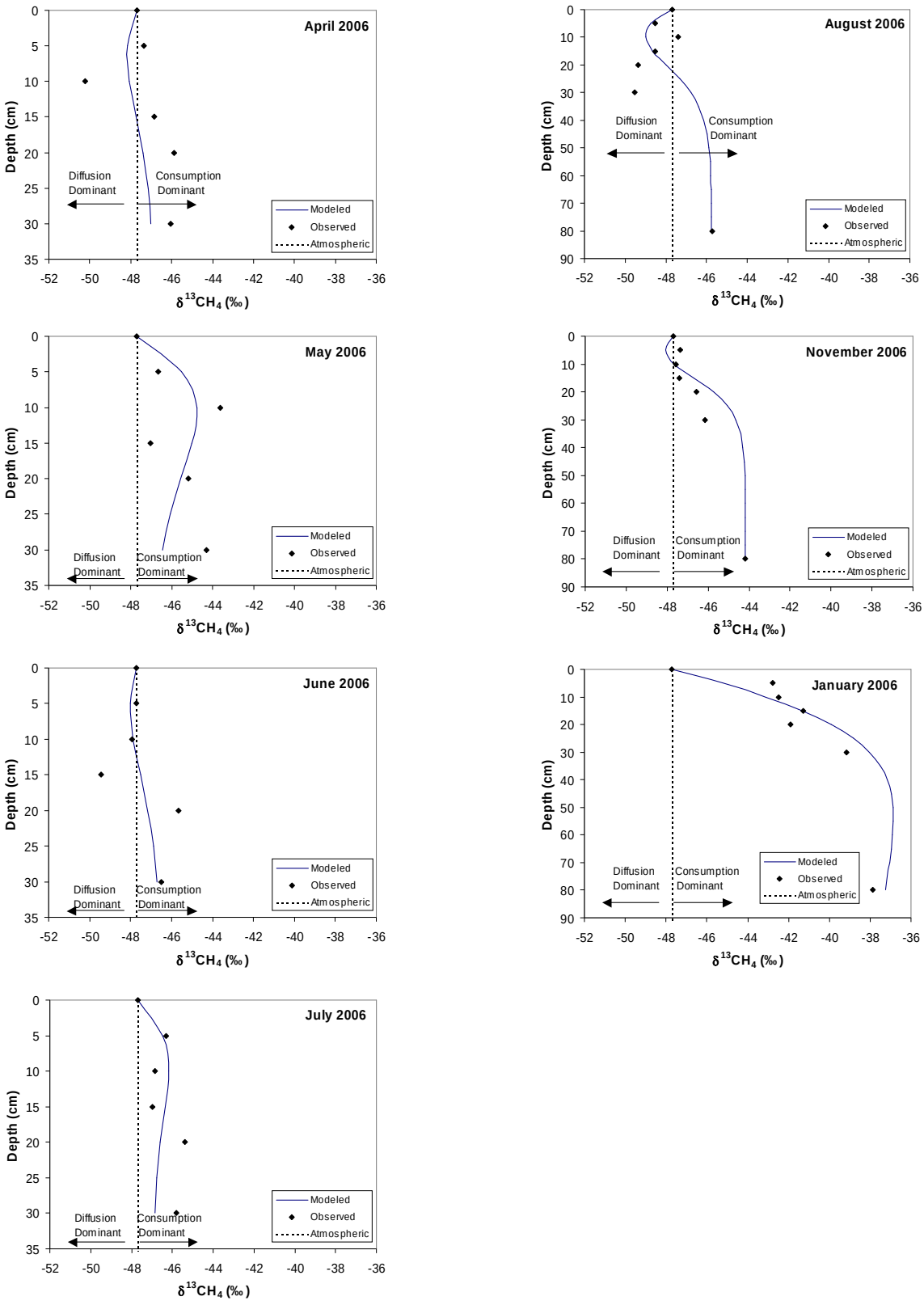

Figure 35: Comparisons between modeled (lines) and observed (points) $\delta^{13}CH_4$ at DF49.

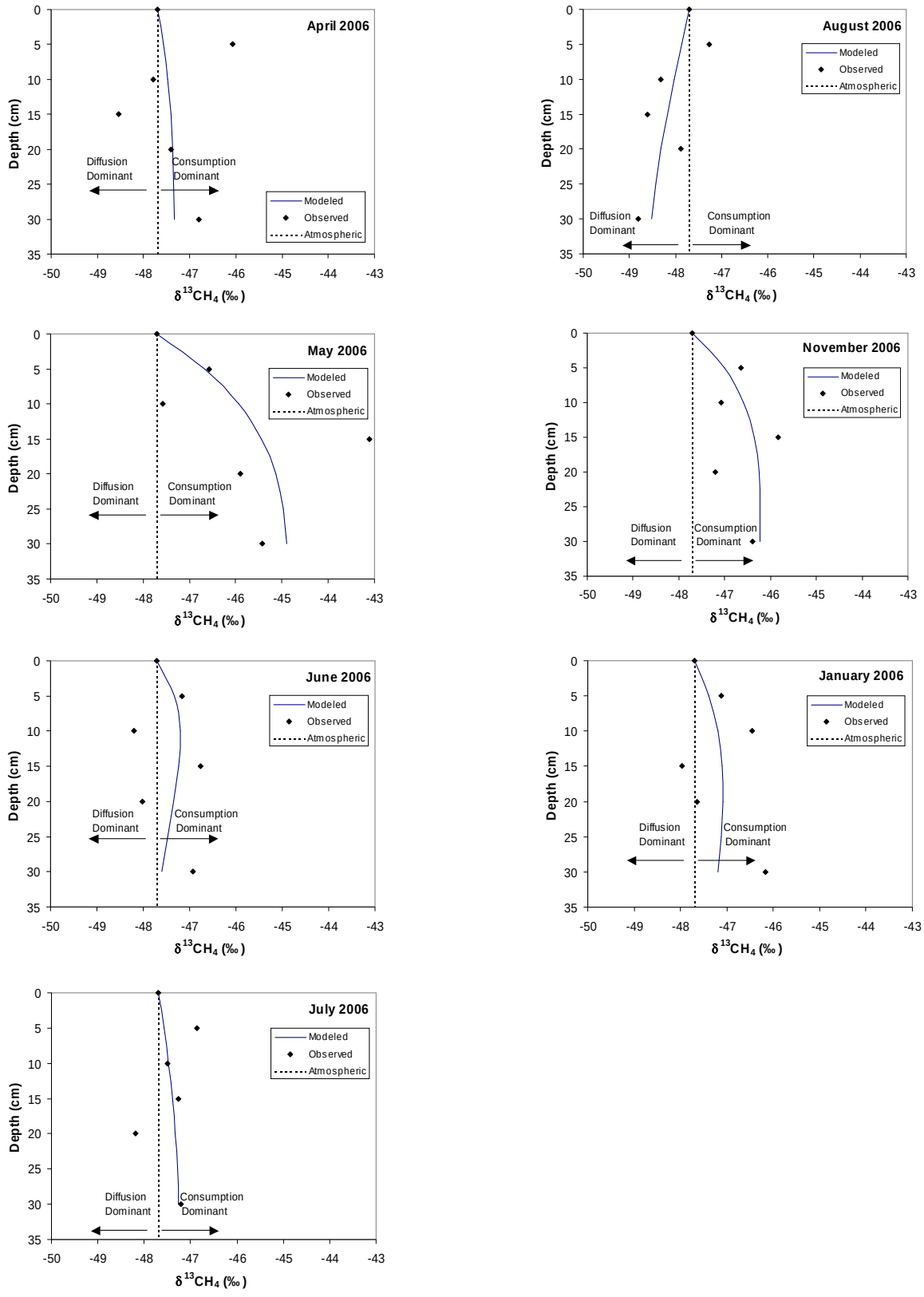

Figure 36: Comparisons between modeled (lines) and observed (points) $\delta^{13}CH_4$ at HDF88.

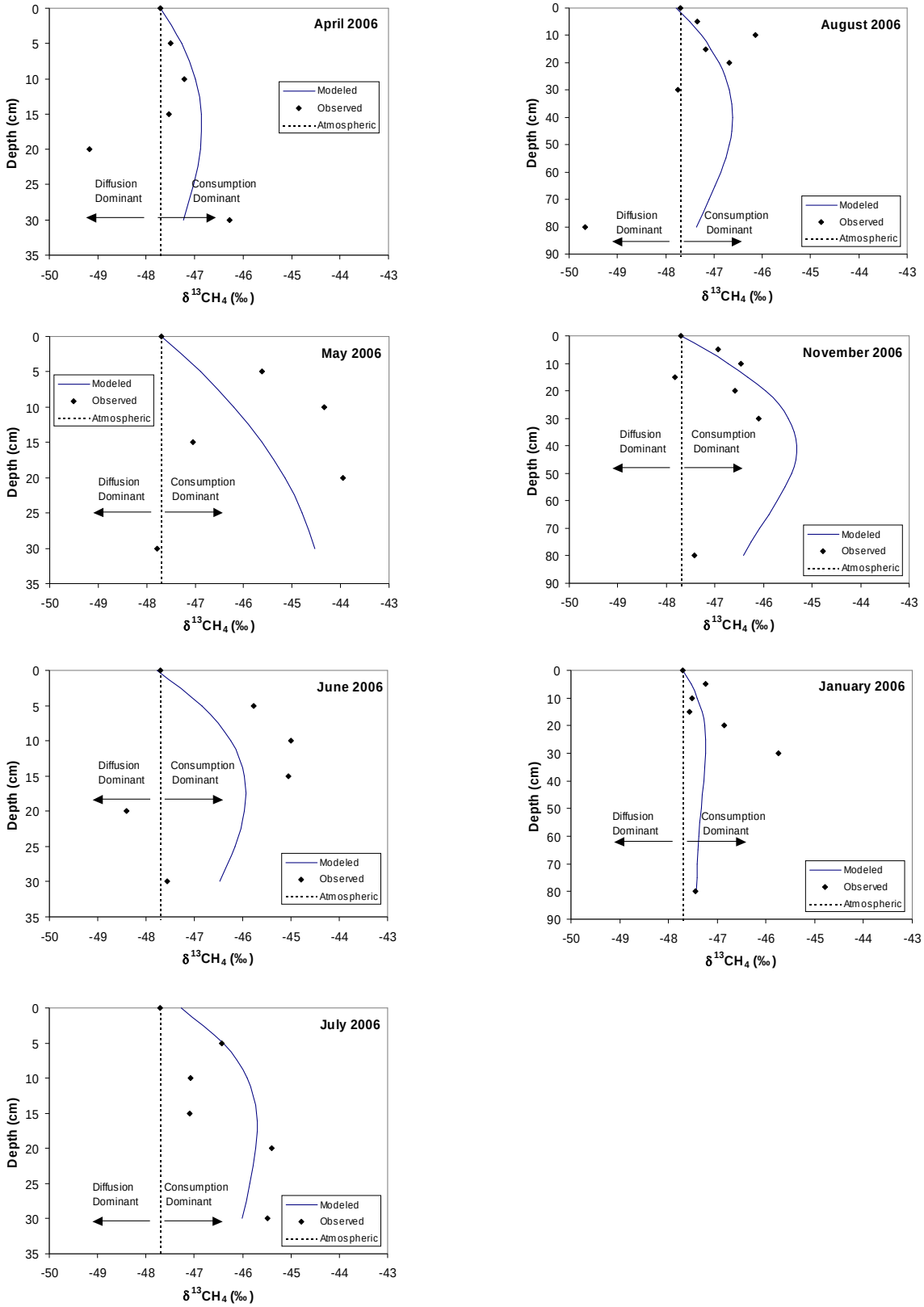

Figure 37: Comparisons between modeled (lines) and observed (points) $\delta^{13}CH_4$ at HDF00.

Equation 4.1.1.2 is unable to fully fit the large ^{12}C-enrichment in HDF00 at 80 cm depth, although a lower ^{12}C-enrichment below 40 cm is still predicted. Assuming that some degree of ^{12}C-enrichment may occur at deeper depths in HDF00, this could be accounted for by the dominance of diffusive fractionation in the absence (or near absence) of methanotrophic activity within that depth range.

Alternatively, methanogenic activity deeper in the soil may be responsible for the presence of ^{12}C-enriched CH_4. However, without an additional 80 cm measurement (with only one viable sample being available for analysis) and in light of the large standard deviations obtained from shallower depths, it is unclear whether the magnitude of the observed ^{12}C-enrichment at 80 cm is actually a genuine feature or an artefact of intra-site variation in $\delta^{13}CH_4$.

Given the larger data scatter within the upper 30 cm of soil, Equation 4.1.1.2 show weaker fits with data sets where the 80 cm depth samples were absent. In any case, the observed $\delta^{13}CH_4$ depth trends are tracked approximately by the modeled depth profiles for $\delta^{13}CH_4$. This indicates that there is a general correspondence of the data with the diffusion/consumption model in most instances.

In the above discussion, exponential trends of $[CH_4]$ decreases with increasing depth are fitted for all datasets. However, during certain periods at DF49 (April, May and July 2006) and HDF00 (April to July 2006), $[CH_4]$ increases with depth below a trend of decreasing $[CH_4]$ in shallower depths. The apparent concentration increases are not associated with more ^{12}C-enriched $\delta^{13}CH_4$ values, as would be expected from methanogenic activity (either via methyl fermentation or carbonate reduction pathways). However, the large sampling standard deviation found in both DF49 and HDF00

indicates that the apparently increasing [CH_4] may be an artefact of intra-site variation and are not representative of true [CH_4] trends.

Using both observed and modelled [CH_4], F_{ox} was calculated using the method described previously (see Section 4.1.1). As with OBS, the calculated values show the largest fraction of CH_4 being oxidized at 5 cm depth, with a general decrease in F_{ox} with depth (Figures 38, 39 and 40). Negative F_{ox} values are occasionally present, although this is likely due to the large standard deviations present in the depth profile [CH_4] measurements.

The observed [CH_4] values also show decreases in F_{ox} as depth increases. Occasionally, observed F_{ox} at 80 cm depth within DF49 and HDF00 are as much as five times larger than that observed at 30 cm. As with the OBS data, this is likely a result of the larger depth interval between 30 cm and 80 cm, as compared to shallower depths (see section 4.1.1).

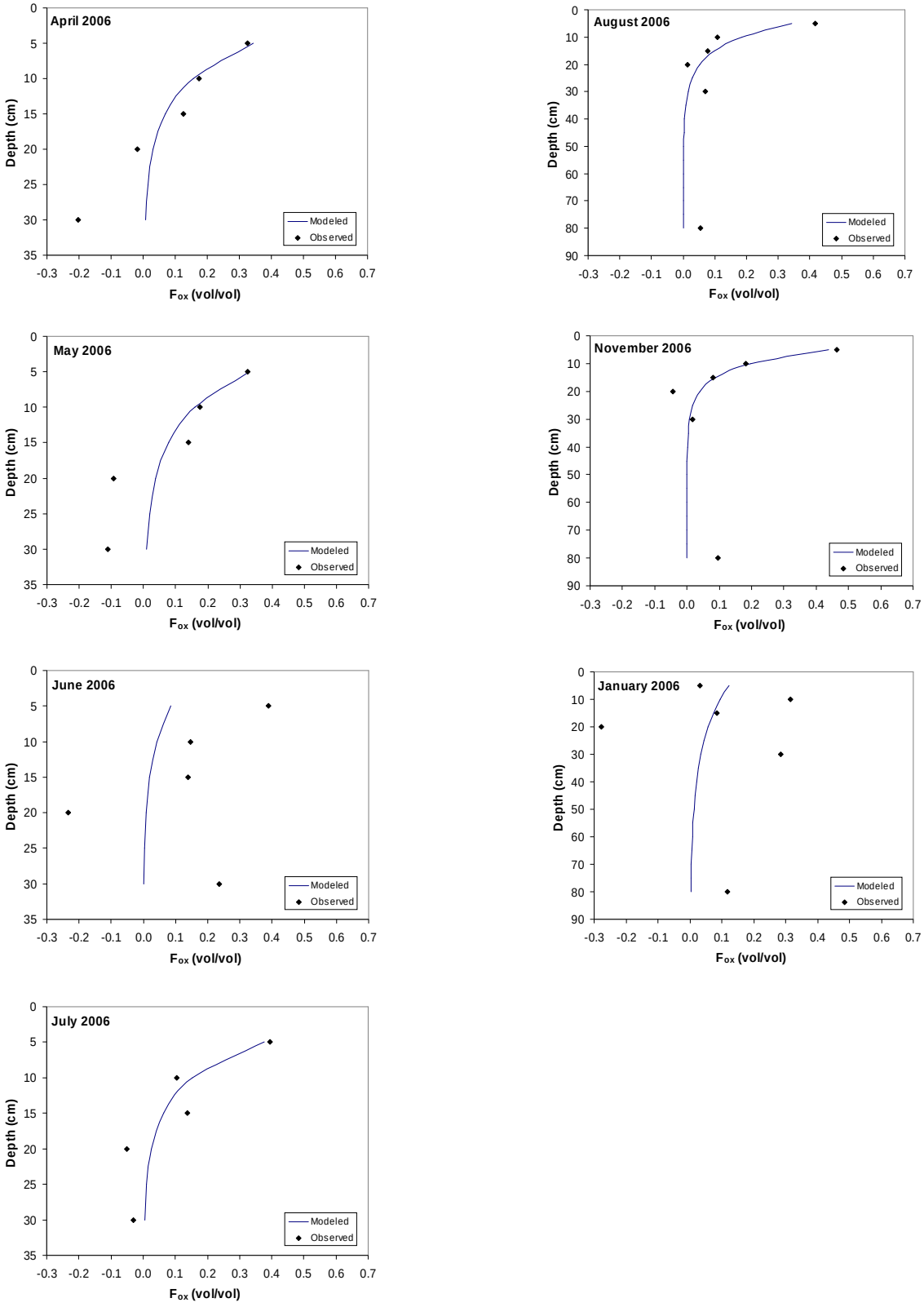

Figure 38: Comparisons between modeled (lines) and observed (points) F_{ox} at DF49.

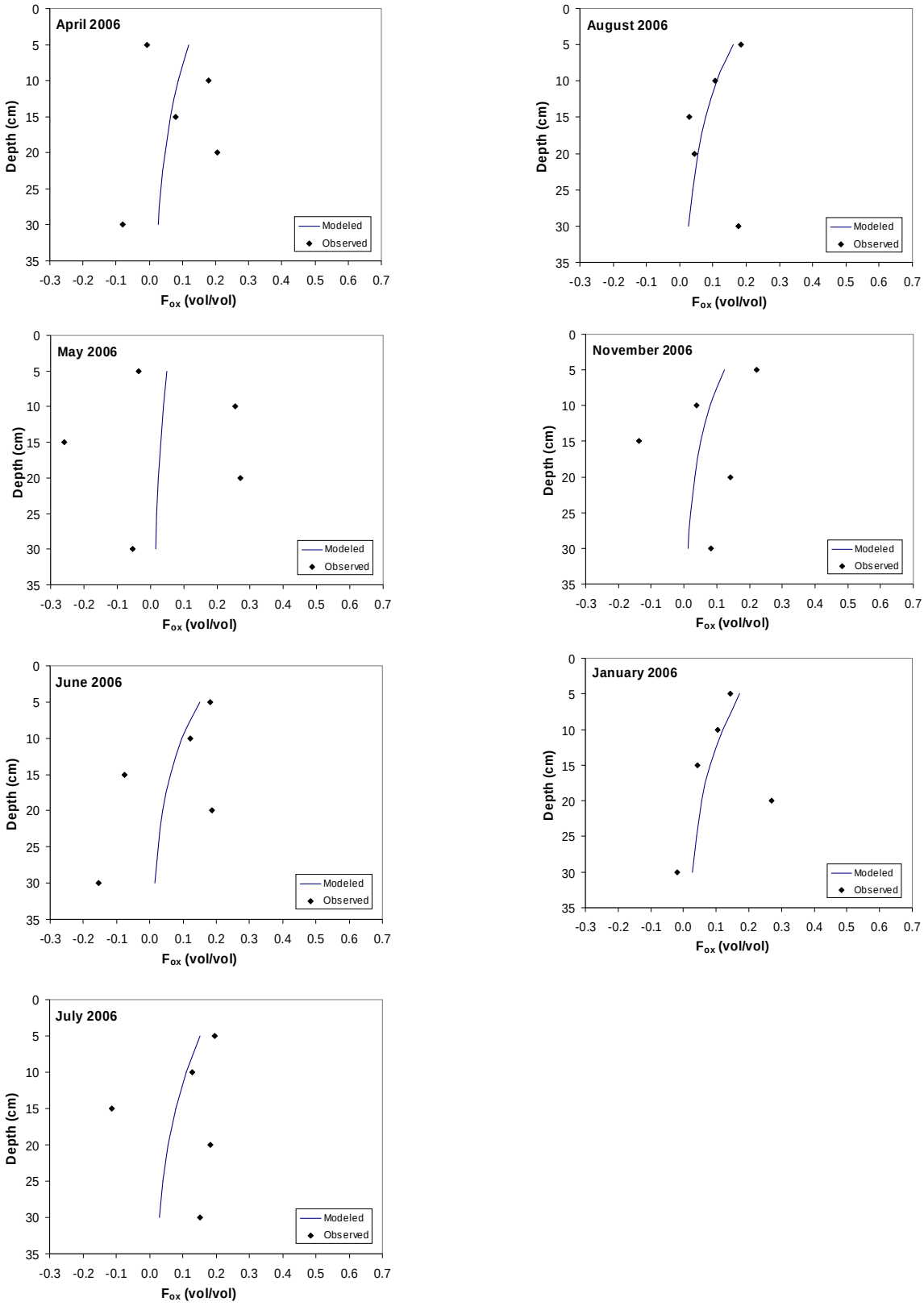

Figure 39: Comparisons between modeled (lines) and observed (points) F_{ox} at HDF88.

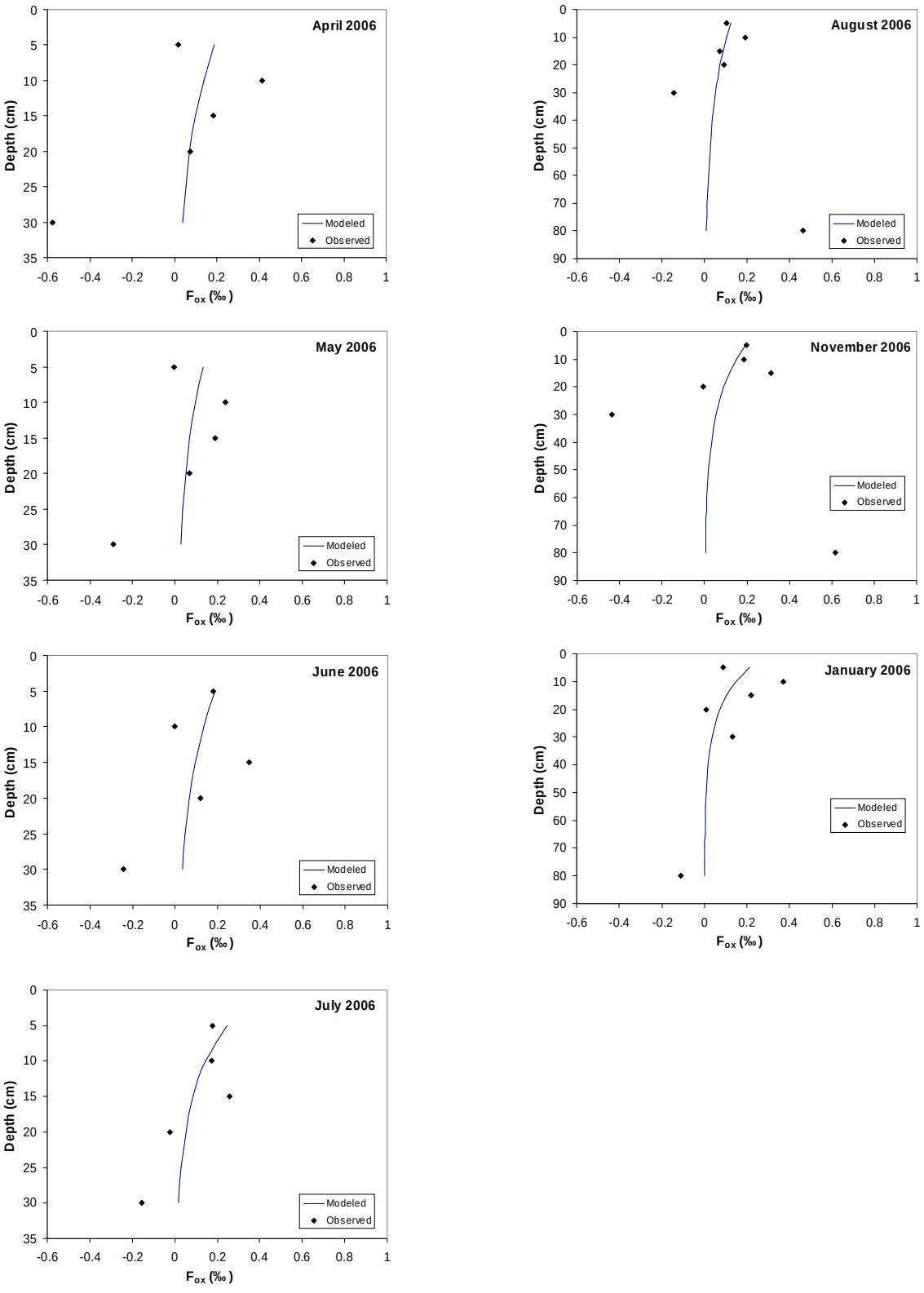

Figure 40: Comparisons between modeled (lines) and observed (points) F_{ox} at HDF00.

Cross-plots of $\delta^{13}CO_2$ vs. $\delta^{13}CH_4$ constructed for all sites show that most of the data lies in the region of methane oxidation in Figures 41 and 42. The apparent magnitude of methane oxidation is not constant from month to month, however, and some months show the majority of data points trending towards atmospheric values. This pattern of scatter is most apparent during August, November and January. As with OBS, the stronger expression of diffusive fractionation during certain months may be the reason for this trend. While mixing between soil and near-ground air could also be a factor, the wet conditions encountered in November and the observed January snow cover makes this a less likely possibility.

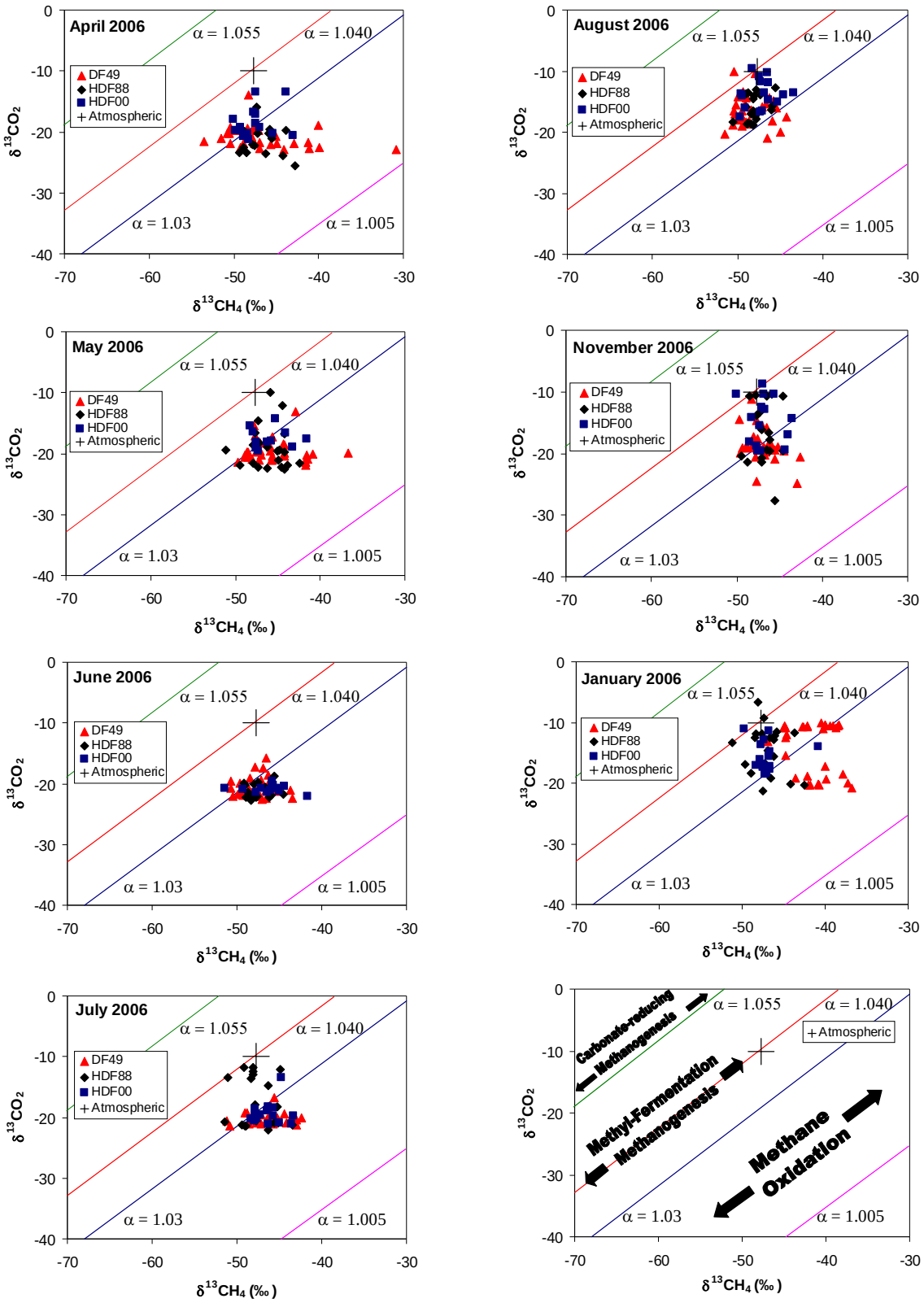

Figure 41: Site-based $\delta^{13}CO_2$-$\delta^{13}CH_4$ cross plot for all BC sites and sampling periods, with a blank plot for reference.

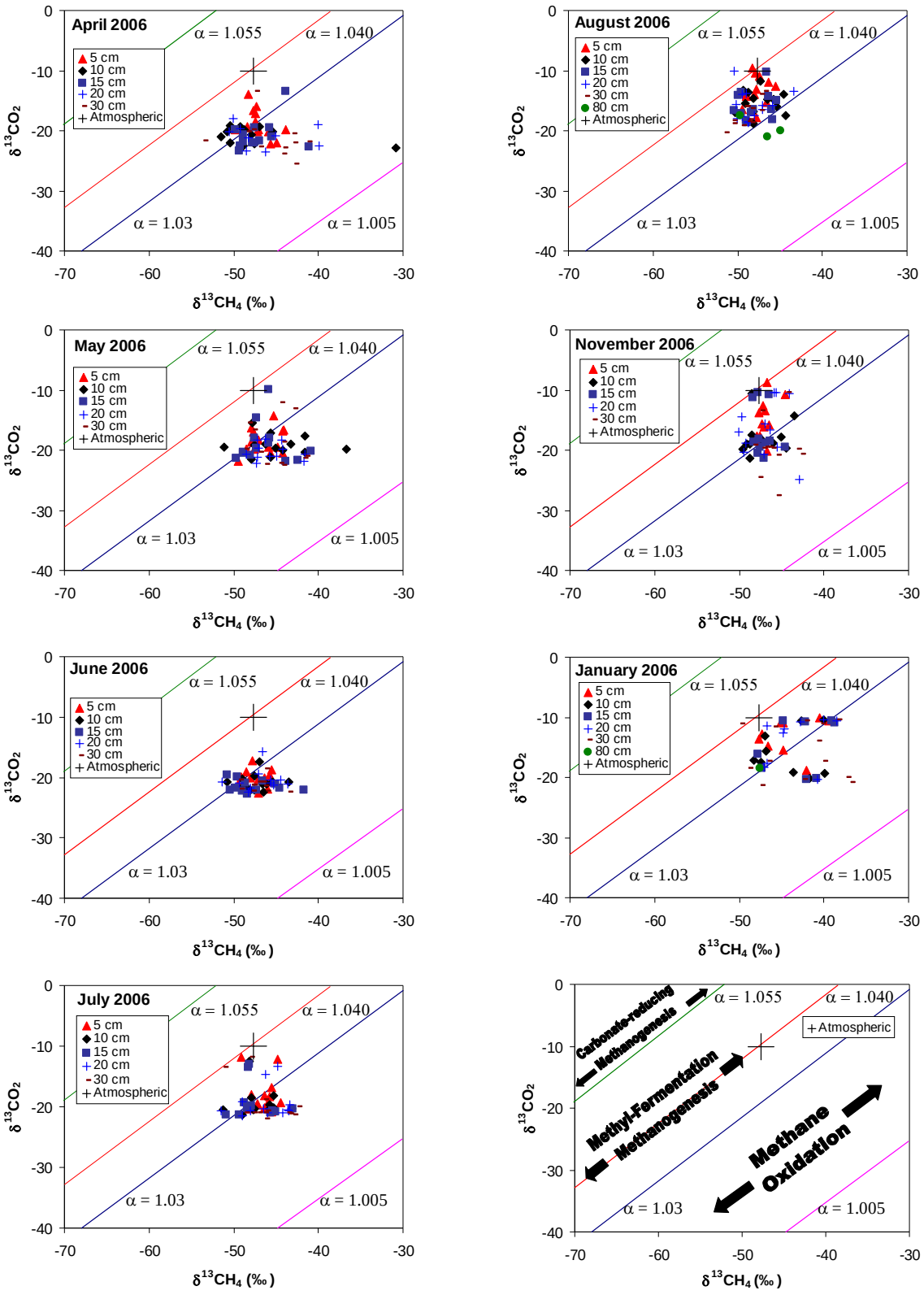

Figure 42: Depth-based $\delta^{13}CO_2$-$\delta^{13}CH_4$ cross plot for all BC sites and sampling periods, with a blank plot for reference.

4.1.3 Comparison of BC and OBS: Inter-site Differences in CH_4 Cycling

The similar uptake rates averaged over the entire sampling season from the DF49 and HDF00 chambers (-2.3 to –3.0 $mg \cdot m^{-2} \cdot d^{-1}$ and –2.2 to 2.9 $mg \cdot m^{-2} \cdot d^{-1}$ at DF49 and HDF00, respectively) suggest that forest age has a minimal influence on CH_4 uptake in temperate forest environments. Although the absence of chamber fluxes at HDF88 make comparisons with DF49 and HDF00 less certain, Equations 4.1.1.3 and 2.5.1 suggests that fluxes within HDF88 (0 to -1.40 $mg \cdot m^{-2} \cdot d^{-1}$ and 0 to -1.50 $mg \cdot m^{-2} \cdot d^{-1}$ using 2.5.1 and 4.1.1.3, respectively) are generally within the same magnitude as those from DF49 (-0.1 to – 3.0 $mg \cdot m^{-2} \cdot d^{-1}$ and -0.3 to -3.2 $mg \cdot m^{-2} \cdot d^{-1}$ using 2.5.1 and 4.1.1.3, respectively) and HDF00 (0 to -1.2 $mg \cdot m^{-2} \cdot d^{-1}$ and -0.6 to -2.3 $mg \cdot m^{-2} \cdot d^{-1}$, using 2.5.1 and 4.1.1.3, respectively) (Figure 43).

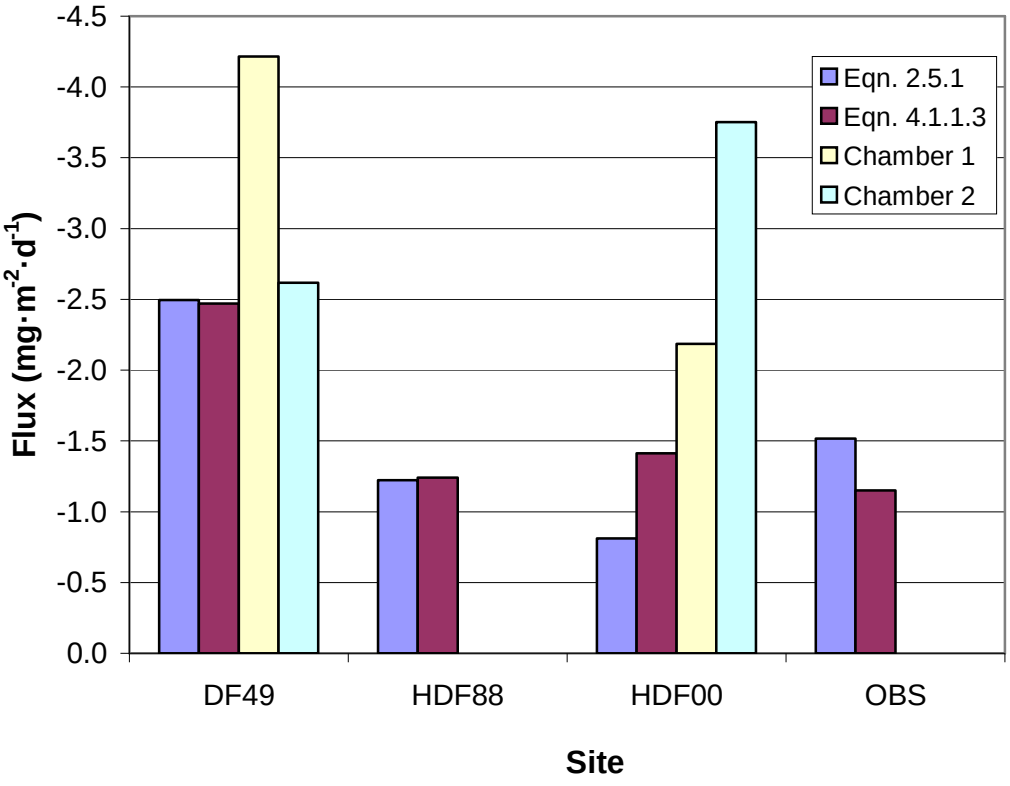

Figure 43: Comparison of maximum CH_4 fluxes at all sties.

Flux rates in OBS calculated by the same method also show a similar range as the BC estimates (-1.5 to -2.3 $mg \cdot m^{-2} \cdot d^{-1}$ and -1.6 to -2.2 $mg \cdot m^{-2} \cdot d^{-1}$, using 2.5.1 and 4.1.1.3, respectively). All sites show the same feature of occasionally ^{12}C-depleted $\delta^{13}CH_4$ relative to atmospheric present in the upper 30 cm of soil during certain times in the summer, showing that diffusive isotopic fractionation may be significant at all sites.

Methanotrophic activity in different locations may only show strong variation with larger differences in short-term soil moisture and temperature values. In the case of OBS and the BC sites, soil moisture and temperature were similar between all locations during the periods of sampling, resulting in similar uptake rates. The similarity of fluxes

between the Vancouver Island sites and OBS suggests that methane uptake is also insensitive to the climatic differences that exist between boreal and temperate forest biomes.

Based on the fluxes calculated from the chamber and depth profile measurements across all BC sites, the largest observed uptake rates are sufficient to completely consume a cubic metre of atmospheric CH_4, per square meter of surface area, within the space of 10 to 21 hours. If this 1 m by 1 m volume of air is extended to the height of the troposphere (average of about 11 km in the middle latitudes; Danielson, Levin and Abrams, 2003), then the range of consumption times span 12 to 26 years for complete consumption of tropospheric methane within that volume of air (Table 13).

Table 13: Estimated consumption times of atmospheric CH_4

Flux Determination	Maximum Fluxes	Time of Consumption	
	($mg \cdot m^{-2} \cdot d^{-1}$)	m^3 Air Volume (hrs)	m^2 x Tropospheric Altitude (years)
Static Chamber	-6.70	4.45	5.59
Eqn. 2.5.1	-3.04	9.80	12.30
Eqn. 4.1.1.3	-3.23	9.22	11.58

Using an estimated total forest area of 64.1 hectares within BC (Natural Resources Canada, 2001), the flux rates calculated in this study can be extrapolated to represent province-wide annual uptake rates. Assuming that site DF49 is the most representative example of a BC forest, due to its age as compared to the other sites, annually averaged fluxes based on both chamber and depth profile measurements (-2.65, -1.5 and –1.7 $mg \cdot m^{-2} \cdot d^{-1}$ based on chamber measurements, Equation 4.1.1.3 and 2.5.1,

respectively) indicates that roughly 3 to 6 metric tons of CH_4 is consumed each year by BC forest soils (Table 14).

Table 14: Estimated mass of CH4 consumed annually in BC and Canadian Forests

Flux Determination	Averaged Fluxes ($mg \cdot m^{-2} \cdot d^{-1}$)	Annual Mass of CH_4 consumed (tons)	
		BC Forest Area (64.1 ha)	Total Canadian Forest Area ($3.1x10^6$ ha)
Static Chamber	-2.65	6.21	3002203.66
Eqn. 2.5.1	-1.75	4.09	1978612.37
Eqn. 4.1.1.3	-1.45	3.40	1646121.92

This is a negligible fraction of the total estimated CH_4 output from BC during 2005, which is estimated at 460,000 metric tons per year in (Environment Canada, 2005). However, if the averaged CH_4 uptake rate from DF49 is extrapolated to the total Canadian forest area (301,000 hectares; Natural Resources Canada, 2001), which results in an estimate of 1.6 to 3.0 Mt of CH_4 consumed per year, the role of Canada's forests as CH_4 sinks becomes mores significant (Table 14).

Based on the 2005 national CH_4 emission estimate of 5.2 Mt, the quantity of CH_4 consumed by forest soils is about 30 % to 60 % of total Canadian CH_4 output (Table 14 and Figure 44). Although admittedly rough estimates of annual CH_4 uptake are used, as data for 5 months were unavailable, these averaged values are still useful in giving a general picture of the significance of forest soil CH_4 uptake within Canada.

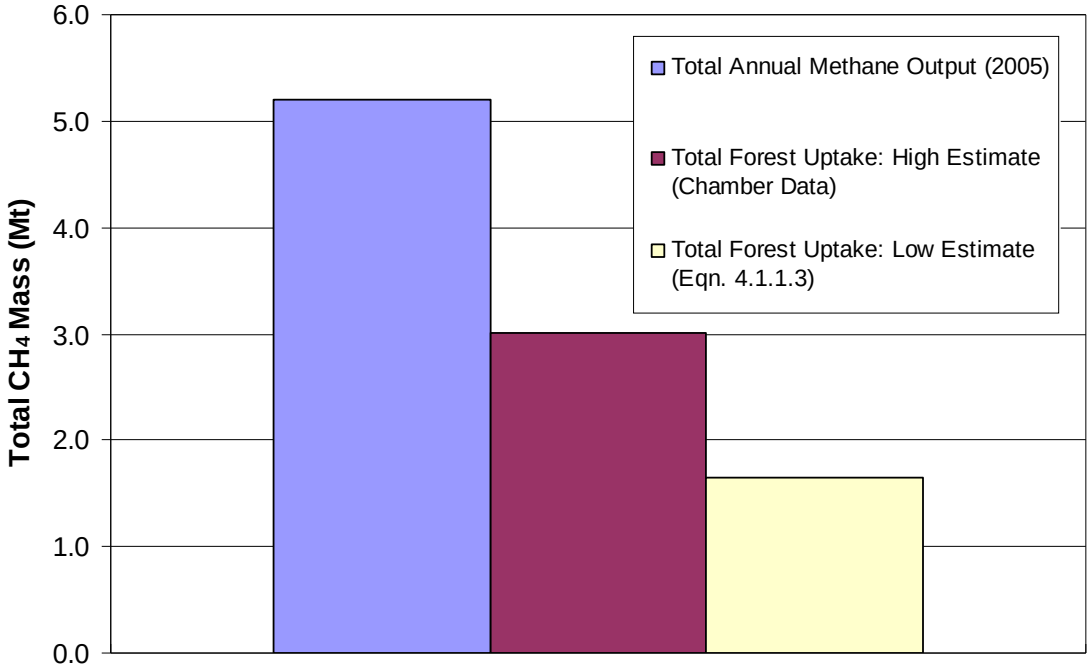

Figure 44: Comparison of estimates of total CH_4 consumed in Canadian forest soils to the total national output of CH_4 (see Table 14 for data).

It is unclear how the continuing rise in global temperatures will affect CH_4 uptake in forest soils. However, given the minimal correlation of CH_4 uptake rate with soil temperature found in this study and in previous research (Dörr, 1993; Castro et al., 1995; Ridgwell et al, 1999), the prospect of large changes in the strength of this CH_4 sink due to higher temperatures appears unlikely. The importance of forest soils as a CH_4 sink will instead depend on current trends in CH_4 emissions, which will either diminish or increase the significance of forest-soil sinks depending on future CH_4 emission rates.

4.2 CO_2 Cycling

4.2.1 CO_2 Dynamics in OBS

The $\delta^{13}CO_2$ and $[CO_2]$ data from the Quebec soil profiles suggests that net production of CO_2 is occurring within the soil. The observed $\delta^{13}CO_2$ range of -20 ‰ to -21 ‰ at 80 cm in OBS is ^{12}C-enriched relative to the $\delta^{13}CO_2$ above the ground surface (based on the averaged near-ground value of –10 ‰; see section 2.4), which is indicative of soil CO_2 produced via heterotrophic and rhizospheric respiration. This is supported by the observed concentration changes, whereby a higher concentration would be expected at deeper depths where CO_2 production is prevalent and the influence of atmospheric CO_2 minimal, as seen in the soil profile data.

A Keeling-type, two component mixing plot of soil $\delta^{13}CO_2$ versus $[CO_2]^{-1}$ using OBS data reveals strong relationships between $\delta^{13}C$ and concentration (Figure 44; see section 1.4). A geometric mean regression is fit to the data (GMR Model II; Sokal and Rohlf, 1995) rather than a simple linear regression, as past studies show that the latter tends to bias the slope value towards smaller values (Sokal and Rohlf, 1995; Pataki et al., 2003). The GMR method involves taking a slope value obtained via linear regression and then dividing it by the R-coefficient of the x and y variables to obtain a revised slope value, from which a new Y-intercept value can also be obtained (Pataki et al., 2003).

The plotted data is then compared to a reference mixing line, using an average $\delta^{13}C$ of previously measured bulk organic matter values minus a 4.4 ‰ ^{12}C-depletion from diffusive fractionation (-23.5 ‰; see Table 15, data courtesy of L. Flanagan), and

averaged near-ground $\delta^{13}CO_2$ and $[CO_2]$ values of -10 ‰ and 433 ppm as the two endmembers.

Table 15: Bulk organic matter $\delta^{13}C$ data from the Fluxnet-Canada database, courtesy of L. Flanagan.

Site	Year	Dominant Species	Replicate	$\delta^{13}C$ (‰)
OBS	2005	*Picea Mariana* (Black Spruce)	1	-26.38
			2	-28.55
			3	-28.01
			4	-28.31
			5	-27.73
			6	-28.15
Average				**-27.86**

Using this method, the OBS data reveals a consistent Y-intercept across all sites and months, with soil $\delta^{13}CO_2$ values of –21.35 ‰, -23.83 ‰, and -22.90 ‰ observed in early June, August, and late August respectively. The average Y-intercept value of all sampling periods is –22.69 ± 1.25 ‰. Differences between the $\delta^{13}C$ of plant organic matter and the estimated $\delta^{13}C$ of soil respired carbon range from 4.0 ‰ to 6.5 ‰, and are similar to the 4.4 ‰ diffusional enrichment found by Cerling (1991).

However, many of the linear regression slopes are steeper than expected for mixing between soil organic matter and atmospheric CO_2 endmembers. Compared to a reference slope based on assumed two-endmember mixing, Keeling-plot slopes retrieved from the OBS data (Figure 45) are up to 37 % larger than the expected value. This implies that at atmospheric concentrations, $\delta^{13}CO_2$ is more ^{12}C-depleted than expected from two-component mixing between soil-derived and near-ground CO_2. Alternatively,

the steeper slope could also suggest that larger-than-expected proportions of near-surface CO_2 with atmospheric $\delta^{13}CO_2$ values exist at OBS.

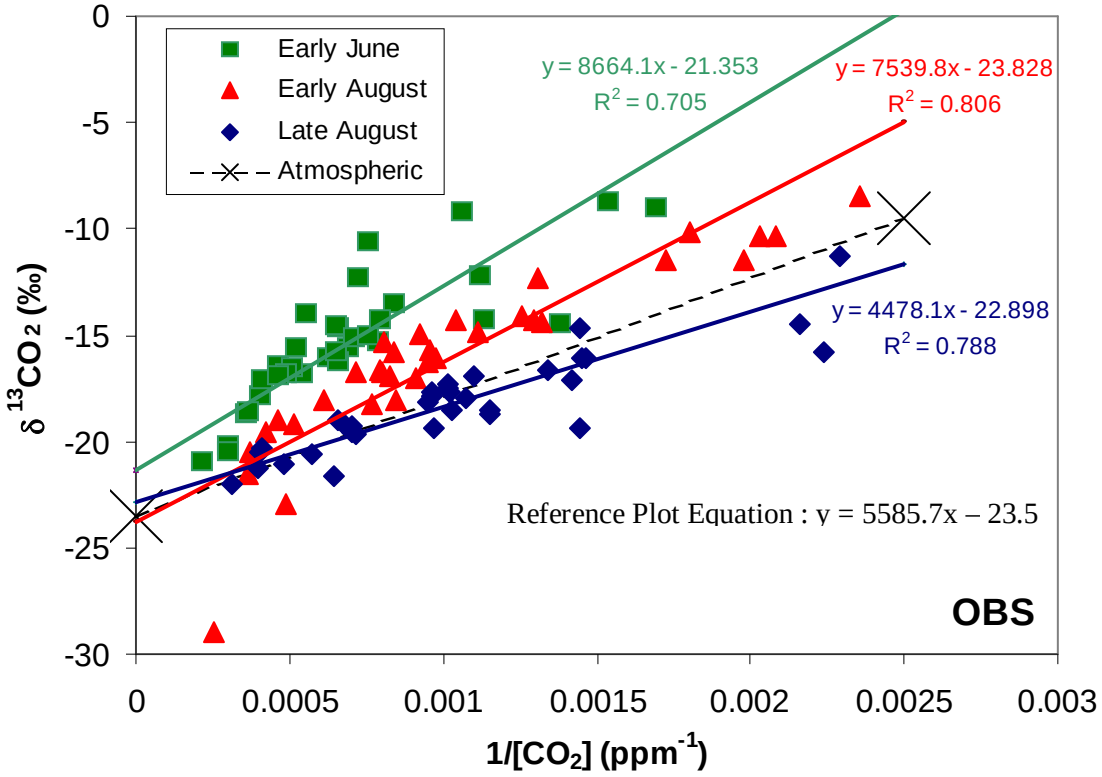

Figure 45: Keeling-type plot for the OBS data.

To assess the validity of a two-endmember mixing model, organic and atmospheric contributions to soil CO_2 are estimated by two approaches and the results compared. The first method is a simple subtraction of atmospheric [CO_2] (as before, using 0.5 m [CO_2] data from the Fluxnet database) from the observed soil [CO_2], and dividing the resulting value by 0.5 m measurements in order to obtain a fraction of soil derived CO_2 (F_{org}).

The second method utilizes a formula derived from the following basic mass-balance Equation (modified from Fry, 2006):

$$\delta_z = \left[\delta_{atm} \bullet (1 - F_{SOM})\right] + \delta_{SOM} F_{SOM} \qquad (4.2.1.1)$$

Where the subscripts *atm* and *SOM* denotes sub-canopy atmospheric values and soil organic carbon respectively and z represents soil depth (measured positively downwards). The δ_{SOM} values used in Equation 4.2.2.1 were derived from the observed Keeling-Plot intercepts for the appropriate period of sampling (see Figure 43).

Available $\delta^{13}CO_2$ and $[CO_2]$ data that was collected 1 m above the ground during May to August of 2005 (Fluxnet-Canada database, courtesy of L. Flanagan) is used to construct a Keeling Plot (Figure 46) that reveals a good linear fit between $\delta^{13}CO_2$ and $[CO_2]^{-1}$.Using this linear relationship, $\delta^{13}CO_2$ values are then estimated from the 0.5 m $[CO_2]$ measurements that were recorded during the times of sampling (see Table 6; data courtesy of Hank Margolis).

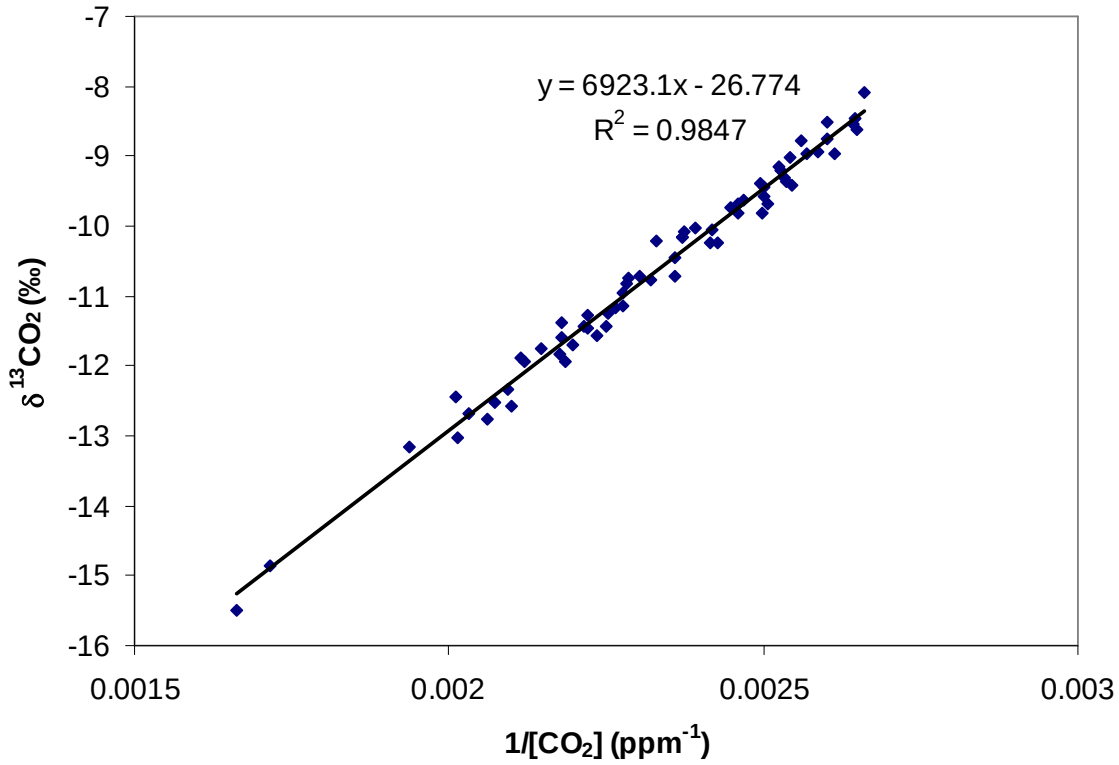

Figure 46: A Keeling Plot constructed using OBS CO_2 measurements from 2005, collected over the period of DOY 143-280 (data courtesy of L. Flanagan).

During late August, Equation 4.2.1.1 showed good agreement with concentration-based F_{org} estimates throughout the depth profile (Figure 47; see Table 16). Trends in early June and August obtained from Equation 4.2.1.1 were more divergent, showing F_{org} values that were consistently lower than the concentration-based estimates within the 0 to 30 cm depth range. Both early June and early August showed smaller divergences at 80 cm depth, in comparison to the shallower depths. However, both F_{org} estimates suggest a greater influence of ambient CO_2 at shallower depths, with larger percentages of SOM-derived CO_2 deeper in the soil column.

Table 16: F_{org} estimations, using observed values and Equation 4.2.2.1

Method of F_{org} Estimation	Depth (cm)	F_{org} (vol/vol) Late June 2005	Early August 2005	Late August 2005
Concentration-based	5	0.63	0.58	0.35
	10	0.74	0.68	0.46
	15	0.74	0.49	0.45
	20	0.76	0.64	0.69
	30	0.84	0.74	0.55
	80	0.89	0.87	0.79
Isotope-based (Eqn. 4.2.1.1)	5	0.24	0.38	0.36
	10	0.45	0.58	0.45
	15	0.48	0.24	0.48
	20	0.48	0.41	0.67
	30	0.70	0.50	0.42
	80	0.84	0.97	0.83

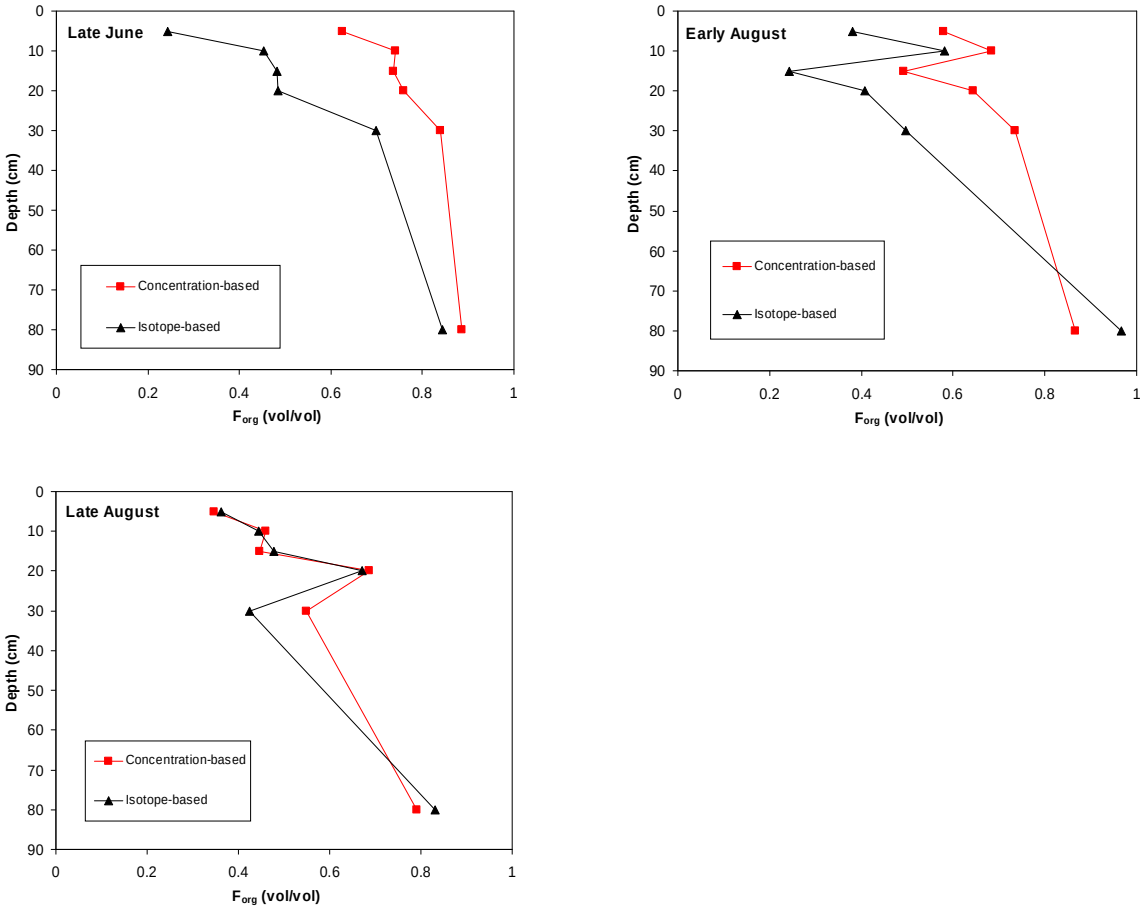

Figure 47: F_{org} profiles in OBS during all periods of study.

As with the Keeling-type plots, the discrepancies between isotope-based and concentration-based F_{org} demonstrate that during certain time periods, either near-surface $\delta^{13}CO_2$ values are heavier than expected or the proportions of near-surface CO_2 (with corresponding atmospheric $\delta^{13}CO_2$ values) are greater than anticipated. Neither conclusions support the application of the atmosphere-SOM mixing model within OBS. The lack of agreement using this simple two-endmember Keeling mixing approach implies that an additional CO_2 endmember is contributing to the CO_2 mass balance.

This CO_2 is either in the form of an additional CO_2 source or sink. The similarity of calculated and observed F_{org} values at 80 cm show that if a third influence on soil CO_2 exists, it is likely present nearer to the soil-atmosphere interface. One postulation is that the CO_2 is potentially derived from oxidized methane, although this would result in the production of ^{12}C-depleted CO_2, which would be 5 ‰ to 20 ‰ more ^{12}C-depleted than precursor materials (see Section 1.4). As the precursor in this case is atmospheric methane, the $\delta^{13}CO_2$ of the produced gas would range from –53 ‰ to –68 ‰, which is far more ^{12}C-enriched than the observed Keeling Plot Y-intercepts.

In addition, the quantities of CO_2 created by oxidized CH_4 would be negligible, since the total amount of CO_2 derived from CH_4 oxidation would be no greater than the atmospheric mixing ratio (1.8 ppm). This amount is only 0.3 % of the lowest observed subsurface CO_2 concentration: 570 ppm at 20 cm depth, within HDF00 during November 2006. Therefore, in light of these small contributions and the ^{12}C-enriched signature of CO_2 derived from CH_4 oxidation, methanotrophic activity is an unlikely influence on the observed Keeling-plot variations.

Another possibility is the influence of CO_2 input contributed by reactions of dissolved carbonates within the soil. While direct measurements of soil carbonate are unavailable at OBS, the acidic soil conditions at OBS (pH = 4; Prevost, 2004) suggests that any amount of subsurface carbonate present at that site is minor. Thus, contributions of CO_2 from carbonate reactions are probably too small to affect the mixing line as observed.

The Keeling plots could show the presence of a CO_2 sink that is acting to fractionate the CO_2 in such a way to leave a relatively ^{12}C-depleted pool of residual CO_2. This ^{12}C-depleted CO_2 would be mixed with the atmospheric and soil-derived CO_2, resulting in a more ^{12}C-depleted near-ground endmember as compared to simpler two-endmember atmosphere-soil organic matter mixing. As an arbitrary example, if a sink were present near the soil surface that acted to reduce near-ground CO_2 by 100 ppm and create a ^{12}C-depletion of 10 ‰ within the residual CO_2 pool, then assuming initial near ground values of 400 ppm and –10 ‰ (which would result in revised values of 300 ppm and 0 ‰), this sink would act to increase the Keeling plot slope from 5400 to 7050 ppm (Figure 48).

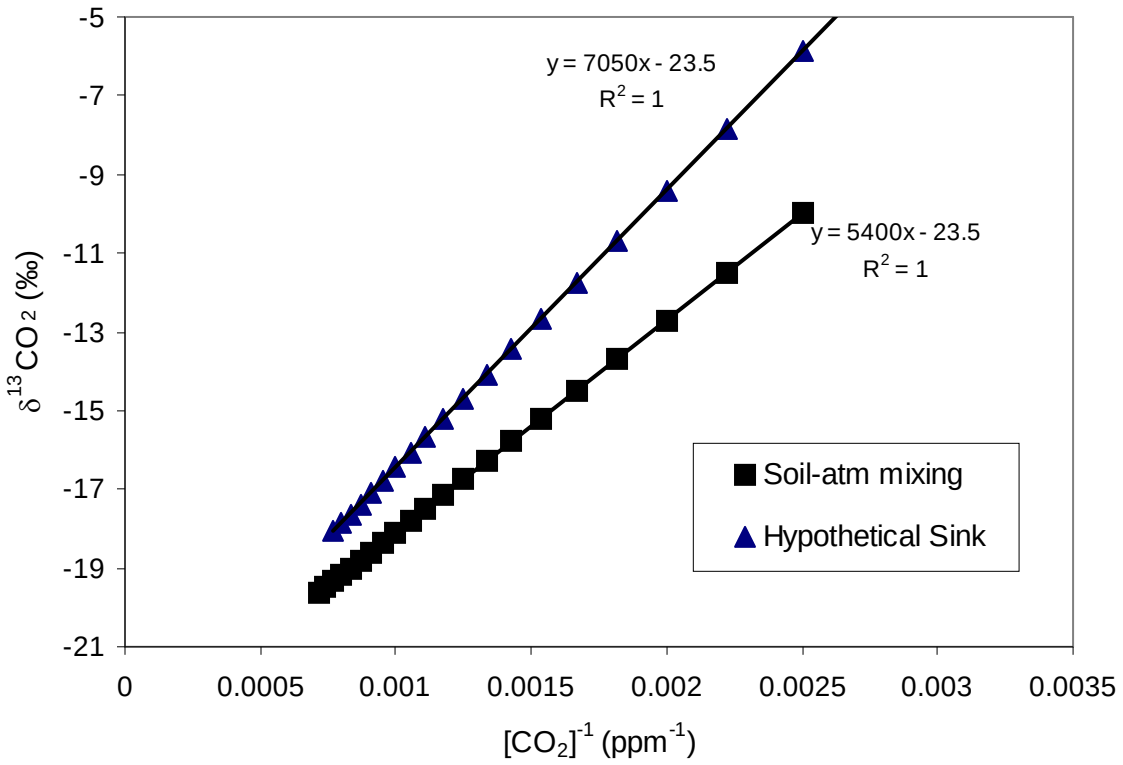

Figure 48: A Keeling plot comparing a two-endmember atmosphere-soil organic matter mixing model, and one with a near-surface sink.

A study by Swanson and Flanagan (2001) found that large portions of soil-respired CO_2 were consumed by moss species present on the floor of a boreal black spruce forest. Average gross photosynthetic CO_2 uptake over several months (May to October of 1996) was about 36 % of the soil-respired output of CO_2. During some months, photosynthetic uptake exceeded soil-respired CO_2 output, resulting in net CO_2 uptake near the forest floor.

Given the environmental similarities between the site studied by Swanson and Flanagan and the OBS site, especially the presence of *Pleurozium* moss cover on the

forest floor, it is likely that similar mechanisms of CO_2 uptake occur on the forest floor at OBS. Furthermore, any such uptake of CO_2 may result in a carbon isotope fractionation that will shift the residual CO_2 towards more ^{12}C-depleted $\delta^{13}CO_2$ values.

Previous research (Lloyd and Farquhar, 1994) has found bulk carbon isotope offsets of 15 ‰ to 19 ‰ between ambient $\delta^{13}CO_2$ and the averaged $\delta^{13}C$ of bulk plant material for various non-tropical forest biomes, while a study by Williams and Flanagan (1996) measured an average ^{13}C discrimination of 19 ‰ in a boreal forest near Cochrane, Ontario.

To explore the effects of photosynthetic uptake on soil respiration at OBS, a three-endmember mixing model is applied to the soil profile data. First, a two-endmember Keeling Plot relationship is established using set atmospheric (-10 ‰, 433 ppm) and SOM (-23.5 ‰ at infinite concentration) endpoints. From this plot (Figure 48), a linear regression is obtained (see Figure 45 for reference plot):

$$\delta_{SA} = \frac{5585.7}{C_{SA}} - 23.5 \qquad (4.2.1.2)$$

where subscript *SA* denotes soil-atmospheric mixed CO_2.

A relationship between observed surface [CO_2] (after photosynthetic uptake) and that expected from two-endmember mixing is then established (Equation 4.2.1.3; modified from Fry, 2006) as well as an isotopic relationship between observed and soil-atmospheric values derived from a mass balance formula (Equation 4.2.1.4; modified from Fry, 2006):

$$\delta_{obs} = \delta_{SA} + 19F_{photo} \quad (4.2.1.3)$$

$$C_{obs} = (1 - F_{photo}) \cdot C_{SA} \quad (4.2.1.4)$$

Where F_{photo} represents the fraction of soil-atmosphere mixed CO_2 consumed by photosynthesis. A photosynthetic isotope fractionation factor ($\Delta^{13}CO_2$) of 19 ‰ is chosen based on the bulk literature values of Lloyd and Farquhar (1994) and moss $\Delta^{13}CO_2$ of Williams and Flanagan (1996).

Upon rearranging Equation 4.2.1.3 to solve for F_{photo}, and substituting it into (4.2.1.4), Equation 4.2.1.5 is obtained:

$$C_{SA} = \frac{C_{obs}}{1 - \frac{\delta_{obs} - \delta_{SA}}{19}} \quad (4.2.1.5)$$

Equation 4.2.1.5 can then be substituted into 4.2.1.2, which is rearranged to solve for δ_{SA}:

$$\delta_{SA} = \frac{(19 \cdot 5585.7) + (-23.5 \cdot 19C_{obs}) - (5585.7 \cdot \delta_{obs})}{19C_{obs} - 5585.7} \quad (4.2.1.6)$$

Once δ_{SA} is known, Equation 4.2.1.3 can be solved for F_{photo}.

With the consideration that discrepancies could exist between the 0.5 m data and near ground CO_2 present at the soil-atmosphere interface (z = 0), near-surface [CO_2] and $\delta^{13}CO_2$ values at z = 0 is obtained by two additional methods. The first method assumes a set atmospheric $\delta^{13}CO_2$ of –10 ‰, and the OBS Keeling plot equations are used to solve for the corresponding [CO_2] value.

A second approach involves the fitting of an exponential curve to soil $^{12}[CO_2]$ and $^{13}[CO_2]$ of the form (Dörr and Münnich, 1990):

$$[CO_2]_z = [CO_2]_\infty (1 - e^{-z\sqrt{G/D_s}}) + [CO_2]_0 \qquad (4.2.1.7)$$

This Equation is a derivation of Fick's second law in a form almost identical to Equation 4.1.1.1, except that the negative loss term *L* is replaced with a positive gain term *G* (Dörr and Münnich, 1990). From the modeled profiles, an estimate of near-surface $^{12}[CO_2]$ and $^{13}[CO_2]$ is obtained and a $\delta^{13}CO_2$ value at z=0 can be calculated.

Regardless of the ambient CO_2 estimate used, all plots show higher F_{photo} in late June, as compared to August (Figure 49; see Table 17). F_{photo} calculations using ambient CO_2 estimated from Equation 4.2.1.7 differ from the other methods in showing a maximum in early August (F_{photo} = 0.47), although this value is similar in magnitude to that calculated in late June (F_{photo} = 0.45). When the 0.5 m CO_2 data is incorporated into 4.2.1.3 instead, lower F_{photo} maxima and minima of 0.03 and -0.08 were obtained for early June and late August, respectively.

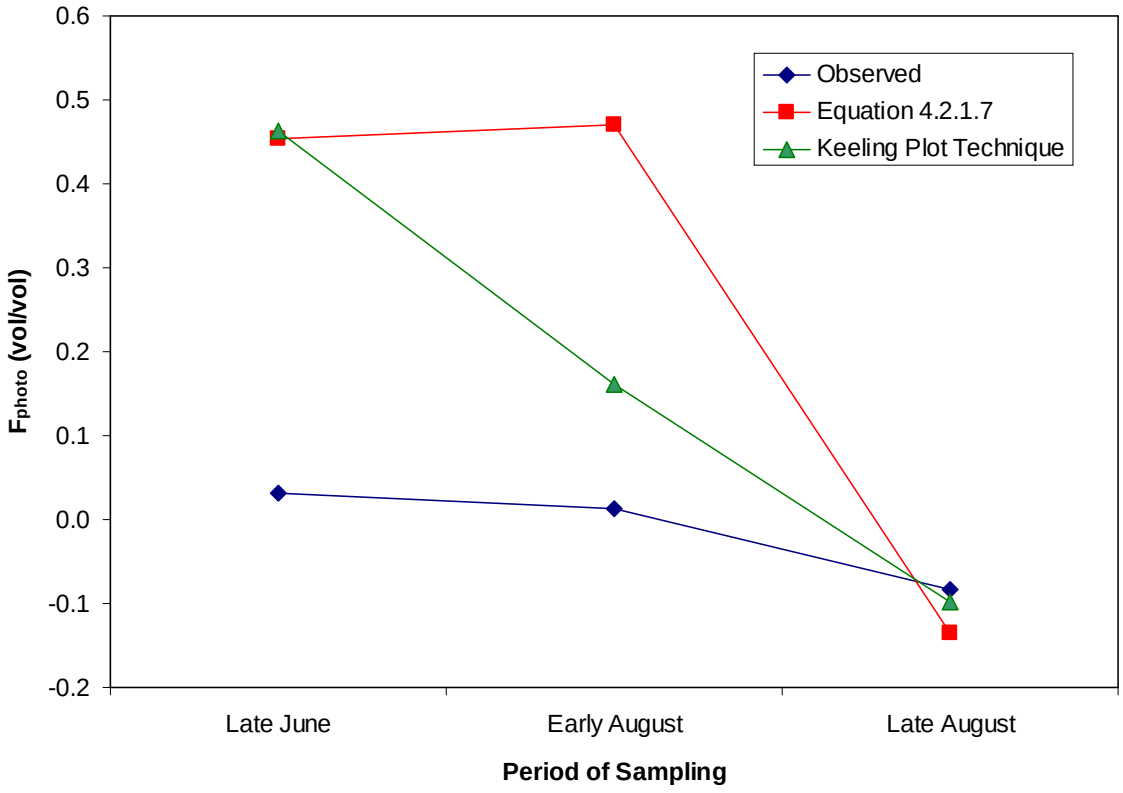

Figure 49: Calculated F_{photo} values, based on various near-surface [CO_2] and $\delta^{13}CO_2$ estimates.

Table 17: Calculated F_{photo}*, based on various near-surface CO_2 estimates and $\Delta^{13}CO_2$ values.*

Method of Near-ground CO_2 Estimation	$\Delta^{13}CO_2$	F_{photo} (vol/vol) 2005		
		Late June	Early August	Late August
Keeling Plot	15	0.71	0.25	-0.15
	19	0.46	0.16	-0.10
	27	0.28	0.10	-0.06
Eqn. 4.2.1.7	15	0.90	0.79	-0.23
	19	0.45	0.47	-0.14
	27	0.23	0.26	-0.07
0.5 m Data	15	0.20	0.06	-0.16
	19	0.03	0.01	-0.08
	27	0.01	0.01	-0.04

All methods of ambient CO_2 estimation showed negative F_{photo} values in late August (-0.14, -0.10 and -0.08 for curve-fitted, Keeling Plot and 0.5 m ambient CO_2 estimates, respectively). These anomalous late August F_{photo} values are likely representative of low photosynthetic uptake during that period. This notion is supported by the close correspondence of observed to calculated F_{org} seen during this period, when only two-endmember mixing is assumed (refer to Figure 47). The apparent negative values may be due to:

a) The large standard deviation of measured [CO_2] and $\delta^{13}CO_2$,

b) The imprecision of the near-surface CO_2 estimates using the Keeling Plot and Curve-fitting approaches,

c) The choice of $\Delta^{13}CO_2$ assumed for all months,

or combinations of these uncertainties.

All F_{photo} estimates obtained with the Keeling Plot and curve-fitted CO_2 estimates are within the range of 0.2 to 1.1 (i.e., net uptake) observed by Swanson and Flanagan (2001). The lower F_{photo} values obtained using 0.5 m CO_2 measurements may indicate that samples taken at that height are not indicative of near-ground CO_2. However, the temporal trend in F_{photo} is similar to that observed when near-ground CO_2 estimates are obtained from the Keeling Plots and Equation 4.2.1.7. This similarity suggests that near-ground processes still exert some degree of influence on CO_2 present at greater heights.

Photosynthetically Active Radiation (PAR) measurements from above the forest canopy were retrieved from the Fluxnet-Canada database for the relevant sampling periods (measured by a LI-COR Quantum Sensor with a precision of ± 5 %; data

courtesy of Hank Margolis), and plotted with sampling time (Figure 50). The plot shows that the highest amount of PAR occurs in early August (123 $\mu mol \cdot m^{-2} \cdot s^{-1}$), followed by early June (93 $\mu mol \cdot m^{-2} \cdot s^{-1}$) and late August (51 $\mu mol \cdot m^{-2} \cdot s^{-1}$) (see Table A19 in appendix). This broadly correlates with the F_{photo} estimates, all of which show higher values in late June and early August than in late August.

As the largest F_{photo} estimates do not coincide with the highest quantity of PAR using the near-ground CO_2 estimates obtained with Equation 4.2.1.7 and the observed 0.5 m data (see Table 9), there likely exists other factors that influence moss uptake and isotopic fractionation of CO_2. In a study carried out by Williams and Flanagan (1996), soil moisture has been found to reduce moss CO_2 uptake when below or above an optimum amount. These authors observed maximum rates of CO_2 assimilation at moss water contents of 7 and 6 (fresh weight/dry weight) for *Pleurozium* and *Sphagnum*, respectively.

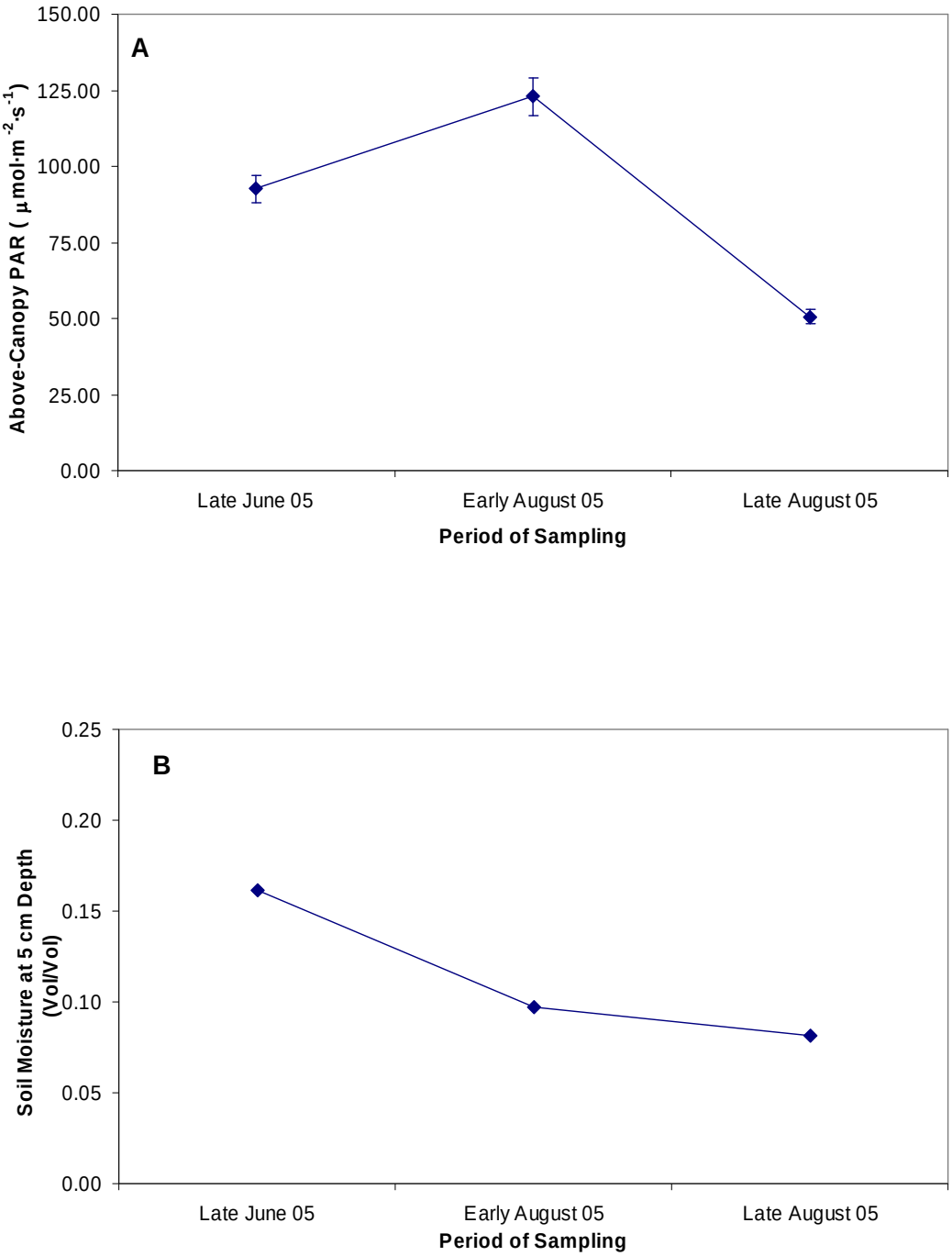

Figure 50: Plots of averaged A) PAR and B) 5 cm soil moisture at OBS over all sampling periods. Error bars represent instrument precision (data courtesy of H. Margolis).

Observed soil moisture at 1-2 cm, measured by Campbell Scientific CS616 soil moisture probes (measurement precision > ± 0.005 % volumetric water content; data courtesy of Hank Margolis) at OBS, shows a decreasing trend from late June to early August (Figure 50; see Table A19 in appendix for data). While not a direct indicator of moss moisture, this trend in soil moisture is likely to be mirrored in moss water content as well. Thus, it is possible that moss water content continued to decrease below an optimum amount over the period of sampling, resulting in a continuous decrease in photosynthetic CO_2 uptake. The influence of soil moisture may have been sufficient to counteract the largest PAR values observed in early August, resulting in F_{photo} values that were lower than in early August or late June.

Williams and Flanagan (1996) also found that photosynthetic ^{13}C-discrimination increased with decreasing soil water content, which ranged from 15 ‰ to 22 ‰ for *Pleurozium* and 15 ‰ to 27 ‰ for *Sphagnum*, over a moss water content range of 15 to 4. If similar relationships between soil moisture and $\Delta^{13}CO_2$ exist in OBS, then the calculated F_{photo} value observed in early and late August might be overestimates since the low soil moisture during those periods would be associated with a larger $\Delta^{13}CO_2$.

To test the sensitivity of F_{photo} to changes in $\Delta^{13}CO_2$, F_{photo} was recalculated using the maximum and minimum $\Delta^{13}CO_2$ (15 ‰ and 27 ‰) observed by Williams and Flanagan (1996). With the lower isotope offset, F_{photo} estimates were 52 % to 6.5 times higher than values utilizing a $\Delta^{13}CO_2$ of 19 ‰, while an isotope offset of 27 ‰ resulted in F_{photo} values being 41 % to 61 % lower (see Table 17). These variations show that the utilization of an accurate $\Delta^{13}CO_2$ value is needed for more precise F_{photo} estimates, which would clarify the role of soil moisture on changes in photosynthetic CO_2 uptake of near-

ground plant species. Unfortunately, in the absence of moss moisture measurements at OBS, it is difficult to solidify any such relationship.

CO_2 flux rates are calculated with Equation 2.5.1 (using the same technique as with CH_4; see section 4.2 and Table A22 in appendix for equations of the $[CO_2]$ curve-fitted data), and by taking the derivative of 4.2.1.7 and substituting it into Equation 2.5.1 (similar to CH_4; see Section 4.2):

$$J = \frac{D_s}{z^*}\left[\left([CO_2]_\infty\right)e^{-z_0/z^*}\right] \qquad (4.2.1.8)$$

Where $z^* = \sqrt{D_s / G}$, or the CO_2 "relaxation depth" (Reeburgh et al., 1997).

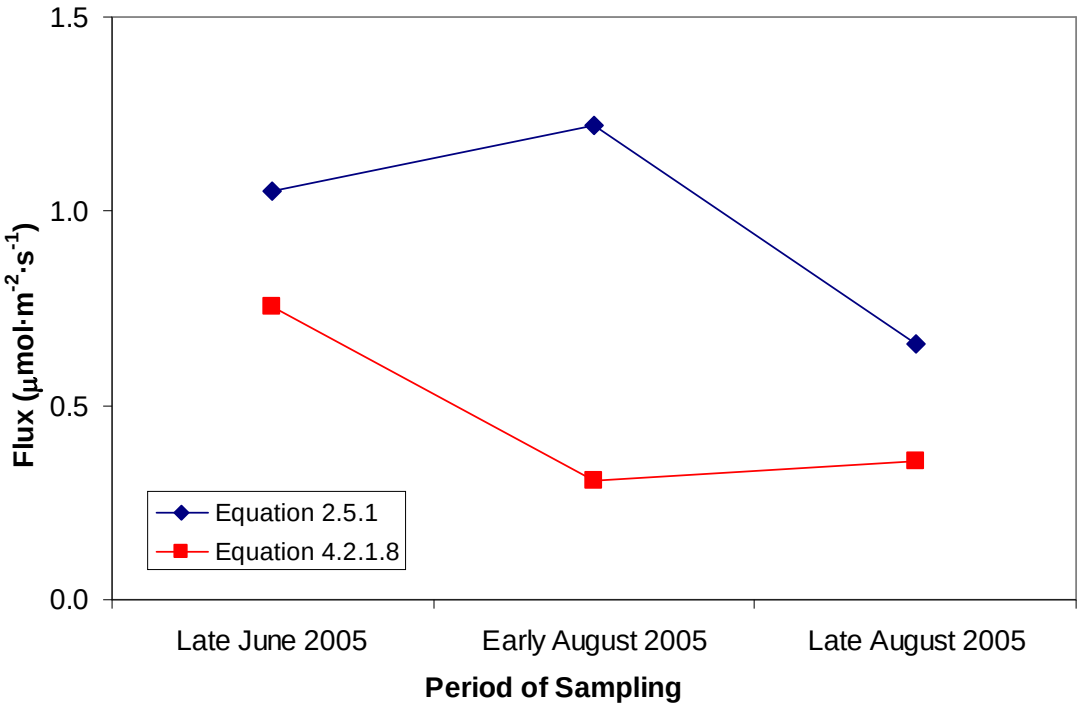

Figure 51: OBS CO_2 flux estimates.

Table18: Calculated CO_2 fluxes at OBS.

Method	CO_2 Fluxes ($\mu mol \cdot m^{-2} \cdot s^{-1}$)		
	2005		
	Late June	Early August	Late August
Eqn. 2.5.1	1.05	1.22	0.66
Eqn. 4.1.1.3	0.76	0.31	0.36

The CO_2 fluxes calculated with Equation 4.2.1.8 are consistently lower than those obtained via Equation 2.5.1 (Figure 51). Temporal trends, if present, are indistinct, although both Equations appear to show higher fluxes in late July (1.1 and 0.8 $\mu mol \cdot m^2 \cdot s^{-1}$, using 2.5.1 and 4.2.1.8, respectively; see Table 18) as compared to late August (0.7 and 0.4 $\mu mol \cdot m^2 \cdot s^{-1}$, using 2.5.1 and 4.2.1.8, respectively; see Table 18 in appendix).

The early August flux maximum calculated by Equation 2.5.1 (1.2 $\mu mol \cdot m^2 \cdot s^{-1}$) is similar in magnitude to the efflux in the preceding period (1.1 $\mu mol \cdot m^2 \cdot s^{-1}$), while the lowest fluxes calculated during the same period by Equation 4.2.1.8 (0.31 $\mu mol \cdot m^2 \cdot s^{-1}$) are similar to rates measured in Late August (0.35 $\mu mol \cdot m^2 \cdot s^{-1}$). Therefore, there is a lack of a clear seasonal trend, which may be due to the narrow range of soil moisture and temperature levels (see Table 6) observed during this period, which may result in correspondingly low variations in flux.

Equation 2.5.1 may be less accurate in determining CO_2 fluxes as opposed to CH_4 fluxes. In addition to being based on a single depth measurement, Equation 2.5.1 assumes fluxes based on concentration differences between 5 cm depth [CO_2] values, and mixing ratios present 50 cm above the soil surface. The studies by Certini et al. (2003) and Jassal et al. (2005) show that in forest soils, maximum CO_2 production occurs at depths

shallower than 5 cm. Substitution of [CO_2] measurements at 5 cm with those closer to the ground surface may result in more accurate assessment of the CO_2 efflux rates. However, the entire [CO_2] depth profile must still be accounted for.

4.2.2 CO_2 Dynamics in Vancouver Island

All of the BC sites show larger subsurface [CO_2] and more ^{13}C-depleted $\delta^{13}CO_2$ with respect to atmospheric values (see Figures 22-25). The finding is consistent with that observed at the OBS site. This indicates the occurrence of net CO_2 production and emission from these soils. Trends of increasing [CO_2] and decreasing $\delta^{13}CO_2$ with depth are clearly visible at most sites, revealing the dominance of CO_2 production throughout the soil column (see Figures 22-25). The chamber measurements provide additional support for this conclusion, showing increases in [CO_2] and decreases in $\delta^{13}CO_2$ occurring over the span of an hour (see Figures 25 and 26, and Table A17 in appendix).

Keeling plots of the BC data shows a linear relationship between $\delta^{13}CO_2$ and $[CO_2]^{-1}$ in all periods of sampling (Figure 52). The Y-intercepts obtained via GMR (see Section 4.2.1) vary little across all sampling periods and sites (Figure 52), with cumulative averages of –22.46 ± 0.82 ‰, -22.92 ± 1.26 ‰, and –21.87 ± 1.21 ‰ for DF49, HDF88, and HDF00 respectively (all values ± 1σ). There appears to be no temporal trend in Y-intercept values, which do not show distinct patterns across the entire period of sampling (Figure 53).

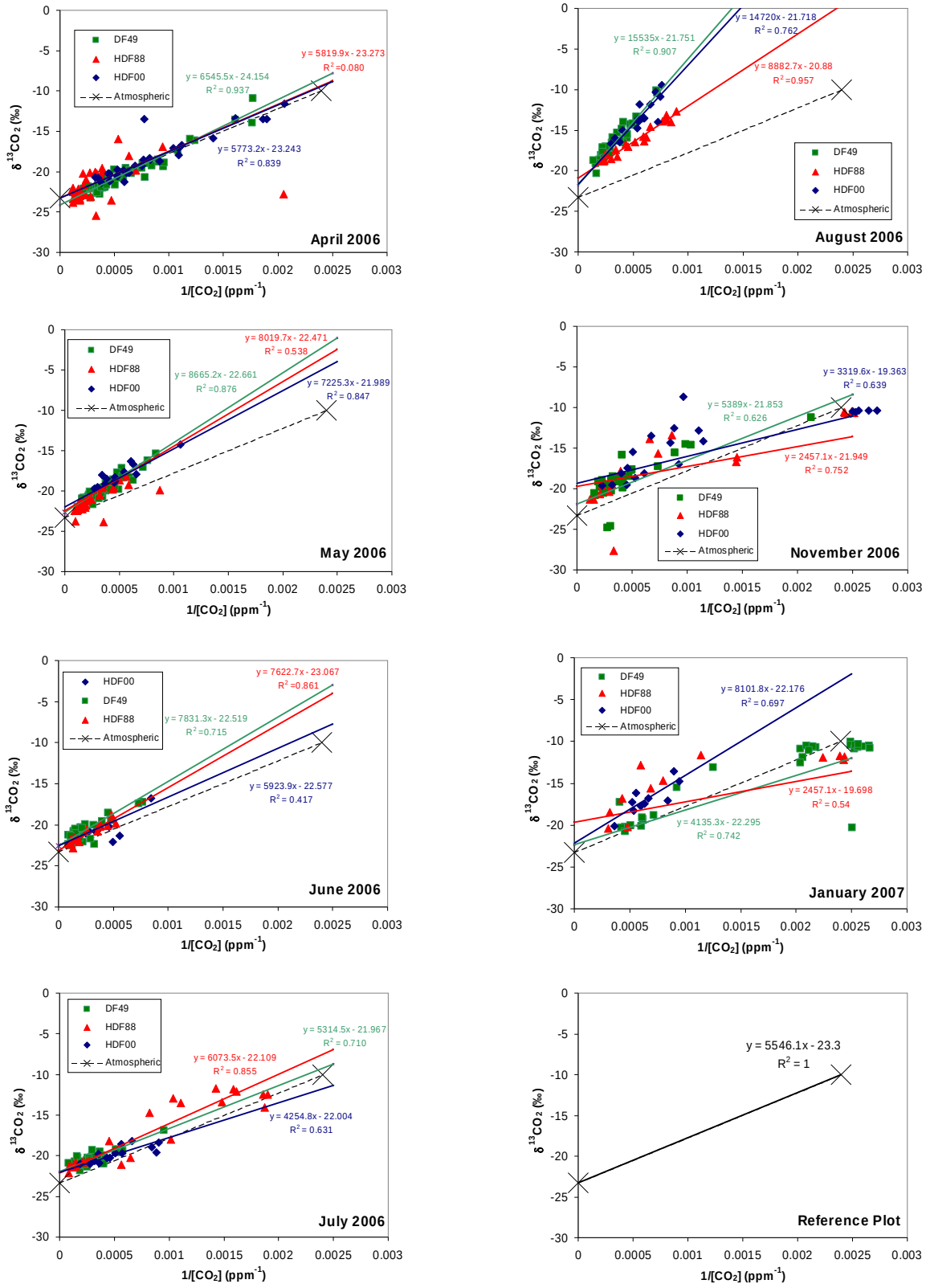

Figure 52: BC Site Keeling Plots.

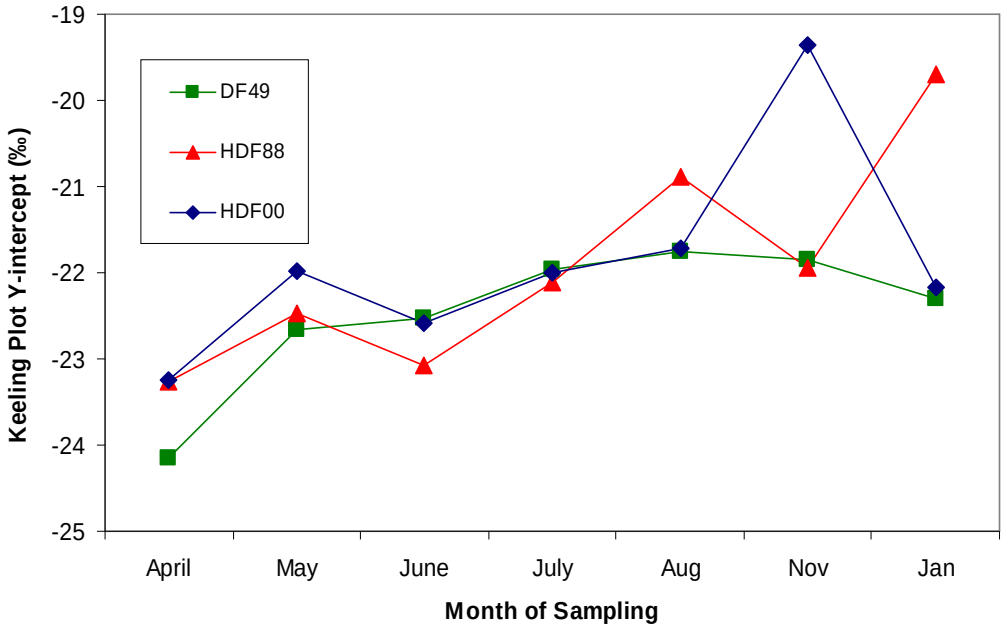

Figure 53: Keeling Plot Y-intercept values in all BC sites.

The Y-intercept values differ from measured bulk plant $\delta^{13}C$ values at DF49 (-27.7 ‰; see Alstad et al., 2006) by 5.2 ‰ to 5.8 ‰. The observed offset is similar in magnitude to the diffusional enrichment value of 4.4 ‰ predicted by Cerling (1991). This suggests that the source of soil respired CO_2 is predominantly plant and heterotrophic respiration, which exhibit values indistinguishable to that of the dominant plant type.

However, the mixing lines are steeper than expected for only SOM-atmosphere mixing at all three BC sites during certain months, as was observed in OBS. Based on two-endmember mixing between averaged near-surface CO_2 measurements (-10 ‰ and 417 ppm; see section 2.4), some of the observed slopes are up to three times steeper. Thus, the BC site soils do not appear to be properly represented by a simple 2-endmember mixing model (see section 2.4).

Equation 4.2.1.1 is applied to data from all BC sites to obtain estimates of F_{org}. These, in turn, are compared to concentration-based F_{org} values, calculated by subtracting atmospheric [CO_2] from depth profile values and dividing by the total observed soil [CO_2] (see section 4.2). The resulting plots (Figures 54, 55 and 56; see Table 20 for data) show that during most months at all sites, there is a tendency for Eqn. 4.2.1.1 to underestimate F_{org}.

The F_{org} discrepancies suggest that soil $\delta^{13}CO_2$ values are more ^{12}C-depleted than expected, assuming simple SOM-atmosphere mixing. The possibility of soil carbonate-derived CO_2 influencing these discrepancies is unlikely, as soil carbonates are absent in all BC site soils (data from the Fluxnet-Canada database, courtesy of T.A. Black).

The addition of the 80 cm data in DF49 show greater agreement between isotope- and concentration-based F_{org} estimates at deeper depths. This raises the possibility of a near-surface influence on what would otherwise be a two-endmember mixing system. The BC site soils are similar to OBS in that a cover of moss or small vascular plants is present in all sites. Therefore, the possibility of plant uptake of near-ground CO_2 is investigated by applying Equation 4.2.1.3 to estimate F_{photo} (see Section 4.2).

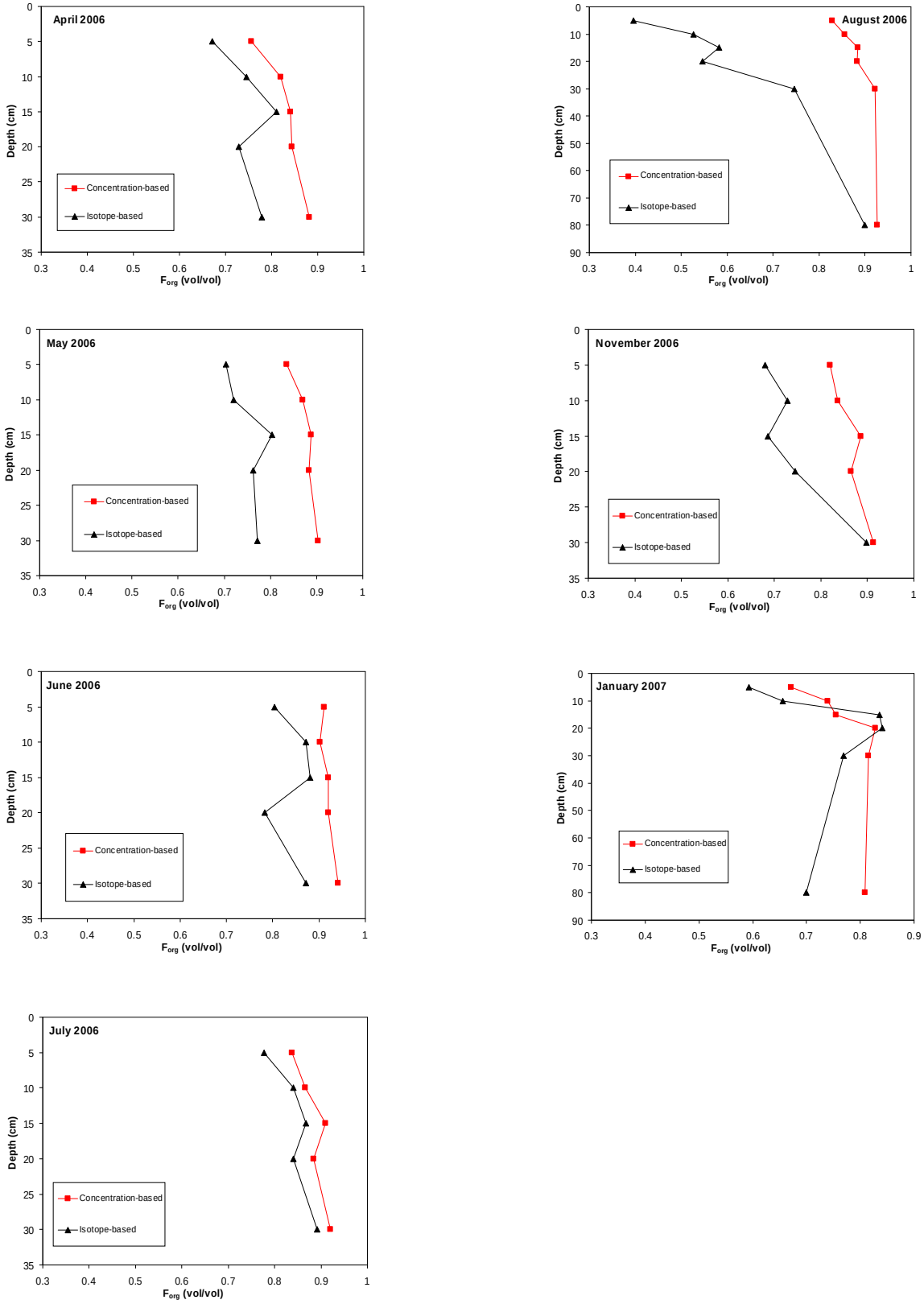

Figure 54: F_{org} profiles in DF49.

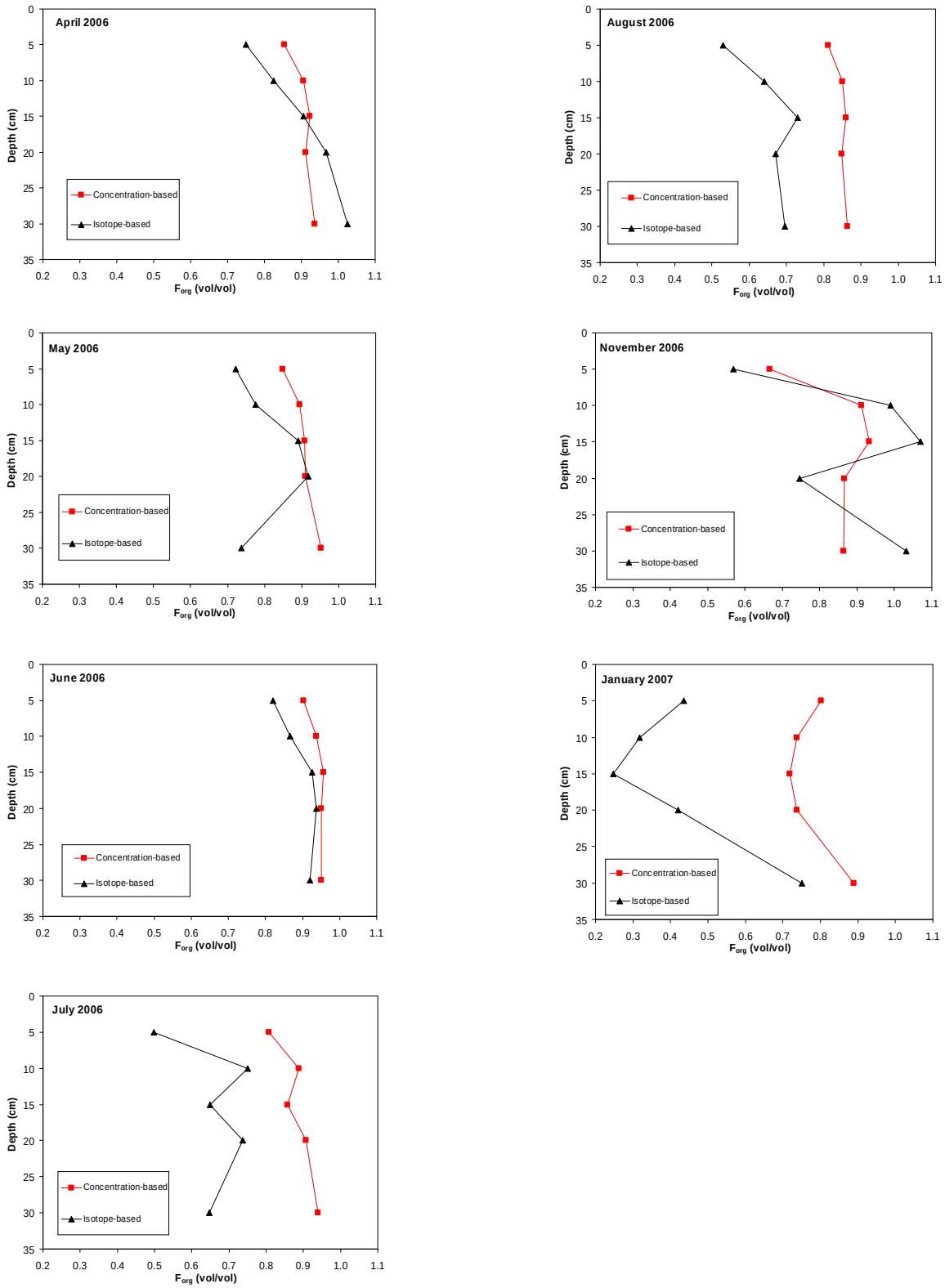

Figure 55: F_{org} profiles in HDF88.

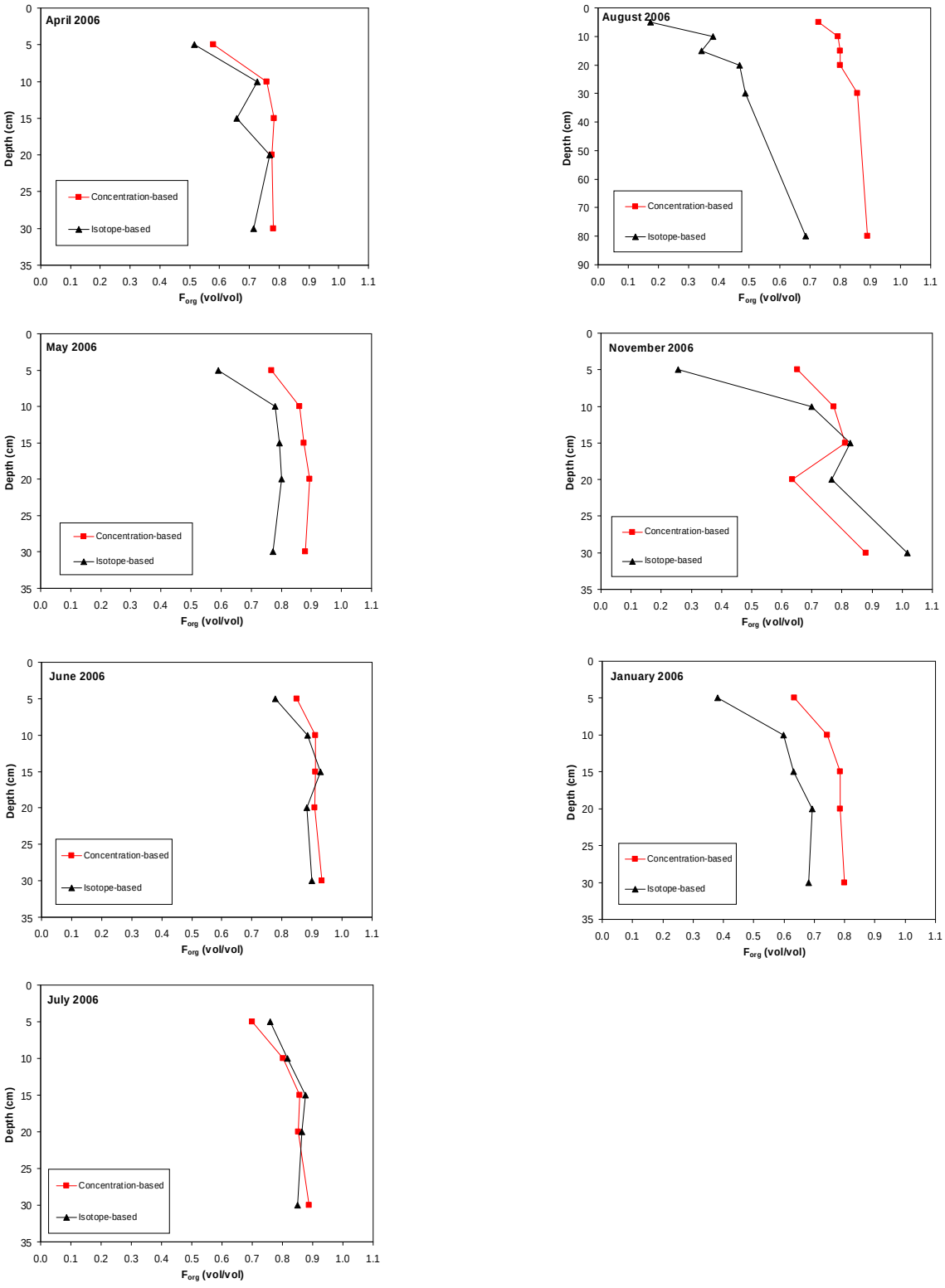

Figure 56: F_{org} profiles in HDF00.

Table 20: F_{org} estimates at all BC sites, using observed data and Equation 4.2.2.1

Site	Method of F_{org} Estimation	Depth (cm)	F_{org} (vol/vol) Apr '06	May '06	Jun '06	Jul '06	Aug '06	Nov '06	Jan '07
DF49	Concentration-based	5	0.76	0.83	0.91	0.84	0.83	0.82	0.67
		10	0.82	0.87	0.90	0.87	0.86	0.84	0.74
		15	0.84	0.89	0.92	0.91	0.88	0.89	0.75
		20	0.84	0.88	0.92	0.88	0.88	0.86	0.83
		30	0.88	0.90	0.94	0.92	0.92	0.91	0.82
		80					0.93		0.81
	Isotope-based (Eqn. 4.2.1.1)	5	0.67	0.70	0.80	0.78	0.40	0.68	0.59
		10	0.74	0.72	0.87	0.84	0.53	0.73	0.66
		15	0.81	0.80	0.88	0.87	0.58	0.69	0.84
		20	0.73	0.76	0.78	0.84	0.55	0.75	0.84
		30	0.78	0.77	0.87	0.89	0.75	0.90	0.77
		80					0.90		0.70
HDF88	Concentration-based	5	0.85	0.85	0.90	0.81	0.81	0.67	0.80
		10	0.91	0.89	0.94	0.89	0.85	0.91	0.74
		15	0.92	0.91	0.96	0.86	0.86	0.93	0.72
		20	0.91	0.91	0.95	0.91	0.85	0.87	0.74
		30	0.94	0.95	0.95	0.94	0.86	0.86	0.89
	Isotope-based (Eqn. 4.2.1.1)	5	0.75	0.72	0.82	0.50	0.53	0.57	0.44
		10	0.82	0.78	0.87	0.75	0.64	0.99	0.32
		15	0.91	0.89	0.93	0.65	0.73	1.07	0.25
		20	0.97	0.92	0.94	0.74	0.67	0.75	0.42
		30	1.03	0.74	0.92	0.65	0.70	1.03	0.75
HDF00	Concentration-based	5	0.58	0.77	0.85	0.70	0.73	0.65	0.63
		10	0.76	0.86	0.91	0.80	0.79	0.77	0.74
		15	0.78	0.88	0.91	0.86	0.80	0.81	0.78
		20	0.78	0.89	0.91	0.85	0.80	0.63	0.78
		30	0.78	0.88	0.93	0.89	0.86	0.88	0.80
		80					0.89		
	Isotope-based (Eqn. 4.2.1.1)	5	0.52	0.59	0.78	0.76	0.17	0.26	0.38
		10	0.73	0.78	0.88	0.82	0.38	0.70	0.60
		15	0.66	0.79	0.93	0.88	0.34	0.83	0.63
		20	0.77	0.80	0.88	0.86	0.47	0.77	0.69
		30	0.71	0.77	0.90	0.85	0.49	1.02	0.68
		80					0.69		

As with OBS, near-ground $[CO_2]$ estimates are obtained by the Keeling Plot method, and by solving Equation 4.2.1.7 at z = 0 for $^{12}[CO_2]$ and $^{13}[CO_2]$, to calculate both $[CO_2]$ and $\delta^{13}CO_2$ at the soil-atmosphere interface. A Keeling Plot relationship

between $\delta^{13}CO_2$ and $[CO_2]^{-1}$ from the 2005 data is used to estimate the $\delta^{13}CO_2$ from the 2 m $[CO_2]$ measurements (Figure 57, data courtesy of L. Flanagan; see Section 4.2.1 for more details).

For sites DF49 and HDF00, near-surface $\delta^{13}CO_2$ and $[CO_2]$ were available in the form of t = 0 chamber measurements, which are incorporated into Equation 4.2.1.6 (see section 4.2.1), and compared to F_{photo} estimates using the Keeling-plot CO_2 estimates (Figure 58 and Table 21).

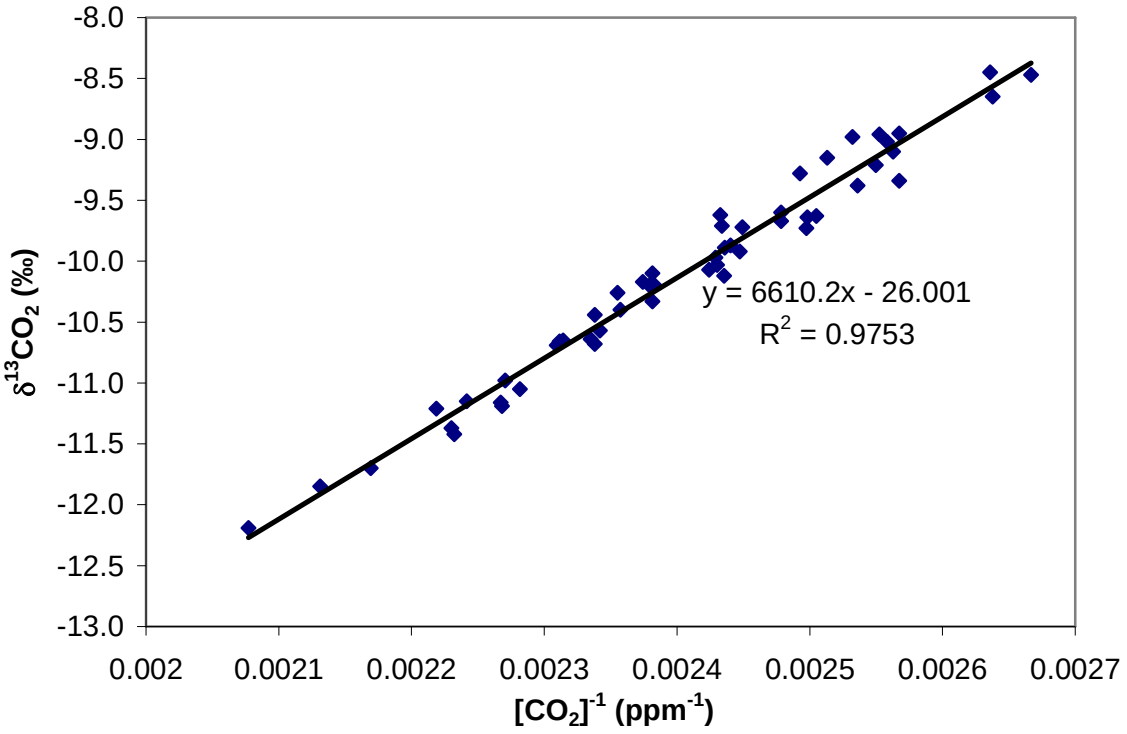

Figure 57: A Keeling Plot using DF49 CO_2 measurements from 2005, collected over the period of DOY 130-284 (data courtesy of L. Flanagan).

Table 21: F_{photo} values from all BC sites, using various methods of near-ground [CO_2] determination, and $\Delta^{13}CO_2$ values.

Site	Method of Near-ground CO_2 Estimation	$\Delta^{13}CO_2$	F_{photo} (vol/vol) 2006 Apr	May	Jun	Jul	Aug	Nov	2007 Jan
DF49	Chamber 1	15	0.07	0.60	0.20	0.17	0.85	0.57	0.46
		19	0.04	0.37	0.13	0.11	0.56	0.35	0.31
		27	0.02	0.21	0.07	0.06	0.33	0.20	0.19
	Chamber 2	15	0.13	0.37	0.20	-0.03	0.66	0.37	0.45
		19	0.08	0.27	0.13	-0.02	0.44	0.23	0.30
		27	0.04	0.17	0.07	-0.01	0.26	0.13	0.18
	Keeling Plot	15	0.39	0.72	0.68	0.28	0.82	0.64	-0.79
		19	0.18	0.46	0.42	0.12	0.60	0.37	-0.17
		27	0.08	0.27	0.24	0.05	0.39	0.20	-0.07
	Eqn. 4.2.1.7	15	0.21	-0.03	0.20	-0.03	0.42	-0.35	0.67
		19	0.10	-0.01	0.13	-0.02	0.25	-0.21	0.21
		27	0.05	-0.01	0.07	-0.01	0.14	-0.12	0.09
HDF88	Keeling Plot	15	0.24	0.70	0.65	0.52	0.76	0.03	0.41
		19	0.10	0.43	0.38	0.27	0.51	0.01	0.19
		27	0.04	0.25	0.21	0.14	0.31	0.00	0.09
	Eqn. 4.2.1.7	15	-1.39	-0.17	-0.44	-5.97	-2.23	-0.24	1.01
		19	-0.51	-0.12	-1.01	0.30	0.16	-0.16	0.62
		27	-0.22	-0.07	0.64	0.10	0.05	-0.09	0.35
	2 m [CO_2] Data	15	0.03	-0.07	0.21	0.08	0.18	0.00	0.02
		19	0.03	-0.05	0.16	0.06	0.14	0.00	0.02
		27	0.02	-0.04	0.12	0.04	0.10	0.00	0.01
HDF00	Chamber 1	15	0.05	0.98	0.81	0.15	1.13	0.66	0.35
		19	0.03	0.73	0.57	0.08	0.80	0.44	0.21
		27	0.01	0.49	0.35	0.05	0.50	0.27	0.12
	Chamber 2	15	0.15	0.70	0.70	0.07	1.20	0.71	0.64
		19	0.07	0.48	0.48	0.04	0.86	0.49	0.37
		27	0.03	0.30	0.30	0.02	0.55	0.30	0.20
	Keeling Plot	15	0.22	0.67	0.43	7.80	0.81	0.28	0.76
		19	0.09	0.40	0.20	-0.62	0.59	0.11	0.51
		27	0.04	0.22	0.10	-0.20	0.38	0.05	0.31
	Eqn. 4.2.1.7	15	0.48	-0.37	0.96	0.48	0.65	1.02	-51.09
		19	-0.35	1.39	0.29	0.06	0.39	0.60	0.17
		27	-0.08	0.13	0.12	0.02	0.22	0.33	0.06

Calculated F_{photo} values show similar seasonal trends, using all near-surface [CO_2] estimates (Figure 58). Within DF49, the largest F_{photo} is observed in August, using all methods of near ground [CO_2] estimation (0.58, 0.46, 0.61 and 0.26 using Chamber 1,

Chamber 2, Keeling Plot and Equation 4.2.1.7, respectively). The lowest values are observed in April, January and November with the Chamber 1 (0.05), Keeling Plot (-0.19), and Chamber 2 (-0.01) near-ground [CO_2] and $\delta^{13}CO_2$ estimates, respectively. The use of Equation 4.2.1.7 for near-ground CO_2 also shows an August maximum (0.26), but differs from the other estimates in showing a low F_{photo} in May (-0.01). As with the near-ground [CO_2] chamber measurements, Equation 4.2.1.7 also show minimum F_{photo} values in November (-0.21).

A maximum August F_{photo} in August (0.82, 0.88 and 0.61 based on near-surface CO_2 obtained via Chamber 1, Chamber 2, and Keeling Plot relationships, respectively) and large F_{photo} values in May (0.75, 0.50 and 0.42 based on near-surface CO_2 obtained via Chamber 1, Chamber 2, and Keeling Plot relationships, respectively) are also observed in HDF00 when near-surface CO_2 data is obtained from the Chamber measurements and the Keeling Plot relationships.

Equation 4.2.1.7 differs by showing an improbably high maximum F_{photo} of 2.5 occurring in May, with a smaller maxima (0.63) occurring in November. In HDF88, the Keeling near-surface CO_2 estimates show the largest F_{photo} values in August (0.53), with a smaller maximum in May (0.45), as in the other two sites. Similarly high F_{photo} values are seen in May (0.16) and August (0.14) when the observed 2 m [CO_2] data is substituted. The usage of near surface CO_2 estimates at HDF88 obtained by Equation 4.2.1.7 differs from the Keeling-plot and observed near-ground data by showing a maximum in January (0.64; see Figure 58).

F_{photo} plots suggest that although Equation 4.2.1.7 is appropriate for calculation of CO_2 fluxes, it does not provide an accurate estimate of near-surface [CO_2] or $\delta^{13}CO_2$. The

similarities between F_{photo} trends obtained from the Keeling near-surface CO_2 estimates and the t = 0 chamber CO_2 measurements and 2 m data indicate that the Keeling Plot estimates more accurately portray actual variations of F_{photo}.

However the Keeling Plot are unlikely to give true magnitudes, as evidenced by the large negative July F_{photo} value seen in HDF00. This is due to the application of –10 ‰ as a near-ground CO_2 value to all months, which does not account for the true variation in near-ground $\delta^{13}CO_2$ that may actually be present (i.e., as seen in the Chamber measurements; see Figure 25). Thus, the Keeling Plot CO_2 estimates are more useful as a general indicator of seasonal F_{photo} trends, rather than the clarification of absolute values.

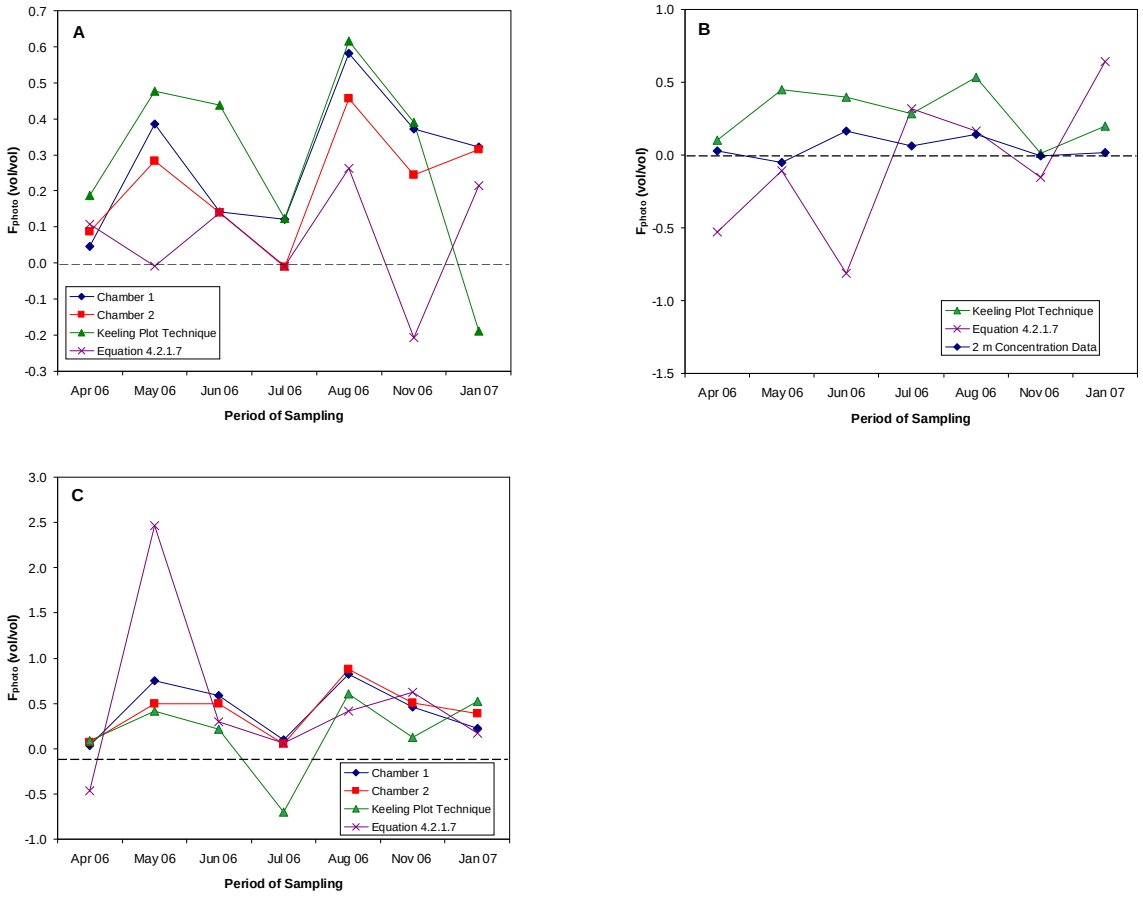

Figure 58: Calculated F_{photo} values at A) DF49, B) HDF88 and C) HDF00, based on various ground level [CO_2] and $\delta^{13}CO_2$ estimates.

The F_{photo} plots are compared to above-canopy PAR measurements (measured with a LI-COR LI190 PAR sensor, with a precision of ± 5 %; data courtesy of T.A. Black) and shallow-depth soil moisture data from the online Fluxnet-Canada database (Figure 59; measured using Campbell Scientific CS615 Soil Probes, with a precision of ± 2 %; data courtesy of T.A. Black) to clarify any relationships with these variables that may exist. While the large PAR levels observed during May in HDF00 and DF49 coincide with the large F_{photo} values calculated from the chamber and Keeling Plot data, the flux maximum in August seen at both sites are associated with smaller PAR levels. This suggests that PAR does not fully account for the variability in near-surface photosynthetic CO_2 uptake in the BC sites.

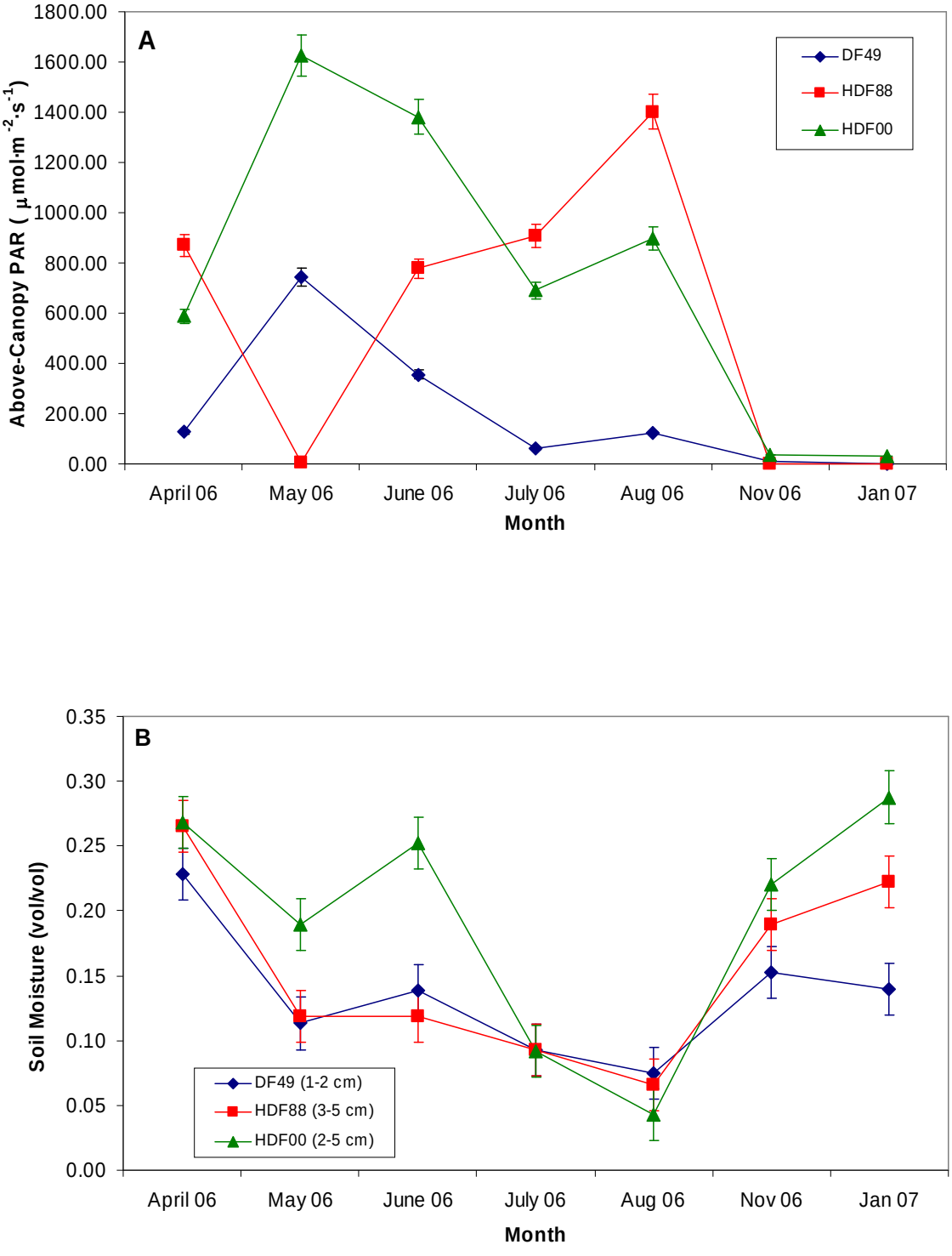

Figure 59: Above-canopy PAR (A) and shallow depth soil moisture measurements (B) at all BC sites (data courtesy of T. A. Black; see Tables A16-18 in appendix).

The soil moisture data show that the driest conditions, which occur during August at all three BC sites (see Tables A16-18 in appendix), may be correlated to the smaller F_{photo} peaks observed during that month. This is likely related to the findings of Williams and Flanagan (1996) that showed correlations between soil moisture and flux strength, well as isotopic fractionation.

It is possible that the low soil moisture observed in August represent optimum levels for photosynthetic activity. However, the lowest observed shallow-depth soil moisture percentage of 8.1 % in OBS during late August, when F_{photo} was shown to be smallest, is still higher than the lowest values observed in the BC sites (7.4 %, 6.5 % and 4.3 % for DF49, HDF88 and HDF00 respectively; refer to Table 5). Therefore, it is more likely that a stronger degree of carbon isotope fractionation occurs due to the drier soil conditions.

As the magnitude of F_{photo} depends on $\Delta^{13}CO_2$, the large F_{photo} calculated in August would be an overestimate if the true $\Delta^{13}CO_2$ is larger than the selected bulk value, due to low moss water content. For example, if the maximum $\Delta^{13}CO_2$ value of –27 ‰ observed by Williams and Flanagan was a genuine August value, then overestimates of F_{photo} become as high as 70 % during that month (see Table 21).

Alternatively, the F_{photo} observed earlier in the growing season would be an underestimate if the real $\Delta^{13}CO_2$ is actually smaller than the chosen value. In this case, substitution of the lowest $\Delta^{13}CO_2$ of –15 ‰ as observed by Williams and Flanagan result in F_{photo} values that are up to three times lower than estimates using a $\Delta^{13}CO_2$ of –19 ‰ during the month of April, when growing-season soil moisture values were highest (see Table 21).

As with OBS, variable $\Delta^{13}CO_2$ is clearly needed for an accurate assessment of site F_{photo}. This requires moss moisture data and $\Delta^{13}CO_2$ data associated with other near-ground plant species at the BC sites. Both of these measurements are unavailable at these sites for this study, making it difficult to clarify the magnitude in which soil moisture affects $\Delta^{13}CO_2$, if such a relationship exists at the BC sites.

CO_2 flux rates are calculated by fitting exponential equations to chamber measurements (see section 4.2) and from the soil profile data using Equations 2.5.1 and 4.2.1.8. Within DF49, similar trends of increasing flux from April to June, and decreasing emissions from June onwards, are present using all three methods (Figure 59; refer to Table 22).

Spatial variation in flux magnitude is observed from the chamber data, with ranges of 0.2 to 2.4 $\mu mol \cdot m^{-2} \cdot s^{-1}$ and 0.6 to 7.7 $\mu mol \cdot m^{-2} \cdot s^{-1}$ seen in Chambers 1 and 2, respectively. The flux range obtained from Equations 4.2.1.8 and 2.5.1 (0.5 to 3.0 $\mu mol \cdot m^{-2} \cdot s^{-1}$ and 0.8 to 5.2 $\mu mol \cdot m^{-2} \cdot s^{-1}$, for Equations 4.2.1.8 and 2.5.1 respectively) are similar to the chamber estimates (Figure 60).

These fluxes fall within the range of 2 to 10 $\mu mol \cdot m^{-2} \cdot s^{-1}$ observed by Drewitt et al. (2002) and Jassal et al. (2004) in past studies undertaken in DF49. Equation 2.5.1 is similar to the chamber measurements in showing the largest fluxes occurring in August, but Equation 4.2.1.8 shows the largest fluxes occurring instead in July. However, the magnitude of fluxes in June (2.5 $\mu mol \cdot m^{-2} \cdot s^{-1}$) and July (3.0 $\mu mol \cdot m^{-2} \cdot s^{-1}$) are similar, with the July fluxes being 21 % larger than those in the previous month.

Table 22: CO_2 fluxes from all BC sites.

Site	Method	Fluxes ($\mu mol \cdot m^{-2} \cdot s^{-1}$)						
		2006						2007
		Apr	May	Jun	Jul	Aug	Nov	Jan
DF49	Chamber 1	1.62	1.73	2.28	1.90	1.01	0.20	
	Chamber 2	0.55	1.68	7.65	3.34	2.65	1.45	
	Equation 2.5.1	0.77	3.20	5.21	3.91	3.41	1.74	0.75
	Equation 4.2.1.8	0.54	2.09	2.50	3.03	2.30	1.23	0.94
HDF88	Equation 2.5.1	0.99	3.53	4.57	2.56	2.91	0.68	1.01
	Equation 4.2.1.8	0.62	1.57	6.75	2.80	4.85	1.29	0.20
HDF00	Chamber 1	0.68	3.60	1.57		0.68	0.53	
	Chamber 2	0.43	2.37		1.49	0.53	1.99	
	Equation 2.5.1	0.58	1.66	2.74	3.23	3.49	1.74	0.75
	Equation 4.2.1.8	0.79	2.37	2.68	1.86	1.19	0.27	0.67

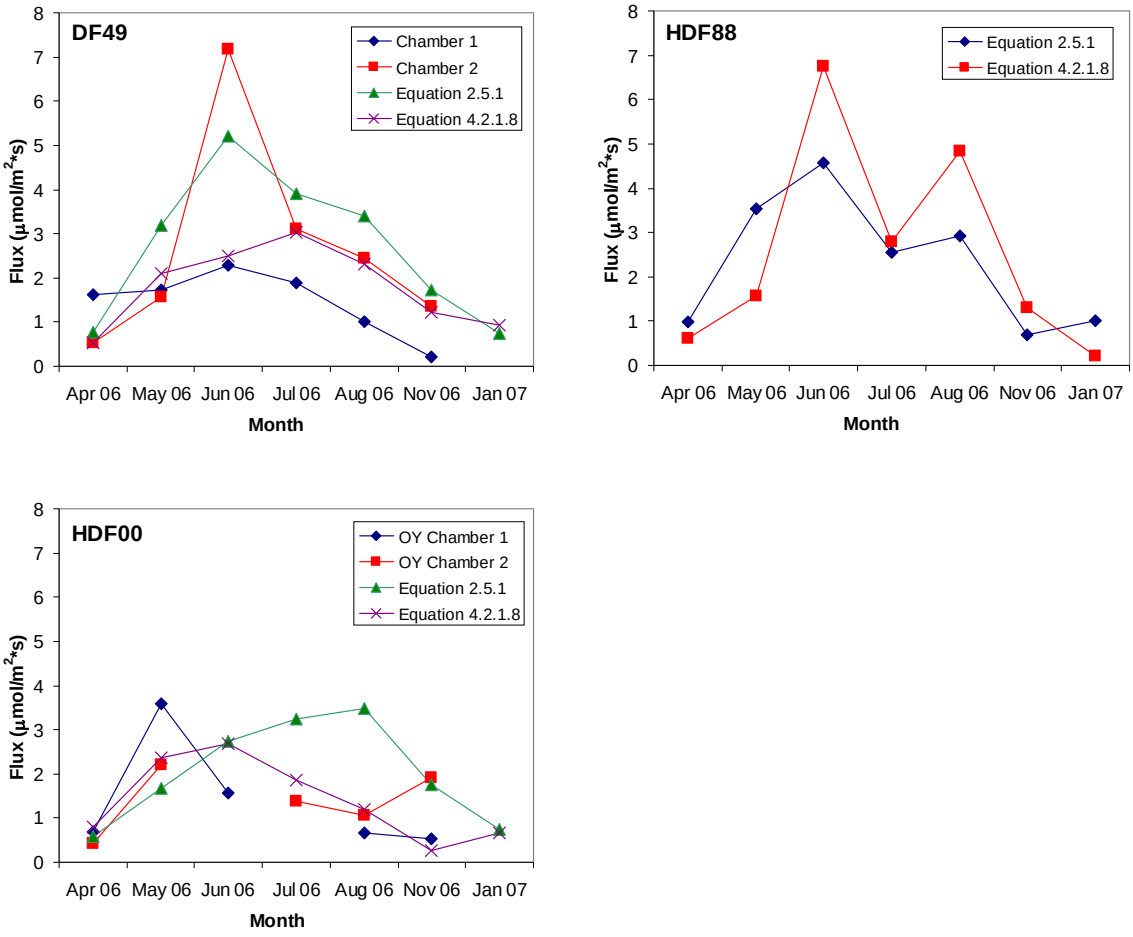

Figure 60: CO_2 flux estimates for all BC sites. Missing data points are omitted, due to poor exponential fitting ($R^2 \leq 0.47$).

From the data available, fluxes from Chamber 1 in HDF00 range from 0.4 to 2.4 $\mu mol \cdot m^{-2} \cdot s^{-1}$ in Chamber 1 and from 0.7 to 3.6 $\mu mol \cdot m^{-2} \cdot s^{-1}$ in Chamber 2, with the largest fluxes observed in May. Equation 4.2.1.8 shows a flux range of 0.3 to 2.7 $\mu mol \cdot m^{-2} \cdot s^{-1}$, with a trend of increasing flux from April to June, when the largest flux is observed.

Afterwards, fluxes decrease until reaching a minimum in November (0.3 $\mu mol \cdot m^{-2} \cdot s^{-1}$), followed by a larger flux in January (0.7 $\mu mol \cdot m^{-2} \cdot s^{-1}$). While the range of CO_2 fluxes obtained from Equation 2.5.1 is similar to the Chamber rates and those obtained using Equation 4.2.1.8 (0.2 to 2.2 $\mu mol \cdot m^{-2} \cdot s^{-1}$), a distinct flux maximum (3.49 $\mu mol \cdot m^{-2} \cdot s^{-1}$) is observed in August rather than May or June.

Although chamber flux measurements were unavailable from HDF88, Equations 2.5.1 and 4.2.1.8 both show flux maxima during June and July, with the largest fluxes occurring in June (6.7 and 4.6 $\mu mol \cdot m^{-2} \cdot s^{-1}$, from Equations 4.2.1.8 and 2.5.1 respectively). Lower fluxes are observed in spring, fall and winter, with Equation 2.5.1 predicting the lowest fluxes in November (0.7 $\mu mol \cdot m^{-2} \cdot s^{-1}$) and 4.2.1.8 predicting the lowest fluxes in January (0.2 $\mu mol \cdot m^{-2} \cdot s^{-1}$).

Calculated emission rates using Equations 2.5.1 and 4.2.1.8 are corrected for soil moisture changes, which were incorporated into the calculation of D_S, in addition to temperature changes associated with the $[CO_2]$ conversion factor (Table 23). These show poor correlations with either variable at all sites of study (Figure 61) ($R^2 \leq 0.33$ and $R^2 \leq 0.06$ for soil temperature and moisture respectively). While the poor correlations may indicate that soil moisture and temperature yield minor influences on soil CO_2 efflux,

varying degrees of photosynthetic uptake may mask any variations in flux rates that are related to either variable.

Table 23: CO_2 fluxes at all BC sites, adjusted for variability in soil temperature and moisture.

Site	Method	Fluxes ($\mu mol \cdot m^{-2} \cdot s^{-1}$)						
		2006						2007
		Apr	May	Jun	Jul	Aug	Nov	Jan
DF49	Chamber 1	1.70	1.84	2.43	2.05	1.09	0.22	
	Chamber 2	0.91	1.68	7.65	3.34	2.65	1.45	
	Equation 2.5.1	3.17	5.65	10.82	6.10	4.80	7.27	3.34
	Equation 4.2.1.8	3.06	7.33	9.79	6.37	3.56	3.36	2.56
HDF88	Equation 2.5.1	5.73	6.44	8.32	3.98	3.89	2.02	3.99
	Equation 4.2.1.8	6.95	3.25	12.30	4.14	6.20	3.79	1.40
HDF00	Chamber 1	0.70	3.87	1.67		0.73	0.56	
	Chamber 2	0.68	2.37		1.49	1.14	1.99	
	Equation 2.5.1	3.35	7.35	11.19	6.57	4.85	4.70	3.72
	Equation 4.2.1.8	2.50	4.71	6.44	2.38	1.34	0.93	2.23

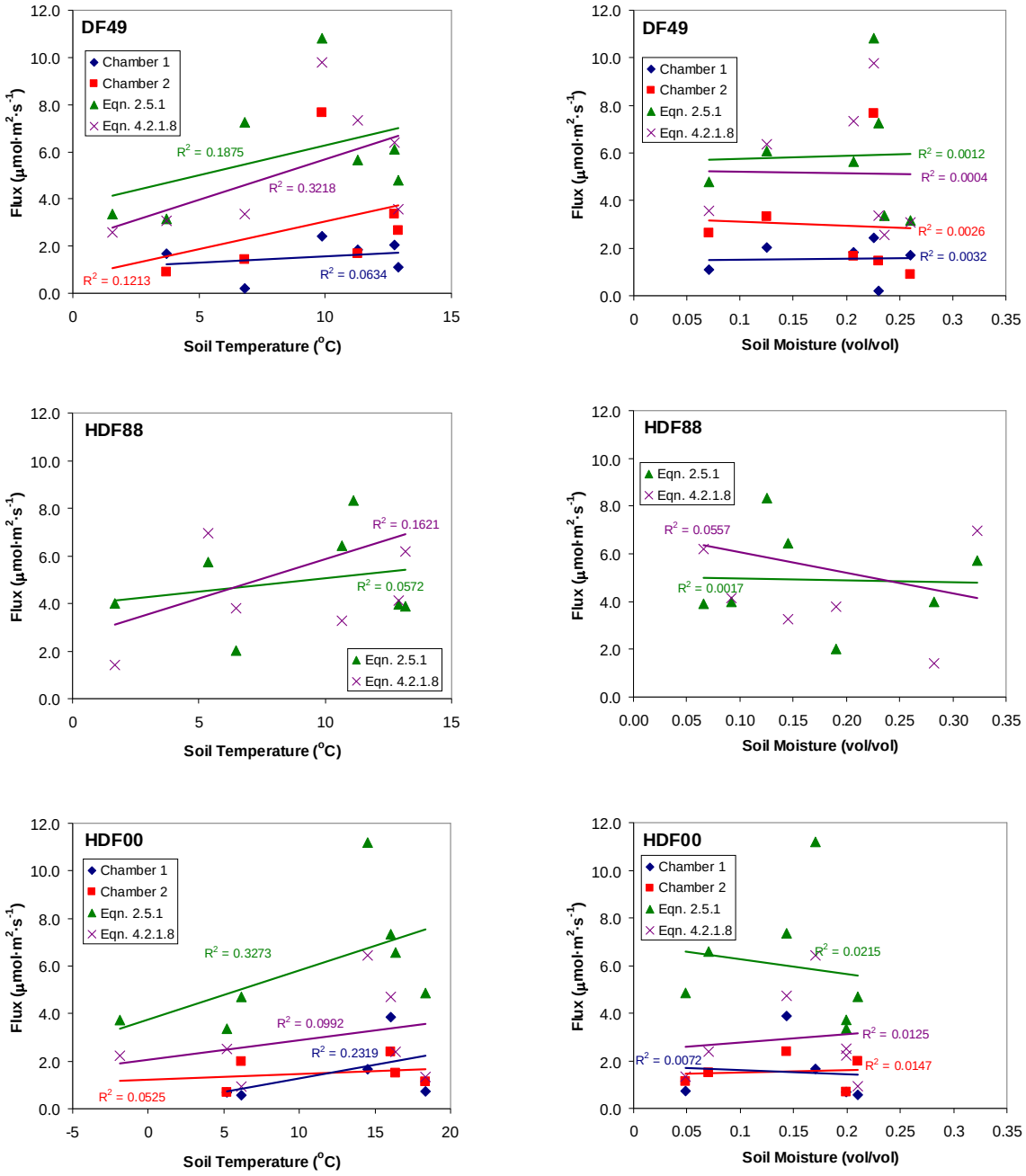

Figure 61: Correlations of BC fluxes with soil temperature and moisture.

4.3 Comparison of BC and OBS sites - Inter-site Differences in CO_2 Cycling

The similarity of the CO_2 flux ranges from HDF88 and DF49 suggests that the two forest sites have indistinguishable CO_2 cycling characteristics (Figure 62). On the other hand, the largest flux observed in the HDF00 chamber measurements (3.6 $\mu mol \cdot m^{-2} \cdot s^{-1}$) is only half of the maximum chamber flux measured in DF49 (7.2 $\mu mol \cdot m^{-2} \cdot s^{-1}$). As well, the maximum fluxes calculated from the HDF00 [CO_2] depth profiles (3.5 $\mu mol \cdot m^{-2} \cdot s^{-1}$ and 2.7 $\mu mol \cdot m^{-2} \cdot s^{-1}$, using 2.5.1 and 4.2.1.8, respectively) are at least 13 % lower than those calculated from DF49 (5.2 and 6.6 $\mu mol \cdot m^{-2} \cdot s^{-1}$, using 2.5.1 and 4.2.1.8, respectively) and HDF88 (4.6 and 6.8 $\mu mol \cdot m^{-2} \cdot s^{-1}$, using 2.5.1 and 4.2.1.8, respectively) using the same equations.

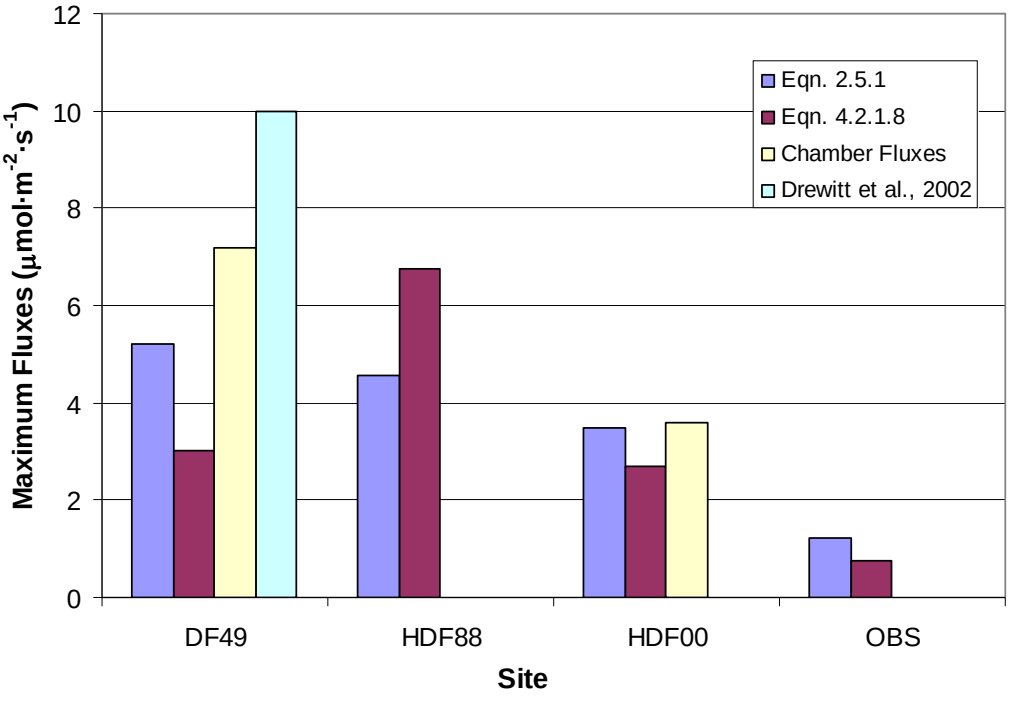

Figure 62: Comparison of maximum CO_2 fluxes at all sites.

The differences in the flux magnitudes of HDF00 as compared to DF49 and HDF88 are likely due to site characteristics. The absence of thick tree cover and the increased exposure of the ground surface at HDF00 could lead to lower accumulations of organic matter at that site. This hypothesis is supported by measurements of the thickness of the organic layer overlying the HDF00 mineral soil surface, which is smaller than that observed in both HDF88 and DF49 (Figure 63; see Table 24).

Past studies have shown that the bulk of CO_2 production occurs within the upper 20 cm of the soil column, with much of it concentrated within the organic topsoil (Certini et al., 2003; Jassal et al., 2005). As well, the results of the present study indicate that CH_4 uptake rates are also largest within the upper 5 cm of soil. This could further contribute to the enhanced shallow-depth CO_2 effluxes, as CO_2 is a by-product of CH_4 oxidation (see Equation 1.2.4, in Section 1.2)

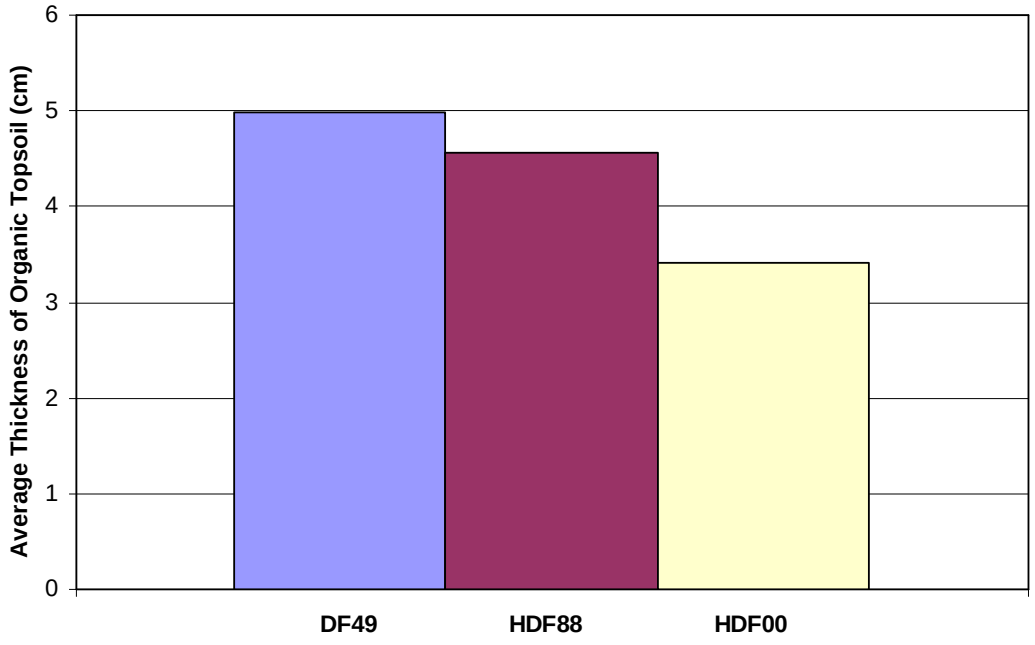

Figure 63: A comparison of organic topsoil thickness at all BC sites.

Table 24: Organic layer thickness at all BC sites.

Site	Avg. Organic Layer Thickness (cm)
DF49	4.99
HDF88	4.57
HDF00	3.41

Thus, if maximum rates of carbon mineralization and methane oxidation occur within the topsoil at OBS, a smaller organic horizon could at least be partially responsible for the lower CO_2 fluxes. In addition, the lower density of tree roots would reduce the amount of CO_2 released by plant respiration. In light of these factors, net CO_2 production in HDF00 is expected to be lower than the output in older forests, while the similarity of environmental characteristics at HDF88 and DF49 (i.e., a greater quantity of full-grown trees and thicker organic ground cover) result in similar subsurface and near-ground CO_2 dynamics.

The range of maximum fluxes calculated from the depth profile data at all BC sites (3.2 to 4.2 $\mu mol \cdot m^{-2} \cdot s^{-1}$and 1.9 to 4.8 $\mu mol \cdot m^{-2} \cdot s^{-1}$ using Equations 2.5.1 and 4.2.1.8, respectively) are 3 to 9 times larger than the largest fluxes calculated from the OBS data (1.2 to 0.8 $\mu mol \cdot m^{-2} \cdot s^{-1}$, using Equations 2.5.1 and 4.2.1.8, respectively). In this case, the lower average annual temperature and precipitation in OBS relative to the BC sites may be responsible for the lower OBS fluxes (see Table 5).

CO_2 efflux has been known to correlate positively with mean annual temperatures and precipitation on a global scale (Raich and Schlesinger, 1992). Therefore, despite the maturity of the forest at OBS and the similarity of soil moisture and temperature conditions during the same months of sampling, CO_2 fluxes may be more sensitive to

differences in climate rather than short term changes in weather or differences in forest age.

Based on these observed relationships, the current rise in global temperatures may result in enhanced CO_2 emission from forest soils. Whether this could act as a positive feedback on CO_2 climate forcing depends on the magnitude of concurrent changes in net primary production (NPP) also associated with rising temperatures. While quantification of NPP changes related to global warming is difficult, it is likely that increases in NPP due to rising temperatures would significantly dampen any enhancement in CO_2 output from soil respiration (Kirschbaum, 1999). Thus, any such increase in soil-respired CO_2 input would probably have a minimal influence on the atmospheric CO_2 burden.

Land clearance may have a stronger influence on global CO_2 dynamics. While clear-cutting of forest environments may act to reduce the accumulation of soil organic carbon and therefore reduce effluxes of soil-respired CO_2, the loss of tree cover would eliminate a large CO_2 sink that normally acts to intercept forest floor emissions (Humpreys et al., 2006). Thus, clear-cutting of forests would convert these areas into net CO_2 sources, despite the reduced soil CO_2 efflux.

5.0 Conclusions

5.1 Summary

Stable isotope and gas concentration data indicate that both BC temperate forest soils and Quebec boreal forest soils act as net sinks of CH_4 and net sources of CO_2. This is further supported by static chamber studies, which show decreasing [CH_4] and increasing [CO_2] with time, implying net consumption of CH_4 and net emission of CO_2 from DF49 and HDF00.

These concentration changes are coupled with increasingly ^{12}C-depleted $\delta^{13}CH_4$, indicating microbial ^{13}C-discrimination during CH_4 uptake, and increasingly ^{12}C-enriched $\delta^{13}CO_2$, indicating the production of ^{12}C-enriched CO_2 from within the soil. BC site CH_4 fluxes obtained from chamber measurements and depth profile calculations range from 0 to –6.8 $mg \cdot m^{-2} \cdot d^{-1}$, while summertime fluxes from OBS show a range of –1.5 to –2.3 $mg \cdot m^{-2} \cdot d^{-1}$. CO_2 fluxes from all BC sites using chamber and depth profile data range from 0.2 to 7.2 $\mu mol \cdot m^{-2} \cdot s^{-1}$, while OBS fluxes range from 0.8 to 1.2 $\mu mol \cdot m^{-2} \cdot s^{-1}$.

Large ranges in $\delta^{13}C$ (± 4.9 ‰ and ± 5.8 ‰ for CH_4 and CO_2, respectively), soil concentration (± 1 ppm and ± 0.23 ppm for CH_4 and CO_2, respectively) and chamber fluxes of CH_4 and CO_2 (± 4.1 $mg \cdot m^{-2} \cdot d^{-1}$ and ± 3.5 $\mu mol \cdot m^{-2} \cdot s^{-1}$ for CH_4 and CO_2, respectively) are indicators of intra-site heterogeneities in factors such as soil moisture, texture, temperature and organic carbon content.

Despite the dominance of methanotrophic activity at all sites, as indicated by the static chamber studies and the low observed soil [CH_4] relative to near-ground values,

^{12}C-enriched $\delta^{13}CH_4$ is observed during some periods of sampling. This may be due to the influence of diffusive fractionation, during which ^{12}C-enriched CH_4 is preferentially mobilized as opposed to ^{13}C-enriched CH_4, which moves slower via diffusive movement.

This suggests that the commonly applied Rayleigh fractionation model is inappropriate and under-defined for use in forest soils. Diffusive fractionation effects result in ^{12}C-enrichment by as much as 1.7 ‰ relative to atmospheric values. This value, while much smaller than the largest observed ^{12}C-depletion (10 ‰, observed at 80 cm depth in January at DF49), is similar in magnitude to the maximum summertime ^{12}C-depletions resulting from methane oxidation at all sites, which range from 0.3 to 4.0 ‰. This degree of diffusive isotopic fractionation is also significant in that it is expressed in the assumed presence of methanotrophic activity. Thus, ^{12}C-enrichment via diffusive fractionation must be taken into account to correctly define CH_4 fluxes in these forest soils.

The CO_2 data cannot be satisfactory explained by a two-endmember atmosphere-SOM mixing model. Keeling Plot techniques often display atmospheric endmembers that are more ^{12}C-depleted than expected. Photosynthetic activity, which can fractionate CO_2 by as much as 27 ‰, could be responsible for the heavier atmospheric endmember. Seasonal variations in calculated F_{photo} values seem to be related to not only PAR levels but also changes in soil moisture, which can affect apparent F_{photo} by either increasing $\Delta^{13}CO_2$ as soil moisture decreases, or by providing an optimum level for maximum photosynthetic activity.

The general similarity of calculated and measured CH_4 uptake rates within all sites during all months of sampling show a weak dependence of CH_4 flux with seasonal

change. As well, CH_4 uptake rates do not appear to be dependent on forest age or climate. CO_2 fluxes show more consistent variation, with HDF00 showing lower fluxes than either DF49 or HDF88, probably due to reduced organic topsoil thickness relative to the other more mature sites. OBS shows smaller fluxes than all of the BC sites, which is likely due to the reduced annual temperatures and precipitation observed in that environment, as compared to the warmer, wetter conditions on Vancouver Island.

Based on the findings of this study, increasing global temperatures are unlikely to significantly affect the strength of forest soils as a CH_4 sink or CO_2 source in the near future. This is due to the observed weak dependence of CH_4 and CO_2 flux on soil temperature. As well, the concurrent increases in plant CO_2 uptake that are expected to accompany any temperature rise would dampen the effects of any increase in soil-respired CO_2 output that may occur. However, clearing of forested areas may convert these environments into net CO_2 sources, given the reduced CO_2 uptake resulting from diminished vegetative cover.

5.2 Directions for Future Research

Given the large variability in gas fluxes encountered in this study, future studies should exercise caution when extrapolating point flux estimates to larger areas and a thorough analysis of site conditions and characteristics should accompany any CO_2/CH_4 flux study carried out within forest environments. Especially important are variables such as soil moisture, temperature and texture, all of which have been found to exert varying degrees of influence on CH_4 and CO_2 dynamics. As well, the installation of additional

chambers at DF49 and HDF00 could help clarify these intra-site variations by providing additional efflux/influx measurements over a larger area.

While the techniques carried out in this study provide valuable tools for the clarification of soil carbon-cycling processes, it may be useful to utilize other methods of flux-determination in conjunction with soil profile and static chamber data. In particular, eddy covariance studies would be particularly valuable, since gas fluxes would be measured over a larger area.

This would theoretically provide a more accurate average flux, since site heterogeneities would exert a lesser influence on EC measurements. Eddy covariance techniques have been successfully applied to ecosystem CO_2 flux measurements at all BC sites and with the advent of robust, fast-response CH_4 concentration analyzers, the same techniques can now be utilized to measure CH_4 uptake as well.

The exact nature of near-surface photosynthetic CO_2 uptake warrants further investigation, as this phenomenon has the potential to dampen or even offset CO_2 emissions from the soil surface. More specifically, information on photosynthetic uptake rates and the $\Delta^{13}CO_2$ associated with surface-level flora, as well as the effects of soil moisture and temperature on photosynthetic rates and isotope fractionation will need to be obtained in order to aid any future study.

References

Alstad, K.P., Lai, C.T., Flanagan, L.B. and J.R. Ehleringer (2007). Environmental controls on the carbon isotope composition of ecosystem-respired CO_2 in contrasting forest ecosystems in Canada and the USA. *Tree Physiol*. **10**: 1361-1374.

Amundson, R., Stern, L., Baisen, Troy, and Y. Wang (1998). The isotopic composition of soil and soil-respired CO_2. *Geoderma*. **82**: 83-114.

Castro, M.S. Steudler, P.A. and J.M. Melillo (1995). Factors controlling methane consumption by temperate forest soils. *Global Biogeochem. Cycles*. **9**: 1-10.

Certini, G. et al. (2003). Carbon Dioxide efflux and concentration in two soils under temperate forests. *Biol. Fertil. Soils* **37**: 39-46

Cerling, T.E. et al. (1991). On the isotopic composition of carbon in soil carbon dioxide. *Geochim. Cosmochim. Acta*. **55**: 3403-3405.

Currie, J.A. (1965). Diffusion within soil microstructure: a structural parameter for soils. *J. Soil Sci*. **16**: 279-289.

Czepiel , P.M., Cril, P.M. and R.C. Harris (1995). Environmental factors influencing the variability of methane oxidation in temperate zone soils. *J. Geophys. Res.* **100**: 9359-9364

Danielson, E.W., Levin, J. and E. Abrams (2003). *Meteorology*. McGraw-Hill College New York.

Davidson, E.A., Savage, K., Verchot, L.V. and R. Navarro (2002). Minimizing artefacts and biases in chamber-based measurements of soil respiration. *Agric. For. Meteorol.* **113**: 21-37.

Dlugokencky, E.J. et al. (2003). Atmospheric methane levels off: Temporary pause or new steady state?. *Geophys. Res. Lett.* **30**: ASC5.1-ASC5.4.

Dörr, H., Katruff, L. and I. Levin (1993). Soil texture parameterization of the methane uptake in aerated soils. *Chemosphere* **26**: 697-613.

Dörr, H. and K.O. Münnich (1990). 222Rn flux and soil air concentration profiles in West Germany: Soil 222Rn as tracer for gas transport in the unsaturated soil zone. Tellus B **42**: 20-28.

Drewitt, G.B. et al. (2002). Measuring forest floor CO_2 fluxes in a Douglas-fir forest. *Agric. For. Meteorol*. **110**: 299-317.

Environment Canada (2005). *National Inventory Report – Greenhouse Gases Sources and Sinks in Canada*. Available online: http://www.ec.gc.ca/pdb/ghg/. Accessed July 5, 2005

Fry, B. (2006). *Stable Isotope Ecology*. Springer New York.

Gupta, S., Tyler, S., and R. Cicerone (1996). Modeling atmospheric $\delta^{13}C$ and the causes of recent changes in atmospheric CH_4 amounts. *Ecosystems*. **3**: 269-282.

Hanson, R.S. and T.E. Hanson (1996). Methanotrophic Bacteria. *Microbiol. Rev*. **60**: 439-471.

Higgins, L.J. et al. (1981). Methane-oxidizing Microorganisms. *Microbiol. Rev*. **45**: 556-590.

Humphreys et al. (2006). Carbon dioxide fluxes in coastal Douglas-fir stands at different stages of development after clearcut harvesting. *Agric. For. Met*. **140**: 6-22.

IPCC (2007). *IPCC Fourth Assessment Report: Climate Change 2007 - The Physical Science Basis*. Cambridge University Press, Cambridge UK: 137-140.

Jang, I. et al. (2006). Methane oxidation rates and their controlling variables: a review and a case study in Korea. *Ecol. Res.* **21**: 849-854.

Jassal, R. et al. (2004). A model of the production and transport of CO_2 in soil: predicting soil CO_2 concentrations and CO_2 efflux from a forest floor. *Agric. For. Met*. **124**: 219-236.

Jassal, R. et al. (2005). Relationship between soil CO_2 concentrations and forest-floor CO_2 effluxes. *Agric. For. Met*. **130**: 176-192.

Keeling, C.D. (1958). The concentration and isotopic abundances of carbon dioxide in rural areas. *Geochim. et Cosmochim. Acta* **13**: 322-334.

Khalil, M.A.K. (2000). Atmospheric Methane: An Introduction. In: *Atmospheric Methane: Its Role in the Global Environment*. M.A.K. Khalil. Springer-Verlag Berlin Heidelberg, New York: 1-8.

Khalil, M.A.K., Shearer, M.J. and R.A. Ramussen (2000). Methane Sinks, Distribution, and Trends. In: *Atmospheric Methane: Its Role in the Global Environment*. M.A.K. Khalil. Springer-Verlag Berlin Heidelberg, New York: 86-97.

Kirschbaum, M.U.F. (1999). Will changes in soil organic carbon act as a positive or negative feedback on global warming? *Biogeochemistry* **48**: 21-51.

Le Mer, J. and P. Roger (2001). Production, oxidation and consumption of methane by soils: A review. *Eur. J. Soil. Biol.* **37**: 25-50.

Lloyd, J., and J.D. Farquhar (1994). 13C discrimination during CO2 assimilation by the terrestrial biosphere. *Oecologia.* **99**: 201-215.

Marshall (1959). The diffusion of gas through porous media. J. Soil Sci. **10:** 79-82.

Millington, R.J. and J.P. Quirk (1961). Permeability of porous solids. *Trans. Faraday Soc*. **57:** 1-8.

Moldrup, P., Olsen, T., Yamaguchi, Y., Schjonning, P. and D.E. Rolston (1999). Modelling diffusion and reaction in soil. IX. The Buckingham-Burdine-Campbell equation for gas diffusivity in undisturbed soil. *Soil Sci.* **164:** 542-551.

Nakano, T. et al. (2004). A comparison of regression methods for estimating soil-atmosphere diffusion gas fluxes by a closed-chamber technique. *Soil Biol. Biochem.* **36**: 107-113.

National Resources Canada (2001). *Canada's National Forest Inventory*. Available online: http://www.pfc.forestry.ca/monitoring/inventory/canfi/index_e.html. Accessed July 5, 2005

Pataki, D.E. et al. (2003). The application and interpretation of Keeling plots in terrestrial carbon cycle research. *Global Biogeochem. Cycles.* **17:** 1673-1676.

Penman, H.L. (1940). Gas and vapour movement in the soil. I. The diffusion of carbon dioxide through porous solids. *J. Agric. Sci.***. 30:** 22-1 – 22-13.

Prévost, M. (1997). Effects of scarification on seedbed coverage and natural regeneration after a group seed-tree cutting in a black spruce (*Picea mariana*) stand. *For. Ecol. Manage*. **94**: 219-231.

Prévost, M. (2004). Predicting Soil Properties from Organic Matter Content following Mechanical Site Preparation of Forest Soils. *Soil Sci. Soc. Am. J*. **68**: 943-949.

Priemé, A. et al. (1999).Spatial variability of CH_4 uptake in a Danish forest soil and its relation to different measurement techniques. *Atmospheric Enviornment* **30**: 1375-1379.

Quay, P.D. et al. (1999). The isotopic composition of atmospheric methane. *Global Biogeochem. Cycles*. **13:** 445-462.

Raich, J.W. and W.H. Schlesinger (1992). The global carbon dioxide flux in soil respiration and its relationship to vegetation and climate. *Tellus B*. **44:** 81-99.

Reeburgh, W.S. et al. (1997). Carbon kinetic isotope effect accompanying microbial oxidation of methane in boreal forest soils. *Geochim. Cosmochim. Acta*. **61:** 4761-4767.

Ridgwell, A.J., Marshall, S.J. and K. Gregson (1999). Consumption of atmospheric methane by soils: a process-based model.*Global Biogeochem. Cycles*. **13:** 59-65.

Savage, K., Moore, T.R. and P.M. Crill (1997). Methane and carbon dioxide exchanges between the atmosphere and northern boreal forest soils. *J. Geophys. Res.* **102:** 29,279-29,288.

Slater, C., Preston, T. and L.T. Weaver (2001). Stable isotopes and the international system of units. *Rapid Comm. In Mass Spectrom.* **15:** 1270-1273.

Snover, A.K. and P.D. Quay (2000). Hydrogen and carbon kinetic isotope effects during soil uptake of atmospheric methane. *Global Biogeochem. Cycles.* **14:** 25-39.

Sokal, R.R. and F.J. Rohlf. *Biometery*. W.H. Freeman, New York. 1995

Stevens, C. (1988). Atmospheric Methane. *Chem. Geol.* **71:** 11-21.

Sugawara, S. et al. (1996). Aircraft measurements of the stable isotopic ratios in atmospheric methane and some of its sources. *Global Biogeochem. Cycles.* **10:** 223-231.

Swanson, R.V. and L.B. Flanagan (2001). Environmental regulation of carbon dioxide exchange in a boreal black spruce ecosystem. *Agric. For. Met.* **108**: 165-181.

Templeton, A.S. et al. (2006). Variable carbon isotope fractionation expressed by aerobic CH_4-oxidizing bacteria. *Geochim. Cosmochim. Acta.* **70:** 1739-1752.

West, A.E. and S.K. Schmidt (1999). Acetate stimulates atmospheric CH_4 oxidation by an alpine tundra soil. *Soil Biol. Biochem.* **31:** 1649-1655.

Whiticar, M.J., Faber, E. and M. Schoell (1986). Biogenic methane formation in marine and freshwater environments: CO_2 reduction vs. acetate fermentation—isotope evidence. *Geochim. Cosmochim. Acta*. **50**: 693-709.

Whiticar, M.J. (1999). Carbon and hydrogen isotope systematics of bacterial formation and oxidation of methane. *Chem. Geol*. **161**: 291-314.

Whiticar, M.J. (2000). Can Stable Isotopes and Global Budgets Be Used to Constrain Atmospheric Methane Budgets? In: *Atmospheric Methane: Its Role in the Global Environment*. M.A.K. Khalil. Springer-Verlag Berlin Heidelberg, New York: 63-85.

Williams, T.G. and L.B. Flanagan (1996). Effect of changes in water content on photosynthesis, transpiration and discrimination against $^{13}CO_2$ and $C^{18}O^{16}O$ in *Pleurozium* and *Sphagnum*. *Oecologia*. **108**: 38-46.

Wuebbles, D.J., and K. Hayhoe (2002). Atmospheric methane and global change. *Earth-Science Reviews.* **57**: 177-210.

APPENDIX

Table A1: CO_2 data collected from OBS

SAS	Depth	Late June 2005		Early August 2005		Late August 2005	
Subsite	(cm)	$[CO_2]$ (ppm)	$\delta^{13}CO_2$ (‰)	$[CO_2]$ (ppm)	$\delta^{13}CO_2$ (‰)	$[CO_2]$ (ppm)	$\delta^{13}CO_2$ (‰)
A-1	5	723.41	-14.52	1053.68	-16.27	869.01	-18.49
	10	894.62	-12.20	2054.05	-22.99	976.49	-17.71
	15	1267.58	-15.37	424.38	-8.46	1041.30	-17.83
	20	2490.22	-17.85	1396.25	-16.76	2454.73	-20.29
	30	1255.11	-14.30	773.63	-14.25	436.40	-11.31
A-2	5	940.44	-9.26	758.07	-14.37	692.94	-14.64
	10	1388.96	-12.32	1027.37	-16.07	910.60	-16.91
	15	1536.72	-15.79	1082.06	-14.96	1039.68	-17.72
	20	1860.06	-16.86	1635.51	-18.09	1395.61	-19.65
	30	2437.20	-17.14	1954.75	-19.15	2473.64	-20.51
B-1	5	1191.55	-13.56	1242.68	-15.29	706.44	-17.12
	10	1524.19	-14.63	1048.05	-15.7	982.97	-17.47
	15	1531.63	-14.61	795.69	-14.08	447.20	-15.76
	20	1927.16	-15.64	1262.49	-16.61	1520.91	-19.02
	30	2060.38	-16.87	961.86	-14.27	1423.69	-19.32
B-2	5	1447.23	-15.59	897.74	-14.87	747.49	-16.68
	10	2155.54	-16.43	1186.64	-15.76	982.97	-17.26
	15	1415.79	-15.13	580.56	-11.44	682.68	-16.08
	20	1975.98	-16.56	1214.22	-16.94	1473.38	-19.21
	30	2163.82	-16.89	2178.84	-19.02	1419.37	-19.60
C-1	5	650.07	-8.78	1247.32	-16.77	1054.27	-18.16
	10	1597.13	-16.07	1097.69	-17.04	970.01	-18.50
	15	1811.05	-13.97	554.36	-10.15	1559.54	-21.62
	20	591.22	-9.01	492.31	-10.37	2071.99	-21.08
	30	3359.03	-20.24	2744.24	-21.56	462.50	-14.50
C-2	5	1320.91	-10.63	505.41	-11.44	689.16	-16.06
	10	1525.13	-16.24	1177.68	-18.07	933.28	-17.99
	15	1328.52	-15.06	1298.34	-18.24	865.79	-18.72
	20	882.68	-14.26	763.97	-12.33	1030.44	-19.42
	30	3345.19	-20.53	480.59	-10.39	690.66	-19.39
1	80	2799.66	-18.69	2688.39	-20.49	2528.93	-21.30
2	80	2724.89	-18.59	2369.83	-19.57	1746.39	-20.55
3	80	4721.48	-20.99	3905.37	-28.95	3185.68	-22.01

Table A2: CH_4 data collected from OBS

SAS Subsite	Depth (cm)	Late June 2005		Early August 2005		Late August 2005	
		$[CH_4]$ (ppm)	$\delta^{13}CH_4$ (‰)	$[CH_4]$ (ppm)	$\delta^{13}CH_4$ (‰)	$[CH_4]$ (ppm)	$\delta^{13}CH_4$ (‰)
A-1	5.00	0.91	-47.86	0.83	-48.64	1.00	-43.72
	10.00	0.98	-47.13			0.31	-39.92
	15.00	0.71	-46.29	0.50	-48.66	1.02	-46.41
	20.00	0.39	-51.95	0.39	-48.16	0.60	-40.68
	30.00			0.86	-48.10	1.13	-47.45
A-2	5.00			0.76	-47.94	1.00	-45.08
	10.00			0.67	-47.28	0.68	-46.89
	15.00	0.88	-49.35	0.46	-49.10	1.09	-43.09
	20.00	1.02	-47.27			0.49	-45.11
	30.00			0.35	-48.13	0.21	-49.45
B-1	5.00	1.33	-48.00	0.82	-48.45	1.61	-49.25
	10.00	1.16	-47.23	0.92	-47.87	1.14	-44.32
	15.00	1.00	-48.29	1.58	-49.39	1.36	-45.45
	20.00	0.78	-47.60	1.05	-46.44	0.82	-44.36
	30.00	0.40	-45.63	0.89	-45.99	0.61	-39.20
B-2	5.00	1.54	-45.02	1.14	-48.60		
	10.00	1.20	-47.89	1.02	-48.44	1.48	-43.74
	15.00	1.41	-46.91	1.13	-47.57		
	20.00	1.18	-47.02	0.83	-46.80		
	30.00	0.70	-47.15	1.00	-46.39	0.71	-45.63
C-1	5.00	1.65	-48.50	1.69	-48.79	1.08	-45.96
	10.00			0.88	-47.33	0.98	-47.54
	15.00	0.93	-46.24	0.54	-48.50	1.08	-45.04
	20.00	1.24	-48.29	0.91	-48.83	1.08	-46.44
	30.00	0.72	-49.30	1.03	-45.68	1.12	-44.98
C-2	5.00	1.37	-48.34	1.85	-47.90	1.11	-44.79
	10.00	1.37	-48.30	0.89	-48.32	1.26	-43.48
	15.00	1.09	-47.32	1.04	-48.07	1.01	-44.01
	20.00	1.04	-48.33	1.20	-48.45	1.28	-43.62
	30.00	0.42	-45.94	1.36	-48.04	1.31	-45.35
1	80.00	0.52	-46.90	0.32	-46.28	0.51	-39.35
2	80.00	0.32	-46.59	0.27	-48.37	0.23	-44.72
3	80.00			0.52	-44.28	0.39	-38.25

Table A3: $\delta^{13}CO_2$ data collected from DF49 (continues onto next page)

SAS	Depth	$\delta^{13}CO_2$ (‰)						
Subsite	(cm)	Apr '06	May '06	Jun '06	Jul '06	Aug '06	Nov '06	Jan '07
A-1	5	-20.62	-19.78					
	10	-20.04	-20.27					
	15	-22.69	-20.14					
	20	-15.93	-18.40					
	30	-22.13	-21.34					
A-2	5	-22.13	-20.82	-21.10	-19.47	-13.97	-18.51	-18.80
	10	-22.83	-20.82	-21.16	-20.25	-14.86	-18.92	-19.29
	15	-22.75	-20.72	-19.98	-19.33	-14.32	-11.27	-10.86
	20	-22.14	-20.83	-20.48	-20.27	-15.86	-18.82	-10.69
	30	-22.67	-20.94	-21.98	-20.07	-18.44	-19.79	-10.60
B-1	5	-19.57	-19.81		-21.80			
	10	-21.40	-19.97		-21.18			
	15	-21.38	-20.77		-21.39			
	20	-23.24	-20.68					
	30	-23.18	-20.95					
B-2	5	-21.96	-20.46	-22.54	-20.38	-16.54	-20.25	-10.09
	10	-21.96	-20.16	-22.04	-20.30	-17.54	-19.65	-10.39
	15	-22.52	-20.92	-22.01	-20.37	-18.10	-20.54	-20.29
	20	-22.58	-21.73	-21.25	-20.98	-18.62	-19.43	-20.29
	30	-21.96	-21.49	-22.38	-21.31	-20.33	-20.59	-10.38
C-1	5	-18.47	-19.55					
	10	-21.13	-19.90					
	15	-21.88	-20.54					
	20	-22.12	-21.16					
	30	-22.42	-13.17					
C-2	5	-19.80	-19.36	-20.07	-19.39	-13.61	-15.85	-10.56
	10	-20.23	-19.53	-21.66	-20.16	-15.50	-19.03	-19.11
	15	-18.99	-21.04	-22.04	-21.00	-18.29		-10.60
	20	-20.78	-20.64	-21.10	-20.71	-17.66	-18.96	-10.46
	30	-21.81	-21.22	-21.30	-21.04	-19.09	-20.87	-20.03
D-1	5	-18.82	-18.27				-17.27	
	10	-20.79	-15.42				-14.65	
	15	-21.98	-20.33				-19.14	
	20	-21.64	-21.07				-15.61	
	30	-17.39	-20.26				-18.50	
D-2	5	-19.34	-18.53	-19.10	-19.63	-14.35		-10.83
	10	-20.68	-18.92	-17.46	-20.15	-16.04		-13.11
	15	-21.66	-19.71	-21.69	-21.40	-16.56		-20.14
	20	-18.91	-18.23	-20.87	-19.21	-17.95		-11.95
	30	-21.61	-20.09	-20.41	-21.06	-18.11		-17.28
E-1	5	-16.15	-17.03					
	10	-13.57	-17.18					
	15	-18.99	-18.88					
	20	-20.44	-19.63					

Table A3 (continued)

SAS Subsite	Depth (cm)	$\delta^{13}CO_2$ (‰) Apr '06	May '06	Jun '06	Jul '06	Aug '06	Nov '06	Jan '07
E-1	30	-20.76	-19.77					-20.81
E-2	5	-13.95	-16.23	-17.28	-16.84	-10.45	-17.66	-15.48
	10	-19.23	-17.70	-22.40	-19.63	-13.32	-19.89	-10.65
	15	-19.52	-18.61	-19.56	-20.00	-14.16	-18.89	-10.54
	20	-20.24	-19.12	-19.48	-20.45	-15.56	-14.50	-10.60
	30	-19.81	-19.78		-20.65	-16.34	-19.16	
F-1	5	-21.34	-20.47					
	10	-22.05	-21.16					
	15	-22.17	-21.39					
	20	-23.03	-21.87					
	30	-14.14	-18.67					
F-2	5	-19.78	-19.74	-20.29	-20.18	-15.34	-17.72	-10.87
	10	-21.00	-21.18	-20.75	-20.56	-17.02	-18.77	-20.25
	15	-21.84	-21.05	-20.89	-20.69	-17.12	-18.45	-10.71
	20	-10.92	-14.96	-15.71		-10.16	-24.82	-12.55
	30	-22.90	-22.00	-18.51	-20.94	-18.77	-24.59	-11.09
1	80					-19.99	-11.75	
2	80					-20.94	-11.43	

Table A4: [CO_2] data collected from DF49 (continues onto next page)

SAS Subsite	Depth (cm)	[CO_2] (ppm) Apr '06	May '06	Jun '06	Jul '06	Aug '06	Nov '06	Jan '07
A-1	5	2207.96	2015.18					
	10	1743.36	3208.32					
	15	2818.69	3720.85					
	20	837.70	1850.44					
	30	4522.96	5284.24					
A-2	5	2748.51	4931.45	5732.72	2713.77	2420.73	2353.87	1390.10
	10	4950.70	5728.54	6019.53	3840.42	2528.32	2415.42	1620.14
	15	2760.06	3279.04	4120.92	3335.76	2097.97	470.50	395.45
	20	4265.79	4953.92	6495.02	5904.88	3169.71	2996.70	391.07
	30	5923.87	6132.08	8406.21	6125.87	4184.90	4870.50	389.97
B-1	5	1648.90	2662.75		5281.22			
	10	2416.19	2676.33		4875.04			
	15	2732.20	2857.36		8699.99			
	20	3531.69	3524.94					
	30	5582.35	3190.77					
B-2	5	2450.00	3589.81	8157.14	3764.88	3230.40	3164.93	400.93
	10	2412.97	3991.11	4500.81	3518.98	3393.16	3350.95	400.93
	15	2943.95	4366.00	6864.01	3707.03	4780.77	4056.70	398.74
	20	2883.57	3844.01	10706.51	4488.93	5088.36	4576.44	2348.59
	30	2653.70	6293.29	11000.02	6166.05	5848.37	6142.49	389.97
C-1	5	1114.30	2176.21					
	10	2609.82	3487.98					
	15	2862.63	3898.33					
	20	3705.60	4333.57					
	30	4630.69	892.36					
C-2	5	1462.52	2499.06	3102.85	1740.17	1789.00	2422.60	375.73
	10	1783.76	2749.50	5070.22	2951.02	2226.24	2789.85	1625.61
	15	1279.35	4661.70	7301.76	6457.01	4565.59		385.59
	20	2562.32	4618.70	6165.45	5152.10	4469.04	4405.95	394.35
	30	4020.41	5955.36	9158.44	2490.96	6323.07	6073.48	1960.81
D-1	5	1116.31	1694.96				1354.81	
	10	1716.53	1198.61				969.04	
	15	2538.24	3805.54				2848.49	
	20	2843.36	4955.88				1122.32	
	30	922.80	2962.97				2115.02	
D-2	5	1050.69	2115.11	2361.52	1930.01	1932.92		374.64
	10	1282.97	2643.89	1361.15	3122.90	2223.95		799.66
	15	1989.33	3272.99	3448.77	3949.80	2417.11		1650.81
	20	1042.99	1888.06	4290.63	1930.86	3570.93		484.56
	30	2319.54	4305.66	4668.29	4391.90	3528.44		2439.76
E-1	5	808.49	1391.07					
	10	620.55	1904.07					
	15	1312.42	2300.61					
	20	1840.31	2898.59					

Table A4 (continued)

SAS	Depth	$[CO_2]$ (ppm)						
Subsite	(cm)	Apr '06	May '06	Jun '06	Jul '06	Aug '06	Nov '06	Jan '07
E-1	30	1905.84	2844.30					2165.48
E-2	5	567.80	1310.82	1298.20	1046.67	1390.77	2011.12	1076.21
	10	1187.45	2081.10	3075.48	1882.12	1874.97	2406.14	468.88
	15	1327.66	2234.52	2507.24	2574.77	2002.45	3193.11	478.03
	20	1525.77	2417.85	2083.25	2396.90	2220.08	1012.25	464.96
	30	1558.08	2396.60		3650.51	2594.82	5143.53	
F-1	5	2466.95	4454.88					
	10	3093.60	5457.27					
	15	3941.82	5832.58					
	20	5279.54	6073.34					
	30	418.47	1592.49					
F-2	5	2009.16	2859.25	4927.06	3408.51	2816.31	2038.90	489.78
	10	2743.40	5186.61	7109.97	3950.65	3988.17	2738.42	2177.24
	15	3852.83	6303.87	7035.66	7130.85	4409.26	3036.74	458.43
	20	563.86	1369.04	1278.97		1395.92	3624.13	491.09
	30	6350.87	8415.66	2201.27	11984.24	7213.98	3241.45	472.80
1	80					5245.01	364.16	2116.86
2	80					5404.69	375.48	

Table A5: $\delta^{13}CO_2$ data collected from HDF88

SAS	Depth	$\delta^{13}CO_2$ (‰)						
Subsite	(cm)	Apr '06	May '06	Jun '06	Jul '06	Aug '06	Nov '06	Jan '07
A-1	5	-20.03	-19.46					
	10	-20.11	-19.58					
	15	-22.54	-21.62					
	20	-22.56	-18.27					
	30	-23.25	-22.49					
A-2	5	-20.20	-19.21	-20.15	-17.96	-13.13	-15.62	-12.87
	10	-22.23	-20.87	-21.49	-20.58	-16.73	-17.83	-6.64
	15	-22.01	-21.35	-21.82	-20.84	-17.01	-19.52	-11.79
	20	-23.50	-23.80	-22.39	-21.08	-17.40	-10.44	-11.70
	30	-23.82	-22.44	-22.32	-21.18	-18.63	-19.59	-20.39
B-1	5	-23.05	-21.88					-19.15
	10	-22.87	-21.56					
	15	-22.81	-21.83					
	20	-9.64	-22.12					
	30	-23.43	-22.35					
B-2	5	-20.18	-21.21	-21.92	-20.85	-17.88	-10.69	
	10	-22.50	-21.69	-22.06	-21.38	-18.88	-21.33	-20.22
	15	-23.38	-22.31	-22.30	-21.30	-18.73	-21.33	-11.87
	20	-23.35	-22.18	-22.05	-21.42	-18.51	-20.68	-12.18
	30	-22.85	-22.48	-22.26	-22.08	-18.27	-19.50	-18.44
C-1	5	-18.06	-18.64					-12.44
	10	-16.87	-19.50					-12.60
	15		-14.57					-9.33
	20	-23.56	-19.83					-13.28
	30		-12.11					-21.36
C-2	5	-19.83	-19.88	-19.89	-11.76	-14.00	-16.16	
	10		-18.23	-20.25	-12.49	-13.59	-10.57	
	15	-19.56	-20.51	-22.78	-13.53	-16.42	-10.46	
	20		-23.84	-21.71	-14.70	-15.76	-16.67	
	30	-25.49	-15.48		-11.82	-13.93	-27.64	
D-1	5		-16.74		-12.50			
	10	-20.37	-18.94		-20.21			
	15		-9.94		-14.06			
	20	-22.11	-21.05					
	30	-23.02	-22.24					
D-2	5	-15.91	-17.63	-18.71	-12.09	-12.65	-13.86	-16.80
	10	-19.89	-19.17	-19.81	-18.22	-14.57	-10.65	-14.71
	15	-21.01	-19.81	-20.59	-12.93	-16.45	-10.68	-15.63
	20	-21.67	-21.22		-20.74	-13.78	-20.38	-16.90
	30		-16.60	-20.77	-13.45	-15.90	-13.40	-11.60

Table A6: [CO_2] data collected from HDF88

SAS	Depth	[CO_2] (ppm)						
Subsite	(cm)	Apr '06	May '06	Jun '06	Jul '06	Aug '06	Nov '06	Jan '07
A-1	5	3100.22	2886.26					
	10	3623.73	2938.04					
	15	8296.45	7451.41					
	20	6982.22	2159.79					
	30	6410.94	10110.16					
A-2	5	2955.91	1704.77	2252.84	983.12	1243.27	1358.33	1675.26
	10	8700.53	4376.07	7084.61	3707.84	2292.32	2545.77	1422.65
	15	8452.71	7132.89	9193.21	4086.27	2204.79	3162.50	409.92
	20	5429.62	10033.28	10254.51	1764.95	2944.73	399.83	417.95
	30	8515.91	11432.08	9313.85	10770.84	4646.19	4428.81	3298.86
B-1	5	3524.70	6080.06					
	10	4341.31	6261.29					
	15	487.18	5086.27					
	20	323.06	5352.69					
	30	6634.91	8405.37					
B-2	5	4767.28	7061.50	8136.70	6778.78	3941.81	411.88	
	10	5184.29	7809.94	9567.96	8388.32	4364.44	6452.06	2094.37
	15	5411.70	6224.79	11757.73	6453.49	4216.72	8500.51	446.66
	20	8548.03	7887.62	5266.23	8336.79	3360.52	4733.34	412.21
	30	5654.16	8833.87	9148.05	12282.96	2812.06	3137.30	3089.88
C-1	5	1580.52	1994.22					1840.21
	10	1062.54	2227.17					1075.77
	15		903.60					1265.92
	20	2136.67	2267.20					1286.59
	30		584.03					6709.85
C-2	5	1435.35	1149.68	1903.34	700.81	1184.46	687.93	
	10		1776.36	2649.47	537.85	1239.17	412.98	
	15	2610.34	3090.74	7533.79	902.95	1665.90	400.93	
	20	318.28	2784.95	5724.16	1221.74	1687.78	691.21	
	30	3013.82	503.31		630.46	1295.24	2981.75	
D-1	5		1465.97		526.15			
	10	2695.31	2319.04		1544.96			
	15		534.81		534.73			
	20	5873.40	4105.73					
	30	5460.77	7226.88					
D-2	5	1865.92	1670.71	2088.10	618.89	1116.07	1508.40	2307.59
	10	2551.72	2643.21	2653.89	2211.07	1529.13	399.83	1254.55
	15	4208.85	3043.49	3886.24	965.28	1929.87	397.64	1457.10
	20	4534.83	5005.86		4610.93	1243.27	3431.97	1638.98
	30		1402.31	2815.67	674.10	1598.88	1165.53	878.39

Table A7: $\delta^{13}CO_2$ data collected from HDF00

SAS	Depth	$\delta^{13}CH_4$ (‰)						
Subsite	(cm)	Apr '06	May '06	Jun '06	Jul '06	Aug '06	Nov '06	Jan '07
A-1	5	-13.48	-16.35				-12.57	
	10	-17.07	-17.63				-14.32	
	15	-13.52	-18.01				-19.52	-16.85
	20	-18.35	-18.14				-10.44	
	30	-15.90	-15.42				-19.59	-13.93
A-2	5	-16.72	-16.66	-20.68	-18.36	-9.50	-12.82	-13.61
	10	-19.29	-19.16		-18.52	-11.80	-15.47	-17.11
	15	-13.52	-17.93	-22.09	-19.81	-10.29	-14.16	
	20	-19.71	-19.31	-20.39	-19.70	-13.50	-10.42	-18.31
	30	-20.18	-19.71	-21.03	-18.90	-13.50	-10.36	-20.08
B-1	5	-11.57	-14.28	-16.81				
	10	-18.69	-18.99	-20.77				
	15	-20.10	-19.64	-21.34				
	20	-20.08		-21.37				
	30	-20.52		-21.33				
B-2	5	-18.56	-18.31	-20.22	-19.58	-11.85	-8.73	-14.79
	10	-19.28	-18.78	-20.74	-20.25	-13.93	-18.11	-17.45
	15	-19.83	-19.50		-20.88	-13.67	-18.71	-16.11
	20	-17.96	-18.46	-20.81	-20.62	-13.97	-17.02	-17.68
	30	-20.55	-19.59	-20.68	-21.00	-15.97	-19.49	-17.27
C-1	5	-18.50						
	10	-20.33						
	15	-21.18						
	20	-21.33						
	30	-20.78						
C-2	5	-17.11	-15.31	-19.51	-18.20	-10.87	-13.45	-12.82
	10	-20.19	-19.79	-21.10	-19.71	-14.74	-17.47	-15.55
	15	-20.73	-20.13	-21.17	-20.28	-15.01	-18.15	-18.53
	20	-21.25	-20.67	-20.88		-16.49	-10.52	-11.39
	30	-13.37	-20.34	-21.41	-21.02	-16.66	-10.41	-11.10
1	80					-10.80	-12.51	-12.05
2	80					-17.55	-10.73	-11.96

Table A8: [CO_2] data collected from HDF00

SAS	Depth	[CO_2] (ppm)						
Subsite	(cm)	Apr '06	May '06	Jun '06	Jul '06	Aug '06	Nov '06	Jan '07
A-1	5	527.08	1642.75				1131.58	
	10	959.26	1845.14				1177.58	
	15	1291.62	2913.42				3162.50	1490.24
	20	1217.13	2926.36				399.83	
	30	712.36	1223.53				4428.81	1028.40
A-2	5	897.63	1592.53	3937.51	1102.42	1309.64	906.29	1110.17
	10	1446.64	2686.68		1777.41	1797.70	1968.94	1185.92
	15	537.29	1521.01	2015.44	2813.93	1411.38	874.40	
	20	1890.92	3640.83	2638.23	1956.39	1659.91	377.54	1857.25
	30	2242.94	3679.64	4012.39	1185.23	1659.91	367.25	2742.77
B-1	5	486.08	945.78	1182.10				
	10	1094.52	2221.78	3584.07				
	15	1575.70	268.59	5131.82				
	20	1635.94		1787.22				
	30	1899.88		6554.19				
B-2	5	1209.73	2180.69	2187.41	1129.13	1527.27	1037.97	1056.62
	10	1326.08	2157.87	2959.67	2168.33	1818.31	1636.67	1575.13
	15	1713.88	3297.67		2780.09	1831.18	1891.79	1786.72
	20	920.95	2590.72	4037.31	3104.23	1370.17	1085.29	1665.25
	30	1901.39	2543.61	6330.79	3569.95	2969.56	2201.43	1908.18
C-1	5	1305.37						
	10	2217.66						
	15	2184.15						
	20	2616.76						
	30	2827.23						
C-2	5	916.43	1503.14	2083.75	1519.17	1333.54	1491.97	936.46
	10	2214.27	4163.39	5922.56	1755.14	1866.96	2178.80	1671.78
	15	3091.92	3937.07	5096.46	2308.00	2446.87	2481.14	2013.98
	20	1700.33	4498.62	7461.46		2656.14	395.45	508.07
	30	621.24	4752.75	5060.29	5290.64	3300.34	391.07	501.53
1	80					1274.73	829.14	404.84
2	80					3469.94	376.51	405.89

Table A9: $\delta^{13}CH_4$ data collected from DF49

SAS	Depth	$\delta^{13}CH_4$ (‰)						
Subsite	(cm)	Apr '06	May '06	Jun '06	Jul '06	Aug '06	Nov '06	Jan '07
A-1	5	-45.60	-48.51	-49.44	-45.99	-49.00	-47.62	-42.09
	10	-30.80	-41.62	-46.56	-43.15	-45.82	-48.74	-39.89
	15	-41.10	-40.86	-49.61	-48.77	-46.30	-48.33	-38.70
	20	-44.25	-44.29	-45.60	-46.48	-47.11		-42.75
	30	-46.92	-41.72	-49.23	-42.37	-48.70	-43.10	-42.20
A-2	20	-50.99					-49.25	
	30						-46.57	
B-1	5	-44.88	-47.61	-47.03	-48.29	-49.46	-46.72	-40.46
	10	-50.43	-44.23	-48.00	-45.74	-44.27	-44.48	-40.04
	15	-49.17		-50.47	-43.00	-45.92	-47.75	-42.01
	20	-39.88	-41.57	-45.30	-44.15	-48.71	-45.52	-40.74
	30	-42.88	-41.44	-43.51	-42.92	-51.53	-42.60	-38.39
B-2	5		-45.67					
	15		-48.07					
C-1	5	-47.08	-45.85	-46.36	-44.45	-49.32	-46.46	-39.46
	10	-50.83	-36.71	-48.99	-45.29	-49.15	-49.05	-43.62
	15		-48.84	-47.29	-45.69	-48.96	-45.91	-44.84
	20	-45.07	-47.20	-43.64	-43.55	-49.52	-45.16	-40.01
	30	-41.22	-42.89	-47.73	-47.12	-49.48	-45.54	-37.26
C-2	15	-47.57						
	20		-48.49					
D-1	5	-48.38	-47.11	-48.49	-47.16	-48.94	-48.07	-45.02
	10	-47.89	-47.75	-46.90	-48.26	-45.43	-47.64	-46.96
	15	-47.00	-48.91	-49.84	-50.85	-50.45	-49.32	-40.85
	20	-39.98	-45.80	-45.65	-48.99	-50.06	-46.95	-44.64
	30	-53.49	-46.93	-49.33	-48.62	-48.68		-40.02
D-2	30						-49.20	
E-1	5	-48.25	-47.63	-47.83	-45.55	-47.93	-47.52	-44.77
	10	-50.43	-45.65	-46.49		-49.34	-49.56	-42.63
	15	-47.52	-45.85	-50.76	-48.01	-49.89	-46.81	-39.06
	20	-50.58	-47.04	-47.11	-43.65	-50.23	-49.66	-38.51
	30	-47.84	-48.66	-42.98	-46.06	-48.40	-48.27	-36.77
E-2	10				-47.31			
F-1	5	-49.83	-44.25	-47.12	-46.35	-46.56	-47.90	-44.79
	10	-51.47	-45.68	-50.74	-51.24	-50.24	-45.95	-41.73
	15	-48.81	-49.72	-48.58	-45.46	-49.59	-46.32	-42.17
	20	-50.36	-41.73	-46.56	-45.53	-50.43	-42.93	-44.81
	30	-44.05	-44.16	-46.28	-47.69	-50.49	-47.65	-40.28
1	80					-44.96	-42.05	-37.11
2	80					-46.51	-46.30	-38.61

Table A10: [CH_4] data collected From DF49

SAS	Depth	[CH_4] (ppm)						
Subsite	(cm)	Apr '06	May '06	Jun '06	Jul '06	Aug '06	Nov '06	Jan '07
A-1	5	0.74	0.84	0.80	0.94	1.04	0.75	1.71
	10	1.25	0.66	0.55	0.54	0.69	0.27	0.97
	15	0.58	0.72	0.49	0.46	0.72	0.35	1.12
	20	1.92	1.73	1.74	1.53	1.47		1.77
	30	1.09	0.52	0.39	0.61	0.58	0.35	0.57
A-2	20	0.38					0.33	
							0.30	
B-1	5	1.06	1.16	0.84	1.09	0.80	0.79	1.66
	10	0.83	1.10	0.89	0.94	1.07	0.86	1.57
	15	0.71		0.61	0.87	0.79	0.54	0.73
	20	0.77	0.86	0.57	0.59	0.52	0.47	0.74
	30	0.54	1.27	0.53	0.91	0.35	0.68	1.18
B-2	5		1.19					
	15		0.71					
C-1	5	1.44	1.17	1.10	0.83	0.85	1.06	1.72
	10	0.44	1.23	0.55	0.62	0.60	0.43	1.21
	15		0.65	0.67	0.75	0.75	0.51	1.01
	20	0.60	0.42	0.64	0.68	0.55	0.46	1.94
	30	0.74	0.68	0.41	0.48	0.54	0.39	0.88
C-2	15	0.74						
	20		0.89					
D-1	5	1.52	1.66	1.45	1.44	0.95	1.09	2.12
	10	1.89	1.45	1.54	2.06	1.32	1.19	0.61
	15	0.55	0.46	0.53	0.46	0.52	0.40	0.95
	20	0.30	0.63	0.80	0.54	0.51	1.21	1.66
	30	1.06	1.13	0.92	0.73	0.79		1.21
D-2	30						0.30	
E-1	5	1.36	1.24	1.12	1.20	1.17	1.21	1.65
	10	0.38	0.28	0.62		0.75	0.40	1.13
	15	0.65	0.72	0.52	0.57	0.71	0.57	1.11
	20	0.44	0.50	0.51	0.63	0.56	0.38	1.08
	30	0.57	0.51	0.66	0.57	0.62	0.42	1.10
E-2	10				0.73			
F-1	5	1.16	1.25	1.30	1.03	1.50	0.88	1.60
	10	0.61	0.68	0.87	0.49	0.73	0.66	1.57
	15	0.80	0.62	0.70	0.80	0.83	0.59	1.25
	20	0.52	0.68	1.78	0.51	0.57	0.55	1.96
	30	2.41	1.96	0.57	1.49	0.54	1.32	1.15
1	80					0.54	0.43	0.83
2	80					0.40	0.30	0.77

Table A11: $\delta^{13}CH_4$ data collected from HDF88

SAS Subsite	Depth (cm)	$\delta^{13}CH_4$ (‰) Apr '06	May '06	Jun '06	Jul '06	Aug '06	Nov '06	Jan '07
A-1	5	-47.15	-44.8	-47.99	-47.89	-47.75	-47.3	-46.18
	10	-47.56	-45.03	-48.68	-47.69	-48.09	-45.08	-48.07
	15	-47.80	-42.39	-44.55	-45.13	-48.38	-44.61	-48.31
	20	-46.25	-47.2	-48.3	-46.02	-47.98	-45.94	-43.69
	30	-44.21	-44.18	-47.77	-43.42	-48.44	-46.14	-42.46
A-2	10						-46.1	
B-1	5	-45.94	-49.41	-45.96	-45.58	-47.84	-44.58	-46.56
	10	-48.84	-47.91	-47.6	-48.93	-48.16	-48.7	-44.13
	15	-49.29	-43.82	-48.96	-49.4	-48.82	-47.07	-47.64
	20	-48.47		-47.99	-48.99	-48.78	-47.12	-46.11
	30	-49.43	-46.27	-46.16	-46.28	-50.48	-46.52	-48.9
B-2	20	-47.34	-47.34					
	30	-46.87						
C-1	5	-43.88	-47.91	-49.14	-49.16	-47.99	-47.07	-48.45
	10	-46.02	-51.15	-49	-48.11	-48.8		-46.69
	15	-45.77	-47.34	-48.35	-48.3	-46.02	-47.83	-47.41
	20	-47.73	-44.18	-48.02	-46.26	-45.86	-46.31	-51.18
	30	-42.72	-44.44	-47.13	-48.07	-47.31	-45.52	-47.46
D-1	5	-47.32	-44.18	-45.57	-44.85	-45.51	-47.63	-47.29
	10	-48.75	-46.2	-47.5	-45.23	-48.19	-48.46	-46.95
	15	-45.53	-45.93	-46.62	-48.11	-48.17	-46.44	-46.16
	20	-47.17	-44.91	-47.76	-51.46	-48.95	-49.44	-49.62
	30	-49.84	-44.56	-46.65	-51.09	-49.02	-47.38	-45.83

Table A12: [CH_4] data collected From HDF88

SAS	Depth	[CH_4] (ppm)						
Subsite	(cm)	Apr '06	May '06	Jun '06	Jul '06	Aug '06	Nov '06	Jan '07
A-1	5	1.87	1.64	1.52	1.47	1.53	1.53	1.52
	10	1.58	1.37	1.25	1.37	1.41	1.86	0.95
	15	1.22	1.69	1.18	1.39	1.17	1.24	0.76
	20	1.46	1.55	1.27	1.66	1.48	1.90	0.76
	30	0.63	1.19	0.47	0.62	0.63	0.43	0.50
A-2	10						1.14	
B-1	5	1.64	1.35	1.49	1.00	1.30	1.42	1.31
	10	1.65	1.45	1.35	1.14	1.26	1.15	1.44
	15	1.48	1.85	1.14	1.10	1.18	1.25	1.78
	20	0.87		0.99	0.95	0.97	0.96	1.04
	30	1.16	1.41	1.26	0.69	0.61	1.84	0.56
B-2	20		1.00					
	30	1.50						
C-1	5	2.56	1.80	1.22	1.29	1.31	1.20	1.57
	10	2.15	1.36	1.26	1.15	1.22		1.86
	15	2.24	1.83	1.45	1.61	1.62	1.90	1.76
	20	1.99	2.18	1.41	1.30	1.42	1.97	0.94
	30	1.29	2.40	1.73	1.60	1.58	2.15	1.98
D-1	5	1.76	2.15	1.65	1.58	1.56	1.47	1.54
	10	1.24	1.43	1.15	1.20	1.22	1.18	1.16
	15	2.17	2.10	1.79	1.60	0.94	1.94	0.82
	20	0.60	0.79	0.54	0.46	0.72	0.46	0.45
	30	0.36	0.58	1.88	0.38	0.52	0.29	0.29

Table A13: $\delta^{13}CH_4$ data collected from HDF00

SAS	Depth	$\delta^{13}CH_4$ (‰)						
Subsite	(cm)	Apr '06	May '06	Jun '06	Jul '06	Aug '06	Nov '06	Jan '07
A-1	5	-47.69	-47.9	-45.86	-45.72	-48.23	-47.15	-47.72
	10	-46.93	-41.59	-43.54	-47.89	-47.37	-43.52	-48.29
	15	-43.87	-47.59	-41.71	-47.89	-46.54	-47.54	-47.54
	20	-49.22	-46.27	-44.46	-43.38	-43.43	-45.7	-47.08
	30	-48.43	-48.23			-46.8	-47.17	-40.79
A-2	5		-44.13					
	10		-47.5					
	15		-45.72					
	30			-47.78	-46.41			
B-1	5	-47.43	-45.33	-45.66	-47.22	-46.37	-46.69	-46.62
	10	-49.26	-43.31	-45.38	-47.6	-44.62	-47.38	-47.46
	15	-49.87	-47.37	-48.45	-44.99	-49.63	-48.3	-47.85
	20	-50.01	-42.8	-51.43	-48.01	-49.48	-50.02	-46.71
	30	-42.98	-47.4	-47.11	-43.63	-49.09	-46.82	-46.61
C-1	5	-47.39	-45.14	-45.8	-46.36	-47.44	-46.98	-47.35
	10	-45.45	-44.95	-46.09	-45.72	-46.43	-48.5	-46.82
	15	-48.86	-47.51	-45.01	-48.39	-45.35	-47.63	-47.32
	20	-48.31	-42.77	-49.33	-44.78	-47.12	-44.03	-46.76
	30	-47.42	-47.7	-46.4	-46.32	-47.33	-44.32	-49.81
1	80					-47.53	-47.53	-47.40
2	80					-49.66	-47.43	-47.50

Table A14:[CH_4] data collected from HDF00

SAS	Depth	[CH_4] (ppm)						
Subsite	(cm)	Apr '06	May '06	Jun '06	Jul '06	Aug '06	Nov '06	Jan '07
A-1	5	1.80	1.67	2.24	1.44	1.33	1.50	1.46
	10	1.22	1.65	1.66	0.95	1.16	1.22	0.90
	15	0.78	0.65	1.03	0.49	0.76	0.45	0.54
	20	0.50	0.67	0.73	0.69	0.94	0.41	0.38
	30	1.47	1.46			1.42	1.16	0.35
A-2	5		1.70					
	10		0.89					
	15		1.98					
	30			0.43	0.44			
B-1	5	2.12	2.36	1.75	1.88	2.07	1.85	1.88
	10	0.94	2.08	2.04	1.47	1.60	1.28	1.22
	15	0.59	0.72	0.72	0.77	1.03	0.55	0.57
	20	0.54	0.96	0.64	0.58	0.61	0.47	0.53
	30	2.00	0.88	0.88	0.90	0.68	0.78	0.37
C-1	5	1.38	1.50	1.21	1.11	1.44	0.98	1.58
	10	0.90	0.90	0.74	1.07	1.03	0.82	0.79
	15	0.69	0.81	0.81	0.83	1.60	0.62	0.63
	20	0.62	1.12	0.56	0.95	1.34	0.77	0.77
	30	2.00	1.98	1.92	1.72	1.55	2.08	0.24
1	80					1.60	1.33	0.85
2	80					0.38	0.23	0.18

Table A15: Chamber data collected from DF49 and HDF00 (continues onto next two pages)

Month	Site	Chamber Subsite	Time Interval (min)	$[CO_2]$	$\delta^{13}CO_2$	$[CH_4]$	$\delta^{13}CH_4$
April '06	DF49	1	0	521.12	-12.70	1.12	-48.47
			3	553.51	-12.83	2.33	-47.71
			9	579.19	-14.47	2.10	-48.54
			14	743.62	-16.76	2.08	-48.48
			60	900.72	-18.69	2.16	-47.88
		2	0	568.18	-12.73	1.04	-44.17
			5	821.56	-18.23	1.16	-47.56
			10	610.06	-15.14	1.16	-46.25
			26	873.82	-16.92	1.05	-45.41
			60	1145.54	-19.29	0.85	-42.56
	HDF00	1	0	497.91	-11.89	2.06	-48.68
			11	537.00	-12.87	2.37	-44.77
			15	586.75	-13.62		
			30	687.57	-15.52	1.62	-44.05
			60	922.54	-17.24	1.15	-39.70
		2	0	461.49	-10.76	1.84	-48.08
			5	491.69	-10.05	2.24	-44.32
			10	509.90	-12.17	1.77	-47.45
			25	552.10	-12.63	1.87	-47.98
			56	567.20	-13.48	1.79	-48.10
May '06	DF49	1	0	636.48	-10.62	1.83	-47.69
			11	873.62	-10.30	1.82	-46.03
			16	773.97	-16.18	1.70	-45.96
			30	1205.76	-15.83	1.63	-45.85
			60	1756.50	-16.76	1.68	-42.56
		2	0			1.15	-46.33
			5	1256.74	-14.76	1.98	-43.94
			15	1473.02	-18.03	1.74	-44.71
			30	1333.21	-18.77	1.72	-40.80
			60	2256.26	-18.75	1.16	-43.13
	HDF00	1	0	1745.55	-8.28	2.19	-47.70
			5	1853.86	-8.62	2.48	-42.43
			15	2111.48	-9.39	1.51	-42.50
			30	2187.19	-10.10	1.04	-40.30
			62	2226.10	-14.66	1.29	-35.79
		2	0	858.17	-10.57	1.40	-48.13
			6	973.26	-12.63	1.83	-46.68
			42	1132.38	-15.94	1.49	-47.21
			60	1140.10	-14.36	1.60	-44.52
			75	709.86	-12.40	1.53	-46.08
Jun '06	DF49	1	0	639.05	-13.17	1.83	-45.47
			5	978.24	-14.38	2.08	-46.65
			10	742.21	-17.09	2.03	-46.28
			15	1107.63	-17.58	1.69	-45.84

Table A15 (continued)

Month	Site	Chamber Subsite	Time Interval (min)	$[CO_2]$	$\delta^{13}CO_2$	$[CH_4]$	$\delta^{13}CH_4$
Jun '06	DF49		30	1227.39	-20.57	1.67	-46.40
			60	2241.48	-21.62	1.47	-44.82
		2	0	695.00	-13.78	1.58	-47.83
			5	766.68	-15.62	1.72	-45.87
			10	1541.24	-21.69		
			30	1701.22	-19.69	1.70	-44.55
			60	2142.69	-20.41	1.37	-42.59
	HDF00	1	0	940.81	-9.73	2.09	-45.65
			10	1698.15	-12.70	1.79	-43.87
			15	1323.39	-13.97	1.53	-43.47
			31	1488.60	-14.75	1.39	-39.26
			60	2085.08	-16.62	1.12	-35.17
		2	0	916.11	-10.76	2.02	-48.11
			5	1747.84	-13.22	2.31	-45.01
			10	3270.67	-14.27	2.11	-44.98
			30	2716.99	-13.75		
			60	2068.48	-18.94	1.34	-45.93
Jul '06	DF49	1	0	499.54	-10.70	1.97	-45.81
			6	547.60	-13.97	1.58	-47.02
			15	591.38	-13.02	1.62	-45.44
			31	1073.75	-20.22	1.35	-44.35
			58	1668.56	-21.94	1.21	-41.74
		2	0	876.34	-17.11	1.00	-46.42
			6	971.61	-18.63	1.55	-43.16
			20	1457.41	-19.25	1.45	-41.42
			30	1907.17	-20.80	0.99	-40.92
			60	2888.22	-21.31	1.05	-38.89
	HDF00	1	0	544.17	-12.27	1.60	-46.14
			7	558.76	-12.65	1.74	-47.31
			18	544.17	-13.55	1.76	-44.55
			30	381.09	-11.11		
			58	565.63	-13.99	1.46	-46.08
		2	0	534.73	-12.51	1.72	-46.20
			5	666.05	-13.76	1.75	-46.93
			15	763.90	-17.21	1.69	-44.07
			30	471.21	-12.05	1.28	-45.00
			60	1477.15	-20.87	1.33	-42.93
Aug '06	DF49	1	0	740.46	-7.66	1.66	-47.63
			5	834.46	-10.58	1.47	-46.56
			62	1356.00	-16.45	0.98	-41.05
			106	1581.36	-17.64	0.82	-38.75
			140	1814.44	-18.53	0.61	-41.58
		2	0	743.03	-10.58		
			5	1000.58	-13.81	1.57	-46.11

Table A15 (continued)

Month	Site	Chamber Subsite	Time Interval (min)	$[CO_2]$	$\delta^{13}CO_2$	$[CH_4]$	$\delta^{13}CH_4$
Aug '06	DF49	2	16	1240.10	-14.78	1.51	-43.80
			30	1433.27	-15.93	1.31	-42.49
			60	1987.00	-17.03	1.27	-39.67
	HDF00	1	0	1029.90	-6.76	1.53	-48.22
			10	1207.71	-7.19	1.14	-46.11
			20	1198.13	-7.68	1.41	-44.74
			34	1176.25	-8.19	1.27	-42.48
			63	1341.75	-9.05	1.02	-41.00
		2	0	1106.50	-5.95	1.77	-47.59
			7	1345.85	-6.70	1.62	-47.89
			17	1211.81	-8.15	1.71	-45.14
			30	1274.73	-7.77	1.63	-46.01
			60	1267.89	-9.65	0.36	-44.34
Nov '06	DF49	1	0	627.51	-9.36	1.71	-46.96
			5	649.11	-10.74	1.67	-45.74
			16	719.07	-13.44	1.36	-46.70
			31	1112.03	-10.94	1.45	-43.95
			61	397.08	-11.12	1.07	-43.18
		2	0	650.14	-12.21	1.20	-47.80
			5	951.55	-12.66	1.53	-47.14
			15	1001.96	-14.18	1.37	-45.17
			30	1091.46	-16.71	1.23	-43.57
			60	1509.11	-18.24	1.06	-41.84
		1	0	781.04	-10.74	1.69	-45.66
			5	402.02	-10.20	1.38	-45.80
			13	809.52	-13.45	1.25	-44.52
			30	387.78	-10.38	1.03	-41.48
			59	1108.57	-14.17	0.25	-34.81
		2	0	905.92	-10.66	1.64	-46.78
			5	750.37	-12.69	1.55	-47.38
			13	1138.15	-9.36	1.61	-45.91
			30	397.64	-10.25	1.48	-44.39
			60	396.54	-10.23	1.27	-44.53
Jan '07	DF49	1	0	845.03	-12.67	2.05	-45.20
			5	1026.58	-20.16	2.50	-43.03
			15	1138.90	-22.47	1.79	-44.86
			30	1202.90	-23.12	2.34	-41.03
			58	481.94	-11.13	1.62	-41.19
		2	0	753.61	-12.27	1.80	-46.17
			5	1149.35	-21.30	1.78	-45.09
			15	481.94	-10.94	2.00	-42.29
			30	476.72	-10.36	1.11	-40.95
			61	479.33	-10.81	1.37	-40.73
	HDF00	1	0	622.51	-12.10	1.61	-48.26

Table A15 (continued)

Month	Site	Chamber Subsite	Time Interval (min)	$[CO_2]$	$\delta^{13}CO_2$	$[CH_4]$	$\delta^{13}CH_4$
Jan '07	HDF00	1	10	721.35	-10.05	1.55	-47.05
			15	631.97	-10.40	1.61	-45.33
			35	645.64	-11.57	1.36	-42.03
			60	245.01	-9.46	0.99	-38.56
		2	0	572.04	-9.99	1.66	-47.73
			5	401.69	-12.00	1.81	-46.18
			16	784.45	-9.65	1.52	-46.51
			33	401.69	-11.47	1.56	-43.72
			60	397.48	-11.69	1.14	-42.36
			64	715.04	-14.29		

Table A16: Soil Moisture and PAR data from DF49

Month/Year	Time of Sampling	Soil Moisture (vol/vol) 1-2 cm	10-12 cm	30-50 cm	70-100 cm	Averaged to 30 cm	Averaged Above-Canopy PAR ($\mu mol \cdot m^{-2} \cdot s^{-1}$)
April 06	13:00-16:00	0.23	0.22	0.18	0.31	0.26	126.14
May 06	14:30-17:00	0.11	0.13	0.13	0.23	0.21	743.60
June 06	12:00-16:00	0.14	0.14	0.12	0.18	0.23	354.92
July 06	12:00-15:00	0.09	0.10	0.10	0.15	0.12	61.68
Aug 06	11:45-15:30	0.07	0.09	0.09	0.14	0.07	123.44
Nov 06	12:18-17:00	0.15	0.16	0.14	0.14	0.23	7.78
Jan 07	9:30-15:30	0.14	0.18	0.17	0.29	0.24	0.00

Table A17: Soil Moisture and PAR data from HDF88

Month/Year	Time of Sampling	Soil Moisture (vol/vol) 3-5 cm	10-15 cm	35-50 cm	70-95 cm	Averaged to 30 cm	Averaged Above-Canopy PAR ($\mu mol \cdot m^{-2} \cdot s^{-1}$)
April 06	16:00-18:00	0.27	0.34	0.35	0.43	0.32	870.26
May 06	11:00-13:00	0.12	0.22	0.24	0.30	0.15	3.58
June 06	20:00-23:00	0.12	0.20	0.19	0.24	0.13	776.99
July 06	20:00-23:00	0.09	0.18	0.16	0.18	0.09	906.84
Aug 06	19:00-22:30	0.07	0.17	0.14	0.16	0.07	1401.81
Nov 06	11:00-13:00	0.19	0.31	0.35	0.46	0.19	0.00
Jan 07	11:00-14:00	0.22	0.32	0.33	0.38	0.28	0.00

Table A18: Soil Moisture and PAR data from HDF00

Month/Year	Time of Sampling	Soil Moisture (vol/vol) 2-5cm	10-20 cm	50-60cm	70-100cm	Averaged to 30 cm	Averaged Above-Canopy PAR ($\mu mol \cdot m^{-2} \cdot s^{-1}$)
April 06	17:00-19:00	0.27	0.36	0.13	0.21	0.20	588.38
May 06	18:30-20:30	0.19	0.27	0.11	0.17	0.14	1624.20
June 06	16:44-19:00	0.25	0.28	0.10	0.15	0.17	1381.80
July 06	15:40-19:00	0.09	0.13	0.07	0.10	0.07	690.27
Aug 06	16:00-18:00	0.04	0.11	0.07	0.09	0.05	898.32
Nov 06	17:30-19:30	0.22	0.32	0.12	0.19	0.21	35.49
Jan 07	16:00-19:00	0.29	0.37	0.13	0.21	0.20	29.41

Table A19: Soil Moisture and PAR data from OBS

Month/Year	Time of Sampling	Soil Moisture (vol/vol) 5 cm	10 cm	20 cm	50 cm	Average of all depths	Averaged Above-Canopy PAR ($\mu mol \cdot m^{-2} \cdot s^{-1}$)
Late June 05	9:00-12:00	0.16	0.16	0.18	0.22	0.18	92.57
Early August 05	9:00-12:00	0.10	0.14	0.13	0.15	0.13	123.00
Late August 05	9:30-12:00	0.08	0.13	0.12	0.14	0.12	50.62

Table A20: Equations of curve-fitted CH_4 concentration data at all BC sites, using Eqn. 4.1.1.2

Site	Carbon Species	Month/ Year	Equation Variables ($y = y_0 + Ae^{-x/t}$)*			Fit (R^2)
			y_o	A	t	
DF49	^{12}C	Apr 2006	0.66535	1.11569	0.06320	0.81
		May 2006	0.63933	1.14171	0.06936	0.82
		Jun 2006	0.57499	1.20605	0.06642	0.85
		Jul 2006	0.64685	1.13419	0.05578	0.96
		Aug 2006	0.46561	1.31543	0.08021	0.96
		Nov 2006	0.36112	1.41991	0.06280	0.96
		Jan 2007	0.79347	0.98757	0.20009	0.71
	^{13}C	Apr 2006	0.00709	0.01187	0.06306	0.81
		May 2006	0.00681	0.01215	0.06980	0.81
		Jun 2006	0.00613	0.01283	0.06630	0.85
		Jul 2006	0.00689	0.01207	0.05593	0.96
		Aug 2006	0.00497	0.01399	0.07990	0.96
		Nov 2006	0.00386	0.01510	0.06266	0.97
		Jan 2007	0.00853	0.01043	0.20248	0.70
HDF88	^{12}C	Apr 2006	0.96695	0.81409	0.16599	0.80
		May 2006	1.36524	0.41580	0.20636	0.33
		Jun 2006	1.04462	0.73642	0.11036	0.67
		Jul 2006	0.81239	0.96865	0.15139	0.84
		Aug 2006	0.82249	0.95854	0.14090	0.95
		Nov 2006	1.16290	0.53740	0.13717	0.61
		Jan 2007	0.78773	0.99331	0.13576	0.88
	^{13}C	Apr 2006	0.01030	0.00866	0.16611	0.80
		May 2006	0.01456	0.00440	0.20980	0.32
		Jun 2006	0.01112	0.00784	0.11073	0.67
		Jul 2006	0.00865	0.01031	0.15144	0.84
		Aug 2006	0.00875	0.01022	0.14092	0.95
		Nov 2006	0.01240	0.00571	0.13761	0.61
		Jan 2007	0.00839	0.01057	0.13601	0.88
HDF00	^{12}C	Apr 2006	0.54896	1.23208	0.15590	0.28
		May 2006	0.90699	0.87404	0.15602	0.53
		Jun 2006	0.63299	1.14805	0.14376	0.71
		Jul 2006	0.69233	1.08871	0.09646	0.83
		Aug 2006	0.95305	0.82799	0.10987	0.87
		Nov 2006	0.76851	1.01253	0.19924	0.47
		Jan 2007	0.51072	1.27032	0.14138	0.94
	^{13}C	Apr 2006	0.00584	0.01313	0.15639	0.28
		May 2006	0.00969	0.00927	0.15627	0.53
		Jun 2006	0.00673	0.01223	0.14461	0.71
		Jul 2006	0.00738	0.01159	0.09675	0.83
		Aug 2006	0.01016	0.00880	0.10999	0.87
		Nov 2006	0.00818	0.01078	0.19973	0.47
		Jan 2007	0.00544	0.01352	0.14147	0.94

Table A21: Equations of curve-fitted CH_4 concentration data at OBS, using Eqn. 4.1.1.3.

Carbon Species	Sampling Period (2005)	Equation Variables ($y = y_0 + Ae^{-x/t}$)*			Fit (R^2)
		yo	A	t	
^{12}C	Late June	0.41180	1.36924	0.14940	0.95
	Early August	0.36664	1.41439	0.15059	0.79
	Late August	0.37515	1.40589	0.17259	0.83
^{13}C	Late June	0.00439	0.01457	0.14937	0.95
	Early August	0.00391	0.01505	0.15034	0.79
	Late August	0.00402	0.01494	0.17334	0.83

Table A22: Equations of curve-fitted CO_2 concentration data at all BC sites, using Eqn. 4.2.1.7

Site	Month/ Year	Equation Variables ($y = y_0 + Ae^{-x/t}$)			Fit (R^2)
		yo	A	t	
DF49	Apr 2006	3481.40	-2993.32	0.12519	0.97
	May 2006	4258.68	-3777.63	0.06597	0.98
	Jun 2006	6223.88	-5574.60	0.07295	0.90
	Jul 2006	5651.52	-5081.62	0.10213	0.90
	Aug 2006	5402.76	-4796.71	0.17277	0.96
	Nov 2006	4972.91	-4352.95	0.16578	0.90
	Jan 2007	2223.84	-1810.15	0.0904	0.93
HDF88	Apr 2006	5786.59	-5355.35	0.09754	0.95
	May 2006	2008139.51	-2007123.53	78.13043	0.93
	Jun 2006	8092.74	-7844.80	0.08079	0.94
	Jul 2006	6089.59	-5728.85	0.17535	0.87
	Aug 2006	5324.85	-4483.64	0.38392	0.87
	Nov 2006	5831.50	-5100.22	0.17050	0.34
	Jan 2007	3494.24	-2859.96	0.25788	0.56
HDF00	Apr 2006	1793.66	-1465.32	0.07195	0.96
	May 2006	3347.10	-3045.11	0.07619	0.97
	Jun 2006	5160.04	-4747.85	0.08775	0.94
	Jul 2006	3903.35	-3522.73	0.17403	0.98
	Aug 2006	3550.13	-2936.32	0.25574	0.95
	Nov 2006	209512.39	-208917.92	26.82168	0.69
	Jan 2007	1945.98	-1580.88	0.08308	0.99

Table A23: Equations of curve-fitted CO_2 concentration data at OBS, using Eqn. 4.2.1.7

Sampling Period (2005)	Equation Variables ($y = y_0 + Ae^{-x/t}$)			Fit (R^2)
	y_o	A	t	
Late June	4161.34	-3421.26	0.52	0.97
Early August	624798.98	-624065.09	222.27	0.93
Late August	18651.49	-17905.80	7.88	0.85

Table A24: Near Ground (1 m) CO_2 data collected at OBS during 2005 (Data courtesy of L. Flanagan; chart continues on next page)

Year	Sampling No.	DOY	Hour	Minute	Night	$[CO_2]$ (ppm)	$\delta^{13}CO_2$ (‰)
2005	1	143	17	48	1	382.7	-8.97
2005	1	143	19	40	1	394.8	-9.32
2005	1	143	22	10	1	400	-9.57
2005	1	143	22	40	1	412	-10.25
2005	1	144	20	25	2	439.5	-11.15
2005	1	144	23	25	2	444.4	-11.43
2005	2	163	18	10	1	400.6	-9.39
2005	2	163	18	40	1	406.6	-9.68
2005	2	163	19	40	1	439.1	-10.96
2005	2	163	20	10	1	437.4	-10.74
2005	2	163	20	40	1	459	-11.6
2005	2	163	21	10	1	583.2	-14.85
2005	2	163	21	40	1	601.5	-15.49
2005	3	177	18	13	1	393.5	-9.01
2005	3	177	18	58	1	405.3	-9.63
2005	3	177	19	25	1	418.2	-10.03
2005	3	177	19	55	1	473.3	-11.88
2005	3	177	20	25	1	429.5	-10.21
2005	3	177	21	25	1	451.5	-11.43
2005	3	177	21	55	1	465.8	-11.75
2005	4	186	18	11	1	392.9	-9.41
2005	4	186	20	10	1	406.7	-9.82
2005	4	186	20	55	1	421.5	-10.15
2005	4	186	22	10	1	437.9	-10.83
2005	4	186	23	10	1	450.3	-11.27
2005	4	187	0	25	1	485	-12.76
2005	4	187	1	10	1	492.6	-12.67
2005	5	199	18	10	1	378.4	-8.53
2005	5	199	19	10	1	399.7	-9.45
2005	5	199	19	40	1	455.1	-11.69
2005	5	199	20	10	1	471.5	-11.94
2005	5	199	20	40	1	414.1	-10.23
2005	5	199	21	10	1	389.2	-8.97
2005	5	200	0	10	1	443.8	-11.25
2005	6	215	17	42	1	390.5	-8.77
2005	6	215	18	10	1	413.5	-10.06
2005	6	215	18	55	1	516.6	-13.15
2005	6	215	19	25	1	497	-12.45
2005	6	215	20	10	1	459.7	-11.84
2005	6	215	20	40	1	434.2	-10.71
2005	6	215	21	40	1	482.5	-12.51
2005	7	234	17	10	1	375.7	-8.08
2005	7	235	0	40	1	384.2	-8.52

Table A24 (continued)

Year	Sampling No.	DOY	Hour	Minute	Night	$[CO_2]$ (ppm)	$\delta^{13}CO_2$ (‰)
2005	7	235	4	10	1	399.1	-9.68
2005	7	235	4	40	1	424	-10.71
2005	7	235	5	10	1	447.6	-11.57
2005	7	235	5	40	1	477.4	-12.33
2005	7	235	6	40	1	459.2	-11.39
2005	8	243	16	50	1	396.3	-9.16
2005	8	243	18	10	1	408.7	-9.73
2005	8	243	18	40	1	421	-10.07
2005	8	243	19	25	1	441.4	-11.17
2005	8	244	0	40	1	496.6	-13.02
2005	8	244	1	25	1	476	-12.57
2005	8	244	1	55	1	450.2	-11.47
2005	9	250	16	35	1	377.5	-8.62
2005	9	250	17	40	1	386.6	-8.93
2005	9	250	18	55	1	395.8	-9.2
2005	9	250	19	25	1	431.1	-10.77
2005	9	250	19	55	1	457.6	-11.93
2005	9	250	20	25	1	423.7	-10.44
2005	10	277	17	38	1	394.4	-9.36
2005	10	277	19	55	1	400.2	-9.81
2005	10	278	15	52	2	384.6	-8.76
2005	10	280	8	10	2	377.9	-8.46
Averaged Values						**433.2**	**-10.64**

Labels: Sampling No. – Period of sampling
DOY – Day of Year
Hour – Hour of sampling (PDT)
Minute – Minute of Sampling
Night – Number of nights over which data was collected

Table A25: Near Ground (1 m) CO_2 data collected at DF49 during 2005 (Data courtesy of L. Flanagan; chart continues on next page)

Year	Sampling No.	DOY	Hour	Minute	Night	$[CO_2]$ (ppm)	$\delta^{13}CO_2$ (‰)
2005	1	130	18	55	1	408.6	-9.92
2005	1	130	21	10	1	419.9	-10.33
2005	1	130	21	40	1	428.3	-10.64
2005	1	131	19	10	2	391.8	-8.96
2005	1	132	3	55	2	440.9	-11.19
2005	1	132	4	25	2	448.4	-11.37
2005	2	145	18	22	1	403.5	-9.67
2005	2	145	19	40	1	411.5	-10.03
2005	2	146	2	10	1	427.7	-10.68
2005	3	172	18	37	1	450.7	-11.21
2005	3	172	19	10	1	438.3	-11.05
2005	3	172	19	40	1	397.9	-9.15
2005	3	172	20	10	1	408.3	-9.72
2005	3	172	21	55	1	412.5	-10.07
2005	3	173	0	40	1	392.2	-9.21
2005	3	173	20	25	2	424.6	-10.26
2005	4	188	18	35	1	401.2	-9.28
2005	4	188	19	25	1	379.1	-8.65
2005	4	188	21	40	1	389.5	-8.95
2005	4	188	22	40	1	409.8	-9.87
2005	5	199	18	27	1	419.6	-10.2
2005	5	199	18	57	1	411.7	-9.97
2005	5	199	20	10	1	400.4	-9.73
2005	5	199	21	40	1	390.2	-9.1
2005	5	200	18	57	2	375	-8.47
2005	5	200	19	25	2	440.4	-10.98
2005	5	202	5	25	3	432.1	-10.65
2005	6	226	17	48	1	419.9	-10.1
2005	6	226	18	25	1	400.3	-9.64
2005	6	226	19	25	1	433	-10.69
2005	6	226	19	55	1	446.1	-11.15
2005	6	226	20	25	1	481.4	-12.19
2005	6	226	22	25	1	461	-11.7
2005	6	226	22	55	1	469.2	-11.85
2005	7	241	17	19	1	411.1	-9.62
2005	7	241	18	10	1	424.2	-10.4
2005	7	241	18	40	1	448	-11.42
2005	7	241	19	55	1	427.7	-10.44
2005	7	241	20	25	1	394.9	-8.98
2005	8	261	16	35	1	410.5	-9.89
2005	8	261	17	10	1	390.9	-9.02
2005	8	261	20	55	1	420.3	-10.2
2005	8	262	1	40	1	410.9	-9.71
2005	8	262	4	55	1	432.6	-10.66
2005	8	262	16	35	2	379.4	-8.45
2005	9	283	15	48	1	410.6	-10.12

Table A25 (continued)

Year	Sampling No.	DOY	Hour	Minute	Night	$[CO_2]$ (ppm)	$\delta^{13}CO_2$ (‰)
2005	9	283	16	25	1	441.1	-11.16
2005	9	283	17	10	1	403.5	-9.6
2005	9	283	17	40	1	389.5	-9.34
2005	9	283	19	10	1	394.3	-9.38
2005	9	284	15	48	2	427	-10.57
2005	9	284	16	40	2	421.2	-10.17
Averaged Values						**417**	**-10.1**

Labels: Sampling No. – Period of sampling
DOY – Day of Year
Hour – Hour of sampling (PDT)
Minute – Minute of Sampling
Night – Number of nights over which data was collected